

Decarboxylation of Poly[*N*-(acryloyloxy)phthalimide] as a Versatile Tool in Polymer Chemistry

Zur Erlangung des akademischen Grades eines

DOKTORS DER NATURWISSENSCHAFTEN

(Dr. rer. nat.)

von der KIT-Fakultät für Chemie und Biowissenschaften
des Karlsruher Instituts für Technologie (KIT)

genehmigte

DISSERTATION

von

M.Sc. Stefan Frech

aus Speyer

1. Referent: Prof. Dr. Patrick Théato
2. Referent: Prof. Dr. Michael Meier

Tag der mündlichen Prüfung: 22.07.2022

für meine Eltern

Declaration of Authorship

Die vorliegende Arbeit wurde im Zeitraum von Juni 2019 bis Juni 2022 am Institut für Technische Chemie und Polymerchemie (ITCP) am Karlsruher Institut für Technologie (KIT) unter der wissenschaftlichen Betreuung von Prof. Dr. Patrick Théato angefertigt.

Ich erkläre hiermit, dass ich die vorliegende Arbeit im Rahmen der Betreuung durch Prof. Dr. Patrick Théato selbstständig verfasst und keine anderen als die angegebenen Quellen und Hilfsmittel verwendet habe. Wörtlich oder inhaltlich übernommene Stellen sind als solche kenntlich gemacht und die Satzung des Karlsruher Instituts für Technologie (KIT) zur Sicherung guter wissenschaftlicher Praxis wurde beachtet. Des Weiteren erkläre ich, dass ich mich derzeit in keinem laufenden Promotionsverfahren befinde, und auch keine vorausgegangenen Promotionsversuche unternommen habe. Die elektronische Version der Arbeit stimmt mit der schriftlichen Version überein und die Primärdaten sind gemäß Abs. A (6) der Regeln zur Sicherung guter wissenschaftlicher Praxis des KIT beim Institut abgegeben und archiviert.

Karlsruhe, den

Stefan Frech

List of Publications

List of Publications

Publications within this Dissertation

- [3] Frech, S.; Molle, E.; Hub, C.; Theato, P. Decarboxylation of Poly[*N*-(acryloyloxy)phthalimide] as a Versatile Tool in Post-Polymerization Modification. *Macromol. Rapid Commun.* **2022**, *43*, 2200068.
DOI: 10.1002/marc.202200068.
- [2] Frech, S.; Theato, P. Synthesizing Polyethylene from Polyacrylates: A Decarboxylation Approach. *ACS Macro Letters.* **2022**, *11* (2), 161–165.
DOI: 10.1021/acsmacrolett.1c00723.
- [1] Frech, S.; Molle, E.; Butzelaar, A.J.; Theato, P. Ethylene-free Synthesis of Polyethylene Copolymers and Block Copolymers. *Macromolecules.* **2021**, *54* (21), 9937–9946.
DOI: 10.1021/acs.macromol.1c01257.

Patent within this Dissertation

- [1] Frech, S.; Theato, P. Decarboxylation of *n*-oxyphthalimide-based polymers. *WO* EP3798242A1.

Other Publications

- [1] Molle, E.; Frech, S.; Grüger, T.; Theato P. Electrochemically-initiated polymerization of reactive monomers *via* 4-fluorobenzenediazonium salts. *Polym. Chem.*, **2021**, *12* (41), 5970-5978. DOI: 10.1039/D1PY00536G.

Conference Contributions

- [1] Synthesizing Polyethylene from Polyacrylates - Decarboxylation as a Versatile Tool in Polymer Chemistry
Poster at the “GDCh Macrosymposium 2021”, October 14th, 2021.

Abstract

Polyethylene (PE) is the most produced plastic worldwide and used for a broad field of applications such as packaging, insulation materials, coatings or even bulletproof vests. The wide range of properties of PE are mainly determined by the structure and architecture and thus by the synthesis method, which consequently plays a major role. Since ethylene gas is mainly used as the monomer in both large-scale production and laboratory synthesis, the targeted synthesis of functional PE and various PE architectures is challenging, but the development of new methods has experienced a rapid growth in recent years. However, most of these methods still rely on gaseous ethylene, which requires additional safety measures to handle a flammable gas, especially on a laboratory scale. Thus, the present thesis deals with the development of a controlled, ethylene-free synthesis method of PE and functional PE. This idea should be realized by a decarboxylation of phthalimide-based active esters. Two different decarboxylation methods, a thermal and a photochemical decarboxylation, were successfully implemented to polymer chemistry and compared regarding their suitability to yield PE polymers from a polyacrylate-based precursor.

In the first project, the synthesis of pure PE by the decarboxylation of poly[*N*-(acryloyloxy)phthalimide] (PAP) should originally be investigated. Herein, the variation of the reaction parameters of the decarboxylation and the analysis of the resulting polymers revealed that the increasing conversion of the phthalimide units resulting in (insoluble) PE units caused the decarboxylation to reach a limitation. To solve this challenge and to circumvent the solubility problem, the focus was laid on the synthesis of precursor block copolymers. By doing so, the phthalimide block should be decarboxylated to yield PE, while the second block enhances the solubility of the polymer during the decarboxylation and the following analysis. Thus, the phthalimide-based precursor block copolymers were synthesized using reversible addition-fragmentation chain-transfer (RAFT) polymerization, which resulted in an excellent control over the polymerization and allowed for the synthesis of defined architectures. Subsequently, a library of different block copolymers with various chain lengths and comonomers was synthesized to i) demonstrate that the architecture of the resulting PE block copolymers can be predefined and ii) evaluate the solubility limits and characteristics of the PE block copolymers. In the next step, these polymers were decarboxylated using both the thermal and photochemical method and the formation of PE block copolymers of different chain lengths was successfully achieved and proven by various analysis methods. However, the analyses also revealed that a side reaction during the decarboxylation resulted in the formation

Abstract

of a comonomer fraction in the PE block. As a consequence of several experiments aiming to elucidate this phenomenon, phenylsilane was identified as the source for the side reaction and was consequently replaced by tributyltin hydride. By using the photochemical method, PE block copolymers were obtained in high purity, however, the thermal decarboxylation featured additional side reactions, which could not be further avoided. The comparison of the results of both methods showed that the photochemical method is clearly superior to the thermal one, and PE polymers were obtained in higher purity using less toxic reactants (nickel(II) chloride). Thus, the first ever controlled and ethylene-free synthesis of PE block copolymers by highly efficient photochemical decarboxylation of a polyacrylate-based precursor was established and the first goal of the present thesis achieved.

In the second approach, the fundamental goal of the present thesis, *i.e.*, the ethylene-free synthesis of pure PE, was further pursued. Since the first project demonstrated that the sophisticated employment of polymer architecture can be used to circumvent the solubility limitation, a cleavable block copolymer, which enables the solubility during the decarboxylation and allows to be subsequently cleaved, was designed. Thus, a macroRAFT agent based on a poly(ethylene glycol) (PEG) ester was synthesized. While the PEG block provides solubility during the decarboxylation, an ester linkage between the blocks allows for the quantitative cleavage of PE by aminolysis and removal of the PEG block. However, a comonomer fraction resulting from a side reaction based on the H-donor phenylsilane was identified and the H-donor subsequently replaced as mentioned before. The decarboxylation was successfully optimized by employing tributyltin hydride as the H-donor. In the next step, the aminolysis was investigated and a one-pot two-step reaction procedure for the decarboxylation and subsequent cleavage was developed. Finally, cleavable precursor block copolymers of three different chain lengths were synthesized to investigate the limitation of this method. The resulting PEs were analyzed in great detail using high-temperature ^1H and ^{13}C NMR spectroscopy, ATR-FT-IR spectroscopy, DSC, and high-temperature SEC, proving the highly efficient decarboxylation and aminolysis as well as the high purity of the material and predefined chain lengths. Thus, the fundamental goal of the present dissertation, the development of a controlled, ethylene-free synthesis of pure PE by decarboxylation of a polyacrylate-based precursor system, was achieved.

The third project dealt with the expansion of the decarboxylation of PAP polymers towards functionalization reactions. First, the *in-situ* Michael-type addition of three different α , β -unsaturated carbonyl compounds during photochemical decarboxylation was successfully performed using the homopolymer PAP, accessing polymers with new functionalities in high

yields and orthogonality. In the next step, nitroxide radical coupling (NRC) was used to attach TEMPO moieties to the polymer. The coupling was successfully performed on both PAP homopolymers and block copolymers. Thus, a new, orthogonal and very mild method to attach TEMPO to a polymer backbone was established. However, the synthesis of TEMPO-functionalized PE by decarboxylation of PAP in the presence of a H-donor (tributyltin hydride) and TEMPO was challenging due to the competing reaction between the TEMPO and the tributyltin radical. Consequently, the decarboxylation was split into two steps, which improved the results, but increased the synthetic effort reducing the advantage of the new method. Nonetheless, a wide range of TEMPO-functionalized copolymers could be obtained by decarboxylation of PAP copolymers followed by NRC. Furthermore, the reduction of the alkoxyamine by zinc and acetic acid, which would result in the formation of poly(vinyl alcohol) and thus represent an alternative synthesis method, failed due to the high steric hindrance of the C-O bond by the methyl groups of TEMPO and the backbone. However, TEMPO-functionalized polymers were successfully employed for the controlled grafting of styrene. To do so, the thermolabile C-O bond of a TEMPO-functionalized block copolymer was homolytically split upon heating in the presence of styrene resulting in the successful formation of a polystyrene graft block copolymer. In summary, the utilization of the decarboxylation of PAP for functionalization reactions exceeded the initial aim of the present dissertation by far. The Michael-type addition allows for the synthesis of polymers with new functionalities and of new structures in high yields, while the first ever combination of NRC with the photochemical decarboxylation of PAP was further employed for the synthesis of graft polymers.

In the last project, the optimized photochemical decarboxylation method evaluated in the first two projects was transferred to the decarboxylation of the methacrylic analogous of PAP poly[*N*-(methacryloyloxy)phthalimide] (PMAP). Due to the additional methyl group at the polymer backbone, polypropylene (PP) polymers should be obtained in a controlled, propylene-free synthesis from a methacrylate-based precursor system. Therefore, PMAP block copolymers were successfully synthesized and subsequently photochemically decarboxylated. However, the detailed analysis of the decarboxylation product and further evaluation of the decarboxylation indicated the degradation of the polymer backbone by β -scission. Subsequently, the reactants of the decarboxylation were extensively varied, but PP block copolymers could not be obtained in high purity and efficiency comparable to PE. Nevertheless, a new and innovative method for the controlled degradation of methacrylate-based polymers was examined, which was also highlighted by a recently published study by the group of Sumerlin.

Abstract

In summary, the first ever ethylene-free and controlled synthesis of PE which is not only relevant to society, but the most produced commodity polymer worldwide from a polyacrylate-based precursor was developed and its high efficiency proven by extensive analysis of the materials. The decarboxylation was successfully transferred from organic chemistry to polymer chemistry by extensive variation of the reaction parameters, eventually identifying the optimal conditions. Furthermore, a sophisticated design of the polymer architecture was used to overcome issues regarding the decarboxylation further allowing for the synthesis of functional PE and PE block copolymers. Additionally, the Michael-type addition, enabling the synthesis of new polymers and NRC with TEMPO were adapted for the decarboxylation of PAP and further a new route to graft side chains was established, creating a new toolbox for polymer chemistry. Thus, in times of growing demands for PE, functional PE and functional polymers in general, a controlled, effective and straightforward alternative to established methods was provided.

Zusammenfassung

Polyethylen (PE) ist der weltweit am häufigsten verarbeitete Kunststoff und wird für vielfältige Anwendungen wie Verpackungen, Isolationsmaterialien, Beschichtungen oder sogar beschusshemmende Westen verwendet. Dabei spielt die Polymerstruktur und -architektur und somit auch die Herstellungsmethode eine zentrale Rolle für die Eigenschaften des Materials. Durch die Verwendung von Ethylengas als Ausgangsstoff in der großtechnischen wie auch labortechnischen Herstellung, ist die gezielte Synthese von funktionellem Polyethylen und verschiedenen Polyethylenarchitekturen herausfordernd, weshalb die Entwicklung neuer Methoden zur kontrollierten Synthese in den letzten Jahren einen enormen Aufschwung erlebte. Jedoch basieren die meisten dieser Methoden weiterhin auf der Verwendung von gasförmigem, leicht entzündlichem Ethylen, das vor allem im Labormaßstab zusätzliche Sicherheitseinrichtungen zur Handhabung erfordert. Daher stand die Entwicklung einer kontrollierten, ethylengasfreien Synthesemethode für PE im Zentrum dieser Arbeit. Diese Idee sollte mittels der Decarboxylierung von Phthalimidaktivestern verwirklicht werden. Zwei Decarboxylierungsmethoden, eine thermische und eine photochemische, wurden im Zuge dieser Arbeit in die Polymerchemie eingeführt und hinsichtlich ihrer Effektivität zur Synthese von PE-Polymeren aus einem acrylatbasierten Vorläuferpolymer verglichen.

Im Rahmen des ersten Projekts wurde zunächst die Synthese von reinem PE mittels der Decarboxylierung des Homopolymers Poly[*N*-(acryloyloxy)phthalimid] (PAP) untersucht. Die Analyse der durch die Variation der Reaktionsparameter (Temperatur, Zeit, Konzentration) erhaltenen Polymere zeigte, dass die Unlöslichkeit des Polymers aufgrund des steigenden Polyethylenanteils die Ursache für die auftretende Limitierung des Umsatzes der Decarboxylierung ist. Um die Löslichkeitsproblematik zu umgehen, wurde der Fokus daher auf die Synthese von Vorläuferblockcopolymeren gelegt. Bei diesen sollte durch die Decarboxylierung des Phthalimidblocks PE erhalten werden, während der zweite Block die Löslichkeit des Polymers während der Decarboxylierung und der darauffolgenden Analyse gewährleistet. Die phthalimidbasierten Vorläuferpolymere wurden hierbei mittels reversibler Additions-Fragmentierungs Kettenübertragungspolymerisation (RAFT), die eine exzellente Kontrolle über die Polymerisation und die Möglichkeit zur Synthese von Blockcopolymeren sicherstellte, synthetisiert. Daraufhin wurde eine Bibliothek verschiedener Polymere unterschiedlicher Kettenlängen und Comonomeren aufgebaut, um i) zu demonstrieren, dass die Architektur der PE-Polymere vordefiniert werden kann und ii) das Löslichkeitslimit sowie die Löslichkeitscharakteristik des PEs zu untersuchen. Die Polymere wurden im nächsten Schritt

Zusammenfassung

sowohl mittels der thermischen als auch der photochemischen Methode decarboxyliert, wobei erfolgreich PE-Blockcopolymere verschiedener Kettenlängen erhalten und diese umfassend analysiert wurden. Die Analyse der erhaltenen Polymere zeigte jedoch auch, dass während der Decarboxylierung eine Nebenreaktion abläuft die in der Bildung einer Comonomerfraktion im PE-Block resultierte. Daraufhin wurde Tributylzinnhydrid als Wasserstoffdonor verwendet und mittels der photochemischen Methode wurden PE-Blockcopolymere in hoher Reinheit erhalten, während mittels der thermischen Methode Polymere mit geringerer Reinheit, die sich nicht weiter erhöhen lies, erhalten wurden. Der Vergleich der beiden Methode zeigte, dass die photochemische Methode der thermischen Methode klar überlegen ist, da Blockcopolymere in höherer Reinheit erhalten und weniger toxische Reaktanden (insbesondere Nickel(II)-chlorid) verwendet wurden.

Im zweiten Ansatz wurde das zugrundeliegende Ziel dieser Arbeit, die ethylenfreie Synthese von reinem PE weiterverfolgt. Da die Ergebnisse des ersten Projekts zeigten, dass der intelligente Einsatz von Polymerarchitekturen genutzt werden kann, um die Löslichkeitslimitierung der Decarboxylierung zu umgehen, wurde ein spaltbares Blockcopolymer, das während der Decarboxylierung die Löslichkeit gewährleistet und in einem weiteren Schritt abgespalten werden kann, entwickelt. Daher wurde im nächsten Schritt ein MakroRAFT-Agens mit einer Polyethylenglycolkette (PEG) synthetisiert. Während die PEG-Kette die Löslichkeit während der Decarboxylierung gewährleistet, kann sie mittels Aminolyse abgespalten werden, um reines PE zu erhalten. In der darauffolgenden Decarboxylierung entstand wiederum eine Comonomerfraktion basierend auf einer Nebenreaktion von Phenylsilan. Im Folgenden wurde die Decarboxylierung auch hier durch den Einsatz von Tributylzinnhydrid an Stelle von Phenylsilan erfolgreich optimiert. Im nächsten Schritt wurde die Aminolyse genauer untersucht und ein zweistufiger Prozess entwickelt, in dem die Decarboxylierung sowie die Spaltung mittels Ethylendiamin nacheinander ohne Zwischenschritt ablaufen. Letztlich wurden Vorläuferpolymere drei verschiedener Kettenlängen synthetisiert, um das Limit der Methode evaluieren. Das erhaltene PE wurde detailliert mittels Hochtemperatur- ^1H und ^{13}C NMR Spektroskopie, ATR-FT-IR Spektroskopie, DSC und Hochtemperatur-SEC analysiert, wobei die hohe Effizienz der Decarboxylierung und der Aminolyse sowie die Reinheit des PEs und die vordefinierten Kettenlängen bewiesen wurden. Damit wurde das fundamentale Ziel dieser Arbeit, die Entwicklung einer ethylenfreien Synthesemethode für PE mittels Decarboxylierung eines acrylatbasierten Vorläuferpolymers erreicht.

Das dritte Projekt befasste sich mit der Erweiterung der Decarboxylierung von PAP um Funktionalisierungsreaktionen. Zuerst wurde eine Michael-Typ Addition mit drei verschiedenen α, β -ungesättigten Carbonylverbindungen erfolgreich an dem Homopolymer PAP durchgeführt und damit der Zugang zu neuartigen Polymer mittels einer hoch effektiven und orthogonalen Methode ermöglicht. Im nächsten Schritt wurde die Nitroxid-Radikal Kupplung (NRC) genutzt, um TEMPO und Derivate in das Polymer einzuführen. Die Kupplung wurde sowohl an Homo- als auch an Blockcopolymeren erfolgreich demonstriert. Die Synthese von TEMPO-funktionalisiertem PE durch die simultane Decarboxylierung von PAP mit einem Wasserstoffdonor und NRC mit TEMPO erwies sich aufgrund der Konkurrenzreaktion zwischen dem Tributylzinn- und dem TEMPO-Radikal als herausfordernd. Daher wurde die Decarboxylierung in zwei Schritte aufgeteilt, was zwar das Ergebnis verbesserte, der synthetische Mehraufwand den Nutzen jedoch zunichtemachte. Nichtsdestotrotz ermöglichte NRC von PAP-Polymeren den Zugang zu einem breiten Spektrum von TEMPO-funktionalisierten Copolymeren. Die im weiteren Verlauf des Projekts angepeilte Reduktion des Alkoxyamins mittels Zink und Essigsäure, die eine alternative Synthesemethode für Polyvinylalkohol darstellen würde, konnte aufgrund der hohen sterischen Abschirmung der C-O Bindung durch die Methylgruppen von TEMPO und des Polymerrückgrats nicht durchgeführt werden. Im nächsten Schritt wurde ein TEMPO-funktionalisiertes Blockcopolymer erfolgreich für eine Pffropfpolymerisation von Styrol verwendet werden. Dabei wurde die thermolabile C-O Bindung zwischen TEMPO und dem Polymerrückgrat in der Gegenwart von Styrol reversibel homolytisch gespalten und erfolgreich ein Polystyrol Pffropfblockcopolymer herzustellen. Zusammenfassend wurde mit der Erweiterung der Decarboxylierung von PAP um Funktionalisierungsreaktionen das Ziel der Arbeit bei weitem übertroffen. Während mittels der Michael-Typ Addition der Zugang zu Polymeren mit neuen Funktionalitäten und neuen Strukturen auf effiziente Weise eröffnet wird, ermöglicht die erstmalige Kombination aus NRC und Decarboxylierung von PAP die neuartige Synthese von Pffropfcopolymeren.

Im Rahmen des letzten Projekts sollte die in den ersten beiden Projekten optimierte photochemische Decarboxylierungsmethode auf das Methacrylat des Phthalimidpolymers Poly[N-(methacryloyloxy)phthalimid] (PMAP) übertragen werden. Durch die zusätzliche Methylgruppe am Polymerrückgrat soll so in einer kontrollierten, propylengasfreien Synthese Polypropylen (PP) erhalten werden. Daher wurden in einem ersten Schritt methacrylbasierte Blockcopolymer synthetisiert und decarboxyliert. Die Analyse des Decarboxylierungsprodukts ließ jedoch darauf schließen, dass eine Zersetzung des

Zusammenfassung

Polymerrückgrats durch β -Spaltung stattfand. Daraufhin wurden die Reaktionsparameter der Reaktion umfassend variiert; PP Blockcopolymere konnten jedoch nicht in vergleichbarer Reinheit und Effizienz erhalten werden. Trotzdem konnte eine neuartige Methode zur kontrollierten Zersetzung von methacrylatbasierten Polymeren untersucht werden. Des Weiteren wurden gewonnenen Erkenntnisse durch eine kürzlich publizierte Studie untermauert.

Zusammenfassend wurde die erste, ethylenfreie und kontrollierte Synthesemethode mittels Decarboxylierung eines acrylatbasierten Vorläuferpolymers für Polyethylen und Polyethylenblockcopolymere entwickelt und die hohe Effizienz der Reaktion durch umfassende Analyse der Polymere untermauert. Dabei wurde die intelligente Verwendung von Polymerarchitekturen dazu verwendet, Herausforderungen im Zusammenhang mit der Decarboxylierung zu überwinden. Durch umfassende Variation und Optimierung der Reaktionsparameter wurde eine optimale Reaktionsführung für die photochemische Decarboxylierung phthalimidbasierter Polymere entwickelt. Außerdem wurde die in-situ Michael-Typ Addition während der Decarboxylierung von PAP als Methode zur Synthese neuartiger Polymere sowie in-situ NRC von TEMPO der Polymerchemie zugänglich gemacht und eine neue Route zur kontrollierten Synthese von Pfropfcopolymeren etabliert und somit ein neuer Werkzeugkasten für die Polymerchemie aufgebaut. Damit wurde in Zeiten eines wachsenden Bedarfs an PE und funktionellen Polyethylenen sowie funktionellen Polymeren im Allgemeinen, eine kontrollierte und effiziente Alternative zu bereits etablierten Methoden geschaffen.

Table of Contents

Declaration of Authorship	I
List of Publications.....	II
Publications within this Dissertation	II
Patent within this Dissertation	II
Other Publications	II
Conference Contributions.....	II
Abstract.....	III
Zusammenfassung.....	VII
Table of Contents	XI
1 Introduction.....	1
2 Theoretical Background.....	3
2.1 Free Radical Polymerization	3
2.2 Reversible-Deactivation Radical Polymerization.....	5
2.2.1 Nitroxide-Mediated Polymerization.....	5
2.2.2 Reversible Addition-Fragmentation Chain-Transfer Polymerization	6
2.3 Polyethylene	10
2.4 Post-Polymerization Modification.....	19
2.4.1 Activated Esters.....	23
2.5 Decarboxylation Chemistry.....	25
3 Motivation and Goal.....	31
4 Results and Discussion.....	33
4.1 Ethylene-free Synthesis of Polyethylene Copolymers and Block Copolymers	34
4.1.1 Synthesis of Poly[<i>N</i> -(acryloyloxy)phthalimide]	36
4.1.2 Decarboxylation of Poly[<i>N</i> -(acryloyloxy)phthalimide]	38
4.1.3 Synthesis of Poly[<i>N</i> -(acryloyloxy)phthalimide] Block Copolymers	42
4.1.4 Decarboxylation of Poly[<i>N</i> -(acryloyloxy)phthalimide] Block Copolymers	46
4.1.5 Recapitulation.....	62

Table of Contents

4.2	Synthesizing Polyethylene from Polyacrylates: A Decarboxylation Approach.....	64
4.2.1	Synthesis of Poly[<i>N</i> -(acryloyloxy)phthalimide]- <i>block</i> -Poly(ethylene glycol) ..	66
4.2.2	Photochemical Decarboxylation of Poly[<i>N</i> -(acryloyloxy)phthalimide]- <i>block</i> -Poly(ethylene glycol).....	69
4.2.3	Thermal Decarboxylation of Poly[<i>N</i> -(acryloyloxy)phthalimide]- <i>block</i> -Poly(ethylene glycol).....	81
4.2.4	Aminolysis of Polyethylene- <i>block</i> -Poly(ethylene glycol)	83
4.2.5	Recapitulation.....	84
4.3	Decarboxylation of Poly[<i>N</i> -(acryloyloxy)phthalimide] as a Versatile Tool for Post-Polymerization Modification.....	85
4.3.1	Michael-type Addition	87
4.3.2	Decarboxylative Thiolation.....	92
4.3.3	Nitroxide Radical Coupling	96
4.3.4	Modification of TEMPO-functionalized Polymers.....	105
4.3.5	Recapitulation.....	113
4.4	Propylene-free Synthesis of Polypropylene <i>via</i> Decarboxylation.....	114
4.4.1	Synthesis of Precursor Polymers.....	115
4.4.2	Decarboxylation of Poly[<i>N</i> -(methacryloyloxy)phthalimide] Block Copolymers 117	
4.4.3	Recapitulation.....	127
5	Conclusion and Outlook	128
6	Experimental Section.....	131
6.1	Instrumentation.....	131
6.1.1	Nuclear Magnetic Resonance (NMR) spectroscopy	131
6.1.2	Size Exclusion Chromatography (SEC).....	131
6.1.3	Attenuated Total Reflection (ATR) Fourier-Transform (FT) Infrared (IR) Spectroscopy (ATR-FT-IR).....	131
6.1.4	Differential Scanning Calorimetry (DSC).....	132
6.1.5	Thermal Gravimetric Analysis (TGA).....	132
6.1.6	Dynamic Light Scattering (DLS).....	132
6.1.7	Light-emitting Diodes (LED) Setup.....	133
6.2	Materials	134

6.3	Procedures for ‘Ethylene-free Synthesis of Polyethylene Copolymers and Block Copolymers’	135
6.3.1	Synthesis of <i>N</i> -(Acryloyloxy)phthalimide <i>via</i> Steglich esterification	135
6.3.2	Free Radical Polymerization of <i>N</i> -(Acryloyloxy)phthalimide.....	136
6.3.3	Free Radical Copolymerization of <i>N</i> -(Acryloyloxy)phthalimide and Oligo(ethylene glycol) methyl ether acrylate.....	137
6.3.4	Synthesis of <i>S, S'</i> - Benzyl propyl trithiocarbonate (BPTT).....	138
6.3.5	Synthesis of Poly[<i>N</i> -(acryloyloxy)phthalimide] Block Copolymers <i>via</i> RAFT polymerization	139
6.3.6	Thermal Decarboxylation of Poly[<i>N</i> -(acryloyloxy)phthalimide] Polymers	142
6.3.7	Photochemical Decarboxylation of Poly[<i>N</i> -(acryloyloxy)phthalimide] Polymers	143
6.4	Procedures for ‘Synthesizing Polyethylene from Polyacrylates: A Decarboxylation Approach’	144
6.4.1	Synthesis of 3-(((Benzylthio)carbonothioyl)thio)propanoic acid (BTTP).....	144
6.4.2	Synthesis of 11-(((Benzylthio)carbonothioyl)thio)undecanoic acid (BTTU)..	145
6.4.3	Synthesis of macroRAFT Agent	146
6.4.4	Synthesis of Poly[<i>N</i> -(acryloyloxy)phthalimide]- <i>block</i> -Poly(ethylene glycol)	147
6.4.5	Photochemical Decarboxylation of Poly[<i>N</i> -(acryloyloxy)phthalimide]- <i>block</i> -Poly(ethylene glycol).....	149
6.4.6	Thermal Decarboxylation of Poly[<i>N</i> -(acryloyloxy)phthalimide]- <i>block</i> -Poly(ethylene glycol).....	151
6.4.7	Aminolysis of Polyethylene- <i>block</i> -Poly(ethylene glycol)	152
6.4.8	One-Pot Two-Step Photochemical Decarboxylation and Aminolysis	153
6.5	Procedures for ‘Decarboxylation of Poly[<i>N</i> -(acryloyloxy)phthalimide as a Versatile Tool for Post-Polymerization Modification’	154
6.5.1	Synthesis of Precursor Polymers.....	154
6.5.2	Michael-type Addition	156
6.5.3	Functionalization of Poly[<i>N</i> -(acryloyloxy)phthalimide]- <i>block</i> -Poly[oligo(ethylene glycol) methyl ether acrylate] with Bis-(4-methoxyphenyl)disulfide	157
6.5.4	Decarboxylative Thiolation of Poly[<i>N</i> -(acryloyloxy)phthalimide]	158
6.5.5	Crosslinking of Poly[<i>N</i> -(acryloyloxy)phthalimide] with Styrene	161
6.5.6	Nitroxide Radical Coupling	162

Table of Contents

6.5.7	Synthesis of Poly[2,2,6,6-tetramethyl-1-(vinyloxy)piperidine]- <i>co</i> -ethylene]..	164
6.5.8	Reduction of Poly[2,2,6,6-tetramethyl-1-(vinyloxy)piperidine] Polymers	166
6.5.9	Grafting of Styrene.....	167
6.6	Procedures for ‘Propylene-free Synthesis of Polypropylene <i>via</i> Decarboxylation’	168
6.6.1	Synthesis of <i>N</i> -(Methacryloyloxy)phthalimide	168
6.6.2	Synthesis of Poly[<i>N</i> -(methacryloyloxy)phthalimide] Block Copolymers	169
6.6.3	Decarboxylation of Poly[<i>N</i> -(methacryloyloxy)phthalimide] Block Copolymers	172
7	Abbreviations	173
7.1	List of Abbreviations	173
8	List of Schemes, Figures, and Tables	178
8.1	List of Schemes	178
8.2	List of Figures.....	183
8.3	List of Tables.....	191
9	Danksagung	192
10	References	194
11	Appendix	211
11.1	Additional Results for ‘Ethylene-free Synthesis of Polyethylene Copolymers and Block Copolymers’	211
11.2	Additional Results for ‘Synthesizing Polyethylene from Polyacrylates: A Decarboxylation Approach’	221
11.3	Additional Results for ‘Decarboxylation of Poly[<i>N</i> -(acryloyloxy)phthalimide as a Versatile Tool for Post-Polymerization Modification’	225
11.4	Additional Results for ‘Propylene-free Synthesis of Polypropylene <i>via</i> Decarboxylation’	227

1 Introduction

Polyethylene (PE) globally ranks number one of the most produced commodity polymers and thus represents a fundamental pillar for the polymer industry and society worldwide. In Europe alone there was a demand of 14.9 million tons of PE in 2020, which accounted for the largest share of plastic production of 30.3%.¹ Besides packaging, PE is used for manufacturing of insulations, pipes, coatings or even bulletproof vests.² Due to this wide range of applications and the high demand, PE deserves fundamental consideration in modern scientific research.^{3,4} Additionally, PE is of great importance from a historical perspective. First accidentally synthesized from diazomethane in 1898 by the German chemist Hans von Pechmann,³ it took another 35 years until the industrial synthesis of PE using ethylene gas was developed in 1933 and patented in 1936 by Eric Fawcett, Reginald Gibson, and Michael Willcox Perrin.⁵ Their discovery marked the starting point for a rapid development resulting in the first major use of the material during World War II. Due to its very low loss-properties as a dielectric, it was used as insulation for cables of the newly developed radar bases in Great Britain, which had a great impact on the course of the war. The actual commercial breakthrough, however, was achieved in the 1950s with the discovery of different metal-catalysts by the German chemist Karl Ziegler allowing for the polymerization under milder conditions.^{3,6,7}

Industrially, PE is nowadays mainly produced from ethylene gas either with Ziegler-Natta-catalysts in a low-pressure reactor to yield high-density PE (HDPE) or in a high-pressure reactor to yield low-density PE (LDPE). However, besides those products, various further types of PE such as linear low-density PE (LLDPE)⁸, ultra-high-molecular weight PE (UHMWPE)⁹ or cross-linked PE (PEX)¹⁰ have been developed over the last decades to meet various demands. While HDPE is mainly used for the production of containers or fibres, LDPE and LLDPE are applied for films. UHMWPE is utilized for more specialized applications such as implants in medicine due to its high chemical resistance, while PEX is used to manufacture pipes due to its high stability, proving the versatility of PE-based products. Even though the employment of ethylene gas allows for a high throughput in industrial reactors, handling gaseous compounds on a laboratory scale requires safety installations and special equipment like an autoclave, which limits academic research within the field.

Since Monteil *et al.*¹¹ demonstrated the first ever reversible addition-fragmentation chain transfer (RAFT) polymerization of ethylene in 2014. The interest in controlled methods for the synthesis of defined PE experienced a rapid growth in the following, since the controlled

Introduction

synthesis of PE allows for the synthesis of functional PE and PE architectures which *inter alia* exhibit new properties and possible applications. Different research groups have demonstrated the implementation of well-studied reversible-deactivation radical polymerization (RDRP) techniques for the synthesis of PE, but all routes still rely on ethylene gas as a monomer.^{12–15} Besides RAFT, processes like the organometallic-mediated polymerization (as demonstrated by Detrembleur *et al.*¹⁶) have been developed, which allows for instance the synthesis of PE block copolymers under high pressures from ethylene gas and suitable polar comonomers such as vinyl acetate¹⁷ or vinyl carbonates¹⁸. However, until today the synthesis of defined PE structures, PE block copolymers or PE-based macromolecular architectures still remains a challenge, mainly due to the use of gaseous ethylene as well as its unreactive nature towards further functionalization.^{2,19–22} Furthermore, the functionalization of polyolefins in general and of PE in particular or the synthesis of functionalized PE is challenging due to a lack of reactive or polar groups.²³

Herein, developing new, straightforward, ethylene-free and controlled synthesis methods for PE should enable the access to different molecular architectures of PE that are of high interest for both industrial and academic research as the rapid development of new techniques for the synthesis of PE and different PE architectures on a laboratory scale as well as the high demand for different types of PE in industry and society proves.

2 Theoretical Background

The following chapters summarize the theoretical background of the present thesis and deal with the polymerization methods, general information about PE, post-polymerization modification and decarboxylation chemistry.

2.1 Free Radical Polymerization

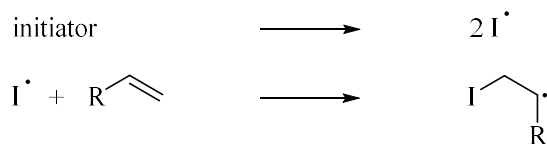
In 1832, Jöns Jacob Berzelius was the first person to call a material “polymeric”, derived from the Greek word πολύς, meaning “consisting of many parts”.²⁴ Later, in 1863, Marcelin Berthelot named the conversion reaction of styrene into a polymeric material a “polymeric transformation”, which was later referred to as polymerization.²⁵ Their work laid the foundation for the subsequent research in polymer chemistry, which resulted in a turning point, when Hermann Staudinger correctly described the formation of polymers as the addition of monomers and introduced the term macromolecule in 1929²⁶ while continuing his pioneering work on the field of polymer chemistry. Staudinger and Kohlschütter eventually described the polymerization of acrylic acid as the addition of monomers to the growing chain in a chain reaction after a previous activation of a monomer in 1935.²⁷

This fundamental work is still the basis for present research in polymer chemistry, while terms such as macromolecule or chain reaction have become indispensable in modern polymer research. With a production share of about 50%, free radical polymerization (FRP) is the industrially commonly used and simplest polymerization technique proving its success story over the last decades.²⁸ Due to its high tolerance towards monomers featuring functional groups and straightforward technical feasibility, FRP is the polymerization technique of choice for many polymeric products all over the world. Elucidation of the mechanism, which is based on three principle steps *i.e.*, initiation, chain growth (propagation), and termination is the basis for the development of other radical polymerization techniques, such as reversible-deactivation radical polymerization (RDRP). The initiation process of FRP is based on the decomposition of an initiator (**Scheme 1a**). The decomposition can be triggered by different means, mostly photochemically or thermally. Common initiators are 2,2'-azobis(2-methylpropionitrile) (AIBN) or benzoyl peroxide.²⁹ Upon decomposition, a radical is formed, which reacts with present monomers and forms a propagating chain (**Scheme 1b**). During propagation, monomer units are added onto the propagating chain end (chain growth polymerization) until termination concludes the chain growth. The two main types of termination are recombination and disproportionation, in both types two growing chains are involved, ending the chain growth as

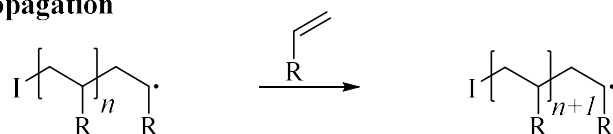
Theoretical Background

demonstrated in **Scheme 1c**.²⁹ Furthermore, also transfer of the propagating radical to *e.g.*, solvent or monomer can lead to termination of the growing chain.

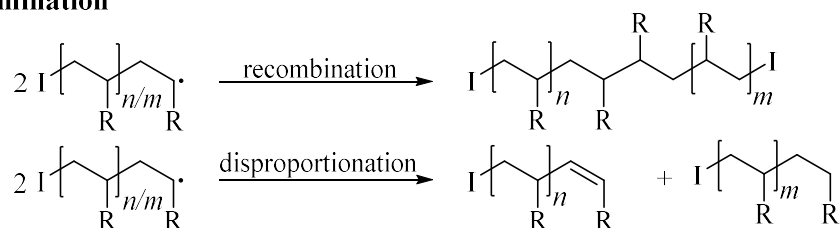
a) initiation



b) propagation



c) termination



Scheme 1: Mechanism of free radical polymerization with three main steps: initiation, propagation, and termination.

Due to the nature of the mechanism, FRP features a high reaction rate with a lifetime of the growing chain in the range of milliseconds to seconds²⁹, leading to the formation of polymers with high molar masses directly at the beginning of the polymerization *i.e.*, at low conversions. This characteristic feature makes FRP even more attractive for industrial production of polymers in comparison to step growth polymerization, in which high molar masses are obtained only at high conversions. However, FRP is not suitable for the synthesis of polymers featuring a narrow distribution ($\mathcal{D} < 1.5$) or different architectures under controlled conditions.

2.2 Reversible-Deactivation Radical Polymerization

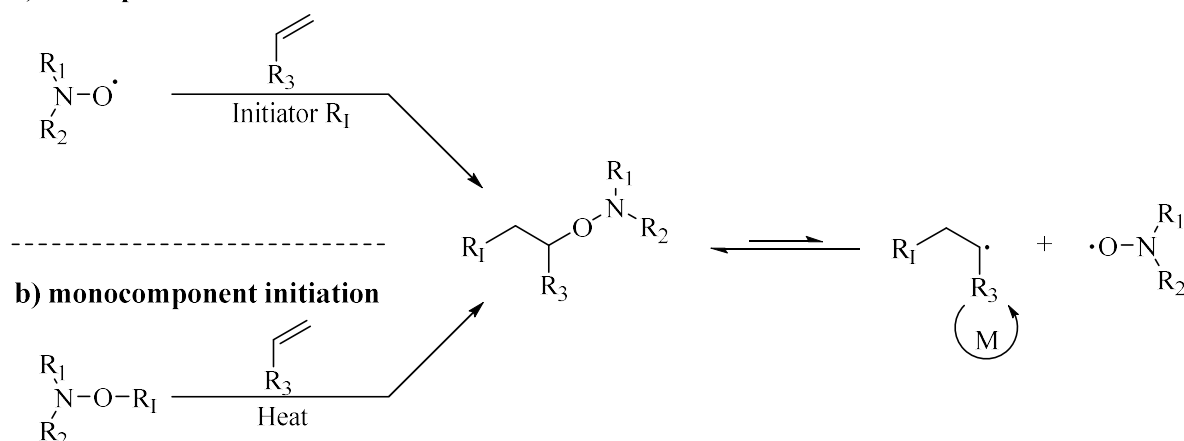
While the synthesis of polymers *via* FRP is limited to homopolymers and copolymers, controlled or living polymerization techniques enable the synthesis of more complex architectures such as block copolymers, brush polymers, or star polymers. The only type of polymerization strictly meeting a criteria of a living polymerization is the anionic polymerization (AP).²⁹ Living polymerizations are characterized by i) the absence of termination reactions, ii) an initiation process, which is magnitudes faster than propagation and iii) active chain ends when all monomer is consumed. Even though AP can be used for the polymerization of various monomers and the synthesis of different polymer architectures, the big disadvantage is the high demand on the purity of solvents, monomers and water-free atmosphere. Therefore, the development of a controlled radical polymerization method with a lower requirement on the atmosphere and purity of reactants was advanced. In 1985, researchers at the Commonwealth Scientific and Industrial Research Organization (CSIRO) developed and patented the first RDRP technique based on a nitroxide as mediator.³⁰

2.2.1 Nitroxide-Mediated Polymerization

Patented in 1985³⁰ and further developed in the following years³¹⁻³⁴, nitroxide-mediated polymerization (NMP) was the first RDRP technique published and employed for the controlled radical polymerization of various monomers. Mechanistically, NMP is based on an equilibrium between an active species, which is a propagating radical alongside a stable nitroxide, and a dormant species, which is an alkoxyamine (**Scheme 2**). The equilibrium between the active and dormant species is shifted towards the dormant species³⁵ and consequently the overall radical concentration is reduced in comparison to FRP. Additionally, the chain growth is frequently interrupted and thus, the propagation is distributed equally between all chains. Originally, as demonstrated in **Scheme 2a**, a bicomponent initiation system was developed for NMP. For those systems, common radical initiators like AIBN were employed in combination with a nitroxide. Initially, 2,2,6,6-tetramethylpiperidinyloxyl (TEMPO) and derivatives thereof were used and developed as nitroxide moieties, which are characterized by sterically hindering methyl groups resulting in the so-called persistent radical effect.³⁵ This effect ensures that TEMPO radicals are stable at room temperature and do not react with other oxygen-based radicals. However, they can reversibly react with carbon-centered radicals. The homolytic split of the labile C-O bond of the alkoxyamine requires temperatures of 120 – 135 °C.³⁶⁻⁴⁰

Theoretical Background

a) bicomponent initiation



Scheme 2: Initiation of nitroxide-mediated polymerization by **a)** a bicomponent system with an initiator or **b)** by a monocomponent system with heat and the mechanism of NMP based on the equilibrium between dormant species (left) and the active species (right) with the propagating radical.

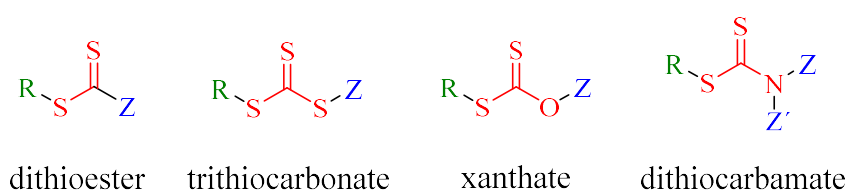
Due to the nature of TEMPO-based radicals, they cannot be used to initiate a polymerization and an additional radical initiator is thus used. Further research of Hawker *et al.*⁴¹ led to the development of a monocomponent initiation system (**Scheme 2b**). In this system an alkoxyamine with a thermolabile C-O bond is used as initiator as it is homolytically cleaved at elevated temperatures. While the carbon-centered radical initiates the polymerization, the nitroxide reversibly reacts with the propagating radical. Since the stability of alkoxyamines is rather high, elevated temperatures (up to 120 °C)³⁷⁻⁴⁰ are necessary for the polymerization. The advantage of NMP is the high versatility of the system due to the reversibility of the mechanism in terms of synthesizing polymer architectures like block copolymers. Furthermore, the high end-group fidelity (TEMPO as end group) opens the possibility for functionalization reactions.

2.2.2 Reversible Addition-Fragmentation Chain-Transfer Polymerization

Reversible addition-fragmentation chain-transfer (RAFT) polymerization was developed significantly later than NMP in 1998 by Thang *et al.*⁴² and therefore represents a rather young RDRP technique. In contrast to other RDRP techniques, RAFT is based on a degenerative mechanism and a so-called RAFT agent, which is a chain-transfer agent and structurally a thiocarbonylthio compound. The RAFT agent maintains an equilibrium between the active and the dormant species and ensures the control over the polymerization. Thus, polymers with predictable molar masses and low dispersities are accessible while the method features a high tolerance towards functional groups and various monomers. Furthermore, RAFT polymerization is characterized by a high end group fidelity and therefore allows for the

synthesis of block copolymers and other polymer architectures⁴³, as well as end group functionalization.^{44,45}

As stated before, the central component of RAFT polymerization is the RAFT agent. Different structures of RAFT agents have been developed (**Scheme 3**), while the simplest structure is the dithioester. Other structures shown in **Scheme 3** are trithiocarbonate, xanthate or dithiocarbamate. All RAFT agents are usually based on a reactive C=S double bond which features the stabilizing Z group (marked in blue) and a labile C-S bond featuring the leaving group R (marked in green).

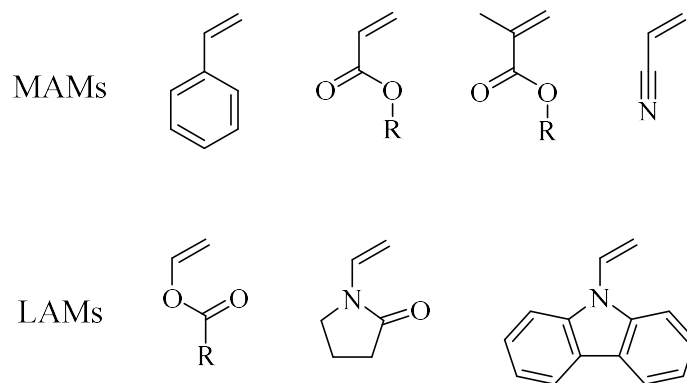


Scheme 3: General structures of four different RAFT agents: dithioester, trithiocarbonate, xanthate, and dithiocarbamate with the stabilizing group Z and leaving group R.

Appropriate selection of the stabilizing and leaving group is crucial for a successful RAFT polymerization. The stabilizing Z group influences the reactivity of the C=S double bond resulting in a balance between the reactivity of the C=S bond towards radicals and the stability of the formed intermediate radical. Therefore, the correct choice over the structure of the stabilizing group is highly dependent on the nature and consequently the reactivity of the monomer. Typical stabilizing groups are phenyl or alkyl groups. In contrast, the leaving group R is required to fragment on the one hand and be able to react with a monomer and initiate a new propagating polymer chain on the other hand. Typical R groups feature isobutylnitril or benzyl groups.

As stated before, the evaluation of suitable R and Z groups for a RAFT agent strongly depends on the reactivity of the monomer. Typically, monomers are divided into two groups depending on the reactivity of the vinyl group: more activated monomers (MAM) and less activated monomers (LAM). MAMs are typically characterized by a good stabilization of the radical, *e.g.*, by phenyl groups (styrene) or esters (acrylates), as shown in **Scheme 4**. In contrast, LAMs feature *e.g.*, heteroatoms next to the vinyl group (**Scheme 4**) and are less stabilized.⁴⁶

Theoretical Background



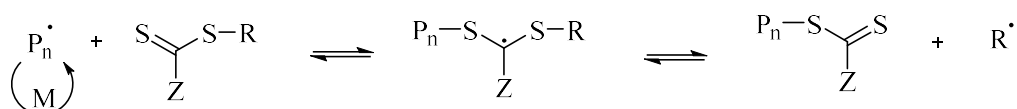
Scheme 4: Examples for MAMs: styrene, acrylates, methacrylates, acrylonitrile, and LAMs: vinylacetates, *N*-vinylpyrrolidone, and *N*-vinylcarbazol.⁴⁶

The high versatility of RAFT polymerization towards different monomeric systems makes it one of the most popular RDRP techniques. Mechanistically, RAFT polymerization is initiated by a common radical initiator like AIBN (**Scheme 5a**).

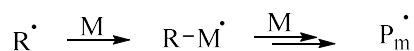
a) initiation



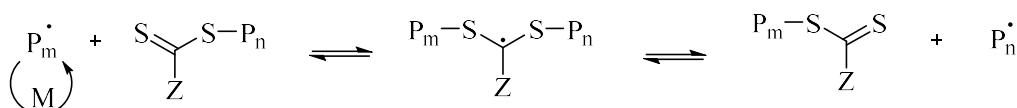
b) reversible chain transfer (pre-equilibrium)



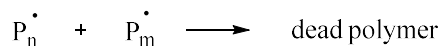
c) reinitiation



d) chain equilibrium (main-equilibrium)



e) termination



Scheme 5: Mechanism of RAFT polymerization including the **a)** initiation, **b)** pre-equilibrium, **c)** reinitiation of a new chain, **d)** main-equilibrium, and **e)** termination.⁴⁶

The radical formed after fragmentation of the initiator reacts with a monomer resulting in a propagating chain. In the next step, the propagating chain reversibly reacts with the RAFT agent forming a stabilized intermediate which can release the leaving group ($R\cdot$) in the pre-equilibrium as shown in **Scheme 5b**. In the third step, the leaving group initiates a new propagating chain upon reacting with a monomer. The propagating radical then further reacts with a RAFT agent to establish the main-equilibrium in which the radical is transferred between the propagating chains. In the last step, the propagating chain is terminated by either recombination or disproportionation similar to FRP (**Scheme 5e**).⁴⁶

Due to the process based on a degenerative mechanism, RAFT features a higher concentration of radicals than other RDRP techniques such as NMP which rely on the reduction of the radical concentration. Therefore, RAFT has the advantage of a higher reaction rate in comparison to other RDRP techniques additional to the already mentioned advantages like tolerance towards a wide range of monomers and functional groups.

Theoretical Background

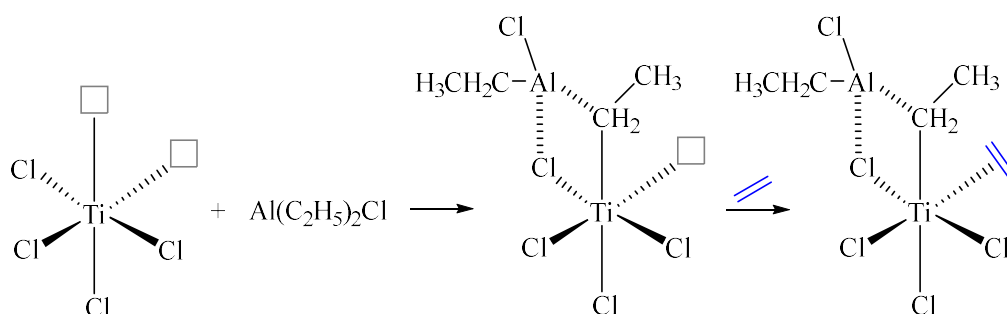
2.3 Polyethylene

PE is the most used commodity polymer worldwide and the simplest polyolefin.^{1,47} In general, polyolefins are a type of polymeric material based on the chemical formula $(\text{CH}_2\text{CHR})_n$, with n displaying the number of monomeric repeating units of the polymer chain. As the simplest of all polyolefins, PE features the formula $(\text{CH}_2\text{CH}_2)_n$, ideally representing a linear polymer chain consisting of CH_2 units. Featuring good processability and required physical properties, PE is the material of choice for many applications in industry and consumer goods. Historically, PE was first discovered by the German chemist Hans von Pechmann in 1898.³ Originally, he was investigating the synthesis and properties of diazomethane when he accidentally discovered PE during distillation of diazomethane as an instable methylation agent, which slowly degrades even at room temperature and can form PE during degradation. His colleagues Eugen Bamberger and Friedrich Tschirner further analyzed the white, waxy residue and postulated that the structure consists of CH_2 repeating units.⁴⁸ Therefore, they called it polymethylene⁴⁸, but there was not yet an application for the material, especially due to the synthesis from toxic and instable diazomethane. 35 years later in 1933 and again by accident, Eric Fawcett and Reginald Gibson discovered the first synthesis of PE from ethylene gas and benzaldehyde under high pressure.⁵ However, it was not until 1935 that Michael Willcox Perrin developed and patented a reproducible method for synthesizing PE at 500 – 1500 bar and 100 – 400 °C.⁵ Since PE features very low loss-properties as a dielectric, it was used as an insulation for cables of the newly developed radar bases in Great Britain during World War II.⁴⁹ In 1951, the American chemists Robert Banks and Paul Hogan discovered the first catalyst for the synthesis of PE under milder conditions based on chromium trioxide at the Phillips Petroleum company.⁵⁰ Yet, the major commercial breakthrough was in 1953, when the German chemist Karl Ziegler developed a titanium-based catalyst for the polymerization of ethylene at lower temperature and pressure at the Max Planck Institute for Coal Research.⁶ The development of a catalytic system allowed for the synthesis of PE while suppressing uncontrolled branching, leading to PE with a higher crystallinity and new properties. However, a problem of those early catalysts were metal impurities in the polymer after production. Together with the Italian chemist Giulio Natta, Karl Ziegler developed the Ziegler-Natta metalorganic catalysts mainly based on metals like titanium, aluminium, or zirconium.^{51,52} In **Scheme 6** the mechanism of the Ziegler-Natta process with the exemplary catalytic system titanium(IV) chloride and diethylaluminiumchloride is shown. In the first step, the active complex is formed from TiCl_4 and the metalorganic compound. Subsequently, the first ethylene monomer unit (blue) adds to the free coordination position of the complex (grey box, **Scheme 6a**). Hereby, the π -electrons

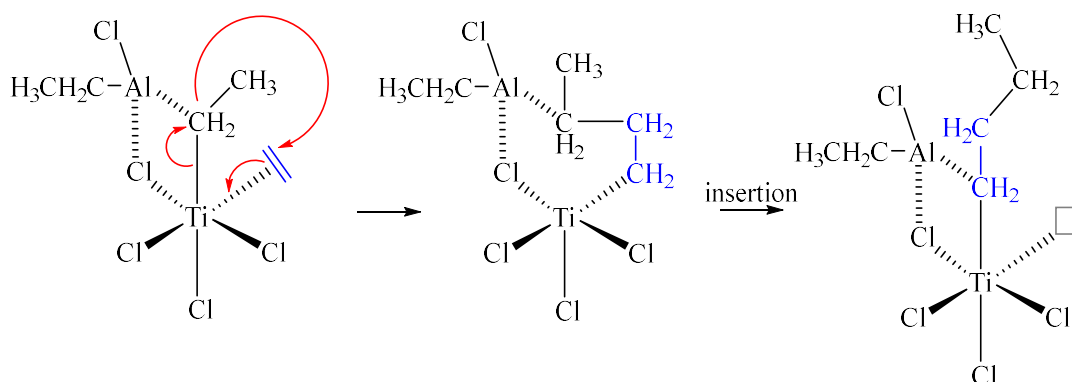
Theoretical Background

of ethylene complex the titanium central atom. In the second step, electrons are rearranged in the complex (red arrows) and a new carbon-carbon bond is formed. The former ethylene unit (blue) is inserted into the carbon-titanium bond (**Scheme 6b**). Thus, the starting structure of the Ti-Al complex with a free coordination position is re-formed (grey box). Another ethylene unit can add to this free coordination position and the process starts from the beginning.

a) formation of Ti-Al complex and addition of ethylene



b) rearrangement of electrons and insertion of ethylene



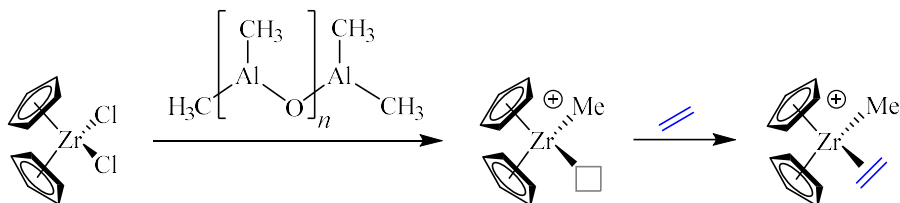
Scheme 6: Mechanism of the Ziegler-Natta process with the exemplary catalytic system TiCl_4 with diethylaluminiumchloride. **a)** Formation of the titanium-aluminium complex and the addition of the first ethylene unit (blue) to the free coordination position (grey box). **b)** Rearrangement of the electrons in the complex after addition of ethylene and insertion of ethylene into the titanium-carbon bond for the formation of a polymer chain.

Giulio Natta further transferred the catalytic system to the synthesis of polypropylene (PP), allowing for the first synthesis of stereotactic PP. While nowadays the major share of PE production is based on Phillips and Ziegler-Natta catalysts, in the 1980s a new type of catalytic system, the Kaminsky catalysts, were developed.⁵³ Kaminsky catalysts are based on

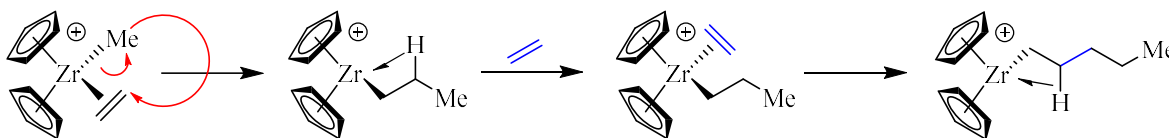
Theoretical Background

metallocenes of titanium or zirconium and are of academic as well as of industrial importance since they allow for the polymerization of α -olefins with high stereoselectivity and a narrower distribution than classical Ziegler-Natta catalysts. In **Scheme 7** the mechanism of the metallocene-catalyzed process and an idealized Kaminsky catalyst are presented.

a) formation of the active catalyst from $ZrCp_2Cl_2$ and MAO and addition of first ethylene unit



b) insertion of ethylene units and growing of the polymer chain

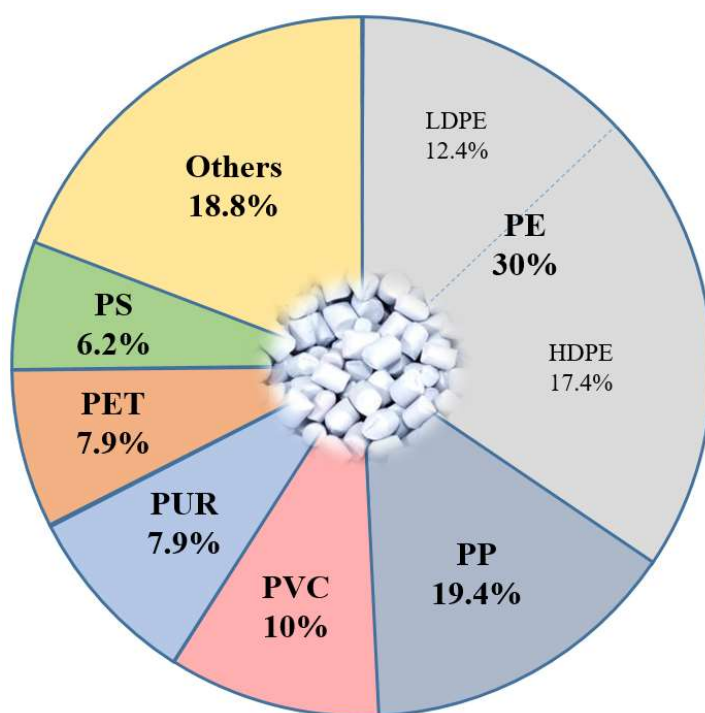


Scheme 7: Mechanism of the synthesis of PE by a metallocene-catalyzed process with a zirconium-based Kaminsky catalyst. **a)** The formation of the active metallocenium ion $ZrCp_2CH_3^+$ from the zirconium-based metallocene catalyst and methylaluminoxane (MAO) and the first addition of a ethylene unit (blue) to the free coordination position. **b)** Insertion of the ethylene unit into the zirconium-carbon bond opening a new coordination position.

In the first step, the zirconium-based metallocene catalyst reacts with the cocatalyst, mostly methylaluminoxane (MAO), to form the active metallocenium ion $ZrCp_2CH_3^+$ and ethylene is added to the free coordination position (**Scheme 7a**). In the second step, the monomer is inserted into the zirconium-carbon bond, opening a new coordination position, which is coordinated by another ethylene unit (**Scheme 7b**). Repetition of this process leads to the formation of a growing chain. The development of those catalytic systems allows for the controlled, industrial synthesis of high amounts of polymers based on α -olefins, from which PE has the highest production share.

As already stated before, PE is the worldwide most produced polymer, with a production share of about 30% in Europe in 2021, followed by another polyolefin, PP, with about 20% production share, resulting in a combined production volume of 50% (**Scheme 8**).^{1,54} This demonstrates the enormous importance of PE and PP for modern society and stresses the

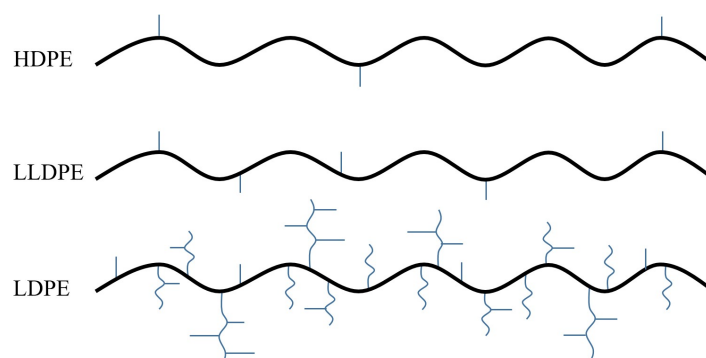
necessity of evaluating alternative synthesis methods and new PE architectures. Further important polymers are poly(vinyl chloride) (PVC) with a production share of 10%, which is used for pipes, insulations or floorings, polyurethanes (PUR) with a production share of 7.9% mainly utilized for foams, poly(ethylene terephthalate) (PET) and polystyrene (PS) (**Scheme 8**).^{1,54}



Scheme 8: Production share of different plastics in Europe in 2021.¹ PE is subdivided into low-density PE (LDPE) and high-density PE (HDPE). PP = polypropylene, PVC = poly(vinyl chloride), PUR = polyurethane, PET = poly(ethylene terephthalate), and PS = polystyrene.

As indicated in **Scheme 8**, commodity PE can be divided in different types depending on its molecular structure, resulting in differences of the mechanical properties such as the crystallinity. The two main types are low-density PE (LDPE) and high-density PE (HDPE). LDPE is produced in a high pressure reactor (1500 - 3000 bar) and at high temperatures up to 200 °C by FRP leading to branching of the polymer chain (**Scheme 9**). Another important type of PE is linear-low density PE (LLDPE), which is analogous to HDPE produced by a Ziegler-Natta polymerization. However, the addition of small amounts of α -olefins like hexene or butene results in the formation of controlled branches as shown in **Scheme 9**.

Theoretical Background



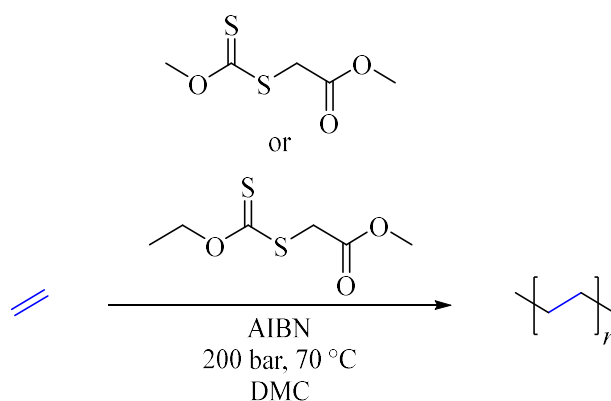
Scheme 9: Presentation of the molecular structure of different types of PE: rarely branched high-density PE (HDPE), slightly branched linear low-density PE (LLDPE) and highly branched low-density PE (LDPE).

Due to its controlled branching, LLDPE features unique rheological properties and is mostly used for packaging as films or sheets.⁸ Furthermore, other types of PE are ultra-high-molecular-weight PE (UHMWPE) which features molar masses of $3.5 - 7.0 \cdot 10^6 \text{ g mol}^{-1}$ and is characterized by a very high toughness and chemical resistance.⁹ Therefore, it is for example used for moving parts in machines or in medicine as implants.⁹ Finally, cross-linked PE (PEX) is produced by crosslinking LDPE, HDPE, or LLDPE by irradiation with an electron beam⁵⁵ or with peroxides^{10,56}. Due to its high impact strength even at low temperatures and high thermal stability, PEX is widely used as tubing to replace copper pipes. The various types of PE demonstrate the impact of the production procedure on the materials properties *i.e.*, glass transition temperature (T_g), melting point (T_m), or ductility.

PE is usually a thermoplastic polymer, which means it becomes flexible and moldable in a specific temperature range. The thermoplastic properties result from the linear structure of PE. Due to its structural composition consisting of CH_2 units and rare branching, PE features both crystalline and amorphous areas resulting in a T_g at around $-100 \text{ }^\circ\text{C}$ and a melting point in the region of $T_m = 90 - 130 \text{ }^\circ\text{C}$.² In order to understand the structure-property relationship in detail, the controlled laboratory synthesis of polymer architectures as well as the examination of the physical properties of the materials are necessary.

On a laboratory scale, PE is synthesized by different methods. Classically, PE is synthesized with ethylene as monomer under high pressure and elevated temperatures in an autoclave. To introduce control over the polymerization, various approaches have been developed in the last years. The first combination of RDRP techniques with the polymerization of ethylene was demonstrated by Monteil *et al.*¹¹ in 2014. They synthesized PE by homopolymerization of ethylene *via* RAFT polymerization¹¹ with two different xanthates at 200 bar and $70 \text{ }^\circ\text{C}$ in

dimethyl carbonate (DMC) as shown in **Scheme 10**. Noteworthy, they proved the controlled nature of the polymerization by chain extension of the polymer, observed little branching and reached molar masses (number average molar mass = M_n) between $M_n = 220 - 2000 \text{ g mol}^{-1}$ and dispersities between $D = 1.4 - 2.3$.

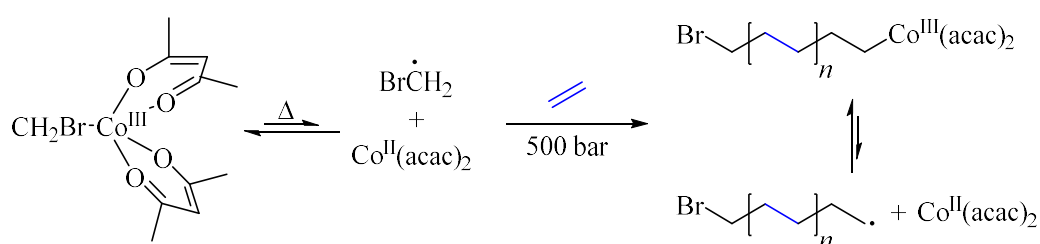


Scheme 10: Polymerization of ethylene with two different xanthates as demonstrated by Monteil *et al.*¹¹

Inspired by the work of Monteil *et al.*, a rapidly growing number of studies on the investigation of controlled synthesis methods for PE was published and the implementation of well-studied RDRP techniques was established, while still relying on ethylene gas as monomer.¹²⁻¹⁵ Besides RDRP, also other methods were invented, like the cobalt-mediated radical polymerization (CMRP) demonstrated by Detrembleur *et al.* in 2019.¹⁶ CMRP is a organometallic-mediated polymerization and allows for the synthesis of PE block copolymers under high pressures from ethylene gas and suitable polar comonomers such as vinyl acetate¹⁷ or carbonates¹⁸. In the first step of the CMRP, the polymerization is initiated by bromomethyl-cobalt(bisacetylacetonate) ($\text{BrCH}_2\text{-Co}(\text{acac})_2$) (**Scheme 11**), featuring a low bond dissociation energy which can be cleaved upon heating resulting in a $\text{BrCH}_2\cdot$ radical and a reduced $\text{Co}^{\text{II}}(\text{acac})_2$ catalyst. The $\text{BrCH}_2\cdot$ radical initiates the polymerization of ethylene at $80 \text{ }^\circ\text{C}$ and an ethylene pressure of 500 bar. During the polymerization an equilibrium between a dormant (Co^{III}) and an active species (Co^{II}) with the propagating radical is formed. The reaction was terminated by the addition of TEMPO, resulting in a radical coupling and serving as an additional analytic element as end group. Little branching was observed by Detrembleur *et al.* and kinetic analyses revealed a drastic impact of the choice of solvent (dichloromethane (DCM), DMC, or 1,2,4-trichlorobenzene (1,2,4-TCB)). SEC analyses revealed that all polymers obtained featured a

Theoretical Background

molar mass $M_n > 2400 \text{ g mol}^{-1}$, but the polymers obtained in DCM and DMC featured a bimodal distribution. The authors suggested coupling reactions as a reason for this bimodal distribution. $^1\text{H NMR}$ spectroscopy revealed in the case of DCM as solvent 49% and in the case of 1,2,4-TCB 19% of chains were initiated by solvent radicals, while only 5% of chains were initiated by solvent radicals in DMC. Even improving the solubility of the PE chain by using an oligo-vinylacetate initiating radical instead of $\text{BrCH}_2\cdot$ resulted in a bimodal distribution. Therefore, and even though a bimodal distribution was obtained by high-temperature SEC analysis, DMC was chosen as solvent for further polymerizations.

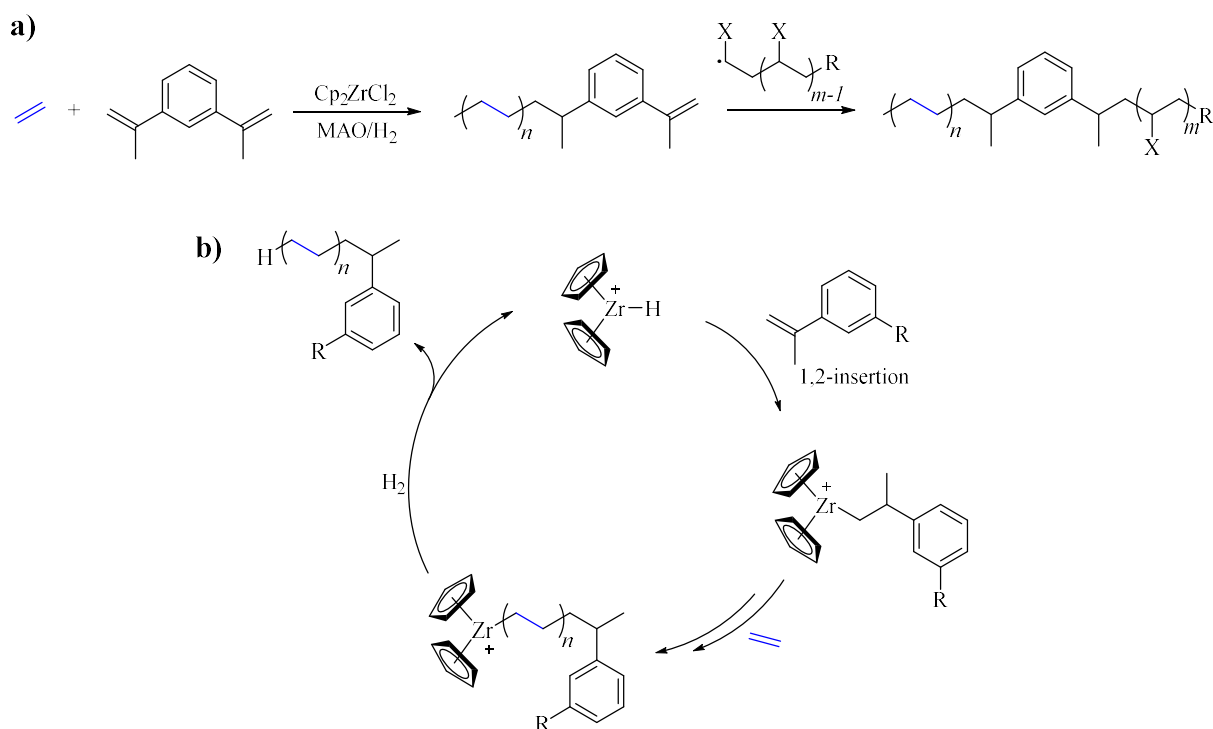


Scheme 11: Mechanism of the cobalt-mediated radical polymerization of ethylene demonstrated by Detrembleur *et al.*¹⁶

Although no full control could be obtained over the homopolymerization, a block copolymerization with vinyl acetate (VAc) was performed. For this purpose, a macroinitiator (PVAc-Co(acac)₂) was used, followed by chain extension with ethylene. The product of the block copolymerization was analyzed by SEC in THF and a shift towards higher molar masses indicated the successful block copolymerization, while an intensive shoulder revealed the presence of coupling products. The detailed analysis of the CMRP of ethylene demonstrates the complex nature of controlled synthesis procedures of PE. Nevertheless, the examination of alternative methods to synthesize PE is by far not at an end. In 2020, the group of D'Agosto^{57,58} introduced the copolymerization of ethylene with vinyl acetate by iodine-transfer polymerization (ITP). Advances in the synthesis of olefin block copolymers have also been achieved *via* chain shuttling polymerization.⁵⁹ Recent developments additionally demonstrated the synthesis of degradable PE-based copolymers.⁶⁰ The synthesis of polyolefin-based block copolymers with styrenes, acrylates, or methacrylates with metallocene-based catalysts was demonstrated by Scott *et al.* in 2018.⁶¹ The authors used a zirconium-based Kaminsky catalyst (Cp_2ZrCl_2) in combination with MAO as cocatalyst and hydrogen to obtain the active catalytic centre (**Scheme 12b**). The homopolymerization of ethylene by a so-called catalytic hydride insertion mechanism was originally published by Chung *et al.*⁶², while Scott *et al.*⁶¹ found that

Theoretical Background

the polymerization of ethylene in the presence of 1,3-diisopropenylbenzene (DIB) allows for the control of the end group. This end group was utilized for the synthesis of block copolymers (Scheme 12a).



Scheme 12: a) Polymerization of ethylene using 1,3-diisopropenylbenzene (DIB), Cp_2ZrCl_2 as catalyst, methylaluminoxane (MAO) as cocatalyst and hydrogen with the following block formation as demonstrated by Scott *et al.*⁶¹ b) Simplified mechanism of the polymerization of ethylene with DIB and Cp_2ZrCl_2 .⁶¹

The mechanism of the homopolymerization of ethylene starts with the 1,2-insertion of DIB to the active catalyst (Cp_2ZrH^+), followed by the insertion of ethylene (blue) into the zirconium-carbon bond and the formation of a PE chain. The propagation is terminated by the addition of hydrogen, resulting in PE with a hydrogen end group and an end group resulting from DIB. For the synthesis of block copolymers, the polymerization of a monomer such as styrene, *n*-butyl acrylate or methyl methacrylate is initiated by benzyl peroxide in the presence of the as-described PE. The resulting material consists of the block copolymer and free homopolymers of the corresponding monomer which was removed by Soxhlet extraction.

Summarized, the functionalization of polyolefins in general and PE in particular is challenging due to a lack of functionalities.²³ Nevertheless, as stated before, all those methods have in common that they still rely on ethylene gas as monomer for the polymerization under pressure.

Theoretical Background

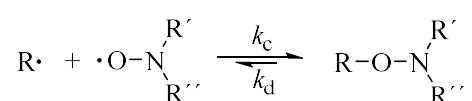
An alternative to the employment of ethylene gas was demonstrated by Shea *et al.*^{63,64} using polyhomologation as a living C1 polymerization with organoboranes. In 2017, Chapman *et al.*⁶⁵ demonstrated the indirect synthesis of polyolefins from an activated ester using dialkyl zinc reagents to introduce alkyl groups to the polymer resulting in polyolefins except polyethylene. In 2022, Sumerlin and coworkers⁶⁶ were the second group after the pioneering work of the present thesis to publish a synthesis method for PE by decarboxylation of a phthalimide-based polymer. In contrast to the studies of the present thesis, Sumerlin *et al.* only focused on copolymers as simple architectures and used a different catalytic system.⁶⁶

2.4 Post-Polymerization Modification

Functional polymers are of fundamental scientific and industrial interest in modern society, requiring high efforts to develop new synthesis procedures and materials. In general, the synthesis of functional polymers can be achieved by two different methods: either by the direct polymerization of a functional monomer or by the chemical modification of the polymer after polymerization, so-called post-polymerization modification (PPM).⁶⁷ While the synthesis of functional polymers *via* PPM requires quantitative reactions, since non-functionalized units in the polymer chain cannot be removed by purification, very much in contrast to organic chemistry, the first method can be challenging due to intolerances of reactants with functional groups or the functionalized monomers are simply not accessible.⁶⁸ Furthermore, PPM can be used to circumvent further issues of directly polymerizing specific monomers, such as ethylene which is gaseous and a safety hazard. Thus, PPM experiences a growing interest in the last decades and opens the pathway to new polymeric materials and architectures.

The first PPM was described in 1839 by Goodyear and Hancock when they observed the vulcanization of rubber with sulfur.^{69,70} In the following years more and more PPM reactions such as the nitration of cellulose for the synthesis of nitrocellulose in 1846 by Schönbein and Böttger were discovered.⁷¹ Since then, the development of new methods for PPM grew rapidly representing a large field of modern polymer chemistry. Especially the development of RDRP techniques resulted in a rapid growth of modification methods, since the straightforward accessibility of various polymer architectures in combination with new functionalities introduced by PPM allowed for the synthesis of materials with new properties. To reach the full potential of the combination of RDRP techniques with PPM methods, so-called click-reactions⁷²⁻⁷⁴ such as the copper-catalyzed azide-alkyne cycloaddition⁷⁵ (CuAAC) or thiol-ene⁷⁶ reactions are essential.

Besides those well-known reactions, another interesting PPM method is nitroxide radical coupling (NRC). NRC describes the reaction between a carbon-centered macroradical and a nitroxide (**Scheme 13**), which in general is highly efficient and orthogonal.³⁵



Scheme 13: Simplified mechanism of the NRC between a carbon-centered radical and a nitroxide.³⁵

Theoretical Background

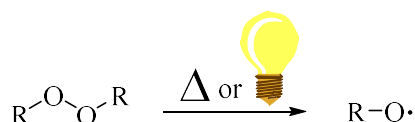
In principle, NRC is the basis for NMP examined in detail in **Chapter 2.2.1**. Here, a stabilized, nitroxide-based radical such as TEMPO is used to reversibly react with the carbon-centered radical of the propagating chain. As explained before, the so-formed C-O bond is thermolabile and can be homolytically split upon heating. Depending on the nature of the alkoxyamine, temperatures in the range of 120 – 135 °C are necessary to split the bond and obtain the nitroxide, which can undergo further coupling reactions.^{37–40} This process is reversible, resulting in the formation of an equilibrium between the active nitroxide and carbon-centered radical (**Scheme 13**, left) and the alkoxyamine (**Scheme 13**, right). The equilibrium is described by the rate constants k_c and k_d , in which k_c describes the rate of the NRC and k_d is the rate of dissociation. The ratio of the constants gives the equilibrium constant K as shown in the following equation.

$$K = \frac{k_c}{k_d} \quad \text{I}$$

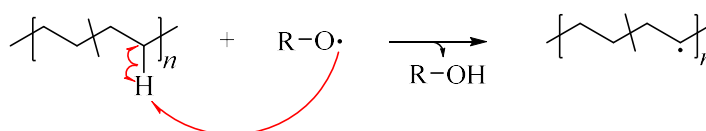
The equilibrium constant K gives information about the predominant species within the equilibrium. Generally, the formation of the stable alkoxyamine is favored leading to a value of K above 1.⁷⁷ For successful NRC or NMP, values between $K = 10^7$ to 10^{11} L mol⁻¹ are necessary.^{40,78} Thereby, the values of the rate constants are typically in the range of $k_c = 10^7 - 10^9$ mol L⁻¹ s⁻¹ for TEMPO moieties which is near the diffusion limit and $k_d = 5 \cdot 10^{-2}$ s⁻¹.⁷⁹ The values demonstrate the stability of the alkoxyamine and the high reaction rate of the NRC.

For different types of polymers, various methods for the formation of the carbon-centered radical have been developed.^{36,80} In most cases polyolefins like PE are used for NRC and the carbon-centered radical is formed with peroxides.⁸⁰ Nevertheless, NRC was successfully performed on polymers like poly(lactide acid),^{81,82} poly(butyl succinate)⁸¹ or unsaturated polyolefins^{83–87}. In the case of NRC on polyolefins such as PE, the polymer, the peroxide, and additives are added to a reaction vessel and the peroxide is decomposed by thermal or photochemical means as shown in **Scheme 14a**.

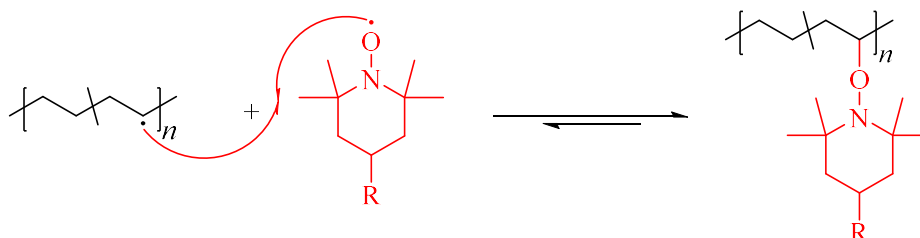
a) decomposition of the peroxide



b) peroxide-induced radical formation at the backbone



c) NRC of TEMPO with the carbon-centered backbone radical



Scheme 14: Different steps of the mechanism of NRC on a PE with a TEMPO derivative (red) as the nitroxide: **a)** The decomposition of the peroxide by heat or under irradiation of light, **b)** the peroxide-induced radical formation at the backbone under H-abstraction and **c)** NRC of TEMPO with the carbon-centered radical at the backbone.

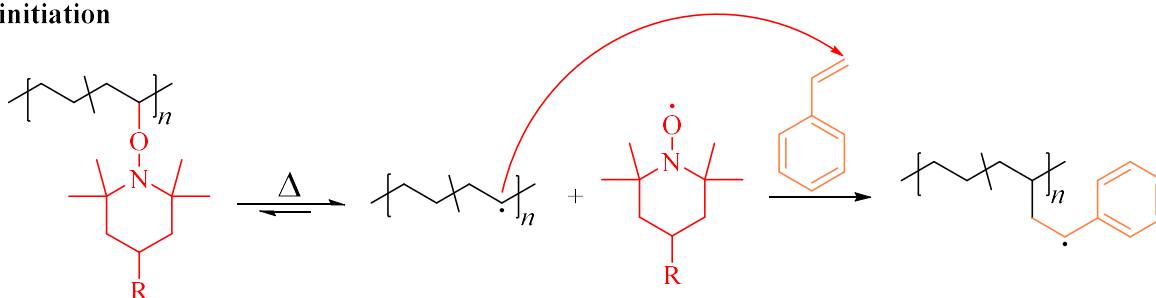
After the decomposition of the peroxide, an oxygen-based radical ($\text{R-O}\cdot$) is formed. Due to the persistent radical effect, the nitroxide radical cannot terminate with the peroxide radical, but reacts with the polyolefin chain. H-abstraction from the backbone by the peroxide leads to the formation of a carbon-centered radical at the polymer backbone and the corresponding alcohol (**Scheme 14b**). In contrast to the peroxide radical, the carbon-centered radical can undergo NRC with the nitroxide and forms a stable alkoxyamine (**Scheme 14c**).

NRC is frequently used in peroxide-crosslinking of polyolefins (PEX) to obtain a higher control over the crosslinking.⁸⁰ Further, another application is grafting of polymer side chains from the backbone by NMP with the TEMPO-functionalized polymers.³⁶ As described in **Chapter 2.2.1**, NMP can be initiated by either a bicomponent system or a monocomponent system from a stable alkoxyamine. In the case of grafting a side chain, the polymerization is initiated by a monocomponent system (alkoxyamine) upon heating as demonstrated on a TEMPO-functionalized PE in **Scheme 15a**. Temperatures > 120 °C result in the homolytical split of the C-O bond of the alkoxyamine (nitroxide and the polymer backbone) under the formation of the

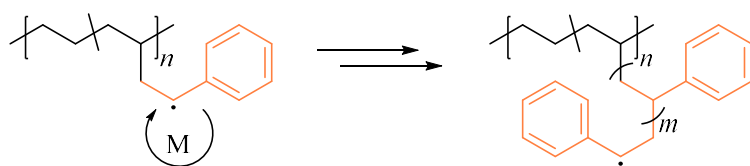
Theoretical Background

nitroxide and the carbon-centered radical at the polymer backbone. The carbon-centered radical initiates the polymerization by reacting with a monomer (exemplarily demonstrated with styrene (orange) in **Scheme 15a**). In the propagating step, more monomeric units are added to the growing side chain (**Scheme 15b**), while the polymerization is controlled by the reversible formation of the dormant alkoxyamine (**Scheme 15c**). Using NMP as a controlled radical polymerization method allows for the controlled grafting of side chains, defining the chain lengths and prevents crosslinking of the material.^{35,36}

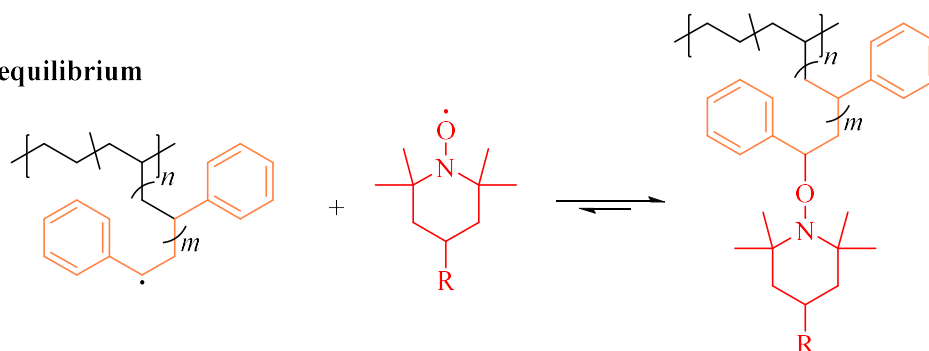
a) initiation



b) propagation



c) equilibrium



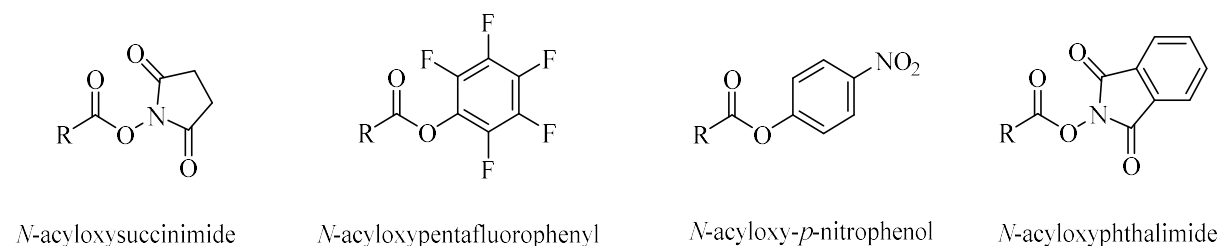
Scheme 15: The three main steps of the mechanism of grafting side chains from a TEMPO-functionalized PE by NMP with **a**) the initiation upon heating to form the nitroxide and carbon-centered radical which initiates the polymerization by reacting with the monomer, **b**) the propagation step, in which monomeric units are added to the side chain and **c**) the equilibrium between the propagating chain and the nitroxide with the stable alkoxyamine.

While the functionalization of polyolefins requires harsh methods like peroxide-induced radical formation, polymers with functional groups allow for PPM with higher selectivity and under

milder conditions. In this regard, so-called activated esters in particular allow for straightforward modification of polymers.

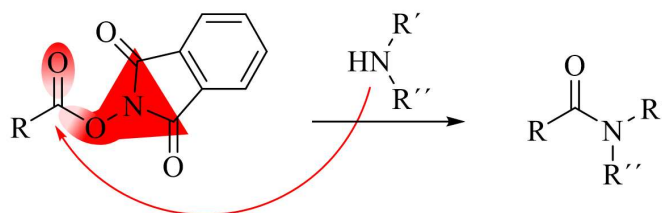
2.4.1 Activated Esters

With their work on ‘reactive’ esters, Batz *et al.*⁸⁸ and Ferruti *et al.*⁸⁹ provided the basis for the application of highly versatile and reactive functional groups, which are still relevant in modern research.^{90,91} Activated or active esters are characterized by the activation of the carbonyl functionality with an electron-withdrawing groups. For the activation, different kind of electron-withdrawing groups have been employed in recent years as shown in **Scheme 16**. Common examples are *N*-hydroxysuccinimide (NHS), pentafluorophenyl (PFP) or *N*-hydroxyphthalimide (NHP) esters while *p*-nitrophenol esters are historically more important.



Scheme 16: Different active esters commonly used in organic synthesis.

Generally, the activation of the ester group makes the ester particularly susceptible to nucleophilic reactions such as hydrolysis or amidation. While they can undergo the same reactions as normal esters, the reactions proceed at a significantly higher reaction rate and with less side reactions. The most prominent example for the application of activated esters is the amidation with an amine to obtain functional amides (**Scheme 17**).



Scheme 17: Amidation of an activated phthalimide-based ester with the reduced electron-density (marked in red) of the carbonyl carbon due to the electron-withdrawing group.

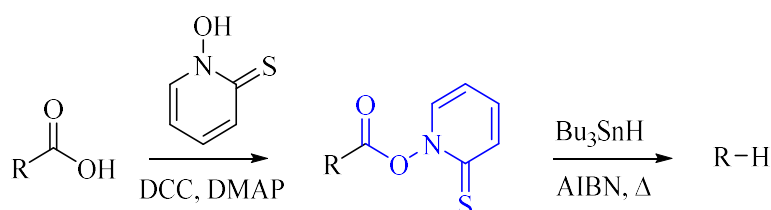
Theoretical Background

By reducing the electron density at the carbon of the carbonyl of the ester, the activation energy is reduced and the free electron pair of the nitrogen can attack faster. As a result, the reaction proceeds at an enhanced rate and in higher conversions. Another advantage of activated esters is the easy synthetic accessibility. Commonly, activated esters like *N*-acyloxysuccinimide are synthesized by Steglich esterification *via* *N,N'*-dicyclohexylcarbodiimide (DCC)-mediated coupling.⁹² The Steglich esterification of the corresponding alcohols with acrylic acid results in the activated ester monomer. Those activated ester monomers, such as *N*-(acryloyloxy)succinimide (NAS) which are crystalline products can be synthesized in high yields and polymerized either by FRP⁹³ or different RDRP techniques^{94–96}. Noteworthy, PFPA is an exception in this regard since it is a liquid and mostly synthesized from acryloyl chloride and pentafluorophenol.⁹⁷

Besides the already mentioned activated esters, *N*-acyloxyphthalimide bearing a phthalimide structural motif deserves particular attention and has become increasingly popular in recent years.⁹⁸ This is not only due to its properties as an activated ester and the proneness towards nucleophiles, but mainly due to the possibilities of performing cross-coupling reactions. Depending on the nature of the carbon bond formed, the cross-coupling results in three different categories: i) $C(sp^3)-C(sp^3)$, ii) $C(sp^3)-C(sp^2)$, or iii) $C(sp^3)-C(sp)$.⁹⁹ The present thesis deals with $C(sp^3)-C(sp^3)$ cross-coupling by decarboxylation and decarboxylative reduction of the phthalimide structural motif as described in more detail in the following chapter.

2.5 Decarboxylation Chemistry

Decarboxylation describes the removal of a carboxyl group from a molecule and is one of the oldest known organic reactions. Not only does it feature a high importance for research, but it also plays an important role in biology, since decarboxylation reactions are an essential part of the metabolism in organisms.^{100–103} This is furthermore underlined by the large number of decarboxylase enzymes, which can be found in the human metabolism.¹⁰⁴ Besides biology, decarboxylations play an important role in chemistry as can be seen by various name reactions based on decarboxylations, such as the Kolbe electrolysis¹⁰⁵, the Kochi reaction¹⁰⁶, or the Hunsdiecker reaction¹⁰⁷. All the mentioned reactions are in principle decarboxylations due to the removal of a carboxylic acid group under the extrusion of CO₂, but originally a decarboxylation described the replacement of a carboxylic acid functionality with a hydrogen atom (reductive decarboxylation), which is not the case for the mentioned reactions. Another important and well-known decarboxylation reaction is the so-called Barton decarboxylation.¹⁰⁸ This reaction originates from Sir Derek Barton's work in cooperation with Schering Plough in the 1970s¹⁰⁹, leading to the invention of the Barton-McCombie deoxygenation, which allows for the selective replacement of a hydroxy group with a hydrogen atom as a radical substitution.¹¹⁰ The pioneering use of a carbonothioyl played an important role in the development of the Barton decarboxylation and the invention of the Barton esters in 1983 as shown in **Scheme 18**.¹⁰⁸

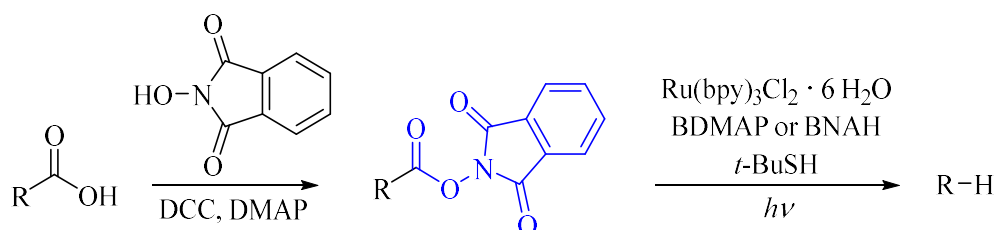


Scheme 18: Synthesis of the Barton ester (marked in blue) *via* Steglich esterification with *N,N'*-dicyclohexylcarbodiimide (DCC) and 4-dimethylaminopyridine (DMAP) followed by the Barton decarboxylation with tributyltin hydride and AIBN upon heating.¹⁰⁸

The Barton decarboxylation is an example for a reductive decarboxylation in which the carboxylic acid functionality is removed and replaced by hydrogen. In contrast, many modern decarboxylation methods aim for the replacement of the carboxylic acid functionality with other compounds like Michael acceptors.

Theoretical Background

In 1988, Okada *et al.*¹¹¹ developed an alternative decarboxylation method based on the phthalimide structural motif introduced in **Chapter 2.4.1**. They developed a new photocatalytic system employing tris(bipyridine)ruthenium(II) chloride hexahydrate ($\text{Ru}(\text{bpy})_3\text{Cl}_2 \cdot 6 \text{H}_2\text{O}$) for the decarboxylation of phthalimide-esters with 1,6-bis(dimethylamino)pyrene (BDMAP) or 1-benzyl-1,4-dihyronicotinamide (BNAH) as reductant and *tert*-butylthiol (*t*-BuSH) as hydrogen source as exemplarily shown in **Scheme 19**.^{111,112} The high suitability of the catalyst $\text{Ru}(\text{bpy})_3\text{Cl}_2 \cdot 6 \text{H}_2\text{O}$ for the decarboxylation of phthalimide activated esters is based on the similar redox potential of both species (Ru : $E_1^{II}/_2 = 1.33 \text{ V vs. SCE}$; *N*-acyloxyphthalimide: $E_{1/2} = -1.26 \text{ to } -1.37 \text{ V vs. SCE}$).¹¹³

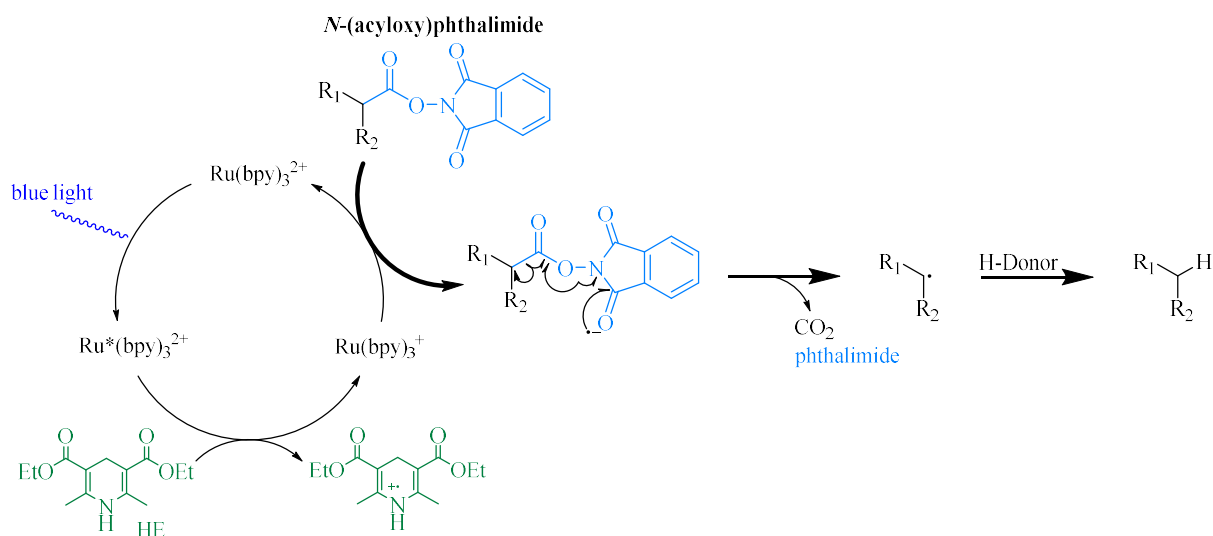


Scheme 19: Synthesis of *N*-acyloxyphthalimide (marked in blue) *via* Steglich esterification with *N,N'*-dicyclohexylcarbodiimide (DCC) and 4-dimethylaminopyridine (DMAP) followed by the metal-catalyzed decarboxylation.^{111,112}

Besides the reductive decarboxylation, they also proved the versatility of the decarboxylation of phthalimide-based esters by replacing the phthalimide motif with halogenes¹¹² or electron-deficient olefins.¹¹⁴ However, the phthalimide-based decarboxylation chemistry was not pursued any further and the potential was only rediscovered in 2015 by Overman *et al.*¹¹⁵. They introduced the decarboxylation of phthalimide-based esters as an innovative method for cross-coupling of sterically-hindered carbon radicals utilizing $\text{Ru}(\text{bpy})_3(\text{PF}_6)_2$, Hantzsch ester (HE) as reductant and *N,N*-diisopropylethylamine (DIPEA) as reductive quencher. From this point on, the investigation of phthalimide-based decarboxylation experienced an exponential growth.^{98,99,113} *Inter alia*, decarboxylative coupling of aspartic acid and glutamic acid derivatives¹¹⁶ was reported as well as the employment of different organocatalysts such as Eosin Y¹¹⁷. In 2020, Mendoza *et al.*¹¹⁸ found photoexcited dihyronicotinamides like nicotinamide adenine dinucleotide (NADH) to be suitable reactants in phthalimide-based coupling reactions.

Mechanistically, the photochemical decarboxylation starts with the excitement of the catalyst ($\text{Ru}(\text{bpy})_3^{2+}$) in a photochemical reaction to a photoexcited state ($\text{Ru}^*(\text{bpy})_3^{2+}$), which

undergoes a reduction by HE in a second step ($\text{Ru}^*(\text{bpy})_3^+$) followed by a single-electron transfer (SET) to the carbonyl of the phthalimide as exemplarily shown for *N*-(acyloxy)phthalimide in **Scheme 20**. The resulting radical can undergo various types of reactions. In the case of a classic decarboxylation, the addition of a H-donor leads to the reductive decarboxylation product, while in the presence of a suitable reactant such as electron-deficient olefins, a Michael-type addition occurs.

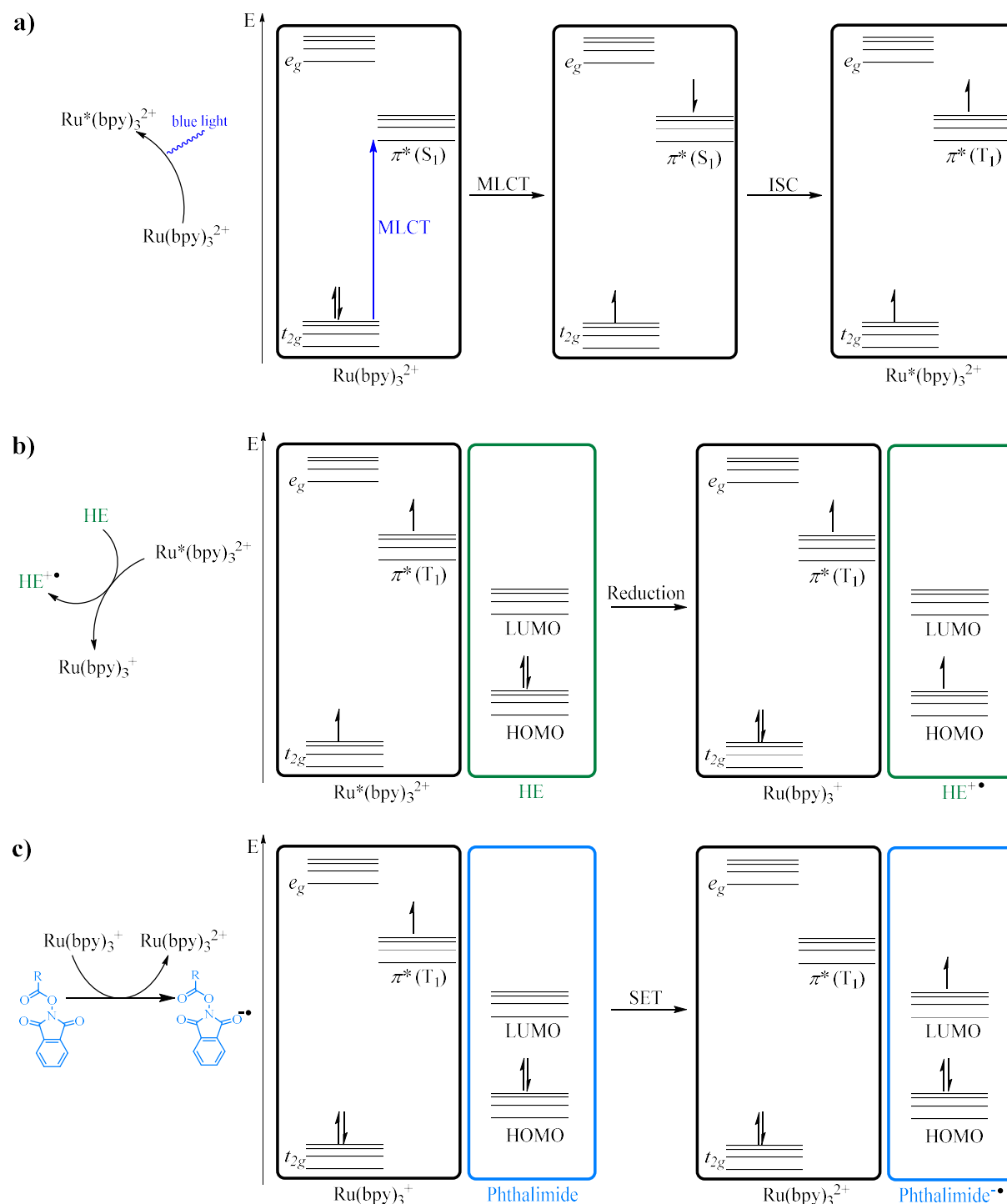


Scheme 20: Mechanism of the photochemical decarboxylation of the phthalimide activated ester *N*-(acyloxy)phthalimide as used in the present thesis with $\text{Ru}(\text{bpy})_3\text{Cl}_2$ as metal catalyst and HE (green) as reductant.^{113,115}

The catalytic cycle consists of different steps and oxidation states of the ruthenium-based catalyst. $\text{Ru}(\text{bpy})_3^{2+}$ is a charge-transfer (CT) complex, more precisely a metal-to-ligand CT (MLCT) complex. Those complexes are characterized by the transfer of an electron from an occupied *d*-orbital of the metal to an antibonding π^* -orbital of the aromatic ligand system. Besides, other CT complexes like ligand-to-metal CT complexes (LMCT), metal-to-metal CT complexes, or ligand-to-ligand CT complexes exist.¹¹⁹ The $\text{Ru}(\text{bpy})_3^{2+}$ complex is characterized by an octahedral symmetry (D_3) as a d^6 complex.¹²⁰ In this system, the t_{2g} metal-centered orbital is fully occupied as shown in the simplified Jablonski diagram in **Scheme 21a**.^{119,121,122} Furthermore, the antibonding π^* -orbital of the ligands are not occupied. The excitation by light (450 nm) leads to the MLCT resulting in an electron transferred from the t_{2g} ground state to the π^* -orbital. By intersystem crossing (ISC) and internal conversion (IC), the electron is

Theoretical Background

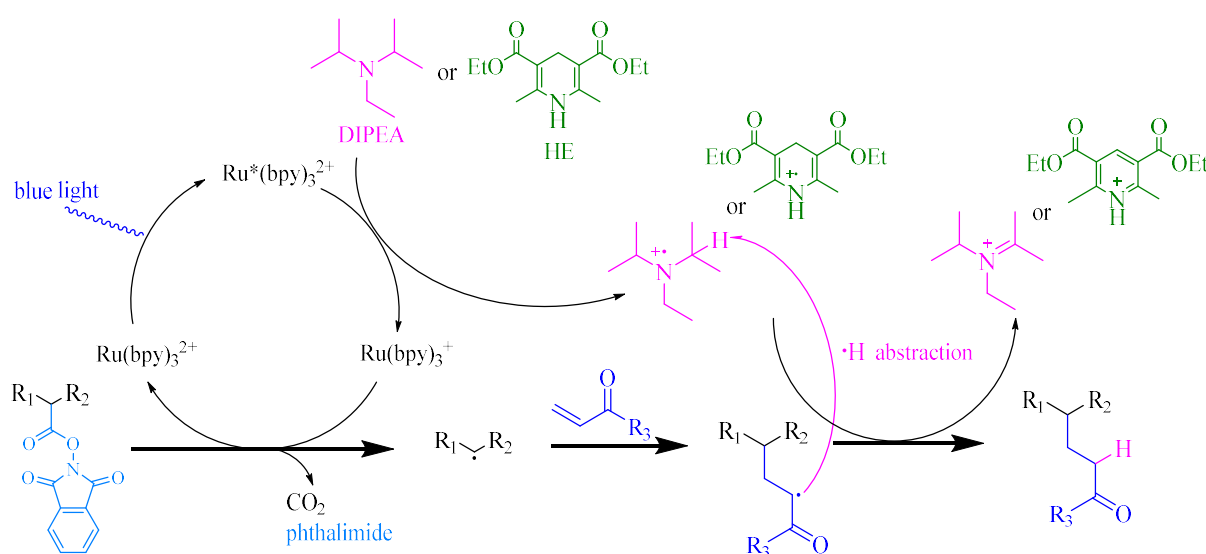
transferred from the π^* singlet state to a more stable π^* triplet state ($\text{Ru}^*(\text{bpy})_3^{2+}$). As just described, HE reduces $\text{Ru}^*(\text{bpy})_3^{2+}$ to $\text{Ru}(\text{bpy})_3^+$ in the next step (Scheme 21b).¹²⁰



Scheme 21: Simplified Jablonski diagram of **a)** excitation of the catalyst $\text{Ru}(\text{bpy})_3^{2+}$, followed by MLCT and ISC to $\text{Ru}^*(\text{bpy})_3^{2+}$ and **b)** reduction of $\text{Ru}^*(\text{bpy})_3^{2+}$ by HE (green) to $\text{Ru}(\text{bpy})_3^+$ and **c)** SET from $\text{Ru}(\text{bpy})_3^+$ to the carbonyl of the phthalimide (red).¹²⁰

The last step of the catalytic cycle is the SET from $\text{Ru}(\text{bpy})_3^+$ to the carbonyl of the phthalimide as shown in the simplified Jablonski diagram in **Scheme 21c**.

Besides the reductive decarboxylation employing a H-donor, cross-coupling reactions or the introduction of electron-deficient alkenes play an important role in modern organic chemistry. Those reactions are based on the same catalytic mechanism as the reductive decarboxylation, but differ from the point when the secondary radical is formed. Instead of the addition of a hydride from a H-donor, the electron-deficient alkene is added in a Michael-type addition (**Scheme 22**).^{115,123,124} After the addition, the radical is located at the α -carbon adjacent to the carbonyl. By H-abstraction from DIPEA (reductive quencher) or HE radical, the final product is formed and the initiation of a polymerization of the alkene is prevented. Additionally, the DIPEA or HE radical is transferred into a stabilized iminium ion. The mechanism demonstrates the necessity to use a reductive quencher to form the desired product and prevent free radical polymerization of the alkene.

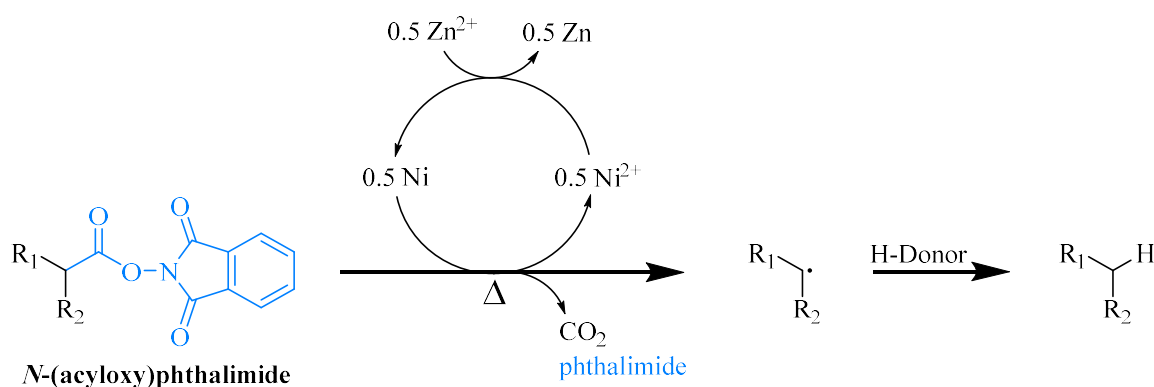


Scheme 22: Mechanism of the photochemical decarboxylation of *N*-(acyloxy)phthalimide with $\text{Ru}(\text{bpy})_3\text{Cl}_2 \cdot 6 \text{H}_2\text{O}$ as metal catalyst, HE (green) or DIPEA (purple) as reductant and radical quencher and the electron-deficient alkene (Michael-acceptor, blue).¹¹⁵

As the already mentioned examples demonstrate, the investigation of the photo-catalyzed decarboxylation of phthalimide-based esters is not yet at an end. In addition to the photo-catalyzed decarboxylation developed by Okada, also the classic Barton decarboxylation was further developed. In 2017, Baran *et al.*¹²⁵ introduced the so-called nickel-catalyzed Barton decarboxylation. To avoid the need of a photochemical reaction set-up, expensive catalysts

Theoretical Background

(Ruthenium), and the handling of instable Barton esters the authors developed a decarboxylation of phthalimide-based esters catalyzed by an inexpensive nickel-catalyst, which can be thermally activated. Furthermore, they introduced phenylsilane as a non-toxic and highly efficient hydrogen source and improved the reaction conditions to synthesize reductive decarboxylation products in high yields. Mechanistically, the nickel-catalyzed thermal decarboxylation is similar to the photochemical one. After activation of the Ni-catalyst by reduction with zinc, an electron from Ni is transferred to the carbonyl of the phthalimide, followed by extrusion of CO₂ and the removal of the phthalimide, leading to the formation of a radical (Scheme 23).

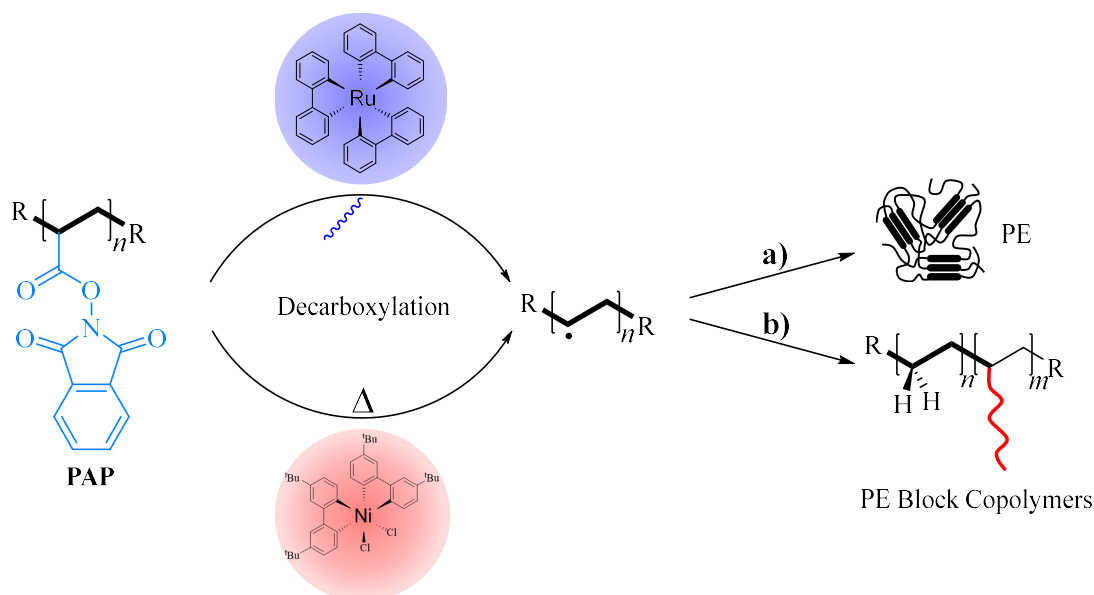


Scheme 23: Mechanism of the thermally-induced, nickel-catalyzed decarboxylation of *N*-(acyloxy)phthalimide as used in the present thesis with NiCl₂ as metal catalyst and zinc as reductant.¹²⁵

This radical can undergo different types of reactions, in case of the presence of a hydrogen source, the reductive decarboxylation product is formed. Besides, Baran *et al.*¹²⁵ also successfully demonstrated the employment of electron-deficient reactants in the reaction entitled as *Giese* reaction. The large number of publications in organic chemistry, especially in recent years, shows the enormous importance and topicality of the decarboxylation of phthalimide-based esters.⁹⁸ On the contrary, the transfer of the scientific findings from organic chemistry to polymer chemistry is a comparatively unexplored area.

3 Motivation and Goal

The growing demand for functional polymers and especially functional PEs makes the development of new synthesis procedures for PE and PE architectures particularly important. Furthermore, the rapidly growing field of decarboxylation chemistry as a part of organic chemistry research offers an attractive opportunity for the scientific transfer to polymer chemistry. Consequently, the present dissertation aims at establishing the first ethylene-free synthesis of PE from a polyacrylate-based precursor system by a decarboxylation approach. This approach is motivated by two advantages: i) removing the necessity to employ ethylene as a gaseous, hazardous monomer, and ii) using an acrylate-based precursor monomer that allows for the employment of RDRP techniques such as RAFT polymerization. While the first advantage offers a wide range of new possibilities for safe academic and industrial research, *e.g.*, for screening experiments, RAFT polymerization allows for the synthesis of defined polymers in terms of molar masses and dispersities. Herein, RAFT polymerization of the acrylate-based precursor monomer should open the pathway to predefined polymers, which result in defined PE after decarboxylation (**Scheme 24a**).



Scheme 24: Pathway of the intended concept of the present thesis. The decarboxylation of the phthalimide-based precursor polymer poly[*N*-(acryloyloxy)phthalimide] (PAP) by either photochemical, ruthenium-catalyzed (top) or thermal, nickel-catalyzed decarboxylation results in the formation of a carbon-centered radical at the polymer backbone. The radical should then be used for **a)** the main goal of the present thesis *i.e.*, the decarboxylative reduction of PAP to obtain pure PE and **b)** the decarboxylative reduction of PAP block copolymers to obtain PE block copolymers.

Motivation and Goal

Furthermore, RAFT polymerization enables the access to various architectures such as block copolymers (**Scheme 24b**). While other methods for the synthesis of PE block copolymers require ethylene gas or are restricted in the choice of comonomers, the decarboxylation approach evaluated in the present dissertation should offer the possibility to synthesize well-defined block copolymers with different comonomers with high efficiency. Furthermore, the decarboxylation of PAP could open the pathway to various PPMs eventually allowing for the synthesis of new and functional polymers.

4 Results and Discussion

In the current chapter, the results of the dissertation are presented and discussed in detail. The four subchapters are sorted logically and are based on each other in terms of content and scientific findings. The individual chapters each represent a self-contained project.

In the first part, the synthesis of the precursor homopolymer, copolymer and block copolymers is described and discussed. Starting with the thermal decarboxylation of the homopolymer, the project is expanded by a photochemical method and the solubility of the polymer is identified as a central aspect of the decarboxylation. The development of a suitable RAFT system allowed for the synthesis of block copolymers used for the synthesis of PE block copolymers with various block length and comonomers. Finally, both decarboxylation methods are evaluated and compared in terms of efficiency and purity of the obtained products.

The second chapter arose from the first project after the solubility of the polymer was identified as a critical factor during decarboxylation. Therefore, a sacrificial block copolymer based on a macroRAFT agent was developed. While the PAP block is decarboxylated, the second block provides solubility during decarboxylation and can be cleaved in a further step. The method demonstrates that it is possible to decarboxylate predefined acrylate-based polymer systems to yield PE.

The third chapter deals with the utilization of the decarboxylation of PAP homopolymers and block copolymers for further functionalization. Michael-type addition is successfully employed and used for the introduction of new functionalities and the synthesis of structurally new polymers. Decarboxylation followed by nitroxide radical coupling with TEMPO is used to lay the foundation for subsequent grafting of side chains from the polymer backbone.

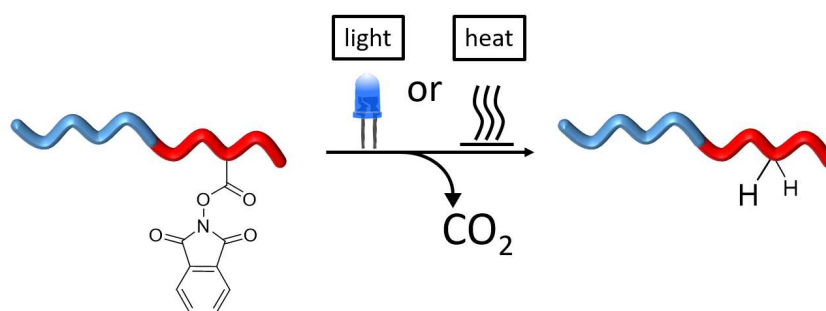
The fourth chapter describes the transfer of the decarboxylation results of the first and the second project onto the methacrylic analogous of PAP, poly[*N*-(methacryloyloxy)phthalimide] (PMAP), with the intention to synthesize PP from a methacrylate-based polymer system. However, the direct transfer of the decarboxylation methods is not possible and the reaction conditions are adapted to avoid the observed degradation of the polymer backbone.

Projects one, two and three were previously published in peer-reviewed journals and one patent as disclosed in the beginning of each subchapter.

4.1 Ethylene-free Synthesis of Polyethylene Copolymers and Block Copolymers

The decarboxylation of phthalimide structural motifs became increasingly popular in organic chemistry over the last few years due to the multiple decarboxylation strategies towards different products which have been established. Furthermore, the introduction of new functionalities to organic molecules *via* decarboxylation of phthalimide-based esters is characterized by high efficiency and orthogonality.⁹⁸ Therefore, those reactions could be of high interest for polymer chemistry and the field of PPM.

In 2017, Baran *et al.*¹²⁵ introduced the so-called nickel-catalyzed Barton decarboxylation, which allows for the reductive decarboxylation of phthalimide-based esters, as a new tool in organic chemistry as shown in **Chapter 2.5**, thus settling the pathway for the chemistry of this thesis. In this chapter, for the first time the decarboxylation of phthalimide-based active esters evaluated in organic chemistry are transferred to polymers in order to synthesize PE derivatives. Thus, phthalimide-based homopolymers, copolymers and block copolymers were synthesized and the efficiency of the decarboxylation was evaluated for different polymeric architectures. Furthermore, two different methods, the nickel-catalyzed decarboxylation based on the work of Baran *et al.*¹²⁵ and an adapted photochemically-induced decarboxylation based on studies of Okada *et al.*¹¹⁴ and Zheng *et al.*¹¹³ as examined in detail in **Chapter 2.5** are studied independently to yield PE-based polymers as shown in **Scheme 25**.



Scheme 25: Ethylene-free synthesis of PE block copolymers by either thermal or photochemical decarboxylation using an acrylate-based precursor polymer.

The decarboxylation of the homopolymer (**Chapter 4.1.2**) was partially evaluated in the master thesis of the author (Stefan Frech) and is thus covered in detail in the master thesis as well as the corresponding publication and patent.^{126–128}

Parts of this chapter and the corresponding parts in the experimental section were adapted with permission from the publication/patent and the master thesis written by the author (Stefan Frech).¹²⁶⁻¹²⁸

Results and Discussion

4.1.1 Synthesis of Poly[*N*-(acryloyloxy)phthalimide]

The catalytic cycle of the decarboxylation is based on a SET from the metal catalyst to the carbonyl of the phthalimide, as explained in detail in **Chapter 2.5**. The structure of the phthalimide is therefore of central importance for the decarboxylation and the resulting carbon-centered radical at the polymer backbone. In the further course of the reaction, this carbon-centered radical couples with a hydrogen originating from a H-donor resulting in a PE chain. Thus, the phthalimide structural motif needs to be linked to the backbone of the polymer *via* an ester bond. The structure of the monomer *N*-(acryloyloxy)phthalimide (NAP, **Figure 1a**) results from this consideration.

The investigation of the decarboxylation of the phthalimide-based polymer poly[*N*-(acryloyloxy)phthalimide] (PAP) started with the synthesis of the monomer NAP, which was synthesized by Steglich esterification from *N*-hydroxyphthalimide and acrylic acid in the presence of 1-ethyl-3-(3-dimethylaminopropyl)carbodiimide hydrochloride (EDC·HCl) and 4-dimethylaminopyridine (DMAP) as catalyst (**Figure 1a**).

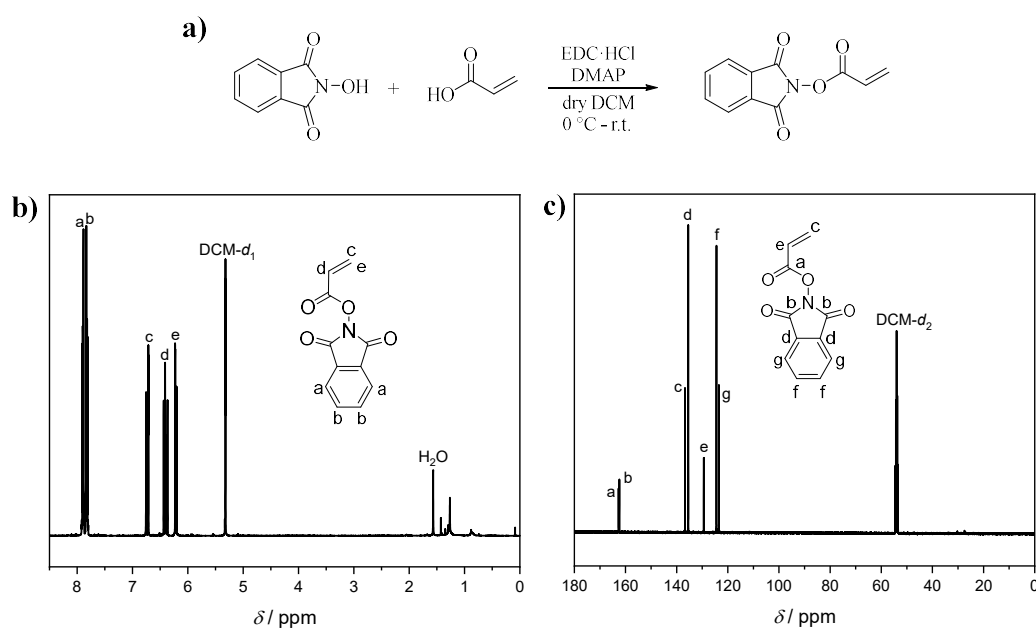


Figure 1: a) Synthesis of the monomer *N*-(acryloyloxy)phthalimide by Steglich esterification as well as the corresponding b) ¹H NMR and c) ¹³C NMR spectrum.

The successful synthesis of NAP in high purity was proven by ¹H NMR (**Figure 1b**) as well as ¹³C NMR (**Figure 1c**) spectroscopy. Subsequently, NAP was polymerized by FRP in dimethylformamide (DMF) at 70 °C using 2,2'-azobis(2-methylpropionitrile) (AIBN) as

initiator to obtain the targeted precursor polymers. As shown in **Table 1** and **Figure 2**, different polymers (**P1 - P4**) were synthesized and analyzed *via* size-exclusion chromatography (SEC) in dimethylacetamide (DMAc) with PMMA calibration. While polymers **P1 - P3** were PAP homopolymers, **P4** was synthesized by the copolymerization of NAP with oligo(ethylene glycol) methyl ether acrylate (OEGMEA, $M_n = 480 \text{ g mol}^{-1}$, $M_n =$ number average molar mass) to obtain poly[*N*-(acryloyloxy)phthalimide-*co*-oligo(ethylene glycol) methyl ether acrylate] (P[AP-*co*-OEGMEA]) as shown in **Figure 2c** and **Figure 2d**.

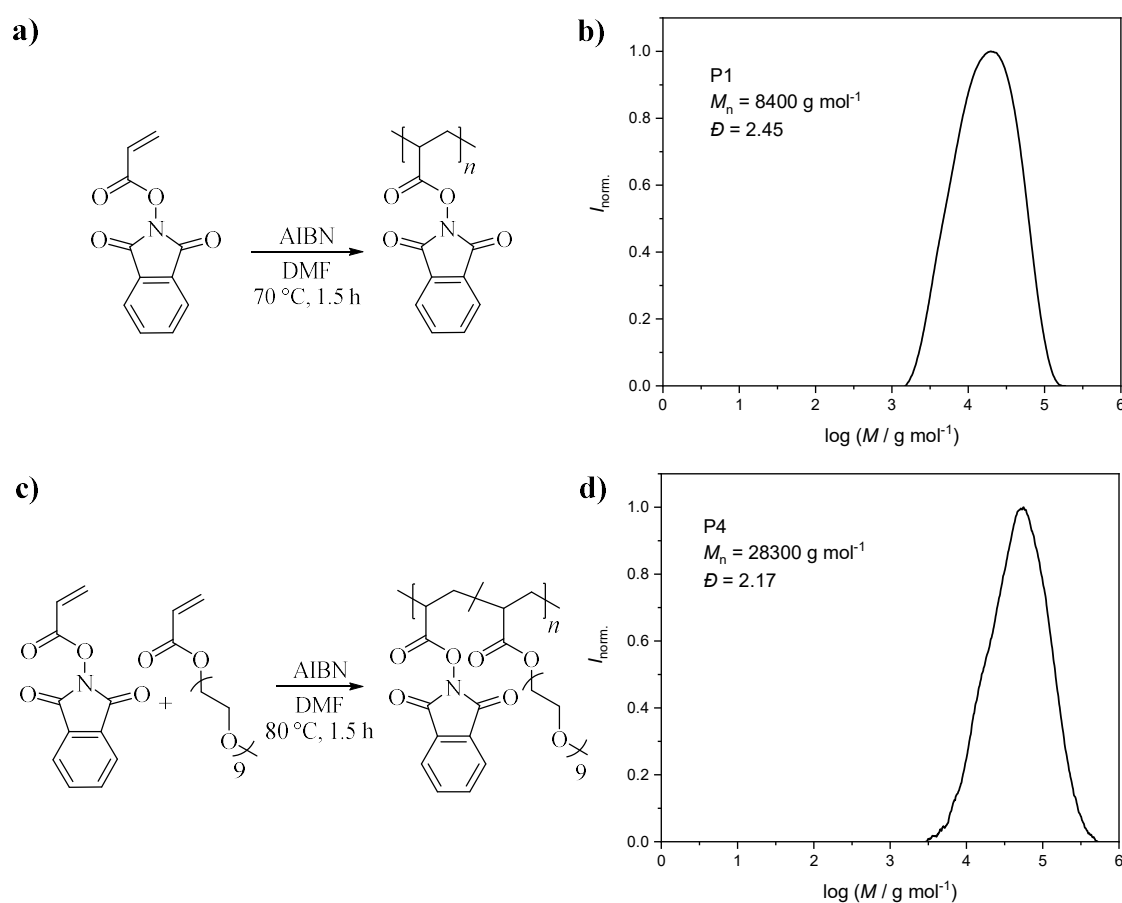


Figure 2: **a)** Polymerization of NAP to PAP and the analysis of PAP (**P1**) by **b)** SEC with DMAc as eluent and PMMA calibration. **c)** Copolymerization of NAP with OEGMEA yielding P[AP-*co*-OEGMEA] (**P4**) and **d)** the corresponding SEC chromatogram in DMAc as eluent using PMMA calibration.

Results and Discussion

Table 1: Overview of the synthesis of different PAP polymers.

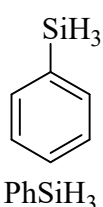
Entry	Polymer [§]	M_n^* [g mol ⁻¹]	\bar{D}^*	DP^*	M_n^\dagger [g mol ⁻¹]	DP^\dagger	$M_{n, \text{theo.}}$ [g mol ⁻¹]	Conv. [#] [%]
1	P1 (HP)	8300	2.25	39	8250	38	27130	30
2	P2 (HP)	2500	1.22	11	1600	7	1600	> 90
3	P3 (HP)	5600	1.56	26	6700	30	27130	25
4	P4 (CP)	28300	1.75	2.17	-	-	57400	-

[§]HP = homopolymer, CP = copolymer with OEGMEA; *calculated by SEC with DMAc as eluent; [†]calculated by ¹H NMR spectroscopy; [#]conv. = conversion, calculated by ¹H NMR spectroscopy.

4.1.2 Decarboxylation of Poly[*N*-(acryloyloxy)phthalimide]

As stated above, the evaluation of the decarboxylation of the PAP homopolymer was partly conducted during the master thesis of the author.¹²⁸ Therefore, the following chapter gives a brief overview of the performed reactions, to provide a basis for the following chapters. More details can be found in the master thesis and the corresponding publication as well as the patent.^{126–128}

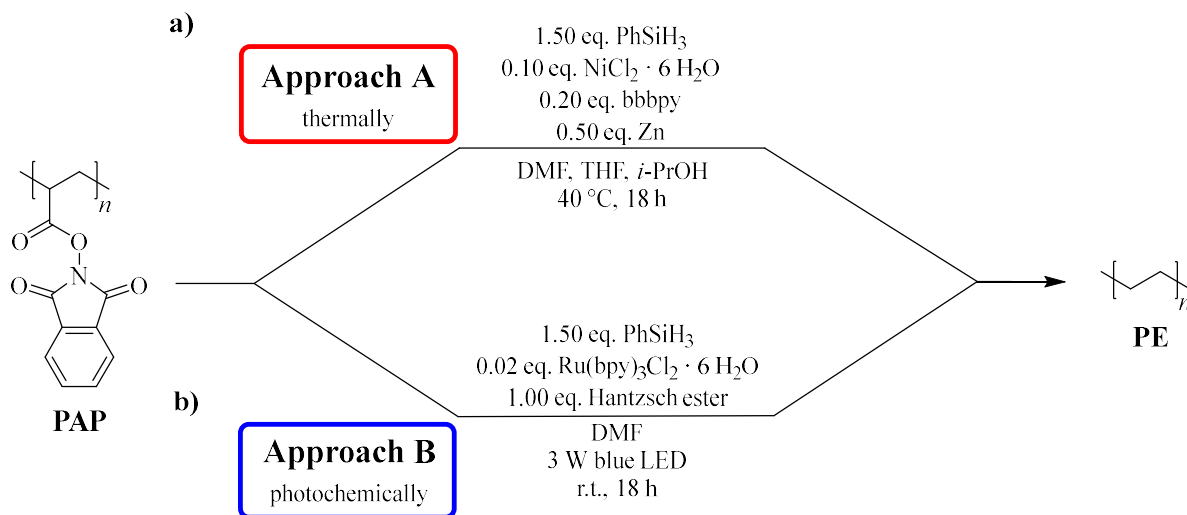
For the decarboxylation reactions of the previously obtained polymers the thermally-induced



Scheme 26:
Structure of phenylsilane.

decarboxylation (approach A, **Scheme 27a**) as firstly report by Baran *et al.*¹²⁵ was examined. To do so, their procedure was adapted meaning 0.50 eq. of zinc, 0.10 eq. of NiCl₂ · 6 H₂O, 0.20 eq. of 4,4'-di-tert butyl-2,2'-dipyridyl (bbbpy), and 1.50 eq. phenylsilane as H-donor (**Scheme 26**) (all equivalents per active ester group) as shown in **Scheme 27a**. Further, the reaction was conducted in DMF as solvent, since it featured good solubility for the polymer as well as the reactants, with addition of tetrahydrofurane (THF) and isopropanol (*i*-PrOH) (DMF:THF:*i*-PrOH 1:0.1:0.01) and at 40 °C as Baran *et al.* found those conditions to yield the most efficient decarboxylation results.¹²⁵ The procedure of Baran *et al.*¹²⁵ was slightly adapted for the use of a polymer as specified in the following. The solubility of the polymer required increased attention, since the homopolymer PAP is soluble in DMF but not in THF or *i*-PrOH. Therefore, the homopolymer (**P1**), catalyst/ligand mixture and the H-donor were separately dissolved, the solutions degassed and the polymer solution was added to the Schlenk tube with the previously added zinc powder, followed by the catalyst and the H-donor. However, the

quick addition of the H-donor after addition of the catalyst solution, as pointed out as a critical step by Baran *et al.* was fully addressed.



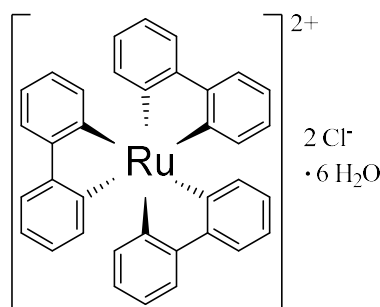
Scheme 27: **a)** Approach A: The thermal decarboxylation of the PAP homopolymer with phenylsilane as H-donor, NiCl₂ · 6 H₂O and bbbpy as catalytic system and zinc as reductant. **b)** Approach B: The photochemical decarboxylation of the PAP homopolymer with phenylsilane as H-donor, Ru(bpy)₃Cl₂ · 6 H₂O as catalytic system and HE as reductant.

After precipitation, the polymer possessed only a poor solubility in common solvents like chloroform, dichloromethane (DCM), toluene or other chlorinated solvents both at room temperature and elevated temperatures. Therefore, ¹H NMR analysis was conducted in a mixture of deuterated dimethyl sulfoxide (DMSO) and DMF (1:1), which featured the best solubility of all tested solvents. The recorded ¹H NMR spectrum (**Figure 53**) revealed that the decarboxylation was not quantitative, but rather a copolymer consisting of units of not decarboxylated PAP as well as PE units was obtained. Thus, the different reaction parameters such as reaction time, temperature and equivalents or the usage of shorter precursor polymers (**P2**, **P3**) were varied, but none of these did improve the decarboxylation result.

Therefore, an alternative method, as firstly described by Okada *et al.*¹¹⁴, based on a photochemical catalytic cycle featuring an electron-transfer from ruthenium to the imide of the phthalimide was investigated. Instead of 1-benzyl-1,4-dihydronicotinamide (BNAH) as reductant, Hantzsch ester (HE) was used due to its high efficiency as a reductant, as described by Overman *et al.*¹¹⁵ in 2015 and Zheng *et al.*¹¹³ in 2018. In relation to the work of Baran *et al.*¹²⁵, the photochemically-induced decarboxylation process of Okada *et al.*¹¹⁴ was adapted,

Results and Discussion

and phenylsilane was employed as the hydrogen source to react with the carbon-centered radical formed at the polymer backbone upon decarboxylation. The conditions of the photochemical



Scheme 28: Structure of the catalyst $\text{Ru}(\text{bpy})_3\text{Cl}_2 \cdot 6 \text{H}_2\text{O}$.

decarboxylation include 0.02 eq. of $\text{Ru}(\text{bpy})_3\text{Cl}_2 \cdot 6 \text{H}_2\text{O}$ (**Scheme 28**), HE (1.00 eq.) and phenylsilane (1.50 eq.) in DMF under the irradiation of three 3 W blue LEDs (450 nm) at room temperature with the homopolymer **P1** as shown in **Scheme 27b** (approach B). The polymer obtained from approach B was similar to the one obtained from the thermally-induced decarboxylation with a decarboxylation degree of $> 90\%$ as calculated by ^1H NMR spectroscopy (**Figure 54**).

Combining the results of both different approaches, it was concluded that the solubility of the polymer during the decarboxylation is a critical factor, since the resulting PE was insoluble in DMF and thus an increasing degree of decarboxylation leads to a reduced solubility of the polymer. However, decreasing the size of the polymer (**P2** and **P3**) to favor the solubility did not result in a higher degree of decarboxylation. Furthermore, the exchange of the solvent to a more suitable one for PE, such as 1,2,4-trichlorobenzene (1,2,4-TCB), is not easily manageable due to insolubilities of the other reactants. Nevertheless, a mixture of DMF and 1,2,4-TCB (1:1) was used in the thermal decarboxylation process while the temperature was increased to 120°C to improve the solubility of the formed PE and simultaneously ensuring the solubility of the reactants and the precursor polymer. The analysis of the product *via* ^1H NMR spectroscopy, however, showed that even the use of this mixture is not sufficient to reach a quantitative decarboxylation of the homopolymer (**Figure 55**).

To overcome further issues with the solubility of the decarboxylated polymer, a copolymer of NAP with OEGMEA ($M_n = 480 \text{ g mol}^{-1}$) was synthesized since the latter is known to be soluble in a wide range of solvents. The corresponding precursor copolymer P[AP-*co*-OEGMEA] (**P4**) featured a comonomer ratio of 1:3 of NAP to OEGMEA and thus exhibited an excellent solubility. Subsequently, the polymer was decarboxylated with the thermally-induced decarboxylation method under the former mentioned standard conditions (**Figure 3a**). The resulting polymer (**P4_{PE}**) still featured a good solubility in common solvents like chloroform and the analysis *via* ^1H NMR spectroscopy revealed a quantitative decarboxylation of the PAP units as indicated by the removal of aromatic phthalimide protons at 7.8 ppm (**Figure 3b**, marked in red). Therefore, the successful formation of PE-units in the copolymer (**Figure 3b**, marked in back) and further the necessity to enhance the solubility during the decarboxylation step by using a soluble comonomer was proven.

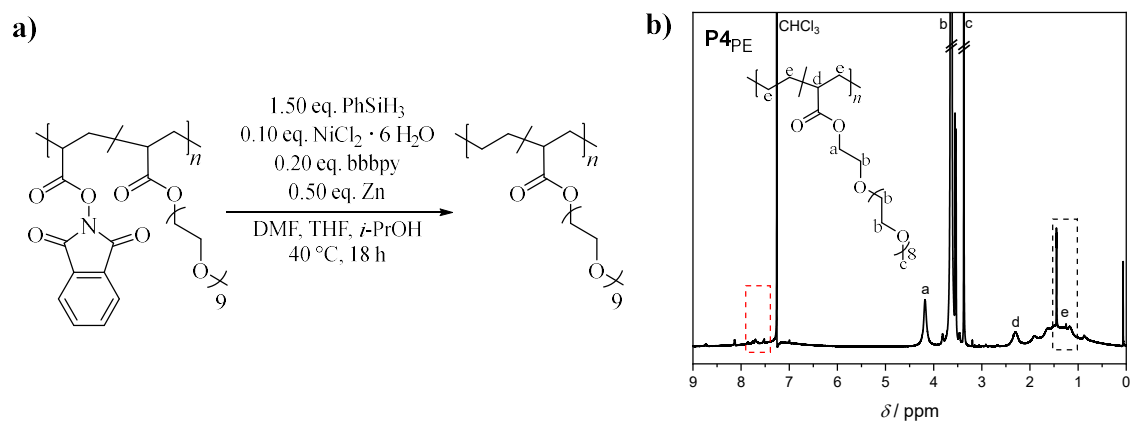


Figure 3: **a)** Thermal decarboxylation of P[AP-*co*-OEGMEA] (**P4**) and the analysis of the product *via* **b)** ^1H NMR spectroscopy.

To ensure the solubility of the polymer during decarboxylation as well as for analysis on the one hand and to further increase the versatility of the method on the other hand in the next step, PAP block copolymers should be synthesized. By doing so, complex structures such as PE block copolymers should be accessible as described in the following chapters.

Results and Discussion

4.1.3 Synthesis of Poly[*N*-(acryloyloxy)phthalimide] Block Copolymers

As one of the most versatile and straightforward RDRP methods RAFT polymerization was selected as the technique of choice for the controlled radical polymerization of NAP. However, a suitable RAFT agent had to be found since the reactivity of the C=C double bond of an activated ester monomer such as NAP differs from the reactivity of standard acrylates. Various commercially available RAFT agents were tested for their ability to control the synthesis of PAP block copolymers, but none of them gave satisfying results. Nevertheless, a recent publication of Chapman *et al.*⁶⁵ described the polymerization of a similar monomer with *S, S'*-benzyl propyl trithiocarbonate (BPTT) as RAFT agent (**Figure 4**).

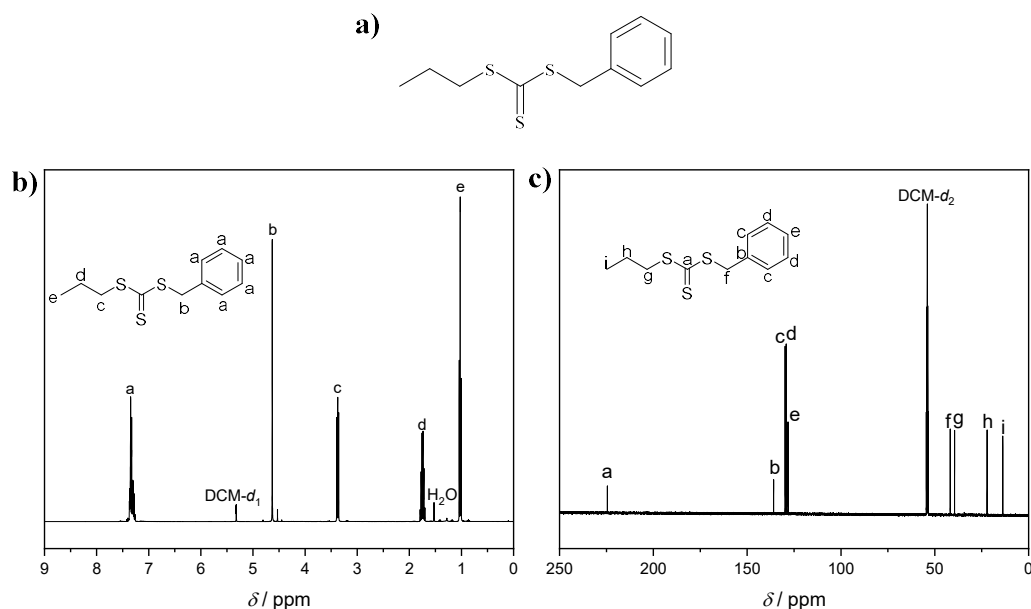


Figure 4: a) Structure of RAFT-agent *S, S'*-benzyl propyl trithiocarbonate (BPTT) and the analysis *via* b) ¹H NMR and c) ¹³C NMR spectroscopy.

Thus, this RAFT agent was synthesized accordingly in high purity (**Figure 4b** and **Figure 4c**) and subsequently employed for the polymerization of NAP. Since the decarboxylation proceeded well with the statistical copolymer **P4**, OEGMEA ($M_n = 480 \text{ g mol}^{-1}$) was chosen again as one of the comonomers for the block copolymerization. As shown in **Figure 5**, the use of BPTT as RAFT agent allowed for the synthesis of poly[*N*-(acryloyloxy)phthalimide]-*block*-poly[(ethylene glycol) methyl ether acrylate] (PAP-*b*-POEGMEA) block copolymers. With this results in hand, sets of different block copolymers with various block lengths and different

comonomers were synthesized by chain extension of PAP with OEGMEA or 2-methoxyethyl acrylate (MEA).

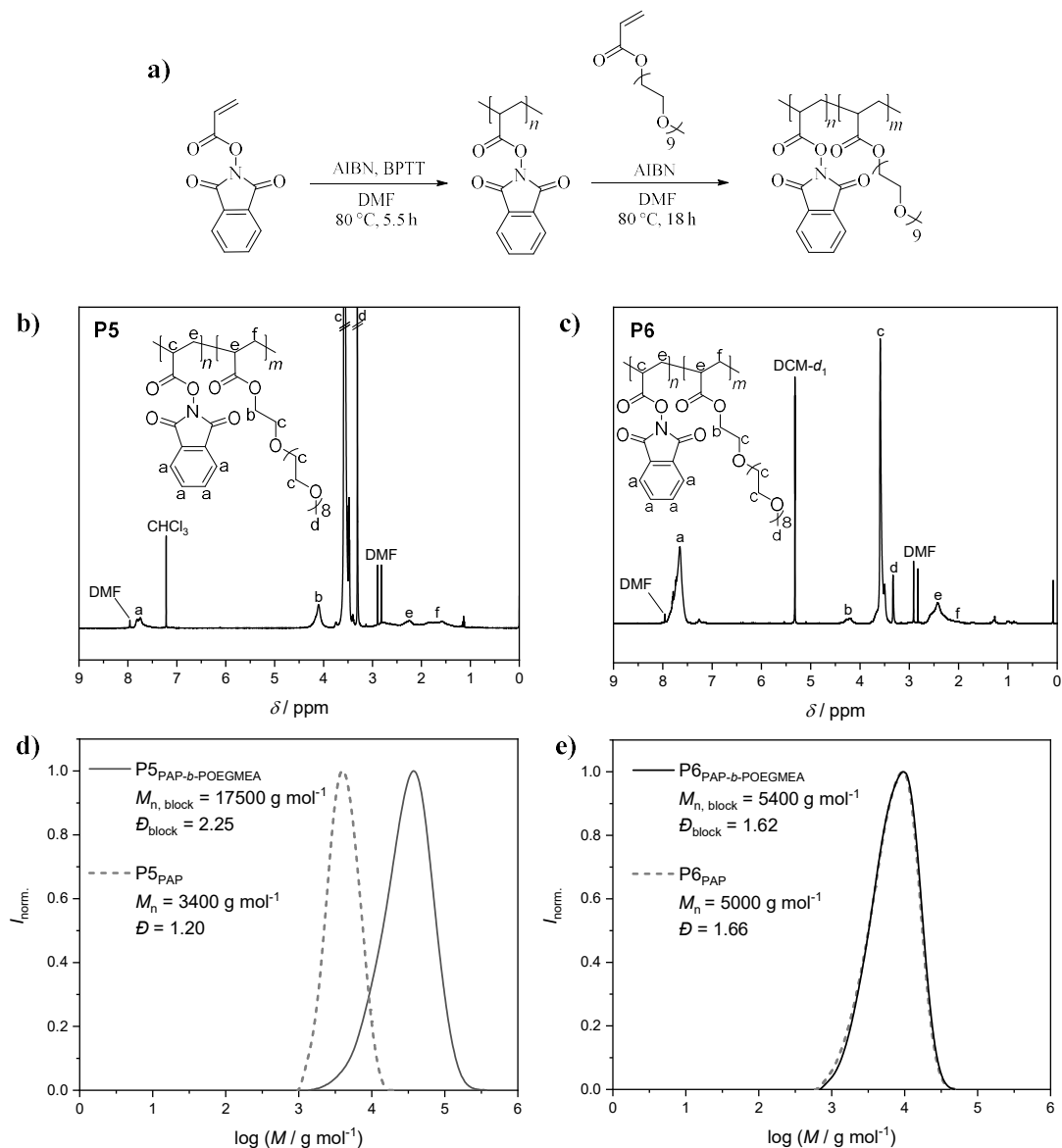


Figure 5: a) Synthesis of PAP-*b*-POEGMEA by chain extension of PAP via RAFT polymerization. b) ¹H NMR spectrum of **P5**. c) ¹H NMR spectrum of **P6** and the corresponding SEC chromatograms in DMAC as eluent with PMMA calibration of d) **P5** and e) **P6**.

The degree of polymerization (*DP*) of the synthesized blocks was intentionally chosen to be in a range of 20 – 30 units, to i) observe material properties of PE while maintaining a decent solubility, hence allowing for an analysis of the polymer and ii) gain a more detailed understanding of the synthesis and methods used in the present thesis. The ¹H NMR spectra of

Results and Discussion

block copolymers **P5** and **P6** presented in **Figure 5** demonstrate the different block ratios. A low intensity of the aromatic signal of the phthalimide units ('a') in comparison to the signals of OEGMEA (4.2 ppm (COOCH₂), 3.7 ppm (CH₂CH₂O) and 3.2 ppm (CH₃)) could be observed for **P5**, while the intensity of the aromatic signal of the phthalimide units was magnitudes higher for **P6**. Further, the SEC chromatograms of both polymers (**Figure 5d** and **Figure 5e**) proved the clean formation of block copolymers by unimodal distributions and an increasing molar mass after block copolymerization.

Thus, three different sets of PAP-*b*-POEGMEA block copolymers were synthesized to be used in decarboxylation reactions (**Table 2**, entry #1-5). Herein, the first set consisted of **P5**, which possessed a degree of polymerization of NAP units of $DP_{\text{NAP, P5}} = 20$ and $DP_{\text{OEGMEA, P5}} = 34$ for the second block and therefore a high OEGMEA content ensuring solubility in various solvents. The second set consisted of polymers **P6** and **P7**, both featuring a drastically decreased size of the OEGMEA block ($DP_{\text{OEGMEA, P6/P7}} = 3$) while at the same time the size of the NAP block was slightly increased to $DP_{\text{NAP, P6/P7}} = 28$. Thus, it was intended to investigate whether such a small block of OEGMEA is already sufficient to provide good solubility during subsequent decarboxylation. The third set of polymers (**P8**, **P9**) was synthesized for kinetic experiments and therefore featured a balanced block ratio of $DP_{\text{NAP, P8/P9}} = 24$ and $DP_{\text{OEGMEA, P8/P9}} = 10$.

Table 2: Summary of block copolymers synthesized and their calculated and theoretical molar masses as well as dispersity.

Entry	Polymer	$M_{n, \text{phth.}}^*$ [g mol ⁻¹]	$M_{n, \text{phth.}}^\dagger$ [g mol ⁻¹]	$M_{n, \text{block}}^{**}$ [g mol ⁻¹]	$M_{n, \text{block}}^{\dagger\dagger}$ [g mol ⁻¹]	D_{block}^{**}
1	P5 (PAP- <i>b</i> -POEGMEA)	3400	4220	17500	20640	2.25
2	P6 (PAP- <i>b</i> -POEGMEA)	5000	6180	5400	7620	1.62
3	P7 (PAP- <i>b</i> -POEGMEA)	4000	5980	5200	7390	1.56
4	P8 (PAP- <i>b</i> -POEGMEA)	3800	5210	9500	10000	1.75
5	P9 (PAP- <i>b</i> -POEGMEA)	4700	3690	8500	9450	1.64
6	P10 (PAP- <i>b</i> -PMEA)	4500	4200	8100	9660	1.57
7	P11 (PAP- <i>b</i> -PMEA)	4900	4600	7000	9020	1.80

*calculated by SEC with DMAc as eluent; †calculated by ¹H NMR spectroscopy; †† $M_{n, \text{block}}$ and D_{block} refer to the entire block copolymer PAP-*b*-POEGMEA.

To widen the scope of comonomers, which can be employed to solubilize the polymer during decarboxylation, MEA was used as comonomer for the block copolymerization to obtain polymers poly[*N*-(acryloyloxy)phthalimide]-*block*-poly(2-methoxyethyl acrylate) (PAP-*b*-PMEA, **P10** and **P11**, **Figure 6**). Both polymers featured a similar DP of NAP ($DP_{\text{NAP, P10/P11}} = 20$) and a $DP_{\text{MEA, P10/P11}} = 11$.

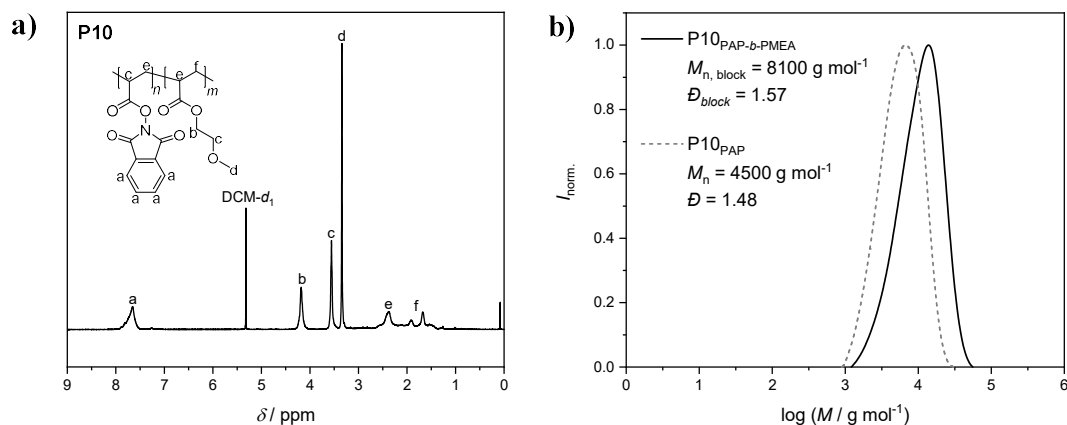
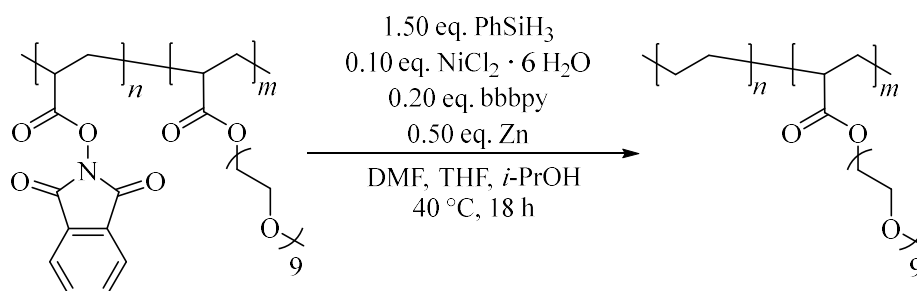


Figure 6: a) ^1H NMR spectrum of PAP-*b*-PMEA (**P10**) and b) the corresponding SEC chromatogram in DMAc as eluent with PMMA calibration.

Results and Discussion

4.1.4 Decarboxylation of Poly[*N*-(acryloyloxy)phthalimide] Block Copolymers

After the successful synthesis of a small library of different block copolymers, their decarboxylation was investigated, thus yielding PE block copolymers. To do so, the thermally-induced decarboxylation method was employed *i.e.*, 0.10 eq. of $\text{NiCl}_2 \cdot 6 \text{H}_2\text{O}$, 0.20 eq. of bbbpy, 0.50 eq. of zinc, and 1.50 eq. of phenylsilane (**Scheme 29**) with respect to the phthalimide active ester, as described under **4.1.2**.



Scheme 29: Thermally-induced decarboxylation of block copolymer PAP-*b*-POEGMEA yielding PE-*b*-POEGMEA.

At first, polymer **P5** with a ratio of 20:34 (NAP:OEGMEA) was used for the decarboxylation. Analogues to the statistical copolymer **P4_{PE}**, block polymer PE-*b*-POEGMEA (**P5_{PE}**) featured a good solubility in various solvents and was therefore analyzed *via* ¹H NMR spectroscopy and SEC as well as attenuated total reflection-Fourier-transform-infrared (ATR-FT-IR) spectroscopy and differential scanning calorimetry (DSC) as shown in **Figure 7**. Evaluation of the ¹H NMR spectrum revealed all expected signals of the POEGMEA block (4.2 ppm (COOCH₂), 3.7 ppm (CH₂CH₂O) and 3.2 ppm (CH₃)) as well as a distinct signal which could be assigned to the PE block (1.2 – 1.5 ppm). Furthermore, the former signal of the aromatic protons of the phthalimide side group was completely removed, indicating a quantitative decarboxylation (**Figure 7b**).

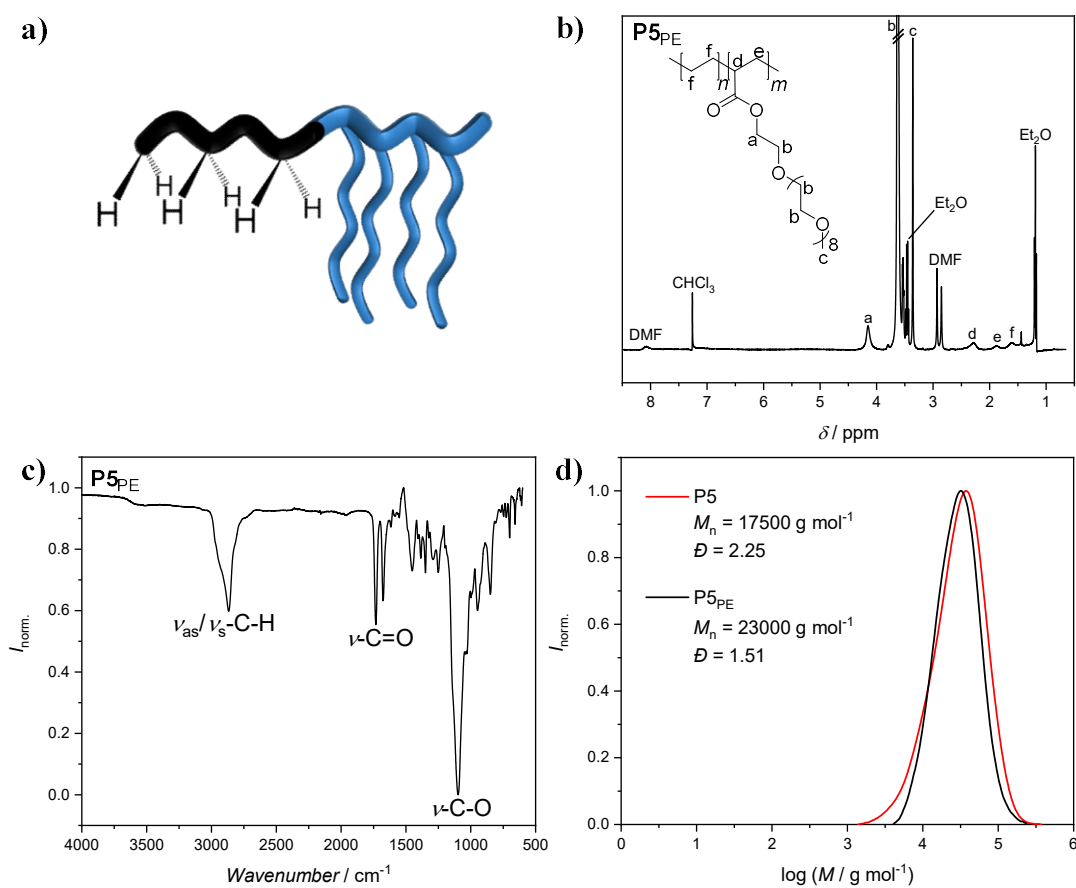
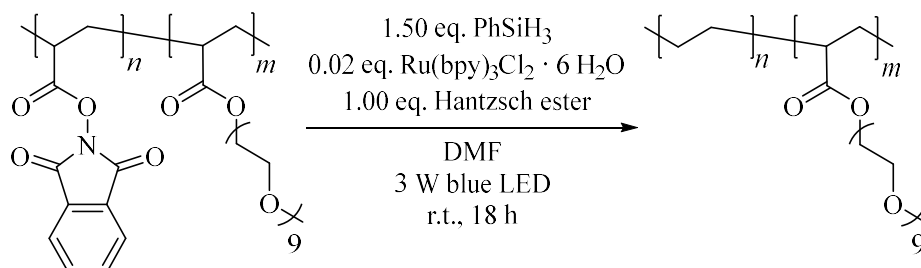


Figure 7: a) Schematic depiction of the block ratios of block copolymer **P5PE**, with PE (black) and POEGMEA (blue) blocks, as well as the analysis of **P5PE** via b) ^1H NMR spectroscopy, c) ATR-FT-IR spectroscopy, and the analysis of the block copolymers before and after decarboxylation by d) SEC with DMAc as eluent and PMMA calibration.

The quantitative removal of the phthalimide unit was once more proven by ATR-FT-IR spectroscopy by the disappearance of the aromatic carbon-hydrogen out-of-plane deformation ($\delta_{\text{oop}}\text{C-H}$) vibration at 690 cm^{-1} (**Figure 7c**). Surprisingly, the SEC trace in DMAc as eluent (**Figure 7d**) showed a slight increase of the molar mass, which was unsuspected, since the decarboxylation of the PAP block and thus the removal of mass should theoretically decrease the total molar mass to around 3600 g mol^{-1} . Though, the analysis demonstrated that the degree of polymerization remains intact and the formation of a network was not observed. This observation will be thus discussed at a later stage. Further, the thermal analysis of **P5PE** via DSC showed neither a melting nor a crystallization point in the temperature range of $0 - 150 \text{ }^\circ\text{C}$ as expected for PE. It was therefore concluded, that the short chain length of the PE block in comparison to the POEGMEA block as well as impurities originating from the catalytic system (polymer was colored light green) hindered the crystallization.

Results and Discussion

To compare the results of the different decarboxylation methods, the same polymer **P5** was additionally decarboxylated *via* the photochemical method. Similar to the decarboxylation of the homopolymer in **Chapter 4.1.2**, the photochemical decarboxylation was performed using 0.02 eq. of $\text{Ru}(\text{bpy})_3\text{Cl}_2 \cdot 6 \text{H}_2\text{O}$, 1.00 eq. of HE and 1.50 eq. of phenylsilane under the irradiation of blue light (440 – 450 nm) at room temperature (**Scheme 30**).



Scheme 30: Photochemically-induced decarboxylation of block copolymer PAP-*b*-POEGMEA yielding PE-*b*-POEGMEA.

Generally, the analysis of the photochemical decarboxylation product revealed similar results as the thermally decarboxylated one did. ¹H NMR analysis showed a comparable spectrum (**Figure 8b**), indicating a successful and quantitative decarboxylation. While the signals of OEGMEA were clearly visible, the signal at 7.6 ppm arising from the aromatic protons of the phthalimide group could not be identified. Furthermore, a signal of low intensity at 1.2 - 1.5 ppm originating from CH₂ repeating units could be found. Analogous to the thermal decarboxylation product, ATR-FT-IR spectroscopy proved the quantitative removal of the phthalimide groups by the disappearance of the aromatic $\delta_{\text{oop}}\text{C-H}$ vibration (690 cm⁻¹) as well as a signal of high intensity corresponding to the asymmetrical ($\nu_{\text{as}}\text{C-H}$) and symmetrical ($\nu_{\text{s}}\text{C-H}$) stretch vibrations of the C-H bond at 2860 cm⁻¹.

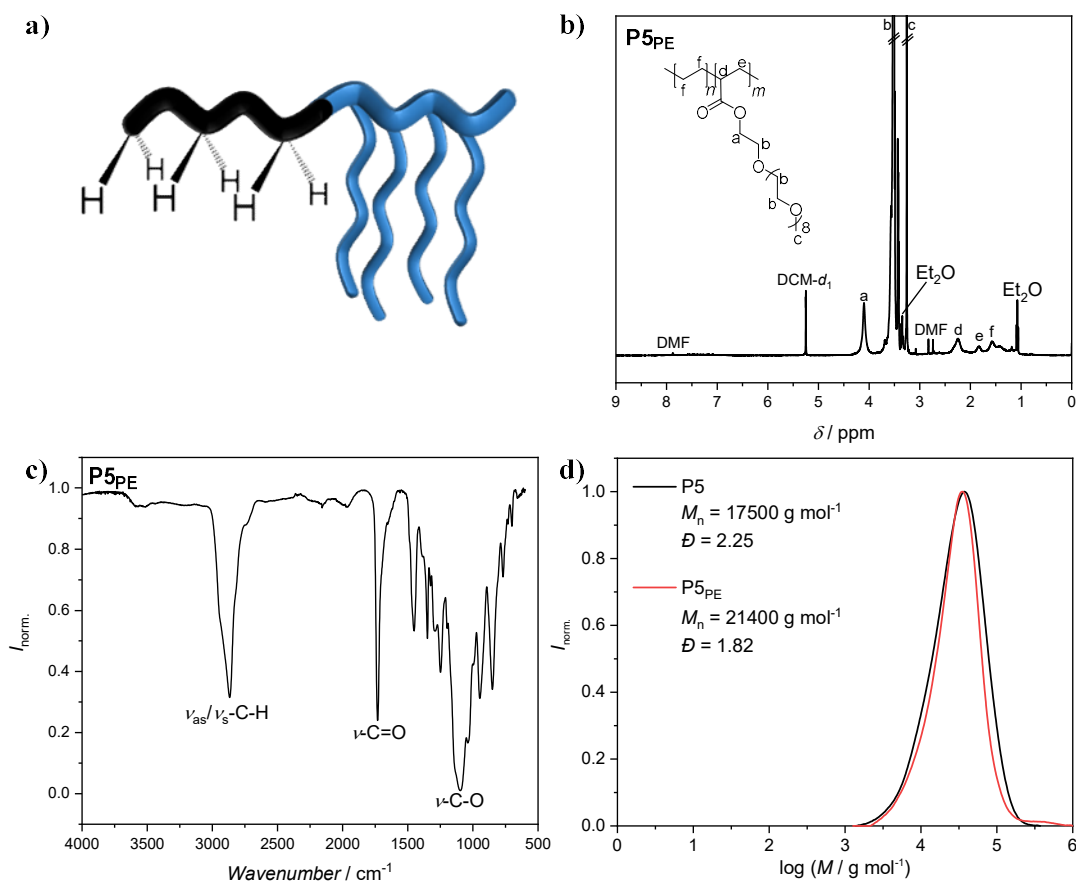


Figure 8: a) Schematic depiction of the block ratios of block copolymer **P5PE**, with PE (black) and POEGMEA (blue) blocks, as well as the analysis of **P5PE** via b) ^1H NMR spectroscopy, c) ATR-FT-IR spectroscopy, and the analysis of the block copolymers before and after decarboxylation by d) SEC with DMAc as eluent and PMMA calibration.

SEC analysis of the polymer showed the intact nature of the chains, while the molar mass slightly increased in contrast to the expected decrease, as observed before for the thermally decarboxylated product. Furthermore, the analysis of the thermal properties of the polymer via DSC showed neither a melting nor a crystallization point in the analyzed temperature range ($0 - 150 \text{ }^\circ\text{C}$), as it would have been expected for PE.

To summarize these results at this stage, it can be concluded that the synthesis of PE block copolymers from acrylate-based precursor polymers can be performed. However, the short PE block and thus a low influence onto the overall properties rendered the analysis (*e.g.*, regarding the thermal properties) rather challenging. Therefore, polymers **P6** (photochemical) and **P7** (thermal) with a high phthalimide and low OEGMEA content were employed for decarboxylation reactions in order to obtain more PE dominant properties.

Results and Discussion

Since the photochemical method seemed to yield better results, the results of the photochemical decarboxylation of polymer **P6** featuring *DPs* of the blocks of 28:3 (NAP:OEGMEA) will be discussed in the following. This particular block copolymer ratio was chosen to evaluate whether such a low amount of OEGMEA can still provide sufficient solubility during the decarboxylation.

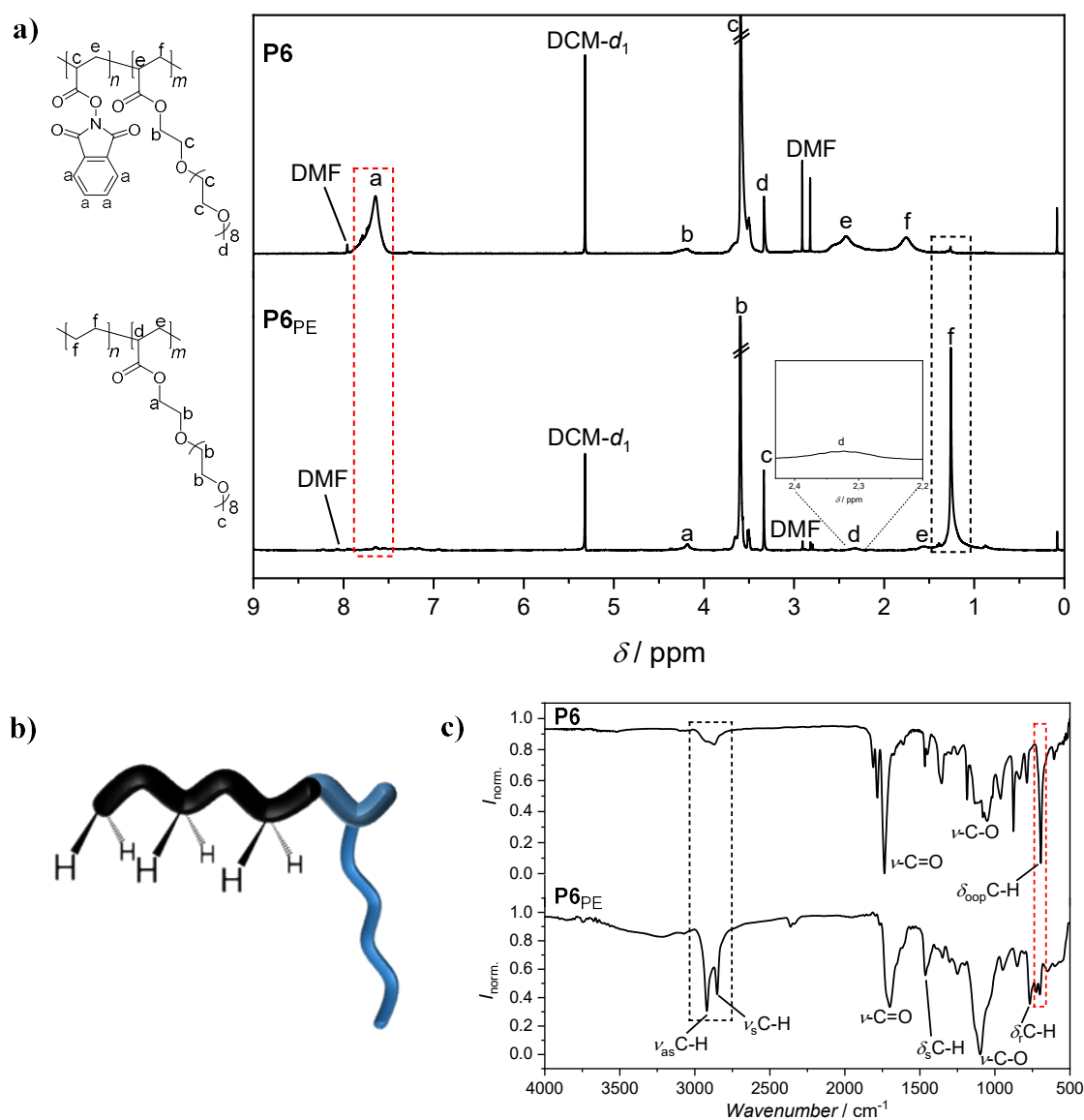


Figure 9: a) ^1H NMR spectra of PAP-*b*-POEGMEA (**P6**) and PE-*b*-POEGMEA (**P6_{PE}**) after photochemically-induced decarboxylation, b) schematic depiction of the block ratios of block copolymer **P6_{PE}**, with PE (black) and POEGMEA (blue) blocks and c) comparison of the ATR-FT-IR spectra before (top) and after (bottom) photochemically-induced decarboxylation.

As shown in **Figure 9a**, the comparison of the ^1H NMR spectra before and after the decarboxylation clearly demonstrated the formation of PE (intensive signal of CH_2 repeating units at 1.25 ppm marked in black). In addition, the quantitative removal of the aromatic proton signal of the phthalimide units can be clearly seen (marked in red). Furthermore, the signals of POEGMEA (4.2 ppm (COOCH_2), 3.7 ppm ($\text{CH}_2\text{CH}_2\text{O}$) and 3.2 ppm (CH_3)) proved the selectivity of the decarboxylation and the intact structure of the second block. ATR-FT-IR spectroscopy (**Figure 9c**) supported these findings revealing a quantitative decarboxylation, as shown by the removal of the aromatic $\delta_{\text{oop}}\text{C-H}$ vibration at 695 cm^{-1} (marked in red) and the arising signals originating from $\nu_{\text{as}}\text{C-H}$ (2923 cm^{-1}) and $\nu_{\text{s}}\text{C-H}$ (2849 cm^{-1}) vibrations (marked in black).

In the next step, SEC analysis of the decarboxylated polymer was planned to be conducted. However, even though the polymer was soluble in DMAc, it did not elute from the column and was not detected by the RI detector of the instrument. It was concluded, that this issue could result from the formation of agglomerates, which could not elute from the column due to their high hydrodynamic radius. To prove this theory, dynamic light scattering (DLS) in DMAc as solvent was conducted. Indeed, the analysis of the precursor polymer PAP-*b*-POEGMEA revealed a hydrodynamic radius R_h of only 4.9 nm, while the radius of the decarboxylated polymer PE-*b*-POEGMEA possessed a roughly 18 times greater value of $R_h = 91\text{ nm}$ (**Figure 10a**). Since the theoretical molar mass and thus the polymers' size drastically decreased (from $M_n, \text{P6} = 7600\text{ g mol}^{-1}$ (**P6**) to $M_n, \text{P6PE} \sim 2200\text{ g mol}^{-1}$ (**P6PE**) calculated by the removal of the molar mass of the phthalimide), such a phenomenon could only be explained by the former postulated formation of agglomerates. As PE itself is insoluble in DMAc, the formation of micelles with PE blocks in the centre and stabilized by POEGMEA on the micelles' surface seems to be energetically favored (schematically depicted in **Figure 10c**). Additionally, the formation of micelles from PE-based block copolymers was also demonstrated by Detrembleur *et al.*¹⁶ proving the conclusion drawn from the results.

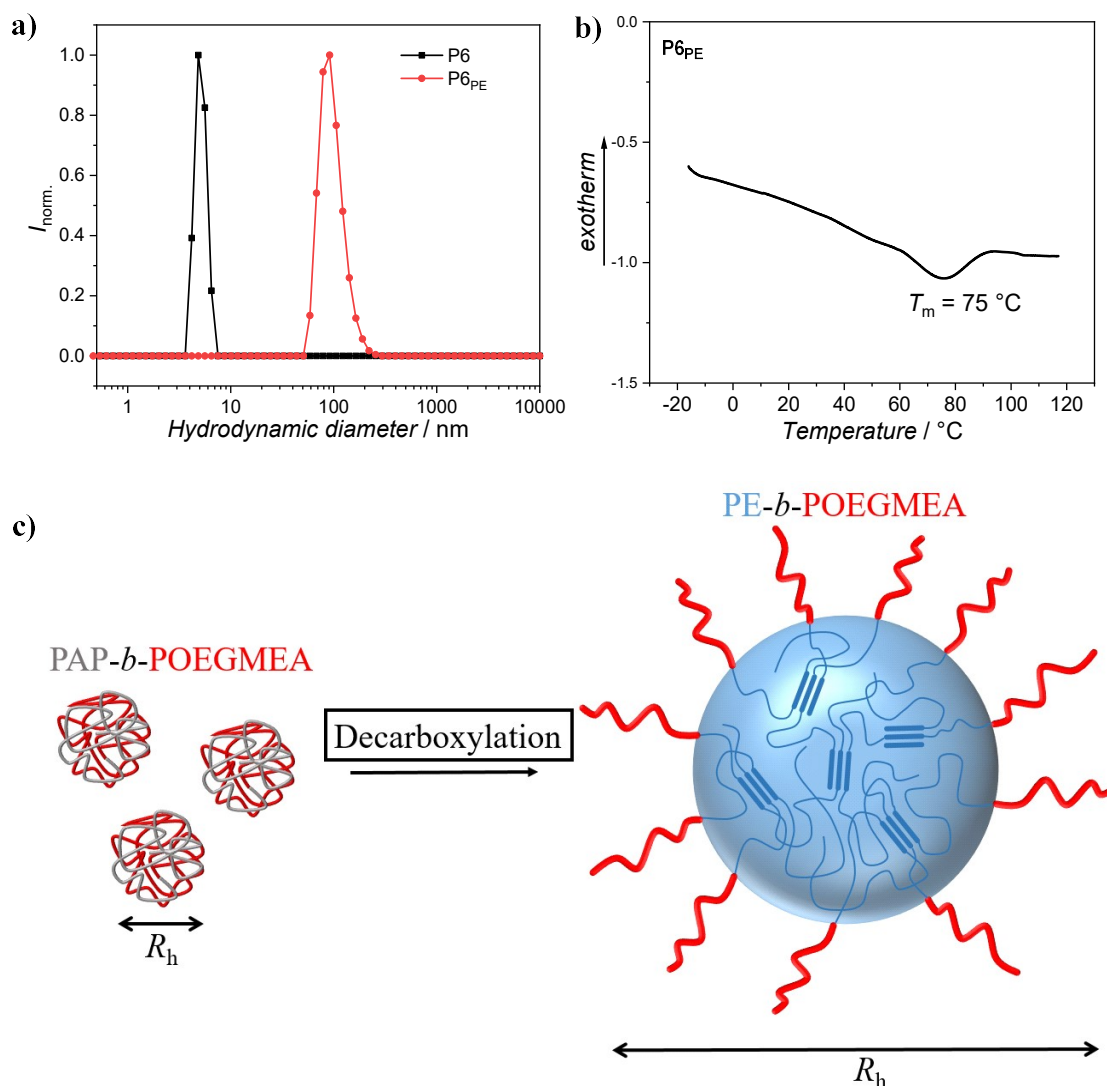
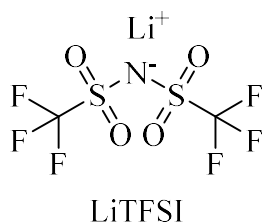


Figure 10: a) DLS analysis of PAP-*b*-POEGMEA (**P6**, black) and PE-*b*-POEGMEA (**P6_{PE}**, red) after photochemically-induced decarboxylation as well as b) DSC characterization of **P6_{PE}** after the addition of LiTFSI to favor the microphase separation and c) schematic depiction of the formation of agglomerates with partly crystalline PE in the core. As a result of the formation of agglomerates, the hydrodynamic radius R_h increases as demonstrated by DLS.

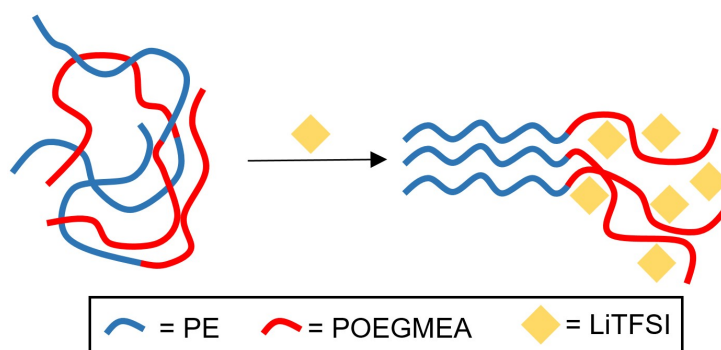
Furthermore, DSC analysis of **P6_{PE}** was performed to prove the formation of PE *via* detection of its melting point. However, as previously observed for **P5_{PE}** no melting point could be recorded. It was concluded that an insufficient phase separation of the two blocks (which is necessary to detect the thermal properties of both blocks separately) due to the short chain lengths of the blocks (especially the PE block) results in a hindered crystallization of PE caused by infiltration of the POEGMEA chains. Therefore, to increase the tendency of microphase

separation, lithium bis(trifluoromethanesulfonyl)imide salt (LiTFSI, **Scheme 31**) was added.



Scheme 31:
Structure of lithium bis(trifluoromethane sulfonyl)imide.

LiTFSI is a lithium salt that is primarily known from battery research, where it is used as a Li-ion source in battery electrolytes.¹²⁹ It is characterized by its good solubility in poly(ethylene glycol) (PEG), while it is insoluble in the PE phase due to its highly polar character. Upon addition the polarity of the POEGMEA phase is increased resulting in a stronger driving force regarding the separation of the PE and POEGMEA phases (**Scheme 32**). As shown in **Figure 10b**, this approach enabled the detection of a melting point at $T_m = 75\text{ }^\circ\text{C}$. However, the as-recorded T_m does not perfectly reach the expected T_m of $90 - 130\text{ }^\circ\text{C}$ for pure PE⁴ (depending on its molar mass). Thus, it was concluded that the necessity of adding LiTFSI in combination with the detection of a low melting point results from a comonomer fraction that hinders the crystallization to some extent. Since ¹H NMR and ATR-FT-IR spectroscopy proved the complete removal of phthalimide units it was considered that the comonomer fraction originates from an unknown side reaction.



Scheme 32: Schematic depiction of the effect of the LiTFSI addition. The salt accumulates exclusively in the POEGMEA phase, increasing the microphase separation and thus enables the crystallization of PE.

As stated in the beginning of the current chapter, polymer **P5_{PE}** with a higher OEGMEA content ($DP_{\text{OEGMEA}} = 34$ vs. $DP_{\text{PE}} = 20$) was analyzed *via* SEC in DMAc as eluent, which showed that the molar mass of the polymer slightly increased after decarboxylation even though it was expected to decrease due to the removal of the phthalimide groups and it was concluded that agglomeration would cause this observation. In contrast, SEC analysis of **P6_{PE}** could not be performed since the polymer did not elute from the column as stated before. To prove the

Results and Discussion

formation of agglomerates also for **P5_{PE}**, the polymer was analyzed *via* DLS. The comparison of the DLS results of **P5** with **P5_{PE}** revealed an increase of the hydrodynamic radius and proved the formation of agglomerates also for polymers with a higher OEGMEA content (**Figure 59**, and **Figure 60**).

The analysis of the thermal decarboxylation product with a comparable polymer (**P7**) revealed some parallels, but also differences. ¹H NMR spectroscopy clearly proved the formation of PE, as a signal of high intensity arose at 1.2 ppm, while the aromatic proton signal of the phthalimide could not be identified (**Figure 11b**).

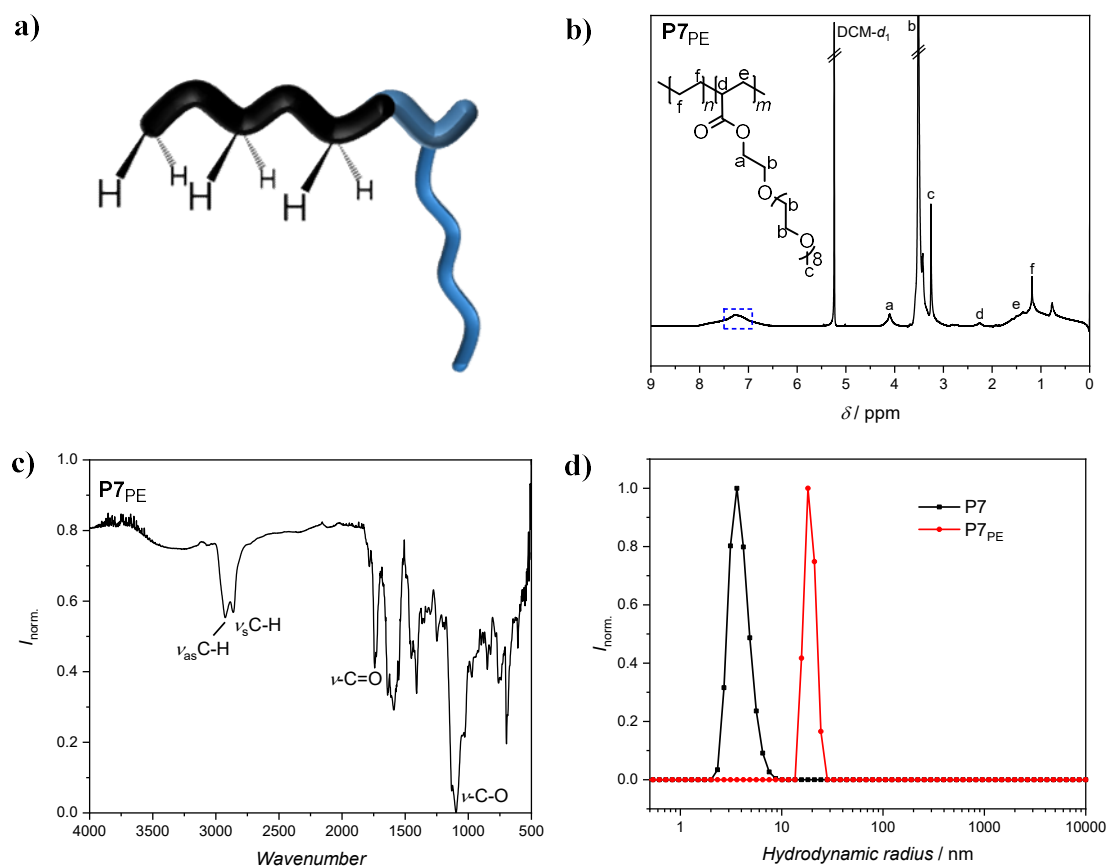
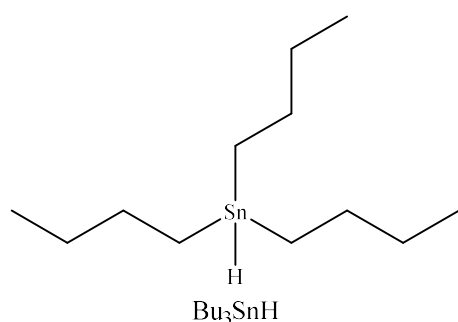


Figure 11: **a)** Schematic depiction of block ratios of block copolymer **P7_{PE}**, with PE (black) and POEGMEA (blue) blocks, as well as the analysis of **P7_{PE}** *via* **b)** ¹H NMR spectroscopy (additional, broad signal at 7.3 ppm marked in red), **c)** ATR-FT-IR spectroscopy, and the analysis of the block copolymers before and after decarboxylation by **d)** DLS.

Additionally, a broad signal at 7.3 ppm appeared after decarboxylation (marked in blue, aromatic signal of the phthalimide at 7.6 – 7.8 ppm), which was considered to result from

residuals of the catalytic system. ATR-FT-IR spectroscopy proved the removal of the signal arising from the vibration of the aromatic $\delta_{\text{oop}}\text{C-H}$ vibration (695 cm^{-1}), as well as the appearance of two signals at 2930 cm^{-1} ($\nu_{\text{as}}\text{C-H}$) and 2856 cm^{-1} ($\nu_{\text{s}}\text{C-H}$) arising from the vibration of CH_2 units (**Figure 11c**). The analysis of the molar mass and distribution by SEC in DMAc as eluent was not possible, since the solution could not be filtered before the measurement. However, DLS analysis showed the agglomeration of **P7PE** to result in a hydrodynamic radius of only $R_h = 18\text{ nm}$ (**Figure 11d**), in contrast to $R_h = 91\text{ nm}$ for the photochemically decarboxylated polymer (**P6PE**). Noteworthy, DSC analysis of **P7PE** neither revealed a melting nor a crystallization point with or without the addition of LiTFSI. It was considered that side reactions resulted in a comonomer fraction that hinders i) the formation of agglomerates as the low hydrodynamic radius demonstrated and ii) the crystallization of the PE block. In comparison to the results of the photochemical decarboxylation of **P6**, the thermally-induced decarboxylation seemed to yield worse results. This led to the conclusion that either the same side reaction occurred to a higher extent, or additional side reactions resulted in an additional comonomer fraction as further evaluated in the following.

The observation of a low melting point ($T_m = 75\text{ }^\circ\text{C}$) in combination with the necessity to add



Scheme 33: Structure of tributyltin hydride.

a salt to further drive the microphase separation in the case of the photochemical decarboxylation led to the consideration that a small comonomer fraction originating from an unknown side reaction hindered the crystallization. Furthermore, the analysis of the photochemically-induced decarboxylation in the next project (**Chapter 4.2.2**) *via* ^1H NMR spectroscopy revealed an impurity in the aromatic region, which could not originate from the phthalimide due to its different shift ($\delta_{\text{phthalimide}} = 7.7\text{ ppm}$ *vs.* $\delta_{\text{impurity}} = 7.3\text{ ppm}$). From the subsequent variation of the reactants and reaction conditions it was concluded that a not further evaluated side reaction of the H-donor phenylsilane caused the formation of a small comonomer fraction hindering the crystallization. Therefore, the H-donor phenylsilane was exchanged by tributyltin hydride (Bu_3SnH , **Scheme 33**) to reduce side reactions comprising phenylsilane (details in **Chapter 4.2.2**). In the following, polymer **P8** with a block ratio of 24:10 (NAP:OEGMEA) was photochemically decarboxylated in the presence of tributyltin hydride instead of phenylsilane (**Figure 12a**). While the ^1H NMR and ATR-FT-IR spectra showed similar results as before (intact nature of the second block as well as the

Results and Discussion

formation of CH₂ with signals intensity according to the block ratio), DLS analysis revealed an even higher hydrodynamic radius of $R_h = 307$ nm ($R_{h, P6PE} = 90$ nm).

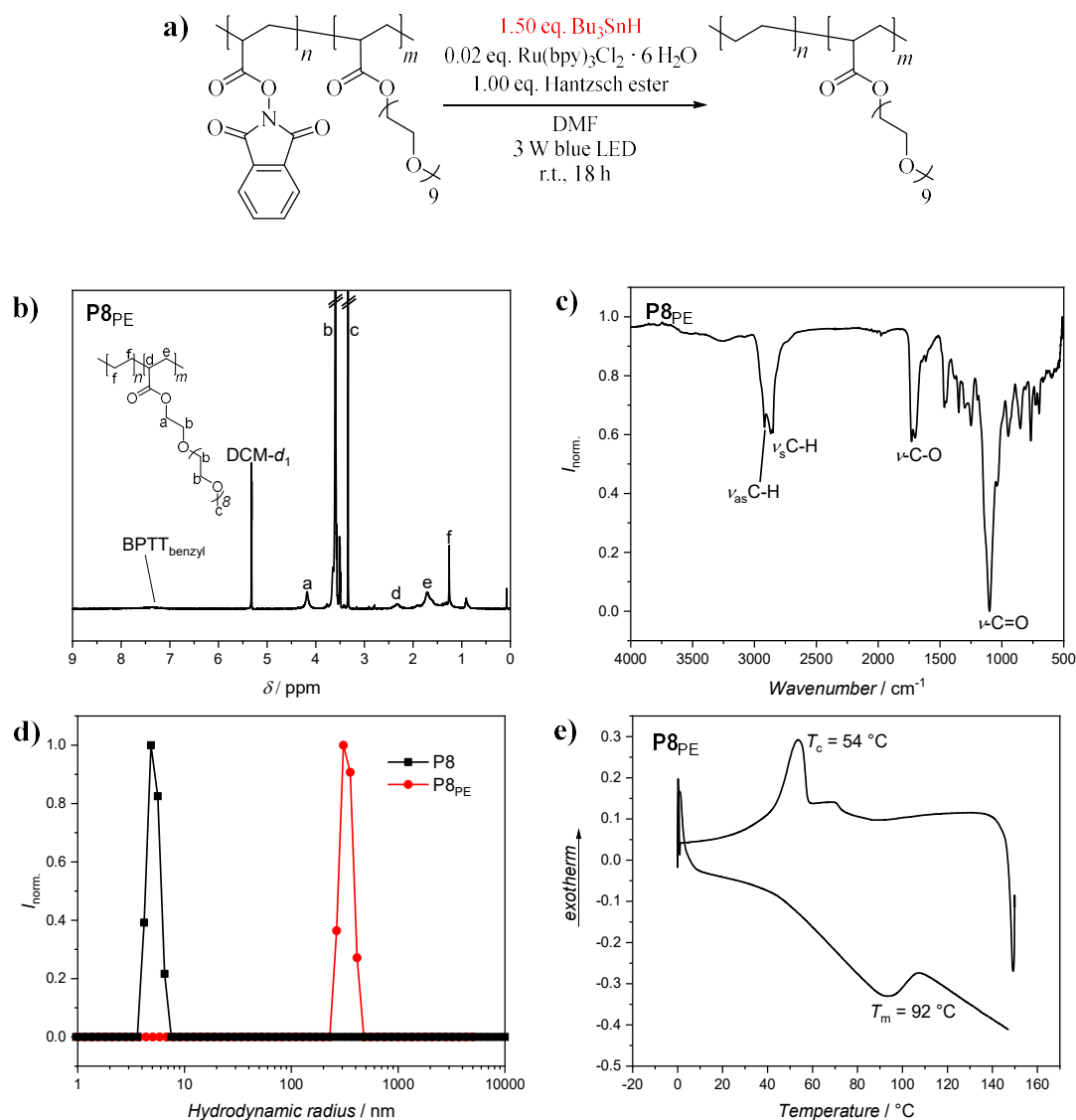
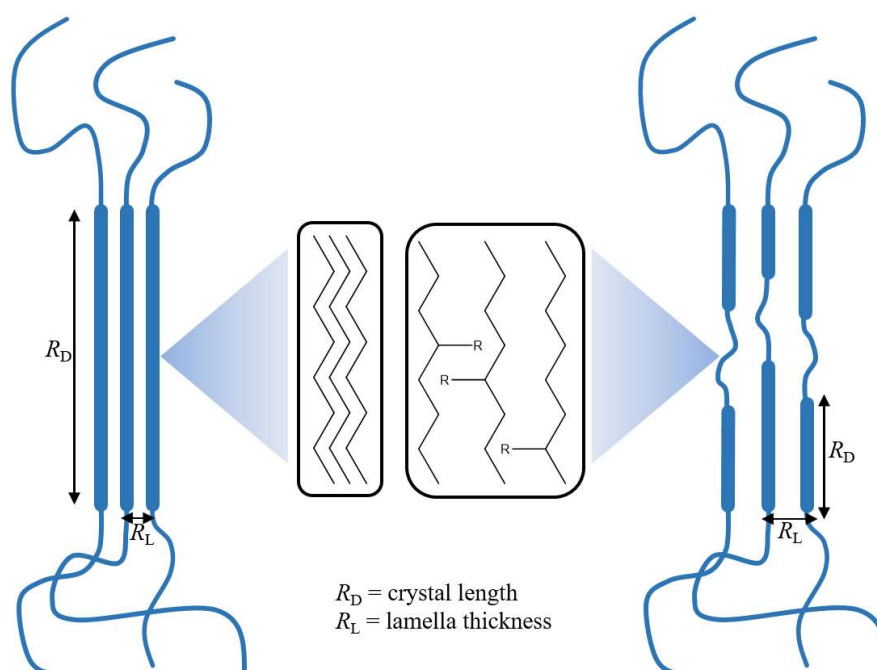


Figure 12: a) Photochemical decarboxylation of PAP-*b*-POEGMEA (**P8**) with tributyltin hydride and the analysis of **P8PE** via b) ¹H NMR spectroscopy, c) ATR-FT-IR spectroscopy, d) DLS and e) DSC revealing $T_m = 92$ °C and $T_c = 54$ °C.

Most importantly, DSC analysis detected a melting point at $T_m = 92$ °C and a crystallization ($T_c = 54$ °C) of the PE chain without further addition of lithium salt proving the successful formation of PE-*b*-POEGMEA. It should be noted that the still comparatively low T_m is caused by the short chain length of the PE, as additionally proven. Thus, commercial PE with a low molar mass (Polyethylene, Sigma Aldrich, average $M_n \sim 7700$ g mol⁻¹, 427799-250G)

purchased from Sigma Aldrich was analyzed *via* DSC and a melting point of $T_m = 94\text{ }^\circ\text{C}$ was detected (**Figure 76**), matching the T_m of the PE block of **P8_{PE}**.

These results, as well as the results evaluated in the next chapter (**Chapter 4.2**), proved the consideration that phenylsilane caused side reactions resulting in the formation of a small comonomer fraction of unknown nature. As concluded, the comonomer fraction caused the lower melting point and the necessity to add a salt to force the phase separation. By exchanging phenylsilane with tributyltin hydride, the formation of this comonomer fraction could be prevented and pure PE was obtained as depicted in **Scheme 34**.



Scheme 34: Schematic depiction of the crystallinity of PE-*b*-POEGMEA after decarboxylation with H-donor Bu_3SnH (left) and hindered crystallization of the PE block due to a small comonomer fraction after the decarboxylation with PhSiH_3 (right). Reduced crystal length (R_D) and increased lamella thickness (R_L) resulting in a decreased crystal size marked.

Since the exchange of phenylsilane with tributyltin hydride successfully improved the results of the photochemical decarboxylation, the thermally-induced decarboxylation of PAP-*b*-POEGMEA (**P9**) with tributyltin hydride as H-donor should be evaluated. Contrary to the expectations, the exchange of the H-donor did not improve the decarboxylation result (**Figure 13**). The ^1H NMR spectrum of **P9_{PE}** still showed a drastic broadening of the signals. While the DLS analysis revealed an increased hydrodynamic radius of $R_h = 95\text{ nm}$ in comparison to the

Results and Discussion

DLS analysis of **P7_{PE}** ($R_h = 18$ nm) (**Figure 13d**), a melting or crystallization of the PE block could not be detected in the analyzed temperature range *via* DSC (**Figure 13e**).

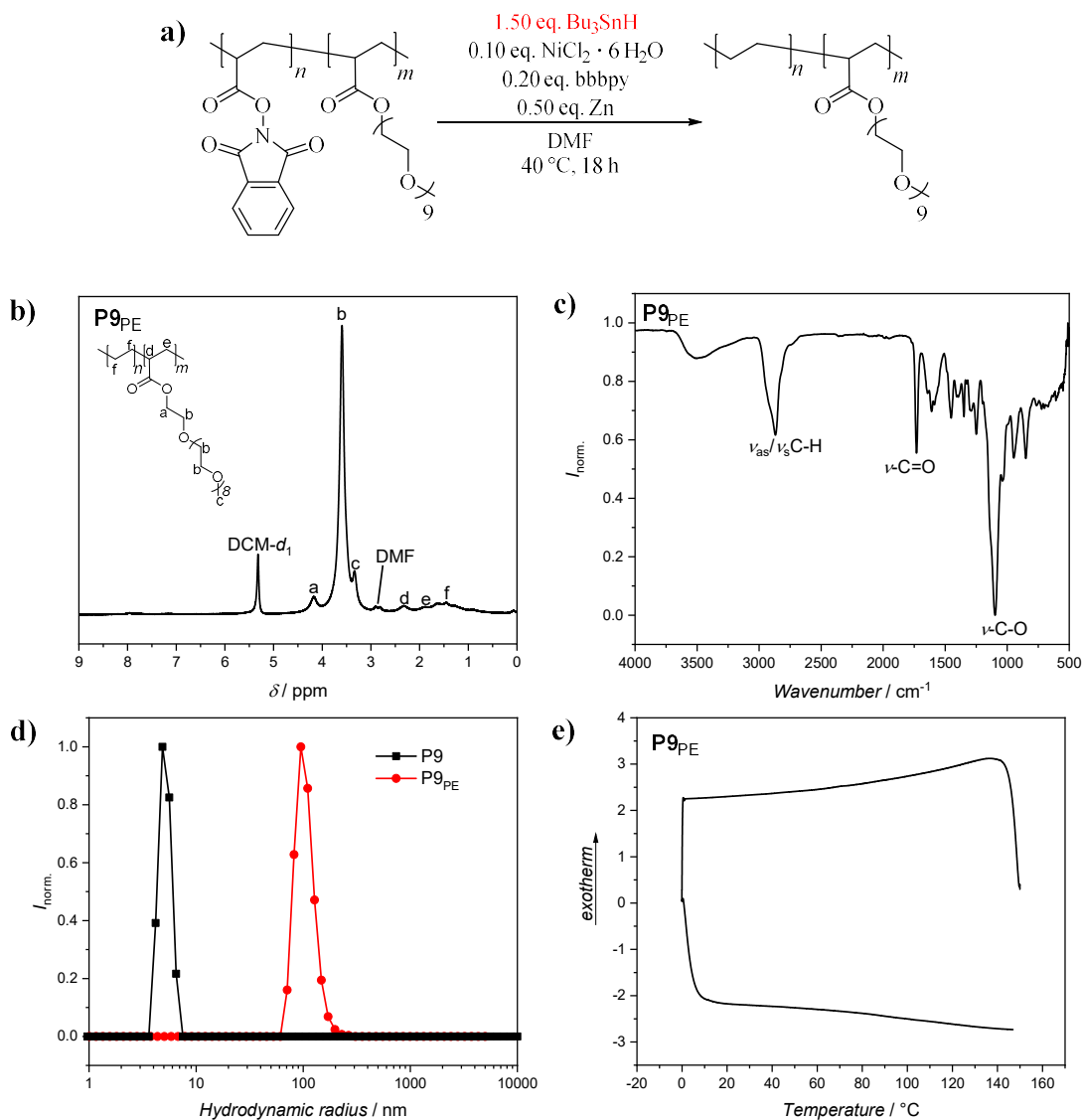


Figure 13: a) Thermal decarboxylation of **P9** with tributyltin hydride and the analysis of **P9_{PE}** via b) ^1H NMR spectroscopy, c) ATR-FT-IR spectroscopy, d) DLS, and e) DSC, which did not reveal a melting or crystallization of the material.

Since the replacement of the H-donor did not lead to a great improvement of the result of the thermal decarboxylation (especially the thermal analysis), the polymer was further purified to remove impurities originating from the catalytic system. It was considered, that residuals of the catalyst would lead to the poor results since the polymer exhibited a green color probably originating from the Ni-catalyst. Generally, the polymers were precipitated several times in diethyl ether and dried under reduced pressure after decarboxylation. For further purification,

dialysis with a prewetted Spectra Pro dialysis membrane (molecular weight cut-off (MWCO) = 1000 g mol⁻¹) was initially performed in DCM, subsequently also in a 1:1 DCM/DMSO mixture, however, both did not remove the impurities. Furthermore, it was tried to pass the polymer through basic aluminium oxide. Since even the purification by dialysis or filtration did not remove the impurities, the former stated conclusion that residuals of the catalytic system caused the poor results was dismissed. Further, it was proven that the catalytic system caused additional side reactions resulting in the formation of an additional comonomer fraction (to the one caused by phenylsilane). As a consequence, the examination of the thermal decarboxylation method was not further pursued.

After the reaction conditions of the photochemical decarboxylation were adjusted and optimized to yield PE block copolymers, the reaction kinetics were examined in more detail. Okada *et al.*^{111,114} stated a reaction time of 2 h of the photochemical decarboxylation of the organic phthalimide ester, while Zheng *et al.*¹¹³ stated to observe full conversion after 24 h. Initially, the decarboxylation of PAP polymers was performed overnight (18 h) which gave full conversion as demonstrated by the former results. To obtain a more detailed understanding and idea about the kinetics of the decarboxylation, the reaction was analyzed using reaction monitoring with polymers **P8** and **P9**. It was found that the photochemical decarboxylation proceeded at a high reaction rate and the reaction thus featured quantitative conversion after only 30 min under the selected conditions (reactants, concentration, solvent, **Figure 64**). Thus, the reaction seemed to proceed faster than Zheng *et al.*¹¹³ observed, however they did not examine the kinetics in detail. Additionally, the kinetics of the thermal decarboxylation were examined. Baran *et al.*¹²⁵ stated a reaction time of the Ni-catalyzed decarboxylation of 1 h for full conversion. The evaluation of the kinetics of the thermal decarboxylation revealed a reaction time of 30 min, similar to the one of the photochemical decarboxylation (and **Figure 65**).

To demonstrate that other comonomers than OEGMEA are suitable to provide solubility during the decarboxylation process, the monomer MEA was employed for the synthesis of PAP-*b*-PMEA (**P10**) and used for decarboxylation to successfully yield PE-*b*-PMEA block copolymers as shown in **Figure 14**. The quantitative removal of the aromatic phthalimide protons (marked in black) as well as an arising signal of CH₂ repeating units (marked in red) was proven by ¹H NMR spectroscopy (**Figure 14a**).

Results and Discussion

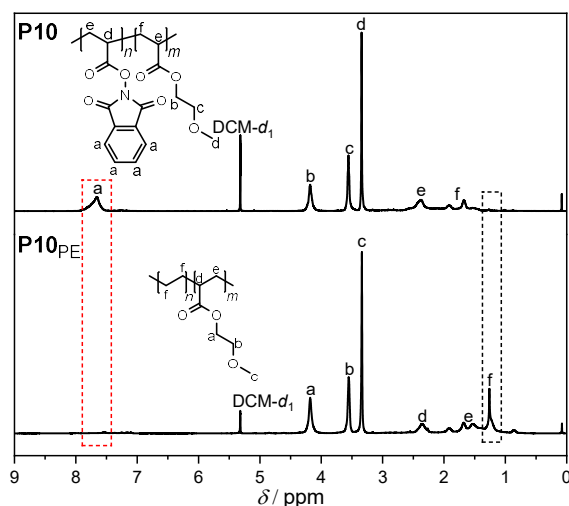


Figure 14: Comparison of the ^1H NMR spectra of **P10** (top) and **P10_{PE}** (bottom). The removal of the aromatic proton signal is marked in red, while the arising signal of PE is marked in black.

The polymer was further analyzed by ATR-FT-IR spectroscopy (**Figure 15**). The comparison of the spectra of **P10** and **P10_{PE}** revealed a disappearance of the $\delta_{\text{oop}}\text{C-H}$ vibration (670 cm^{-1} , marked in red) and an increased intensity of the signals of the $\nu_{\text{as}}\text{C-H}$ (2940 cm^{-1}) and $\nu_{\text{s}}\text{C-H}$ (2890 cm^{-1}) vibration, stating the successful decarboxylation and formation of PE.

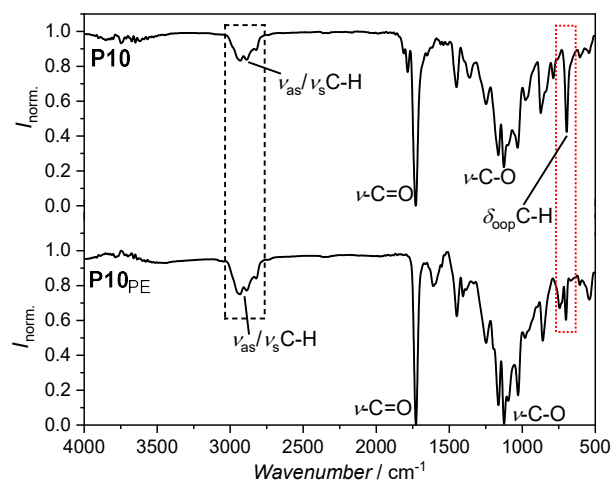


Figure 15: Comparison of the ATR-FT-IR spectra of **P10** (top) and **P10_{PE}** (bottom). The removal of the $\delta_{\text{oop}}\text{C-H}$ vibration is marked in red, while the arising signal of the C-H vibration of PE is marked in black.

Furthermore, the intensity of the signals of the ν -C=O (1730 cm^{-1}) and ν -C-O (1120 cm^{-1}) vibration of PMEA decreased as expected. The decarboxylation of PAP-*b*-PMEMA (**P11**) was also performed with the thermal decarboxylation method. The analysis of the obtained polymer **P11**_{PE} via ^1H NMR and ATR-FT-IR spectroscopy revealed comparable results to the thermal decarboxylation of PAP-*b*-POEGMEA block copolymers. In the ^1H NMR spectrum, a broadening of the signals was observed, while the intensity of the PE signal (1.23 ppm) was rather low (**Figure 67**). However, the ATR-FT-IR spectrum indicated a quantitative conversion of the PAP units by a complete removal of the δ_{oop} C-H vibration (690 cm^{-1} , **Figure 68**).

The direct comparison of the two decarboxylation methods revealed that the photochemical method is clearly superior to the thermal one, due to the following advantages: i) the PE obtained by the photochemical decarboxylation had a significantly higher purity and side reactions that could result in a comonomer fraction were not observed when tributyltin hydride was employed. ii) Furthermore, the process itself is simpler since only the H-donor and the polymer had to be dissolved, deoxygenated and added separately to the reaction flask, while for the thermal method the catalyst had to be dissolved and mixed with the ligand in an additional step. iii) Nickel(II) chloride, which was the basis of the catalyst of the thermal method, is both toxic and carcinogenic, while the reactants of the photochemical method (with the exception of Bu_3SnH) are far less toxic. The only disadvantage of the photochemical method is the increased effort due to the photoreaction itself resulting in a more complex practical setup (see **Chapter 6.1.7** for more details), which was required due to additional safety measures using high power LEDs. Furthermore, the setup only allowed for the temperature to be adjusted to a limited extent. Nevertheless, the photochemical method was clearly preferred and used in the further course of this thesis.

In the following paragraph the photochemical decarboxylation approach should be compared to other controlled synthesis methods for PE block copolymers. The central aspect of the present chapter was the development of an ethylene-free and controlled synthesis procedure for PE polymers and thus to circumvent employing ethylene gas and handling a flammable, gaseous component, which represents the greatest advantage of this method. As a disadvantage the low atom economy of the approach could be mentioned. This results from the removal of the phthalimide (representing 80% of the molar mass of the PAP block). Methods based on ethylene gas generally do not feature a comparable low atom economy depending on the conversion of the monomer during the polymerization. Nevertheless, the recovery of the phthalimide after the precipitation should be possible as demonstrated in organic chemistry,¹¹¹ but was not examined

Results and Discussion

in the course of the present thesis. Besides those central aspects related to the ethylene-free approach, further advantages and disadvantages in comparison to other techniques should be pointed out in the following. A well-known approach for the synthesis of PE block copolymers is the cobalt-mediated radical polymerization (CMRP) as demonstrated by Detrembleur *et al.* in 2019 (see **Chapter 2.3** for details).¹⁶ In contrast to the presented decarboxylation approach, this method suffers from coupling reactions resulting in the formation of a mixture of diblock and triblock copolymers (unimodal SEC data of PE from decarboxylation provided in **Chapter 4.2.2**). Furthermore, the full control over the polymerization of ethylene was not obtained as stated by the authors and the choice of comonomers is mostly limited to vinyl acetate (VAc). Contrary, the control of the RAFT polymerization of the precursor monomer NAP as well as the controlled chain extension with OEGMEA and MEA was demonstrated. Besides those two monomers, other comonomers such as styrene or methyl acrylate should also be suitable for the block copolymerization. In a different study, Scott *et al.* demonstrated an approach based on classic Kaminsky catalysts ($\text{ZrCp}_2\text{Cl}_2/\text{MAO}$ (methylaluminoxane), see **Chapter 2.3** for details).⁶¹ They introduced the synthesis of PE block copolymers with styrene or acrylates (*n*-butyl acrylate, methyl methacrylate) as comonomers in high yields. However, the authors observed various side reactions during the polymerization of *n*-butyl acrylate such as backbiting, β -scission, chain transfer, high dispersities when targeting high yields, and an increased effort for the purification of the block copolymers such as PE-*i*-DIB-*b*-PMMA (purification by Soxhlet extractor) was necessary. In contrast, the decarboxylation approach features less side reactions, less demand for purification and a predefined architecture. Thus, the controlled synthesis of PE by the photochemical decarboxylation of PAP represents an alternative method with advantages over established procedures based on ethylene gas.

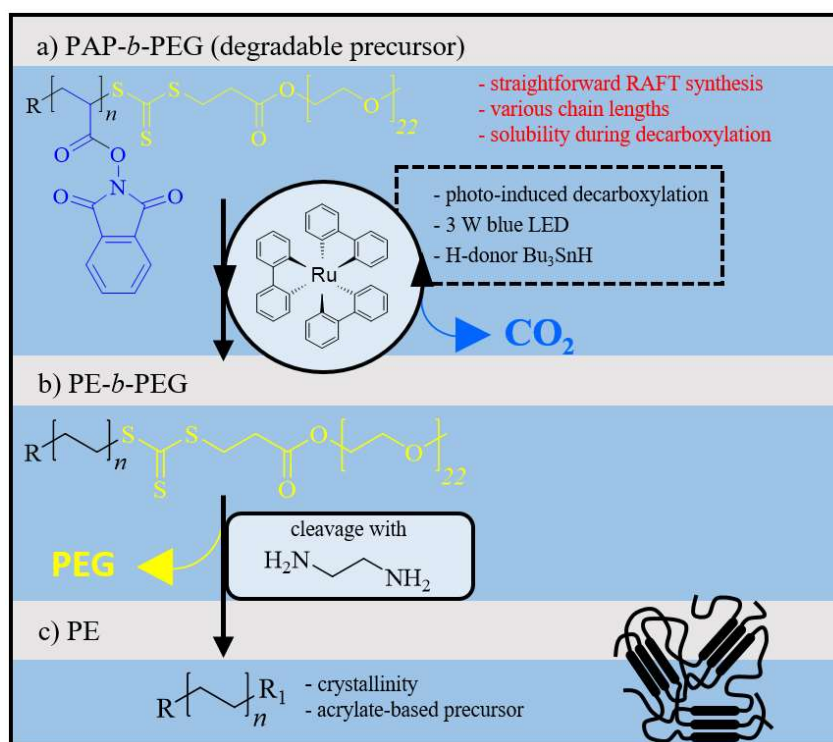
4.1.5 Recapitulation

In summary, the decarboxylation of different polymer systems based on the phthalimide activated ester *via* both a photochemical and a thermal decarboxylation method was studied and both methods independently evaluated in regards to their suitability to yield PE polymers. The decarboxylation of PAP homopolymers synthesized by FRP led to the consideration that the polymer lacks solubility during the reaction. This consideration was proven by employing a copolymer with OEGMEA as comonomer for decarboxylation, demonstrating the necessity to enable the solubility of the polymer during decarboxylation. Therefore, the adaption of the decarboxylation method towards PE homopolymers was postponed and further investigated in the following chapter (**Chapter 4.2**). Thus, the focus was laid on block copolymers in the first

project, which should enable a quantitative decarboxylation by providing solubility. RAFT polymerization was chosen for the synthesis of PAP block copolymers, and subsequently the chain lengths and ratios of two employed comonomers, OEGMEA and MEA, as well as of NAP were varied and a library of block copolymers was synthesized. In the following, both decarboxylation methods were used to yield PE block copolymers. All polymers were analyzed by various characterization techniques, such as ^1H NMR spectroscopy, ATR-FT-IR spectroscopy, DLS and DSC. Especially the DSC results indicated the formation of a comonomer fraction during the decarboxylation. For the photochemical decarboxylation, the H-donor phenylsilane was found as the source of this side reaction (see also **Chapter 4.2.2**), while for the thermal decarboxylation additional side reactions occurred. By exchanging the H-donor to tributyltin hydride, the formation of PE block copolymers by photochemical decarboxylation of the PAP precursor polymers was successfully conducted. This first combination of a RAFT polymerization of an acrylate monomer with an efficient decarboxylation strategy for PPM opens the synthetic avenue toward unprecedented polyethylene copolymers and block copolymers. Yet, the current state of the methodology is clearly limited to low molar mass PE copolymers and block copolymers. Furthermore, the photochemically-induced method is preferred over the thermally-induced method since less toxic reagents, *e.g.*, nickel(II) chloride are used and less side reactions were observed.

4.2 Synthesizing Polyethylene from Polyacrylates: A Decarboxylation Approach

The second project arose from the first project, as soon as the successful synthesis of the block copolymers was established and it became obvious that the lack of solubility limits the quantitative decarboxylation of PAP homopolymers. As the decarboxylation of PAP-*b*-POEGMEA (**P6**, $DP_{\text{OEGMEA}} = 3$, **Chapter 4.1.4**) demonstrated, already a low molar mass fraction of PEG provides sufficient solubility for the block copolymer during decarboxylation. Thus, the idea to synthesize a degradable block copolymer yielding pure PE after degradation was developed. The requirements for the degradable block copolymer were i) a straightforward synthesis of the polymer, ideally with RAFT polymerization, ii) sufficient solubility of the polymer during the decarboxylation, and iii) a simple and efficient cleavage of the sacrificial block as shown in **Scheme 35**.



Scheme 35: Overview of the project idea to obtain pure PE from **a)** a soluble, degradable block copolymer which can be quantitatively decarboxylated to yield **b)** a degradable PE block copolymer which can be cleaved to yield **c)** PE.

Therefore, a macroRAFT agent based on a well-soluble PEG block (**Scheme 35**, marked in yellow) was used for the RAFT polymerization of NAP (blue) to obtain the degradable

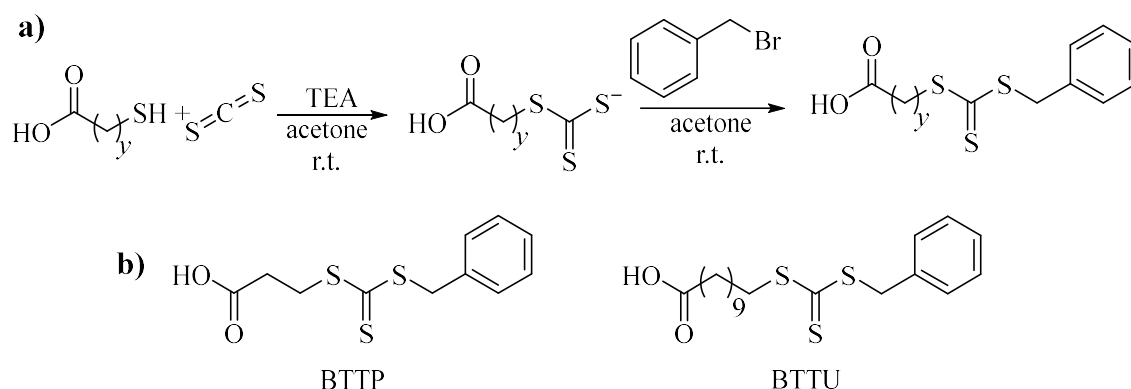
precursor polymer PAP-*b*-PEG (**Scheme 35a**). Additionally, RAFT polymerization allows for the synthesis of a defined precursor and thus of predefined PE and a predictable molar mass. The sacrificial block copolymer is then used in a decarboxylation step to obtain PE-*b*-PEG (**Scheme 35b**). Herein, solubility provided by the PEG block allows for a quantitative decarboxylation. In the last step, PE-*b*-PEG is cleaved at the trithiocarbonate and/or ester junction, the PEG block can be removed by washing and pure PE is obtained (**Scheme 35c**).

Parts of this chapter and the corresponding parts in the experimental section were adapted with permission from a publication written by the author (Stefan Frech).¹³⁰

Results and Discussion

4.2.1 Synthesis of Poly[*N*-(acryloyloxy)phthalimide]-*block*-Poly(ethylene glycol)

First, a suitable design of the macroRAFT agent for the polymerization of NAP had to be found. It was intended to build the macroRAFT transfer agent on the same structural motif as the previously employed RAFT agent BPTT, since it featured a suitable reactivity and provided good control over the polymerization of NAP. Further, the basic structure should be extended by a PEG chain, which provides solubility during the decarboxylation and linked in a way, which enables the cleavage in a second step. Since the reactivity of the leaving group of the RAFT agent (benzyl) is critical for the control, it was planned to attach the PEG chain to the stabilizing moiety of the RAFT agent. This position additionally offers the possibility to cleave the PEG chain *via* aminolysis of the trithiocarbonate. In order to easily link the PEG chain to the RAFT agent, the latter one should be functionalized with an acid functionality to enable the esterification with poly(ethylene glycol) methyl ether (mPEG₁₀₀₀) forming a macroRAFT transfer agent with an additional cleavable ester next to the trithiocarbonate junction. To do so, two different RAFT agents with a terminal carboxylic acid functionality were synthesized as shown in **Scheme 36**. At first, 3-(((benzylthio)carbonothioyl)thio)propanoic acid (BTTP) was synthesized with 3-mercaptopropanoic acid as thiol. For the synthesis of the second RAFT agent 11-(((benzylthio)carbonothioyl)thio)undecanoic acid (BTTU), 11-mercaptoundecanoic acid was employed as the thiol. Subsequently, both were used for the polymerization of NAP to test their suitability.



Scheme 36: **a)** Synthesis of the basic structure of the RAFT agents and **b)** detailed structure of the RAFT agents 3-(((benzylthio)carbonothioyl)thio)propanoic acid (BTTP) and 11-(((benzylthio)carbonothioyl)thio)undecanoic acid (BTTU) evaluated for the synthesis of the degradable PAP block copolymers.

Since the study in the former chapter (**Chapter 4.1**) showed that a small number of OEGMEA units already improved the solubility of the block copolymer significantly, mPEG₁₀₀₀ was chosen for the synthesis of the macroRAFT agent. Due to superior results of the polymerization (lower dispersity) and the less bulky structure, BTTP was chosen and converted by Steglich esterification with mPEG₁₀₀₀ to yield the macroRAFT agent BTTP-mPEG₁₀₀₀ (**Figure 16a**).

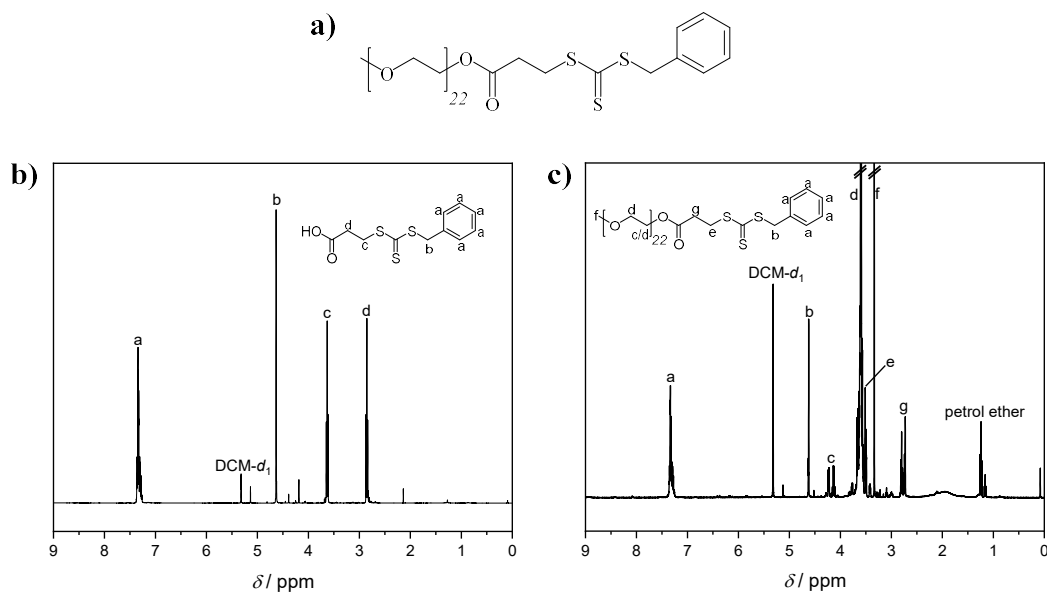


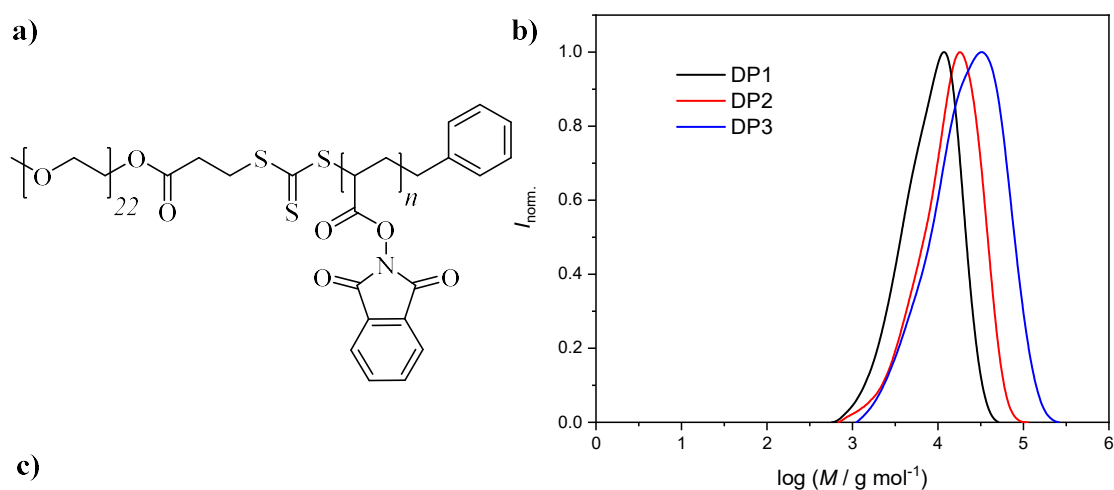
Figure 16: a) Structure of the macroRAFT-agent BTTP-mPEG₁₀₀₀ and the ¹H NMR spectra of b) BTTP and c) BTTP-mPEG₁₀₀₀.

Additionally, BTTP was esterified with mPEG₂₀₀₀ and polymerized with NAP (SEC shown in **Figure 69**). It was intended that the longer PEG chain (44 units *vs.* 22 units) would allow for the synthesis of a longer PE chain, since an increased solubility should be provided in comparison to the shorter PEG chain. This RAFT agent, however, did not control the polymerization and an asymmetrical SEC chromatogram was obtained. Therefore, this approach was dismissed and all further polymerizations were conducted using BTTP-mPEG₁₀₀₀.

Next, NAP was polymerized with BTTP-mPEG₁₀₀₀ to obtain a series of block copolymers PAP-*b*-PEG (**DP1-DP4**, **Figure 17a**) ranging from 5900 – 14000 g mol⁻¹ and with a corresponding degree of the polymerization of $DP = 20 - 60$, as shown **Figure 17**. Different degrees of polymerization were chosen to prove the possibility to predefine the molar mass of PE by comparison of the molar mass of the precursor with the obtained PEs. It is crucial to note, that

Results and Discussion

for the polymer with the highest DP (**DP3**), 500 equivalents of NAP were used in the polymerization resulting in degree of 60 units in the polymer chain, clearly proving the limit of the method. Polymers **DP1** to **DP3** were used for the photochemical decarboxylation while **DP4** was used for additional experiments and evaluation of the thermal decarboxylation method.



Entry	Polymer	M_n^* [g mol ⁻¹]	D^*	M_n^\dagger [g mol ⁻¹]	DP^\dagger	$M_{n, \text{theo}}$ [g mol ⁻¹]	conv.^\dagger [%]
1	DP1	5900	1.74	5829	21	5612	98
2	DP2	9400	1.90	9301	37	12122	74
3	DP3	13700	2.37	14292	60	109772	20
4	DP4	5200	1.81	5672	20	5612	95

*calculated by SEC with DMAc as eluent; † calculated by ¹H NMR spectroscopy, conv. = conversion.

Figure 17: **a)** Structure of the precursor polymer PAP-*b*-PEG and **b)** the SEC chromatograms of the three different polymers **DP1-3** in DMAC as eluent and PMMA calibration and **c)** overview of the molar masses of the precursor polymers.

4.2.2 Photochemical Decarboxylation of Poly[*N*-(acryloyloxy)phthalimide]-*block*-Poly(ethylene glycol)

The evaluation of the synthesis of pure PE by the above-mentioned strategy was started after the first results of the decarboxylation of block copolymers (**P6**, Chapter 4.1.4) were obtained. Those results indicated, that already a low molar mass fraction of PEG is sufficient to solubilize the block copolymer during the decarboxylation and, furthermore, that the photochemical decarboxylation method is superior to the thermal one. Thus, the second project mainly focuses on the photochemical decarboxylation. Additionally, the optimization of the reaction conditions for both projects (Chapter 4.1.4 and the current project) was mainly conducted on the degradable block copolymer system, although the formation of the comonomer fraction was already discovered in Chapter 4.1.4. Due the higher phthalimide content of the degradable precursor block copolymers (especially **DP2** and **DP3**), the intensity of the signals of the comonomer fraction resulting from a side reaction during the decarboxylation was higher in the ^1H NMR spectra and thus the influence of the variation of the reaction parameters could be analyzed in greater detail as demonstrated in the following.

After the successful synthesis of the three different polymers **DP1-3** with increasing chain lengths of the PAP chain, the photochemically-induced decarboxylation under standard conditions (1.50 eq. phenylsilane, 0.02 eq. $\text{Ru}(\text{bpy})_3\text{Cl}_2 \cdot 6 \text{H}_2\text{O}$, 1.00 eq. of HE, 3 W blue LEDs) was conducted (Scheme 37).



Scheme 37: Photochemical decarboxylation of PAP-*b*-PEG with phenylsilane as H-donor to yield PE-*b*-PEG.

The obtained block copolymers featured a good solubility of **DP1_{PE}** and **DP2_{PE}** and a worse but still sufficient solubility of **DP3_{PE}**. Subsequently, all polymers were analyzed by ^1H NMR, ATR-FT-IR spectroscopy, and DSC. In **Figure 18a** the exemplary comparison of the ^1H NMR spectra before (PAP-*b*-PEG, **DP2**, top) and after (PE-*b*-PEG, **DP2_{PE}**, bottom) the decarboxylation of **DP2** is presented. The formation of PE during the decarboxylation could be

Results and Discussion

clearly identified in the ^1H NMR spectrum by a new signal arising at ~ 1.2 ppm (**Figure 18a**, bottom), and the disappearance of the backbone signals of PAP (marked in black) as well as of the aromatic proton signals (marked in red). Noteworthy, the signals of the PEG chain could still be identified in the spectrum after the decarboxylation at 4.24 ppm (COOCH_2), 3.5 ppm (OCH_2CH_2) and 3.2 ppm (CH_3), respectively, stating that PAP was successfully decarboxylated while the overall block copolymer architecture stayed intact, yet being converted from PAP-*b*-PEG to PE-*b*-PEG.

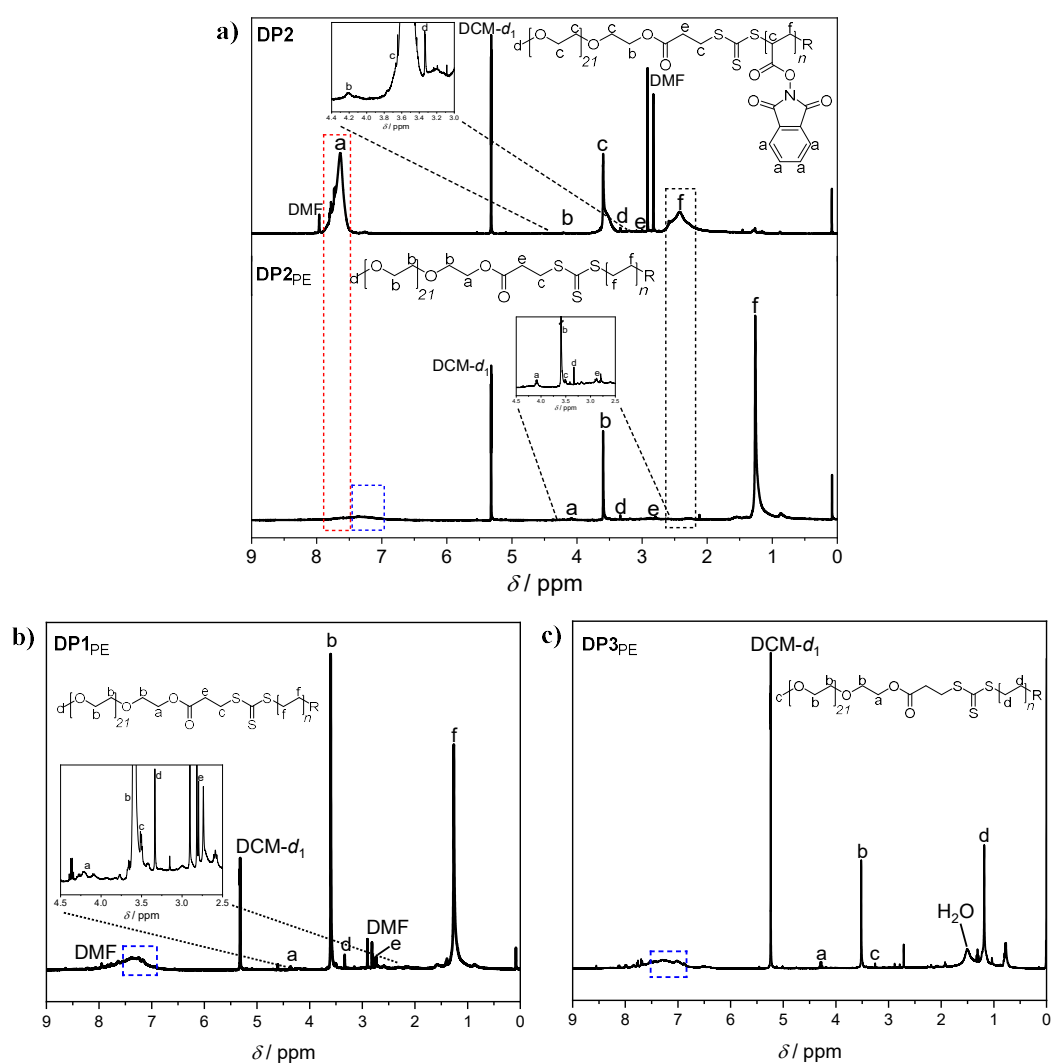
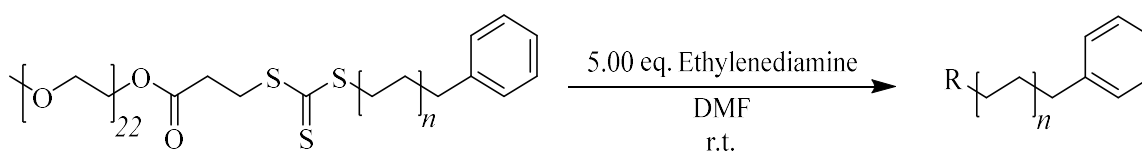


Figure 18: a) Comparison of the ^1H NMR spectra of DP2 before (top) and after (DP2_{PE}, bottom) the decarboxylation. b) ^1H NMR spectrum of DP1_{PE}. c) ^1H NMR spectrum of DP3_{PE}.

Beside those expected signals an additional, broad signal of low intensity at 7.3 ppm (marked in blue) could be identified in the ^1H NMR spectrum after the decarboxylation for all three polymers (**Figure 18a, b, and c**), indicative for an unknown but noticeable side reaction as further analyzed in the following. Nevertheless, ATR-FT-IR spectroscopy confirmed the removal of the active ester as seen by the disappearance of the $\nu\text{-C=O}$ vibration of the phthalimide active ester at 1734 cm^{-1} and the appearance of new signals at 2921 cm^{-1} ($\nu_{\text{as}}\text{C-H}$), 2848 cm^{-1} ($\nu_{\text{s}}\text{C-H}$), while the signal of the $\nu\text{-C-O}$ vibration (1049 cm^{-1}) of PEG could be identified stating that the overall polymer composition stayed intact (**Figure 19a, middle**).

Even though, the signal at 7.3 ppm in the ^1H NMR spectra indicated a slight impurity, the block copolymers PE-*b*-PEG were cleaved to yield pure PE and prove the concept. To do so, the cleavage was conducted by an aminolysis of the ester and/or trithiocarbonate junction, which would result in the desired product (**Scheme 38**). For this, ethylenediamine was identified as a suitable reactant.¹³¹



Scheme 38: Aminolysis of PE-*b*-PEG cleaving the connection between both blocks, to obtain pure PE.

The cleavage yielded a precipitated product that was insoluble in common solvents. Hence, ATR-FT-IR spectroscopy and DSC were used for characterization (**Figure 19**). The ATR-FT-IR spectrum of the decarboxylated and cleaved polymer derived from **DP2 (PE2)** clearly indicated the removal of the PEG chain. Further it revealed the typical C-H vibrational signals at 2920 cm^{-1} ($\nu_{\text{as}}\text{C-H}$), 2846 cm^{-1} ($\nu_{\text{s}}\text{C-H}$), 1450 cm^{-1} ($\delta_{\text{s}}\text{C-H}$), and 721 cm^{-1} ($\delta_{\text{r}}\text{C-H}$), identical to the ATR-FT-IR spectrum of commercially available PE (**Figure 75**).

Results and Discussion

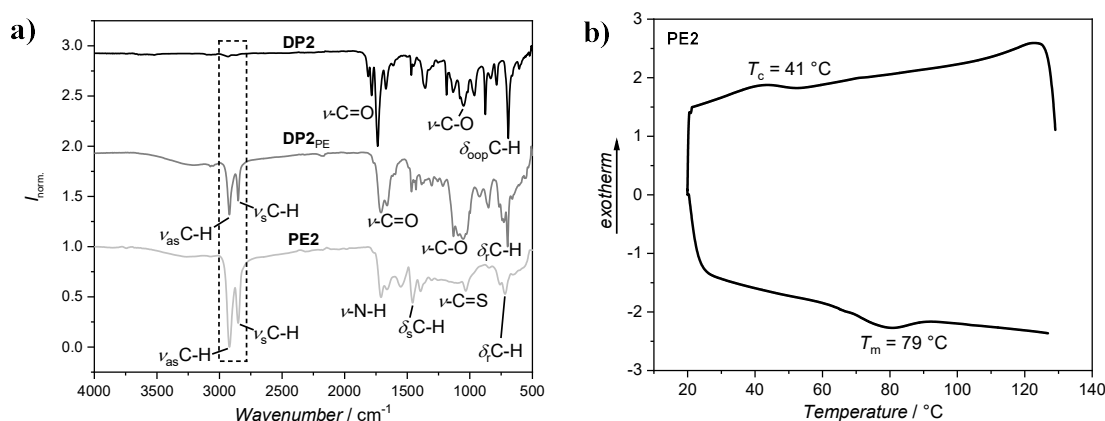


Figure 19: a) ATR-FT-IR spectra of the **DP2** precursor (top, black), after decarboxylation (**DP2_{PE}**, middle, grey) and after cleavage (**PE2**, bottom, light grey). b) DSC chromatogram of **PE2** obtained after decarboxylation and cleavage of **DP2**.

However, additional signals at 1704 cm^{-1} ($\nu\text{-N-H}$) and 1027 cm^{-1} ($\nu\text{-C=S}$) were found as a result of remaining rests of unremoved ethylene thiourea (ETU), which is formed as a product of the aminolysis. The DSC characterization of the as-obtained **PE2** (Figure 19b) showed crystallization (during cooling) and melting (during heating) with a melting point at $T_m = 79\text{ }^\circ\text{C}$, which was lower than expected for pure PE. However, these results prove the feasibility of the idea for an indirect synthesis of PE. Additionally, it needs to be mentioned, that the DSC analysis was performed without further preparation of the samples (addition of a salt) as done in the first project (see Chapter 4.1.4). Yet, the fact that the observed melting temperature T_m alongside with the observation of the small additional broad signal in the ^1H NMR spectra, led to the assumption that the standard H-donor phenylsilane could cause side reactions within the decarboxylation step. PPMs are known to be very sensitive to small amounts of side reactions since repeating units with side products (comonomer fraction) cannot be removed and thus lead eventually to changes in the polymer properties. These side reactions most likely result in a small comonomer fraction bearing an unknown structural motif, hence, being responsible for the reduction of the T_m . In contrast to the sufficient utilization in organic chemistry, the reaction conditions of the photochemically-induced decarboxylation needed to be improved in order to be viable for its application in polymer chemistry. Consequently, the decarboxylation step as well as the cleavage step were optimized and a variation of the decarboxylation parameters was performed. Herein, the standard conditions included phenylsilane as H-donor in an excess of 1.50 equivalents per phthalimide ester at a concentration of $0.013\text{ mmol mL}^{-1}$ with respect to the polymer (Table 3, entry #1). The evaluation of the decarboxylation of **DP2** was performed

by ^1H NMR analysis and the change of the respective signal at 7.3 ppm was followed. Further, the percentage change of the signals intensity was calculated with respect to the signal of the CH_3 group of the PEG chain and calculated by the following equation:

$$\text{Reduction [\%]} = 100 - \left[\frac{\text{Integral at 7.35 ppm Standard}}{\text{Integral at 7.35 ppm Variation}} 100 \right] \quad \text{II}$$

To alter the reaction conditions, the equivalents of phenylsilane were reduced from 1.50 to 1.20 equiv., which did not lead to a great reduction of the signal intensity (reduction of 9%, **Table 3**, entry #2, **Figure 20a**, **Figure 71**). In a second approach, the concentration of the polymer was reduced in half, which lead to a substantial but not sufficient decrease of the intensity of the signal at 7.3 ppm (**Table 3**, entry #3, **Figure 20b**, **Figure 72**).

Table 3: Variation of the reaction parameters of the decarboxylation reactions with PAP-*b*-PEG.

Entry	H-donor	Conc. [mmol mL ⁻¹]	Eq. H-donor	Add. reactant	Aromatic signal's intensity*
1	PhSiH ₃	0.013	1.5		Standard conditions – 100%
2	PhSiH ₃	0.013	1.2		91%
3	PhSiH ₃	0.005	1.5		65%
4	PhSiH ₃	0.013	1.5	<i>i</i> -PrOH	34%
5	PhSiH ₃	0.005	1.5	<i>i</i> -PrOH	41%
6	Bu₃SnH	0.013	1.5		No signal

*calculated by ^1H NMR spectroscopy.

As an additional variation of the synthetic parameters isopropanol (*i*-PrOH) was added (10 mol% with respect to PhSiH₃), which is known to form complexes with phenylsilane, increasing its H-donor ability.^{125,132} The addition led to an improvement of the decarboxylation results, by judging from the ^1H NMR spectrum (**Table 3**, entry #4, and **Figure 20c**, **Figure 73**). Yet, also the combination of the addition of *i*-PrOH and a lower concentration of the polymer

Results and Discussion

did not further improve the reaction, as observed by ^1H NMR spectroscopy (**Table 3**, entry #5, and **Figure 20d**, **Figure 74**).

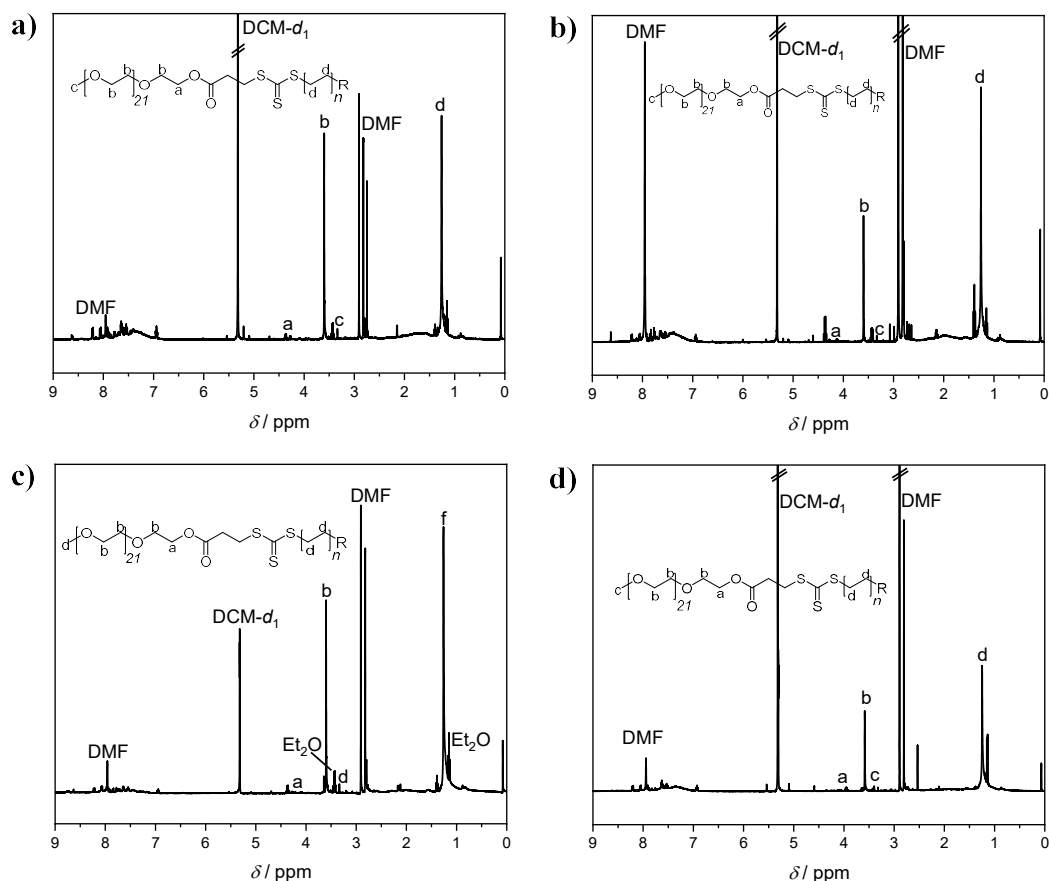


Figure 20: ^1H NMR spectra of PE-*b*-PEG (DP₂PE) after photochemically-induced decarboxylation with **a**) reduced equivalents of phenylsilane, **b**) reduced concentration with respect to the polymer, **c**) additional *i*-PrOH and **d**) reduced concentration and additional *i*-PrOH. Solvent: DCM-*d*₂.

Since the variation of the reaction conditions did not result in a complete removal of the side reactions, phenylsilane was substituted and tributyltin hydride was found to be a potent H-donor (**Figure 21a**), as already demonstrated by Sir Derek Barton.¹¹⁰ The exchange led to an excellent improvement of the decarboxylation reaction according to ^1H NMR and ATR-FT-IR spectroscopy (**Table 3**, entry #6). The ^1H NMR spectrum of DP₃PE, which was obtained *via* the decarboxylation of PAP-*b*-PEG (DP₃) using Bu₃SnH, showed the characteristic signals of the PEG chain as well as an intensive signal of protons of the PE chain at 1.25 ppm (**Figure 21b**). In the following, the obtained PE was analyzed in great detail.

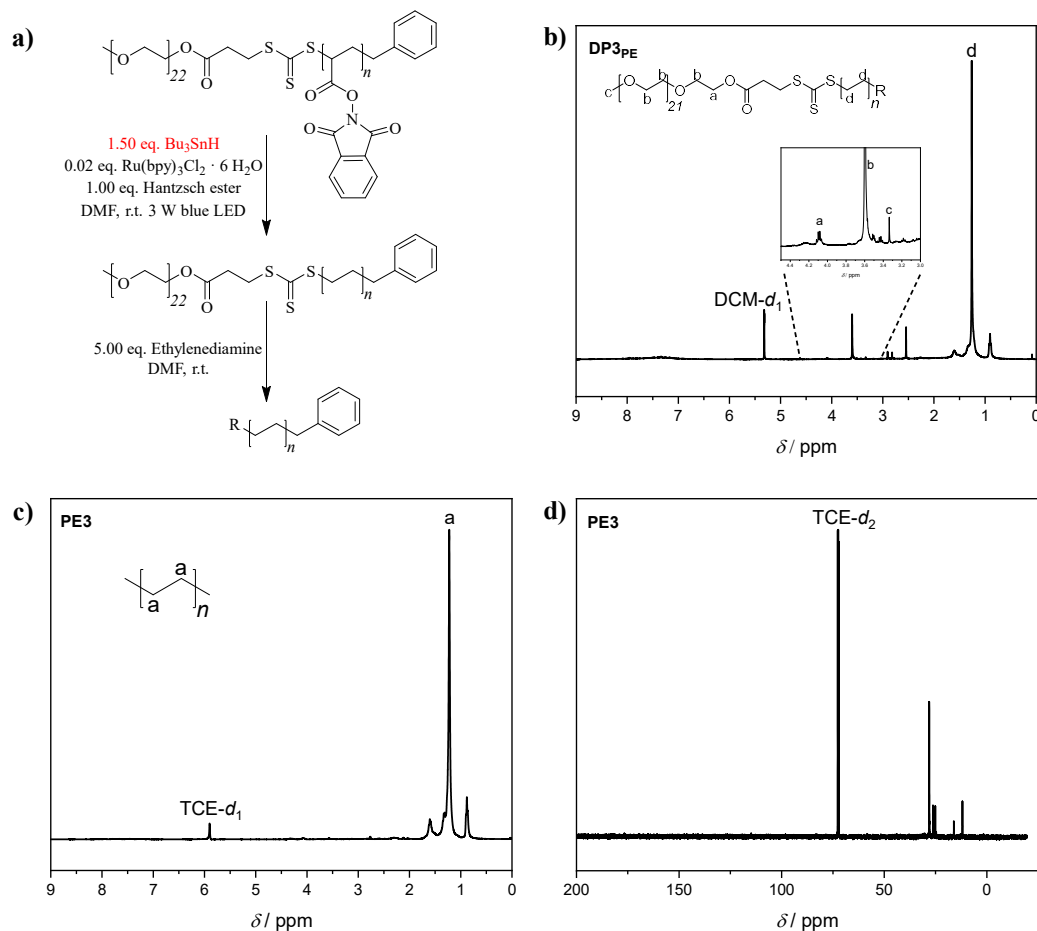


Figure 21: a) Decarboxylation of PAP-*b*-PEG under optimized conditions followed by cleavage with ethylenediamine. b) ^1H NMR spectrum of **DP3PE** after decarboxylation with Bu_3SnH , solvent: $\text{DCM-}d_2$. c) HT- ^1H NMR spectrum of **PE3** derived from **DP3PE** after cleavage with ethylenediamine, solvent: $\text{TCE-}d_2$ and d) HT- ^{13}C NMR spectrum of **PE3** derived from **DP3** after cleavage with ethylenediamine, solvent: $\text{TCE-}d_2$.

High-temperature (HT)- ^1H and ^{13}C NMR analysis in deuterated tetrachloroethane ($\text{TCE-}d_2$) at 90 °C were performed to prove the linear structure and the high purity of PE (**Figure 21c** and **Figure 21d**). The ^1H NMR furthermore proved the quantitative decarboxylation as well as the quantitative aminolysis. In the spectrum, besides the deuterated solvents' signal, only the intensive signal of the CH_2 group of PE at 1.25 ppm could be identified, proving the improved purity of the formed PE derived from **DP3**. In the ^{13}C NMR spectrum, the carbon of the CH_2 groups can be clearly identified at 29.8 ppm, while signals with a downfield shift indicating a branching could not be found. In addition to the obtained NMR results, the comparison of the ATR-FT-IR spectra of **DP3PE** and **PE3** obtained after cleavage revealed the removal of the carbonyl vibrational signal of the ester at 1685 cm^{-1} , as well as of the $\nu\text{-C-O}$ vibration of the

Results and Discussion

ether bond of the PEG chain at 1074 cm^{-1} (**Figure 22a**). Even more, the ATR-FT-IR spectrum of PE showed the characteristic signals originating from the different vibrations of PE ($\nu_{\text{as}}\text{C-H}$ at 2919 cm^{-1} , $\nu_{\text{s}}\text{C-H}$ at 2948 cm^{-1} , $\delta_{\text{s}}\text{C-H}$ at 1468 cm^{-1} , and $\delta_{\text{r}}\text{C-H}$ at 720 cm^{-1}). Further, the previously observed signals at 1704 cm^{-1} ($\nu\text{-N-H}$) and 1027 cm^{-1} ($\nu\text{-C=S}$) were not present anymore.

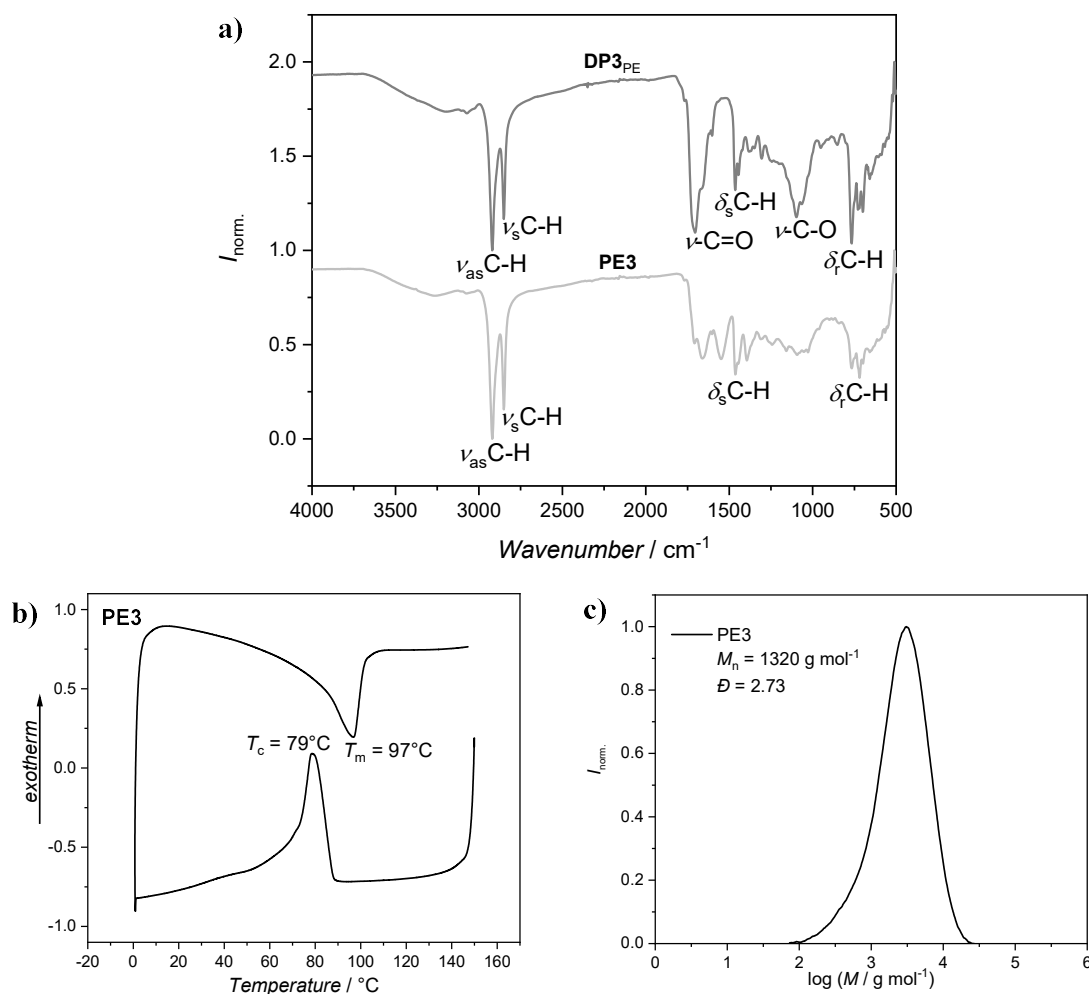


Figure 22: a) Comparison of the ATR-FT-IR spectra of **DP3_{PE}** before (top, black) and **PE3** after (bottom, grey) cleavage with ethylenediamine at room temperature. Analysis of **PE3** by b) DSC and c) HT-SEC in 1,2,4-TCB at $160\text{ }^{\circ}\text{C}$.

Additionally, DSC analysis revealed a melting point of $T_m = 97\text{ }^{\circ}\text{C}$, corresponding to a low molar mass PE, as compared with a commercially available PE ($T_m = 94\text{ }^{\circ}\text{C}$, **Figure 76**). Furthermore, high-temperature SEC (HT-SEC) in 1,2,4-TCB at $160\text{ }^{\circ}\text{C}$ was conducted (calibration with polystyrene standards) as shown in **Figure 22c**. The analysis revealed a molar

mass of $M_n = 1320 \text{ g mol}^{-1}$ for **PE3** ($D = 2.73$, $DP = 47$). The value was found to be in good agreement with the DP determined for the precursor polymer, even though the comparison of those values is only relative since different calibrations were used for the analyses. Most importantly the chromatogram featured a symmetrical, monomodal shape without any shoulders. In comparison to the precursor polymer **DP3_{PE}**, the dispersity increased only slightly from $D = 2.37$ to $D = 2.73$. This could be explained by the definition of the dispersity ($D = \frac{M_w}{M_n}$) and the average values. Hereby, M_n is the arithmetic mean or number average of the molar mass of the polymer, whereas M_w describes the weight average, in which the relative mass fraction is weighted. Thus, chains with a higher molar mass contribute to M_w in a larger extend than smaller chains. The removal of the phthalimide groups during the decarboxylation step has a smaller impact on M_w , since larger chains have a higher proportionate weight here, resulting in a lower percentage decrease of M_w in comparison to M_n . Therefore, the increase of the dispersity D is in good agreement with the expectation.

In addition to **DP3**, also **DP2** featuring a $DP = 37$ and **DP1** with a $DP = 21$ were decarboxylated with Bu_3SnH , cleaved with ethylenediamine and analyzed. The analysis of the decarboxylation and cleavage products of **DP2** is shown in **Figure 23**. The ^1H NMR spectrum of **DP2_{PE}** proved the formation of PE-*b*-PEG and the intact nature of the polymer by revealing signals of the PEG chain (4.2 ppm (COOCH_2), 3.7 ppm ($\text{CH}_2\text{CH}_2\text{O}$) and 3.2 ppm (CH_3)) on the one hand and of PE on the other hand (1.25 ppm, **Figure 23b**) In contrast to the analysis of **PE3**, the HT- ^1H NMR spectrum of **PE2** (**Figure 23c**) showed the signal of the benzyl end group of the RAFT agent and a signal of low intensity at 2.3 - 2.5 ppm which probably originates from a thiol end group (CH_2SH). Furthermore, a signal of low intensity originating from ETU, resulting from the aminolysis of the trithiocarbonate with ethylenediamine as shown in **Figure 23a**. The signal of the end group of **PE2** can be identified due to the lower molar mass of **PE2** in comparison to **PE3**, additionally proving the successful synthesis of PE with different molar masses. Furthermore, DSC analysis revealed $T_m = 95 \text{ }^\circ\text{C}$ and $T_c = 81 \text{ }^\circ\text{C}$ (**Figure 23f**), which is in good agreement with the expected T_m in the range of 90 – 100 $^\circ\text{C}$. Unfortunately, the analysis of **PE2** via HT-SEC in 1,2,4-TCB could not be conducted as planned, since technical problems occurred at PSS and a chromatogram could not be obtained.

Results and Discussion

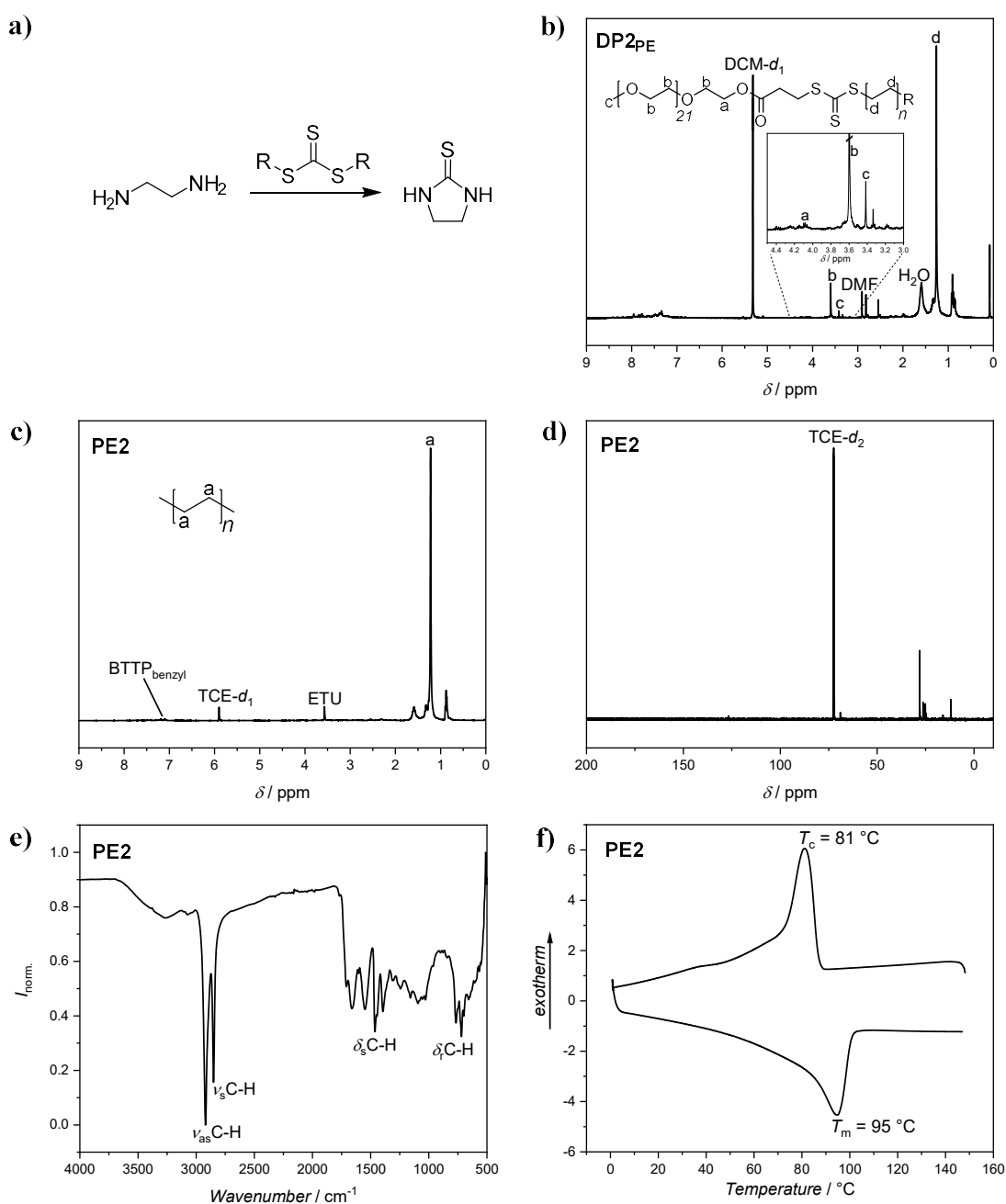


Figure 23: a) Formation of ethylene thiourea (ETU) from ethylenediamine in the presence of a trithiocarbonate like BTTP. b) ^1H NMR spectrum of PE-*b*-PEG (**DP2PE**), solvent: $\text{DCM-}d_2$. Analysis of **PE2** via c) HT- ^1H NMR spectroscopy, benzyl end group and ETU marked, solvent: $\text{TCE-}d_2$ and d) HT- ^{13}C NMR spectroscopy, solvent: $\text{TCE-}d_2$. e) ATR-FT-IR spectrum and f) DSC chromatogram of **PE2**.

In line with the analysis of **DP2PE**, the analysis of **DP1PE** proved the clean formation of the decarboxylated block copolymer without any side reactions (**Figure 24a**). In comparison to the HT- ^1H NMR spectrum of **PE2**, the HT- ^1H NMR spectrum of **PE1** showed signals of the benzyl end group in even higher intensity, as expected for the lower molar mass and shorter chain

length (**Figure 24b**). Additionally, two signals of low intensity originating from ETU (3.6 ppm) and the thiol end group (2.5 ppm) could be identified in the HT- ^1H NMR spectrum.

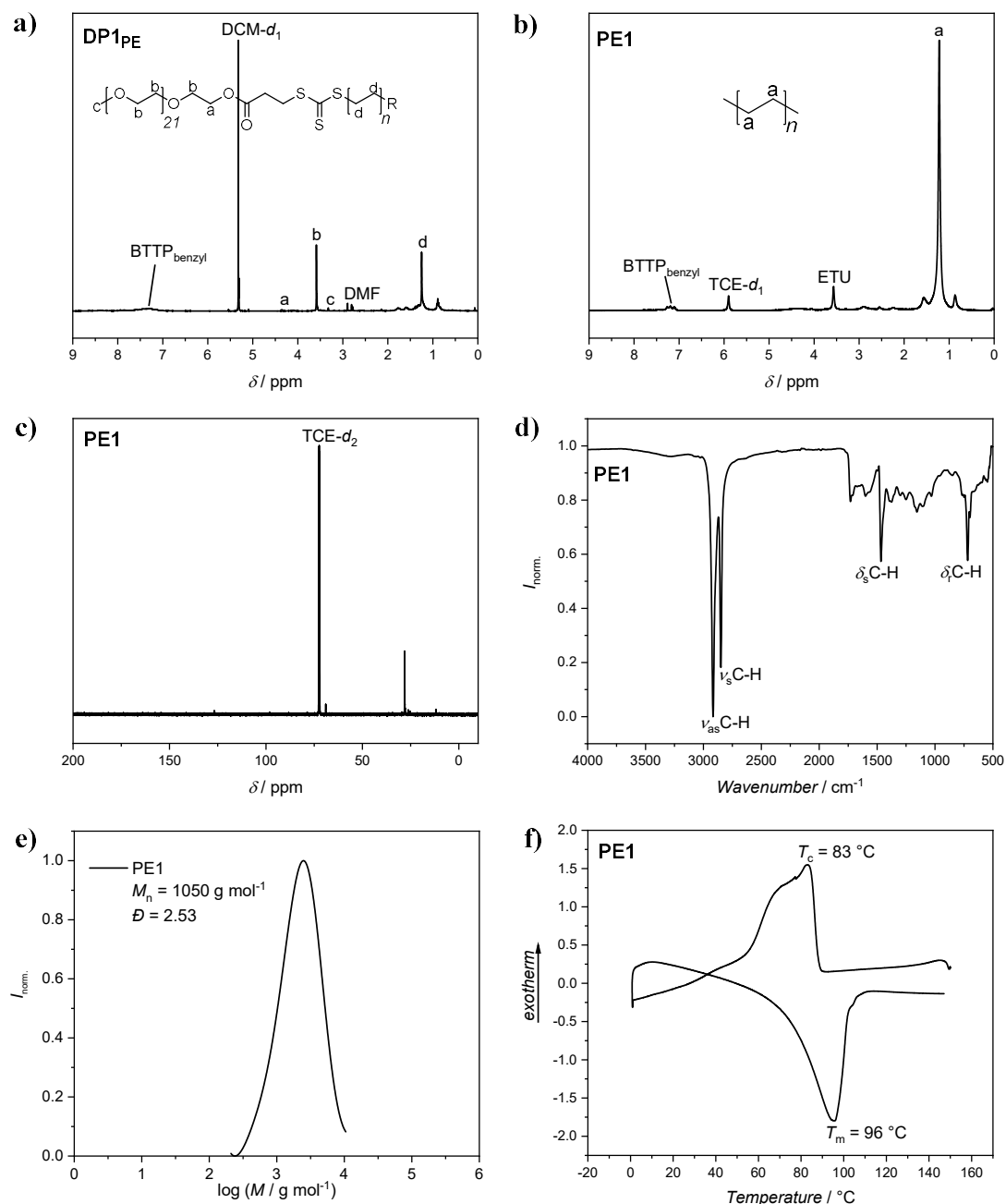


Figure 24: **a)** ^1H NMR spectrum of PE-*b*-PEG (DP1), solvent: $\text{DCM-}d_2$. Analysis of PE1 via **b)** HT- ^1H NMR spectroscopy, benzyl end group and ETU marked, solvent: $\text{TCE-}d_2$, **c)** HT- ^{13}C NMR spectroscopy, solvent: $\text{TCE-}d_2$, **d)** ATR-FT-IR spectroscopy, **e)** HT-SEC in 1,2,4-TCB at 160 $^{\circ}\text{C}$ and **f)** DSC.

Results and Discussion

The analysis of **PE1** via HT- ^1H NMR spectroscopy furthermore revealed a signal at 29.8 ppm originating from CH_2 units, while signals at higher shift originating from branching or rare crosslinking of the chains could not be observed. In addition, the intensive vibrations of PE (ν_{as} at 2919 cm^{-1} , ν_{s} at 2948 cm^{-1} , δ_{s} at 1468 cm^{-1} , and $\delta_{\text{r}}\text{-CH}_2$ at 720 cm^{-1}) could be identified in the ATR-FT-IR spectrum, while HT-SEC in SEC analysis of **PE1** revealed a molar mass of $M_{\text{n}} = 1050\text{ g mol}^{-1}$ ($DP = 37$), a unimodal shape of the chromatogram and an increased dispersity ($D = 2.53$) as expected. Thus, HT-SEC analysis of **PE3** and **PE1** proved the intact nature of the PE chains after cleavage. DSC analysis showed $T_{\text{m}} = 96\text{ }^\circ\text{C}$ and $T_{\text{c}} = 83\text{ }^\circ\text{C}$, which is in good agreement with the DSC analysis of commercial PE (**Figure 76**).

In comparison to other controlled synthesis methods of PE, the presented approach features several advantages. As stated in **Chapter 4.1.4**, the most important is to circumvent employing ethylene gas and thus the handling of a flammable, gaseous component. Furthermore, the chain length of PE can be predefined (although the maximum chain length is limited), while as the only disadvantage the low atom economy could be mentioned. The first controlled synthesis method of PE by RAFT polymerization of ethylene was developed by Monteil *et al.* in 2014 (see **Chapter 2.3** for details).¹¹ They developed a RAFT system for the homopolymerization of ethylene at $70\text{ }^\circ\text{C}$ and 200 bar, reached molar masses in the range of $220 - 2000\text{ g mol}^{-1}$ and dispersities in the range of $D = 1.4 - 2.3$ and thus in a comparable range as the PEs obtained in the present study. Subsequently they performed a chain extension of PE ($M_{\text{n}} = 500\text{ g mol}^{-1}$, $D = 1.7$) with ethylene to prove the end group fidelity. The SEC analysis of the polymer resulting from the chain extension revealed a shift towards higher molar masses, however, additionally a shoulder and high dispersities ($D = 3.4$) originating from a fraction of chains that could not be reinitiated were observed. In contrast, Detrembleur *et al.* reached molar masses in the range of $1800 - 4200\text{ g mol}^{-1}$ which are slightly higher than the one obtained in the present study.¹⁶ Nevertheless, the authors could not demonstrate the full control over the polymerization, while they observed transfer reactions and slight branching of the PE. Contrary, branching or transfer reactions were not observed in the present study.

The current subchapter impressively demonstrated the necessity of quantitative reactions for PPM of polymers, since a comonomer fraction based on side reactions caused the low T_{m} and the corresponding signal in the ^1H NMR spectra of the polymers obtained by the photochemically-induced decarboxylation with phenylsilane (see also **Scheme 34**). Furthermore, the importance of intelligent deployment of polymer architecture to overcome common challenges regarding polymers such as solubility issues was highlighted.

4.2.3 Thermal Decarboxylation of Poly[*N*-(acryloyloxy)phthalimide]-*block*-Poly(ethylene glycol)

Besides the photochemical decarboxylation of PAP-*b*-PEG, the thermally-induced decarboxylation method was simultaneously investigated to yield PE-*b*-PEG. For the evaluation of the method the degradable block copolymer PAP-*b*-PEG (**DP4**) featuring a $DP = 20$ was used. The decarboxylation was first performed under former evaluated standard conditions, meaning 0.50 eq. of zinc, 0.10 eq. of $\text{NiCl}_2 \cdot 6 \text{H}_2\text{O}$, 0.20 eq. of bbbpy and 1.50 eq. of phenylsilane, all equivalents with respect to the activated ester groups of the polymer. Similar to the results described in **Chapter 4.1.4**, the proper analysis of the resulting polymer was hindered by residues of the catalyst, which could not be removed quantitatively from the polymer. The analysis of PE-*b*-PEG obtained from thermally-induced decarboxylation *via* ^1H NMR spectroscopy (**Figure 25a**) reveals signals of the intact PEG chain (4.22 ppm (COOCH_2), 3.58 ppm ($\text{CH}_2\text{CH}_2\text{O}$), and 3.42 ppm (CH_3)) as well as a signal at 1.25 ppm of the formed PE and an additional broad signal at 7.3 ppm originating from an unknown side reaction (marked in blue). Noteworthy, all signals in the spectrum feature an extensive broadening, probably due to impurities originating from the nickel-catalyst.

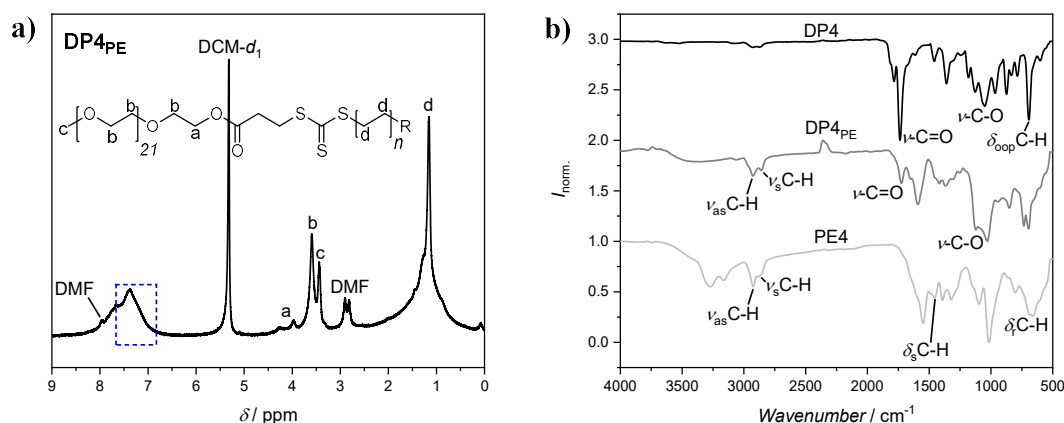


Figure 25: a) ^1H NMR spectrum of **DP4PE** after thermally-induced decarboxylation of **DP4** with phenylsilane and b) analysis *via* ATR-FT-IR spectroscopy of **DP4** (top, black), **DP4PE** (middle, grey) and **PE4** (bottom, light grey).

Additionally, the analysis *via* ATR-FT-IR spectroscopy revealed various signals resulting from impurities and side reactions during the decarboxylation. In the spectrum of the decarboxylated polymer **DP4PE**, signals of low intensity at 2925 cm^{-1} and 2945 cm^{-1} originating from $\nu_{\text{as}}\text{C-H}$

Results and Discussion

and $\nu_s\text{C-H}$ vibrations could be identified, while the signal of the phthalimide ester at 1690 cm^{-1} was removed after decarboxylation stating that the decarboxylation could be performed in a quantitative fashion, but besides CH_2 units, side reactions caused the formation of a comonomer fraction. The spectrum of **PE4** revealed the common signals of PE ($\nu_{\text{as}}\text{C-H}$ at 2925 cm^{-1} and $\nu_s\text{C-H}$ at 2948 cm^{-1}), while the $\delta_s\text{-C-H}$ and $\delta_r\text{-C-H}$ vibrational bands featured a low intensity. Furthermore, additional signals at $3100 - 3300\text{ cm}^{-1}$ and 1050 cm^{-1} could be identified, which could not be assigned to the product. In contrast to the results of the photochemically-induced decarboxylation and in accordance with the results in **Chapter 4.1.4**, the DSC analysis of the obtained material revealed neither a melting nor a crystallization indicating the formation of comonomer fractions, which hindered the crystallization. As evaluated in the previous chapter (**Chapter 4.2.2**), the H-donor phenylsilane was therefore exchanged with tributyltin hydride. The $^1\text{H NMR}$ spectrum of **DP4PE** (after decarboxylation with Bu_3SnH , **Figure 26a**), revealed an intensive signal at 1.45 ppm which could be assigned to CH_2 units. Nevertheless, the higher shift of the signal (the PE signal was expected at 1.25 ppm , compare **Chapter 4.2.2**) could originate from an additional comonomer fraction resulting from a side reaction. Furthermore, additional signals at $7.5 - 7.9\text{ ppm}$ and 0.9 ppm (marked in blue) arose from this comonomer fraction.

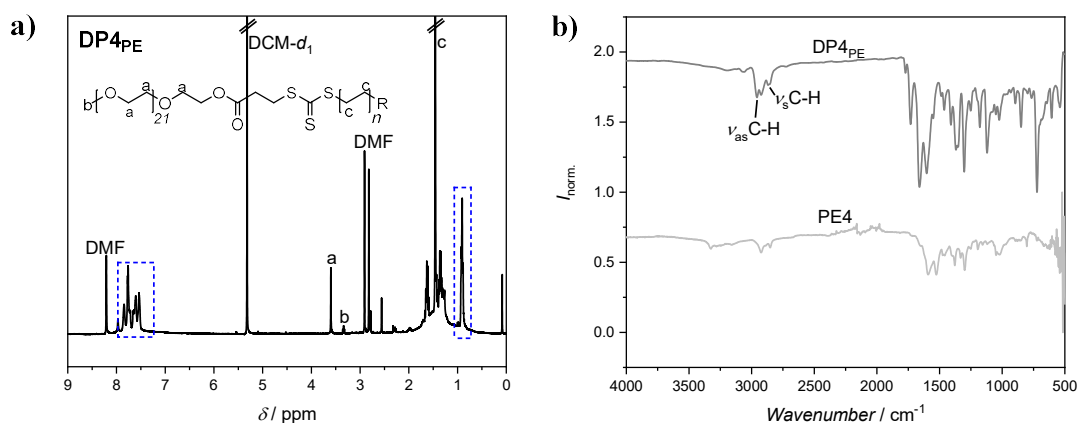


Figure 26: a) $^1\text{H NMR}$ spectrum of **DP4PE** after thermally-induced decarboxylation with Bu_3SnH and the corresponding b) comparison of the ATR-FT-IR spectra of **DP4PE** and **PE4**.

In line with these results, the DSC analysis of the obtained material did once more not reveal any melting or crystallization. Summing all these results up, the approach of optimizing the thermally-induced decarboxylation for the synthesis of PE was consequently discarded.

4.2.4 Aminolysis of Polyethylene-*block*-Poly(ethylene glycol)

After the successful optimization of the photochemical decarboxylation method, the cleavage of the block copolymers by aminolysis was further investigated. Thus, **DP2_{PE}** (PE-*b*-PEG) obtained from decarboxylation under the previously optimized conditions was chosen as a model for different aminolysis approaches, while the results were judged by DSC measurements. Initially, the cleavage was performed with ethylenediamine in DMF at room temperature. Thus, in the first step the reaction temperature was increased to 80 °C (below the melting point of PE and the boiling point of ethylenediamine at 116 °C) and the cleavage was performed in DMF to raise the reaction rate and efficiency. The analysis *via* DSC revealed a melting point of $T_m = 94$ °C (**Figure 27a**), which is comparable to the one obtained from the cleavage of **DP2_{PE}** at room temperature ($T_m = 95$ °C).

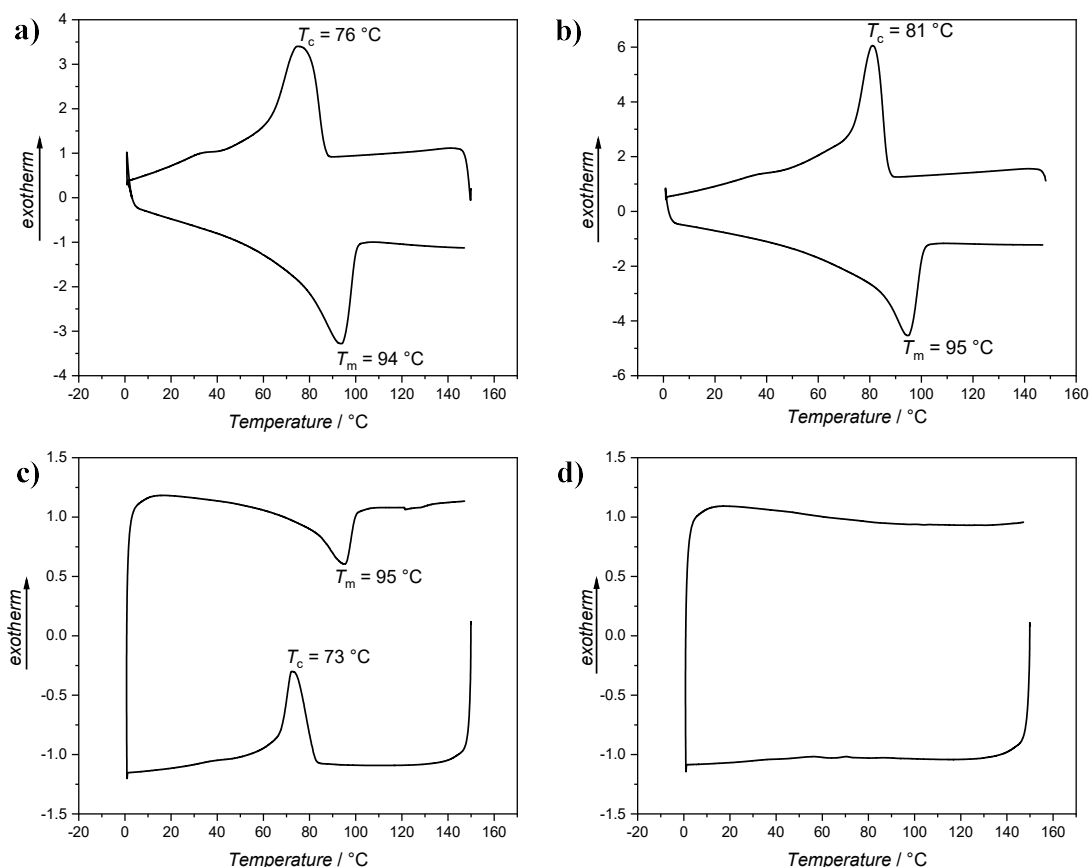


Figure 27: DSC analysis of the different approaches for the cleavage of **DP2_{PE}** with ethylenediamine: **a)** Cleavage in DMF at 80 °C, **b)** cleavage in DMF at 80 °C, after direct addition of ethylenediamine to the decarboxylation mixture (one-pot two-step procedure, **c)** cleavage in 1,2,4-TCB at 80 °C and **d)** cleavage of PE-*b*-PEG with LiAlH₄.

Results and Discussion

Furthermore, a one-pot two-step approach was performed. To do so, ethylenediamine was dissolved in DMF, deoxygenated and added to the preheated decarboxylation mixture (80 °C). Here, DSC analysis revealed a melting point of $T_m = 95$ °C (**Figure 27b**) and the highest enthalpy of fusion observed ($H_{\text{fus}} = 39$ J g⁻¹). Next, the cleavage was performed in 1,2,4-TCB at 80 °C. 1,2,4-TCB was chosen since PE formed during the reaction should remain in solution and therefore any side reaction due to precipitation should be avoided. Yet, the PE obtained in both solvents featured similar properties ($T_m = 95$ °C, **Figure 27c**) as the one obtained in DMF. Finally, LiAlH₄ was chosen as an alternative reducing agent. Unfortunately, **DP2PE** featured only a low solubility in THF, thus the concentration of the polymer had to be drastically reduced, which rendered this approach not suitable for the cleavage of PE-*b*-PE. Furthermore, neither a crystallization nor a melting of the polymer could be observed (**Figure 27d**).

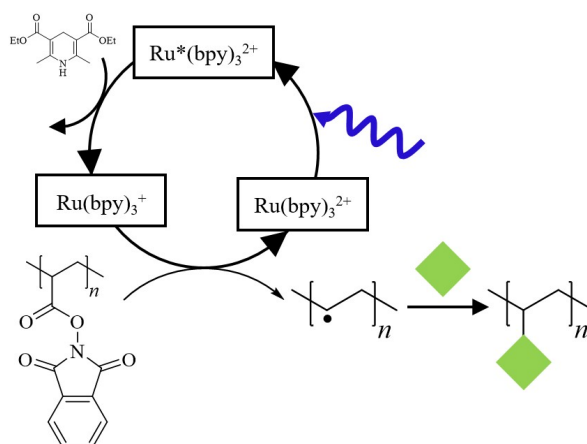
In summary, ethylenediamine was found to be a very suitable and versatile reagent for the aminolysis of PE-*b*-PEG, while the choice of solvent seemed not to be critical for the cleavage as long as it is suitable for the precursor polymer PE-*b*-PEG.

4.2.5 Recapitulation

In conclusion, the synthesis of PE from an acrylate-based precursor block copolymer was successfully performed using the previously described, highly efficient photochemically-induced decarboxylation approach combined with a subsequent cleavage of a sacrificial block copolymer. To do so, RAFT polymerization of the acrylate-based precursor monomer was used for the synthesis of the sacrificial precursor block copolymers, allowing for a prediction and control of the degree of polymerization of the obtained PE. Both, the decarboxylation method and the block copolymer cleavage were optimized by varying various reaction parameters such as concentration and H-donor (decarboxylation) or solvent (reduction), which enabled ultimately to conduct the reaction in a one-pot two-step procedure. As such, a fundamentally new method for the synthesis of PE *via* a post-modification approach has been presented that lays the foundation for an academic exploration of unprecedented PE-based polymers, copolymers, and block copolymers.

4.3 Decarboxylation of Poly[*N*-(acryloyloxy)phthalimide] as a Versatile Tool for Post-Polymerization Modification

The third project arose as a side project from the first project, since the application of phthalimide active esters is not only limited to reductive decarboxylation, but is frequently used for cross-coupling reactions in organic chemistry as described in detail in **Chapter 2.5**.^{98,99} Various studies on organic molecules have already demonstrated the versatility of the decarboxylation of phthalimide-based structural motifs, but yet those reactions were not transferred to polymers. While in the former projects the secondary, carbon-centered radical formed at the polymer backbone during the decarboxylation was used to introduce hydrogen by employing a H-donor, this carbon-centered radical additionally should be used for the modification of the polymer with other suitable reactants (**Scheme 39**). Therefore, different methods were evaluated regarding their suitability for the functionalization of PAP precursor polymers.



Scheme 39: Functionalization of PAP *via* photochemical decarboxylation using the carbon-centered radical formed at the polymer backbone.

One of the most studied reactions of the phthalimide structural motif is the Michael-type addition of α , β -unsaturated carbonyl compounds, whereby various types of catalytic systems and reactants are used.^{114–118,133–135} Michael-type additions not only lead to the formation of a new C-C bond, but also allow for the introduction of new functionalities to the molecule with high yields and efficiency. In the following subchapter, the Michael-type addition should be transferred to polymer chemistry employing PAP polymers.

Results and Discussion

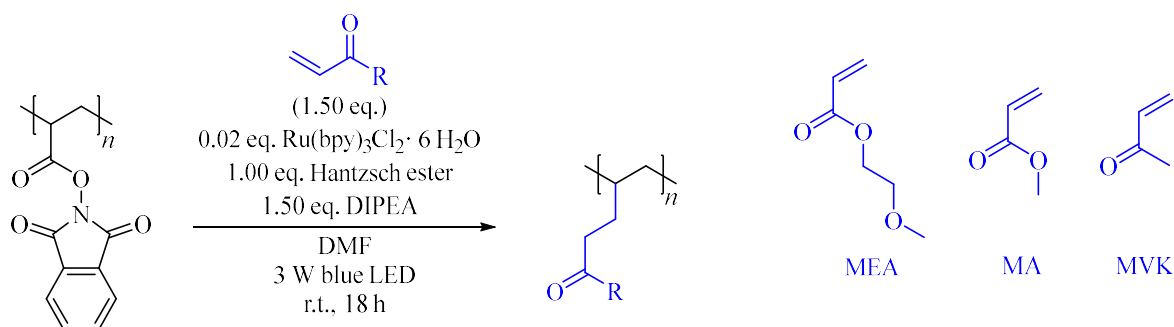
Another way to functionalize polymers employing radicals at the polymer backbone is the so-called nitroxide radical coupling (NRC).^{35,40,77} NRC is based on the coupling of a persistent, nitroxide-based radical *e.g.*, TEMPO-based persistent radicals, with carbon-centered radicals. This coupling method is widely known, *e.g.*, for end group functionalization and used on different types of polymers. Especially the introduction of TEMPO functionalities to a polymer backbone, for example on polyolefins, represents a growing field of research.³⁵ However, most of those methods lack control and require harsh conditions like laser-based etching or the employment of peroxides.⁸⁰ Nevertheless, an advantage of NRC is its high efficiency and the possibility to further make use of the TEMPO functionality at the polymer, for instance to perform grafting reactions or introduce more complex architectures such as brush polymers.¹³⁶

Consequently, within this project new synthetic routes exploring the decarboxylation of PAP and the subsequent functionalization using Michael-type addition of α , β -unsaturated carbonyl compounds and NRC should be developed.

Parts of this chapter and the corresponding parts in the experimental section were adapted with permission from a publication written by the author (Stefan Frech).¹³⁷

4.3.1 Michael-type Addition

As previously described, the photochemical decarboxylation evaluated in the present thesis is based on a SET from the metal catalyst to the carbonyl of the phthalimide structural motif resulting in a carbon-centered radical after release of CO₂ and removal of the phthalimide. Within the current chapter, this carbon-centered radical should be employed for Michael-type addition reactions. Thus, a homopolymer PAP (**FP1**) with a molar mass of $M_n = 6700 \text{ g mol}^{-1}$ and a dispersity of $D = 1.20$ was synthesized by RAFT polymerization (**Table 19**) and subsequently used for decarboxylative Michael-type additions with α, β -unsaturated carbonyl compounds (Michael acceptors). Following the evaluation of decarboxylation reactions on PAP for the synthesis of PE and PE-block copolymers with a hydrogen-donor in the former chapters (**Chapters 4.1** and **4.2**),^{126,130} herein only the photochemical decarboxylation method employing Ru(bpy)₃Cl₂ · 6 H₂O as catalyst was used for the functionalization of PAP.



Scheme 40: Decarboxylative Michael-type addition of PAP with α, β -unsaturated carbonyl compounds 2-methoxyethyl acrylate (MEA), methyl acrylate (MA), and methyl vinyl ketone (MVK).

As model Michael acceptors, methyl acrylate (MA), 2-methoxyethyl acrylate (MEA) and methyl vinyl ketone (MVK) were chosen (**Scheme 40**). MA and MEA were chosen due to their electron poor double bond, which makes them good Michael acceptors and due to their characteristic signals in ¹H NMR spectra at 3.0 – 4.2 ppm, which can be clearly distinguished from the signals of PAP. To widen the scope of usable reagents, MVK representing a vinyl ketone was additionally employed for the PPM. Decarboxylation reactions and Michael-type additions were performed in-situ using Ru(bpy)₃Cl₂ · 6 H₂O (0.02 eq.), HE (1.00 eq.), Michael acceptor (1.50 eq.) and *N,N'*-diisopropylethyl amine (DIPEA, 1.50 eq.) as reductive quencher^{138,139} (**Scheme 40**). As explained in detail in **Chapter 2.5**, a reductive quencher is required for the Michael-type addition of α, β -unsaturated carbonyl compounds to prevent the

Results and Discussion

initiation of a polymerization after the addition of the first double bond. Thus, DIPEA was chosen due to its ability to undergo a reduction during the decarboxylation similar to HE and to stabilize a radical by forming an iminium ion under H-abstraction.^{138,139}

First, the decarboxylative Michael-type addition with MEA and PAP (**FP1**) was performed to yield **FP1-MEA**. The comparison of the ¹H NMR spectra before and after the decarboxylation with MEA is presented in **Figure 28a**.

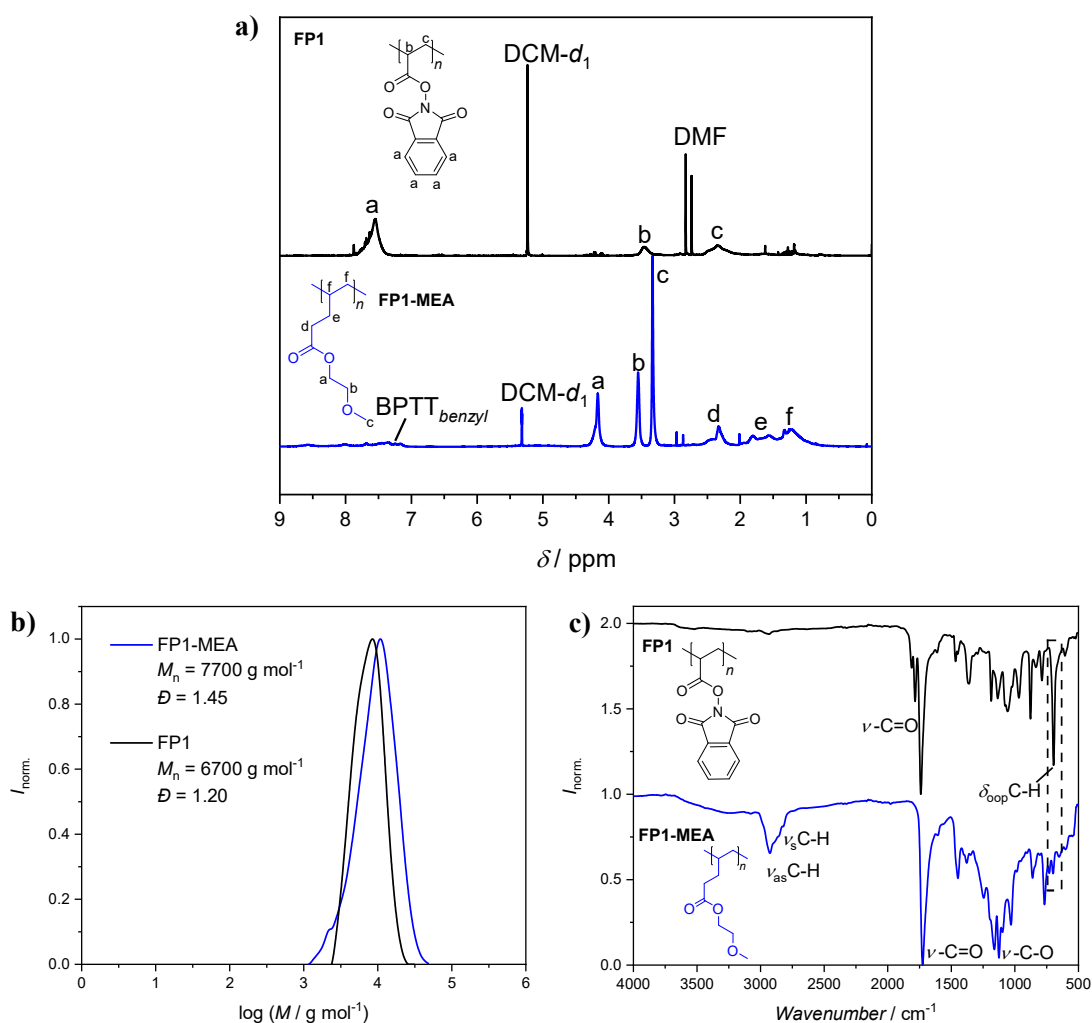


Figure 28: **a)** Comparison of the ¹H NMR spectra of PAP (**FP1**) (top, black) and after the Michael-type addition of MEA (**FP1-MEA**, bottom, blue); solvent: DCM-d₂. **b)** SEC chromatogram of **FP1** (black) and **FP1-MEA** (blue). **c)** Comparison of the ATR-FT-IR spectra of **FP1** (top, black) and **FP1-MEA** (bottom, blue).

The removal of the aromatic proton signal of the phthalimide (7.8 ppm) as well as the arising signals of MEA (4.17 ppm, 3.55 ppm, 3.33 ppm) can be clearly identified, proving the quantitative exchange of the phthalimide with MEA. Additionally, SEC analysis (**Figure 28b**) revealed the intact structure of the polymer by a unimodal distribution with a slight shift towards higher molar masses. This shift towards a higher molar mass is contrary to the expectation, since the molecular weight of MEA (155 g mol⁻¹) is slightly lower than the molecular weight of the phthalimide (217 g mol⁻¹). Nevertheless, the difference is within the tolerance of the instrument. Furthermore, the analysis of the ATR-FT-IR spectra before (top, black) and after (bottom, blue) the Michael addition with MEA (**Figure 28c**) proved the successful functionalization. The spectrum of the functionalized polymer **FP1-MEA** featured an additional vibrational band at 2919 cm⁻¹ originating from $\nu_{\text{as}}\text{C-H}$ vibration of the additional CH₂ units of MEA and only one band at 1730 cm⁻¹ which can be assigned to the carbonyl vibration of the ester. In addition, the intensive signal of the $\delta_{\text{oop}}\text{C-H}$ vibration at 697 cm⁻¹ disappeared after the decarboxylation, stating a complete removal of the phthalimide groups.

In addition to MEA, other α , β -unsaturated carbonyl compounds should be used to obtain a broader range of substrates, which can be employed for the Michael-type addition and to prove the effectivity of the method. Thus, MA was chosen as a second acrylate-based Michael-acceptor and used for the Michael-type addition analogously to the functionalization with MEA. Again, ¹H NMR analysis (**Figure 29a**) revealed a quantitative decarboxylation (no signal at 7.8 ppm of aromatic phthalimide protons) and the intensive signal of the CH₃ group of MA at 3.65 ppm.

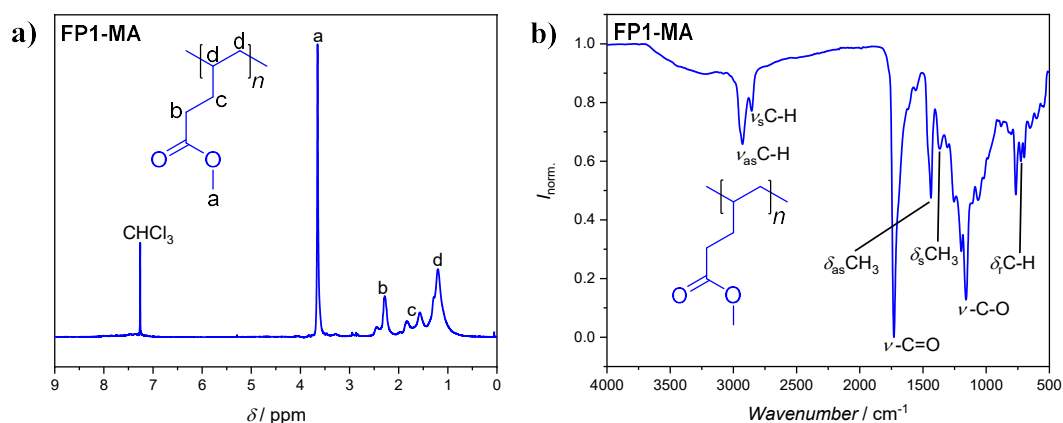


Figure 29: Analysis of **FP1-MA** via **a)** ¹H NMR spectroscopy and **b)** ATR-FT-IR spectroscopy.

Results and Discussion

Furthermore, ATR-FT-IR spectroscopy proved the formation of the product without impurities as no signal of the $\delta_{\text{oop}}\text{C-H}$ vibration at 697 cm^{-1} (aromatic C-H vibration of the phthalimide) could be identified and signals at 2930 cm^{-1} ($\nu_{\text{as}}\text{C-H}$) and 2850 cm^{-1} ($\nu_{\text{s}}\text{C-H}$) proved the presence of additional C-H vibrations.

Lastly, MVK was used as Michael-acceptor, which was especially chosen due to its different chemical nature, representing an α, β -unsaturated ketone and not an acrylate. This should furthermore demonstrate the versatility of the phthalimide-based decarboxylation and widen the scope of usable Michael-acceptors. The results of the successful functionalization are shown in **Figure 30**. In agreement with the functionalization of **FP1** with MEA and MA, the functionalization of **FP1** with MVK was performed in a quantitative fashion as proven by ^1H NMR and ATR-FT-IR spectroscopy. While the ^1H NMR spectrum of **FP1-MVK** proved the quantitative decarboxylation by the removal of the phthalimide proton signal (7.8 ppm), the intensive signal of the CH_3 unit of the ketone at 2.14 ppm (**Figure 30a**) proved the successful addition of the ketone. Additionally, in the ATR-FT-IR spectrum two intensive signals at 2930 cm^{-1} ($\nu_{\text{as}}\text{C-H}$) and 2850 cm^{-1} ($\nu_{\text{s}}\text{C-H}$) and the signals at 1450 cm^{-1} ($\delta_{\text{as}}\text{CH}_3$), 1356 cm^{-1} ($\delta_{\text{s}}\text{CH}_3$), and 1160 cm^{-1} ($\delta_{\text{oop}}\text{C-C}$) confirmed the functionalization with MVK, whereby the disappearance of the $\delta_{\text{oop}}\text{C-H}$ vibration at 697 cm^{-1} verified the complete removal of the phthalimide.

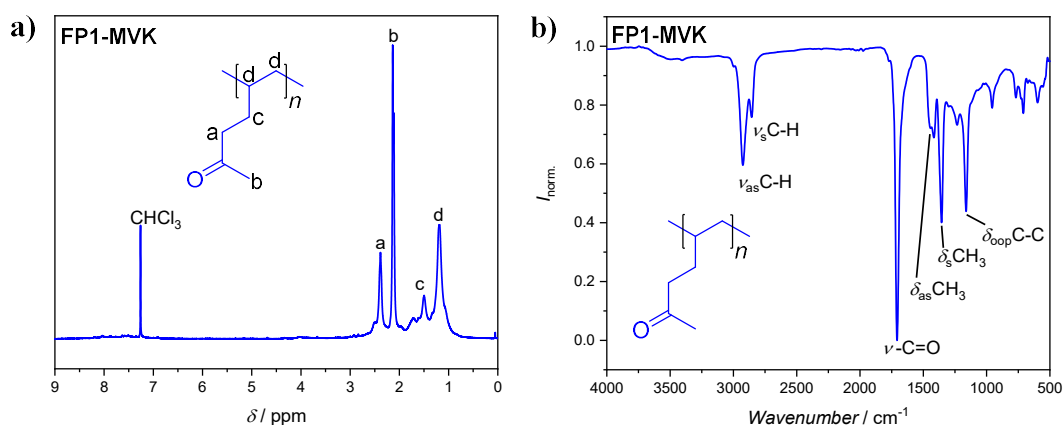


Figure 30: Analysis of **FP1-MVK** via **a)** ^1H NMR spectroscopy and **b)** ATR-FT-IR spectroscopy.

In summary, it was successfully demonstrated that the decarboxylative Michael-type addition onto PAP can be performed with different Michael-acceptors.

As stated before, the decarboxylation was performed in the presence of DIPEA as a reductive quencher, which features a wide application in cross coupling reactions in organic chemistry.^{98,99,138,139} The addition of a Michael-acceptor or a monomer in the absence of a reductive quencher, however, should result in the initiation of a polymerization and either in the formation of a cross-linked polymer or in a graft polymer. To prove the hypothesis, an additional experiment was performed to test, if the polymer is cross-linked by the addition of a monomer to the decarboxylation of PAP or a graft polymer can be obtained. In contrast to the α , β -unsaturated carbonyl compounds MEA, MA and MVK chosen for the Michael-type addition with DIPEA, styrene was chosen as the monomer for the crosslinking since styrene is easily polymerizable, features a high tolerance towards solvent or impurities like small amounts of oxygen and is frequently used for grafting side chains.^{36,140,141} The side chain polymerization of styrene on **FP1** was performed with the same procedure as before, but in the absence of DIPEA and more equivalents of the monomer (30 eq., **Figure 31a**). The side chain polymerization resulted in the formation of an insoluble polymer (**FP1-CL**). The insolubility of the polymer indicated that the polymer was cross-linked by styrene as schematically depicted in **Figure 31a**.

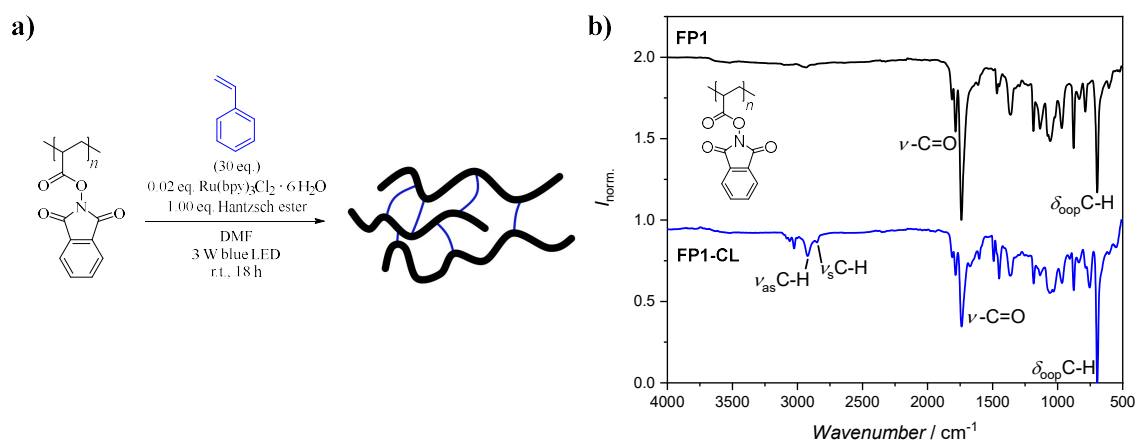


Figure 31: **a)** Side chain polymerization of styrene on **FP1** in the absence of DIPEA and formation of a cross-linked polymer (**FP1-CL**). **b)** Comparison of ATR-FT-IR spectra of **FP1** (PAP) (top, black) with **FP1-CL** (bottom, blue).

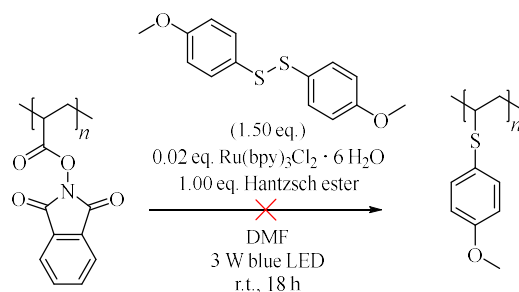
Due to the insolubility, ATR-FT-IR spectroscopy was used to analyze **FP1-CL** (**Figure 31b**). In the spectrum of the resulting polymer (blue, bottom) additional signals of low intensity at 3022 cm^{-1} , 2927 cm^{-1} (ν_{as}) and 2846 cm^{-1} (ν_{s}) arose, indicating the formation of CH_2 units of

Results and Discussion

the polystyrene backbone. Furthermore, the signal at 697 cm^{-1} originating from the $\delta_{\text{oop}}\text{C-H}$ vibration of styrene and the phthalimide featured an increased intensity proving the presence of styrene. Additionally, the experiment demonstrated the necessity to employ a control agent for the synthesis of graft polymers, as successfully performed and presented in **Chapter 4.3.4**. In summary, the Michael-type addition of α, β -unsaturated carbonyl compounds on PAP polymers was successfully demonstrated enabling the synthesis of new polymers

4.3.2 Decarboxylative Thiolation

After the successful transfer of the Michael-type addition from organic chemistry to polymers, other methods described in organic chemistry should be adapted and performed on phthalimide-based polymers as described in the following. At first, disulfides should be employed for decarboxylative functionalization of phthalimide-based precursor polymers. Herein, the weak disulfide bond should be prone to react with the carbon-centered, secondary radical at the backbone to result in a functionalized polymer. Therefore, bis-(4-methoxyphenyl)disulfide was chosen as reactant due to its easy handling, low odour nuisance and good detectability in ^1H NMR spectroscopy (**Scheme 41**).

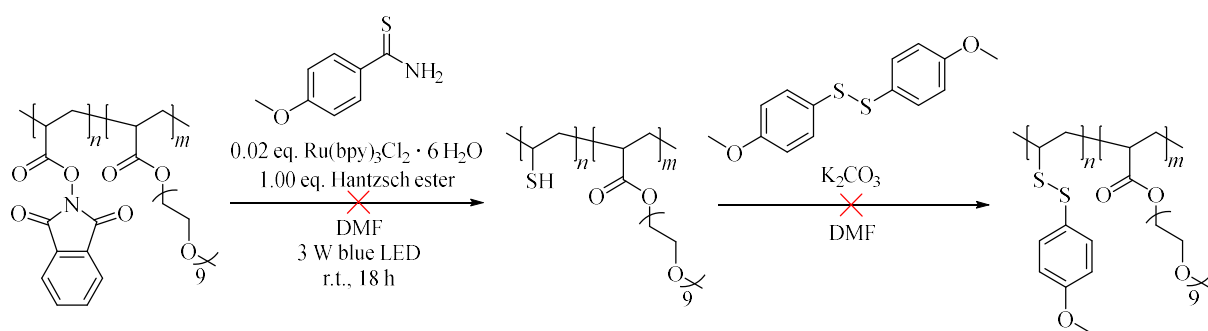


Scheme 41: Decarboxylative functionalization of **FP1** with bis-(4-methoxyphenyl)disulfide.

The decarboxylation was performed following the same procedure as for the Michael-type addition, with the difference that employing DIPEA as a radical quencher was not necessary and the Michael-acceptor was exchanged by the disulfide. In the ^1H NMR spectrum of the decarboxylation product of **FP1** only one intensive signal at 1.26 ppm and in the aromatic region as well as a signal of low intensity at 3.5 - 4.0 ppm originating from the methoxy group of the disulfide could be identified (**Figure 77**). Thus, it was concluded, that the decarboxylation of the phthalimide reached full conversion, but either the disulfide or the solvent abstracted hydrogen, resulting in the formation of CH_2 units, while only a small amount

of disulfide was added to the polymer chain and additional side reactions occurred (signals in the aromatic region). The abstraction of hydrogen from solvent¹¹¹ or thiols¹³⁴ is commonly known, whereas the abstraction from solvent is a competing reaction in many cross-coupling reactions. To circumvent this issue, other thiol sources as described by Cao *et al.*¹³⁴ should be investigated.

In 2020, Cao *et al.*¹³⁴ demonstrated the decarboxylative thiolation of phthalimide-based active esters with different thiol sources. They found 4-methoxythiobenzamide to be a potent thiol source and developed a two-step process to introduce different sulfur-based functionalities. In the first step, they introduced a thiol using 4-methoxythiobenzamide, which they further converted using a disulfide to obtain the disulfide-functionalized product. This approach was adapted to the block copolymer PAP-*b*-POEGMEA (**FP2**) with OEGMEA ($M_n = 480 \text{ g mol}^{-1}$) as comonomer (see also **Table 20**). The block copolymer was herein chosen to circumvent solubility issues and simplify the purification of the polymer by precipitation.



Scheme 42: Decarboxylative thiolation of **FP2** with 4-methoxythiobenzamide followed by functionalization with bis-(4-methoxyphenyl)disulfide.

The analysis of the reaction product of the first step *via* ¹H NMR spectroscopy (**Figure 32a**) proved the intact nature of the polymer by revealing signals of the PEG side chain (4.2 ppm (COOCH₂), 3.7 ppm (CH₂CH₂O), and 3.3 ppm (CH₃)) as well as of the backbone of POEGMEA. Furthermore, a broad signal at 1.25 ppm was identified, which could be assigned to CH₂ repeating units (marked as PE), while a signal correlating with the thiol could not be identified. It was concluded that in contrast to the findings of Cao *et al.*, either the H-abstraction from 4-methoxythiobenzamide or from the solvent dominated over the thiolation. In their study, Cao *et al.*¹³⁴ stated to observe the competing reaction between the transfer of the thiol or hydrogen to the carbon-centered radical, but they found 4-methoxythiobenzamide to be the

Results and Discussion

most suitable reactant with the highest transfer of thiol. Thus, the difference in the observation could either result from the different catalytic system employed by Cao *et al.* or the steric hindrance of the polymer. Nevertheless, the reaction was repeated and a one-pot two-step reaction as demonstrated by Cao *et al.*¹³⁴ was performed.

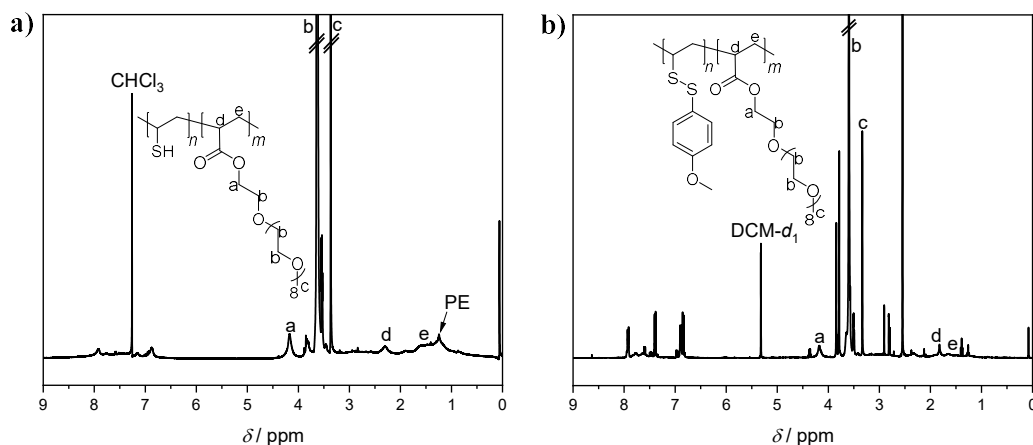


Figure 32: ^1H NMR spectra of **a)** the decarboxylative thiolation of **FP2** with 4-methoxythiobenzamide and **b)** the following functionalization in a one-pot two-step process with bis-(4-methoxyphenyl)disulfide.

In the ^1H NMR spectrum of the resulting polymer (**Figure 32b**), the signals of PEG (4.2 ppm (COOCH_2), 3.7 ppm ($\text{CH}_2\text{CH}_2\text{O}$), and 3.3 ppm (CH_3)) could be identified. In addition, several signals appeared in the aromatic region, but those could not be assigned to the functionalized polymer due to their splitting pattern, which resulted from organic impurities rather than a polymer. It was concluded that the reaction did not proceed as intended, but H-abstraction from 4-methoxythiobenzamide or solvent occurred as proven by the signal of low intensity at 1.26 ppm probably originating from CH_2 units. In a last experiment, Eosin Y was used as the catalyst in the decarboxylation process (**Figure 33a**), since Cao *et al.*¹³⁴ used it as an inexpensive organocatalyst. The procedure was adapted and Eosin Y (0.02 eq. per active ester group), DIPEA as the reductant (instead of HE, 1.10 eq. per active ester group), 4-methoxythiobenzamide (1.00 eq. per active ester group), bis-(4-methoxyphenyl)disulfide (2.00 eq. per active ester group), and potassium carbonate (2.00 eq. per active ester group) were used for the two-step reaction. The comparison of the final reaction product and the intermediate (thiol) *via* ^1H NMR spectroscopy (**Figure 33b**) revealed signals of low intensity assigned to the POEGMEA block (4.2 ppm (COOCH_2), 3.7 ppm ($\text{CH}_2\text{CH}_2\text{O}$), and 3.3 ppm

(CH₃) in both cases, but neither a signal of the thiol, nor aromatic signals of bis-(4-methoxyphenyl)disulfide. It was considered, that although the phthalimide side groups were removed with a conversion of > 90%, the following thiolation could not be performed.

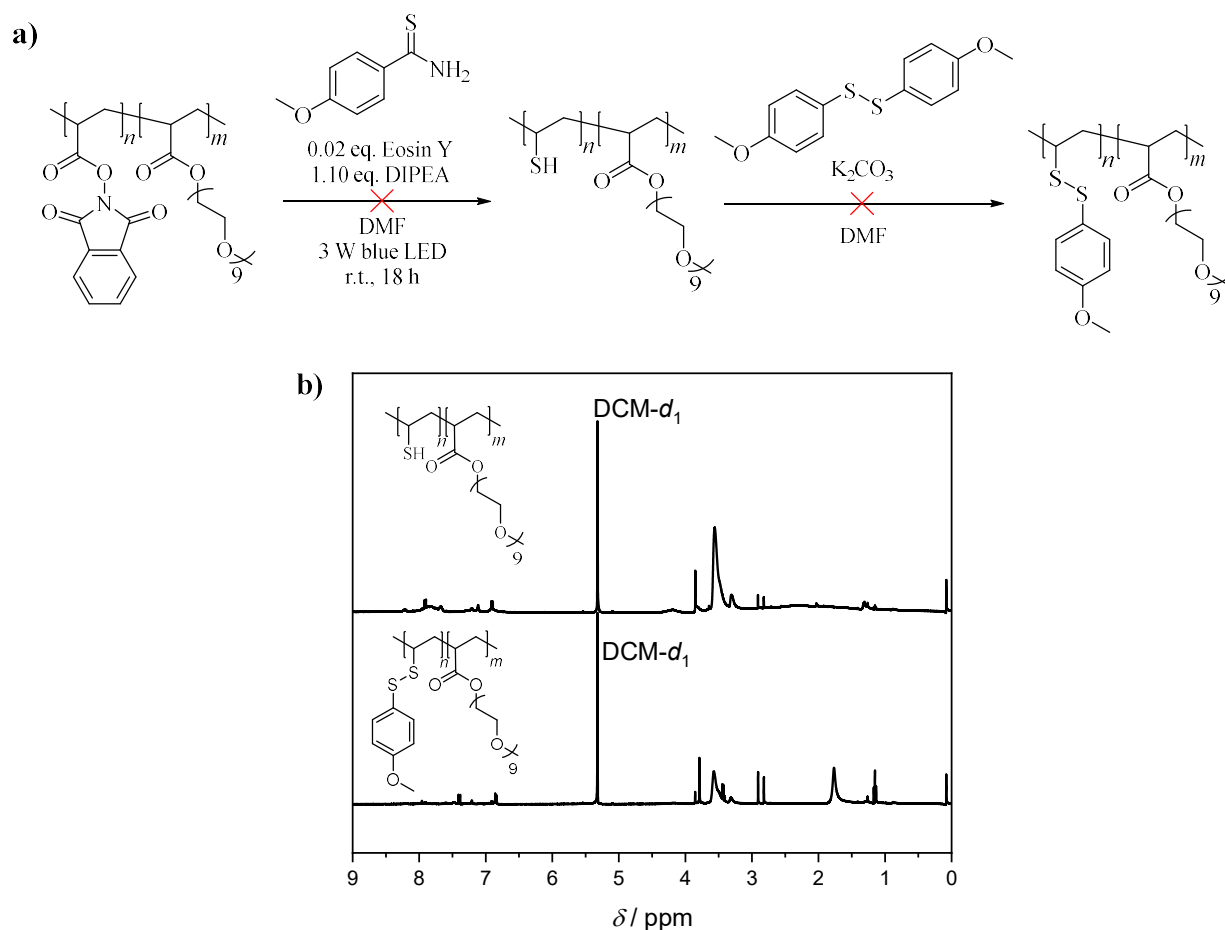


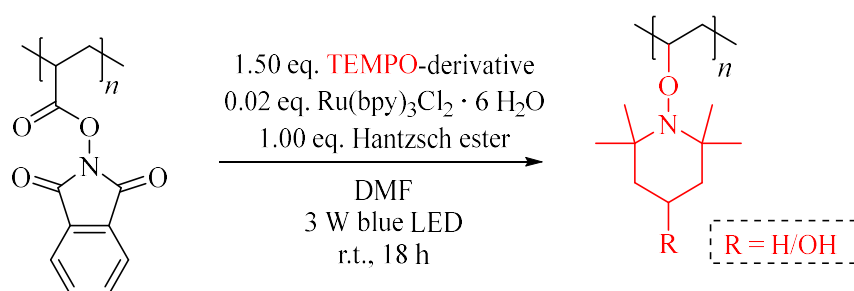
Figure 33: **a)** Decarboxylative thiolation with Eosin Y as the catalyst as used by Cao *et al.*¹³⁴ and **b)** the comparison of the ¹H NMR spectra of the first step (top) and the second step (bottom) of the reaction.

Furthermore, the few signals (beside the signals of POEGMEA) in the ¹H NMR spectra could not be assigned to specific side products, such as the introduction of hydrogen by H-abstraction resulting in CH₂ units. Since even the exchange of the catalytic system and employing the exact same conditions like Cao *et al.* did not improve the result, the idea of introducing sulfur-based molecules to PAP was dismissed to focus on other functionalization methods as presented in the following.

Results and Discussion

4.3.3 Nitroxide Radical Coupling

The Michael-type addition of α , β -unsaturated carbonyl compounds has already successfully proven the possibility of employing the carbon-centered radical for the functionalization of PAP. Another well-known reaction of carbon-centered radicals is the so-called nitroxide radical coupling (NRC), in which a nitroxide reacts with the radical under formation of an alkoxyamine (details in **Chapter 2.4**). Moreover, NRC is a common tool in polymer chemistry and frequently used in combination with peroxide-initiated crosslinking or functionalization.^{40,142–145} Additionally, the common polymerization and block building technique nitroxide-mediated polymerization (NMP) is based on the mechanism of NRC.^{146,147} As explained in detail in **Chapter 2.4**, stabilized nitroxides such as 2,2,6,6-tetramethylpiperidin-1-yl)oxyl (TEMPO) are reactive towards carbon-centered radicals^{40,77} but do not react with oxygen-centered radicals or terminate with themselves due to the persistent radical effect.¹⁴⁸ In the case of the decarboxylation process developed in the course of this thesis, the secondary radical formed at the polymer backbone should be used for NRC with TEMPO-derivatives. To do so, NRC with TEMPO-based radicals was conducted on the homopolymer PAP (**FP1**). Photochemically-induced decarboxylation was employed (0.02 eq. $\text{Ru}(\text{bpy})_3\text{Cl}_2 \cdot 6 \text{H}_2\text{O}$, 1.00 eq. HE) with TEMPO or (4-hydroxy-2,2,6,6-tetramethylpiperidin-1-yl)oxyl (TEMPO-OH, 1.50 eq.) (**Scheme 43**) instead of the hydrogen-donor.



Scheme 43: Decarboxylative NRC on PAP with TEMPO or TEMPO-OH.

Both, the decarboxylation and in-situ TEMPO or TEMPO-OH addition proceeded quantitatively without further optimization of the reaction conditions. The ^1H NMR and ATR-FT-IR spectroscopy analyses of the polymer after functionalization with TEMPO-OH to poly[2,2,6,6-tetramethyl-1-(vinyl)oxy)piperidin-4-ol] (**PTEMVPO**) are exemplarily shown in **Figure 34a** and **Figure 34b**. In the ^1H NMR spectrum the typical signals of the proton next to the hydroxy group (4.3 ppm) and the backbone proton (3.75 ppm) as well as the intensive

signals of the methyl groups of TEMPO-OH (1.02 ppm) could be identified, while the aromatic proton signal of the phthalimide (7.8 ppm) could not be identified, stating a quantitative decarboxylation and functionalization with TEMPO-OH. The results of the ^1H NMR analysis were further corroborated by ATR-FT-IR spectroscopy. On the one hand, the vibration of O-H at 3370 cm^{-1} and the intensive C-H vibration at 2931 cm^{-1} ($\nu_{\text{as}}\text{C-H}$) originating from TEMPO-OH could be observed, while on the other hand the removal of the aromatic C-H (δ_{oop}) vibration at 695 cm^{-1} demonstrated the quantitative removal of the phthalimide.

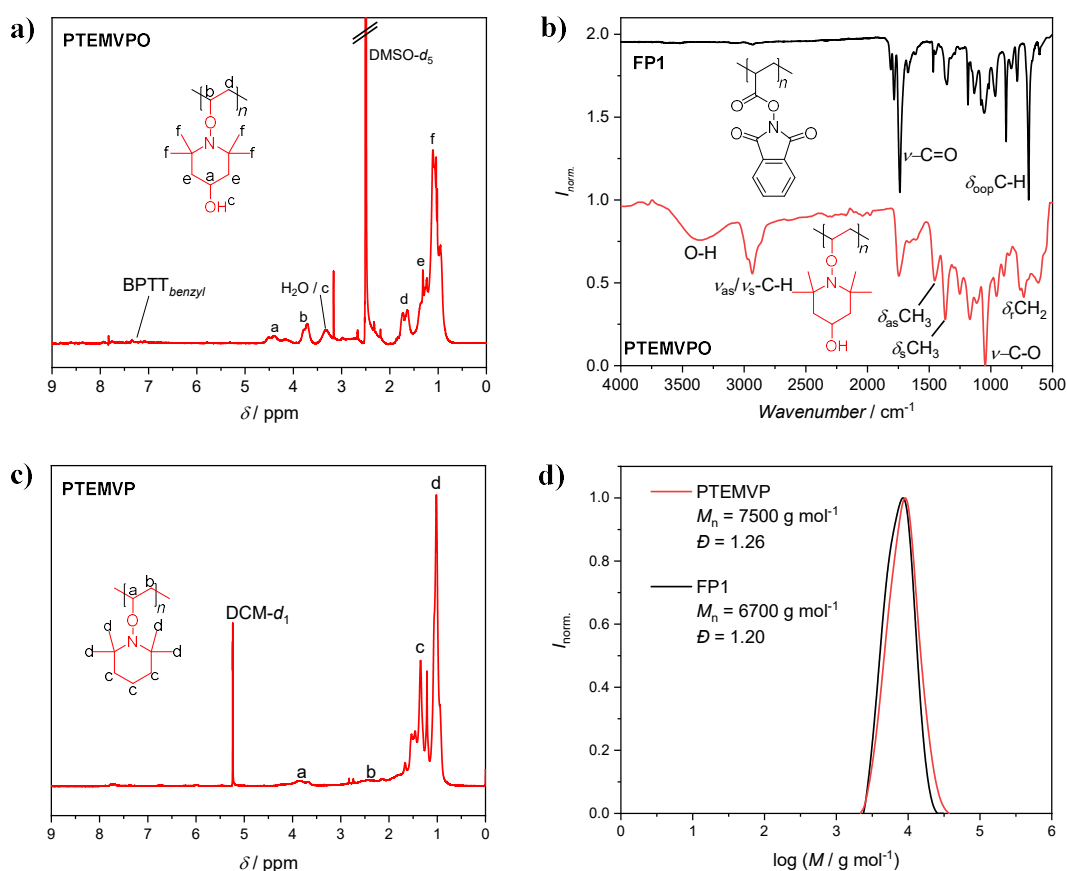


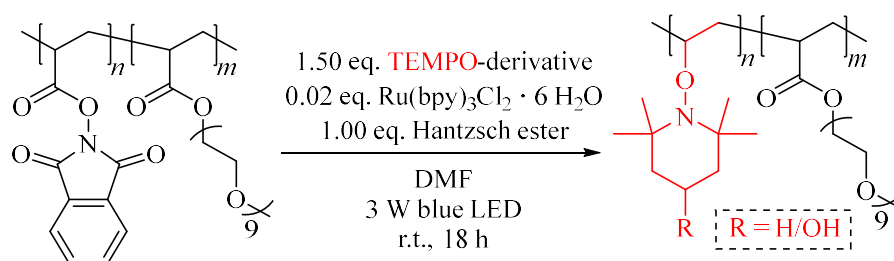
Figure 34: a) ^1H NMR spectrum of **PTMVP** after decarboxylation of PAP with TEMPO-OH; solvent: $\text{DMSO-}d_6$. b) Comparison of ATR-FT-IR spectra of **FP1** (top, black) and **PTMVP** (bottom, red). c) ^1H NMR spectrum of **PTMVP** after decarboxylation of PAP with TEMPO; solvent: $\text{DCM-}d_2$. d) SEC chromatogram of **PTMVP** and precursor **FP1** in DMAC as eluent with PMMA calibration.

The analysis of the TEMPO-functionalized polymer poly[2,2,6,6-tetramethyl-1-(vinylxy)piperidine] (**PTMVP**) via ^1H NMR (Figure 34c) and ATR-FT-IR spectroscopy revealed similar results as for **PTMVP** and proved the successful decarboxylation.

Results and Discussion

Furthermore, SEC analysis (**Figure 34d**) proved the intact nature of the polymer after decarboxylation followed by NRC, by revealing a monomodal distribution. In both cases, the molar mass of the polymers was slightly increased in comparison to **FP1** even though the molar masses of TEMPO and TEMPO-OH themselves are slightly lower than the one of the phthalimide. However, the deviation is within the tolerance of the SEC and the bulky structure of TEMPO results in a lower flexibility of the chain, eventually increasing the hydrodynamic radius.

Thus, the functionalization of PAP using both TEMPO-derivatives could be performed without further optimization of the reaction conditions. Additionally, and especially for further reactions of TEMPO-based polymers, the decarboxylative NRC was investigated on block copolymers with OEGMEA ($M_n = 480 \text{ g mol}^{-1}$) as comonomer (**FP2**, PAP-*b*-POEGMEA, **Table 20**) as shown in **Scheme 44**.



Scheme 44: Decarboxylative NRC on PAP-*b*-POEGMEA with TEMPO or TEMPO-OH.

The decarboxylative NRC of the block copolymer proceeded quantitatively with both TEMPO derivatives, without noticeable side reactions as proven by ¹H NMR and ATR-FT-IR spectroscopy (**Figure 35**). Similar to the functionalization of the homopolymer, the disappearance of the aromatic proton signal of the phthalimide (7.8 ppm) as well as the appearance of the signals of the TEMPO methyl groups (1.03 ppm) can be clearly identified (**Figure 35a**). Additionally, the presence of the signals of POEGMEA (4.2 ppm (COOCH₂), 3.7 ppm (CH₂CH₂O) and 3.2 ppm (CH₃)) indicated the successful decarboxylation and subsequent NRC functionalization on different polymer architectures. Furthermore, ATR-FT-IR spectroscopy proved the quantitative decarboxylation of the phthalimide groups by removal of the aromatic C-H (δ_{oop}) vibration at 695 cm⁻¹.

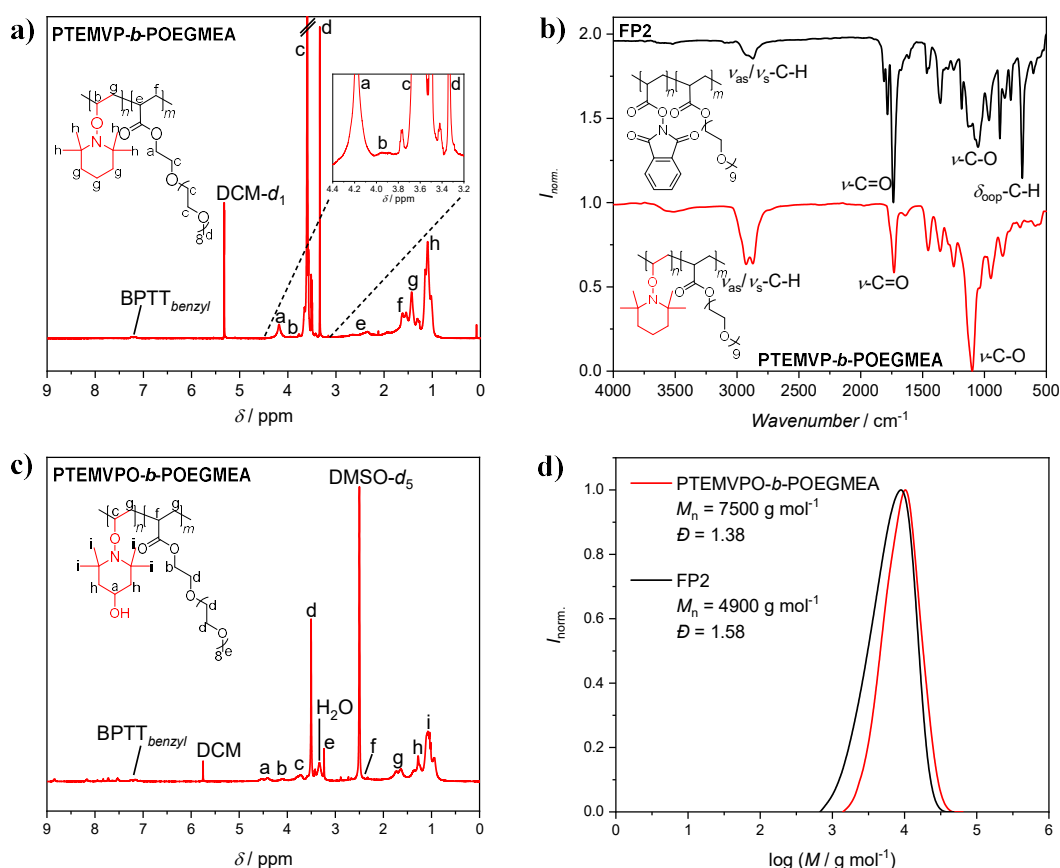
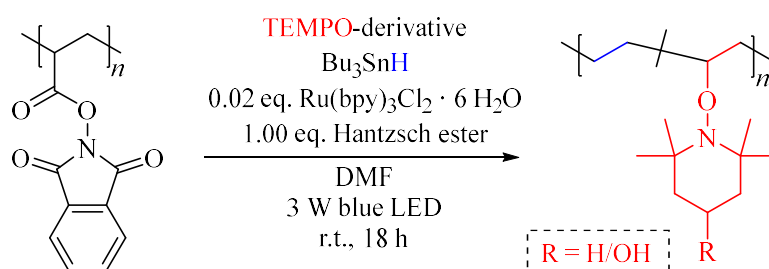


Figure 35: **a)** ^1H NMR spectrum of **PTEMVP-*b*-POEGMEA** after decarboxylation of **PAP-*b*-POEGMEA (FP2)** with TEMPO; solvent: $\text{DCM-}d_2$. **b)** Comparison of ATR-FT-IR spectra of **FP2** (top, black) and **PTEMVP-*b*-POEGMEA** (bottom, red). **c)** ^1H NMR spectrum of **PTEMVPO-*b*-POEGMEA** after decarboxylation with TEMPO-OH; solvent: $\text{DMSO-}d_6$. **d)** SEC chromatogram of **PTEMVPO-*b*-POEGMEA** and precursor **FP2** with DMac as eluent and PMMA calibration.

Finally, block copolymer **FP2** was functionalized with TEMPO-OH to obtain **PTEMVPO-*b*-POEGMEA** and analyzed by ^1H NMR (**Figure 35c**) and ATR-FT-IR spectroscopy. Comparable to the ^1H NMR spectrum of **PTEMVPO** homopolymer, signals of the proton next to the hydroxy group (4.3 ppm) and the backbone proton (3.75 ppm) as well as the intensive signals of the methyl groups of TEMPO (1.02 ppm) could be identified besides the signals of POEGMEA. The overall polymer architecture and POEGMEA block were not affected by NRC on the PAP chain as judging from the spectra and the SEC chromatogram (**Figure 35d**). In summary, a new and controlled synthesis route to access TEMPO-functionalized polymer systems was established. In the following those systems are further modified.

Results and Discussion

To demonstrate the versatility and application of the decarboxylative NRC of phthalimide-based precursor polymers, further PPMs should be performed. As described in the theoretical part (**Chapter 2.4**), NRC is commonly conducted on polyolefins like PE to obtain TEMPO-functionalized polyolefins such as poly(ethylene-*co*-TEMVP), which can be further used to obtain PE graft polymers.^{143,144} High temperatures and for instance the utilization of peroxides are necessary to form radicals at the polymer backbone for a successful functionalization.⁸⁰ Thus, the formation of a carbon-centered radical at the polymer backbone by decarboxylation of PAP followed by NRC with TEMPO should be used as an alternative and comparably mild pathway towards TEMPO-functionalized polyolefins (**Scheme 45**). Herein, it was planned to perform the decarboxylation using TEMPO and the H-donor simultaneously, to functionalize the polymer with TEMPO on the one hand and to obtain PE units by the H-donor on the other hand.



Scheme 45: Synthesis of poly(ethylene-*co*-TEMVP) from PAP by simultaneous decarboxylation with TEMPO/TEMPO-OH and Bu₃SnH as H-donor.

First, the equivalents of TEMPO and the H-donor Bu₃SnH used for the decarboxylation had to be evaluated. Initially 1.20 eq. of Bu₃SnH and 0.20 eq. of TEMPO were chosen, while employing 0.02 eq. of Ru(bpy)₃Cl₂ and 1.00 eq. of HE (**Table 4**, entry #1). This specific ratio of H-donor to TEMPO was chosen to i) ensure a quantitative decarboxylation by adding an excess of H-donor/TEMPO and ii) to obtain a polymer which mainly features the properties of PE with only a few TEMPO units which could be used for grafting. However, the decarboxylation under the given conditions resulted in the formation of an insoluble polymer. It was concluded that either the relative fraction of CH₂ units was too high and the polymer could not be dissolved due to its polyolefinic character or side reactions occurred causing the insolubility. To circumvent the solubility issue, TEMPO was exchanged with TEMPO-OH (0.30 eq.) featuring a superior solubility, while 0.80 eq. of Bu₃SnH were employed (**Table 4**, entry #2). Here, a soluble polymer was obtained, which could be analyzed *via* ¹H NMR

spectroscopy in deuterated DMSO (**Figure 78**). The analysis revealed signals of TEMPO-OH, signals in the aromatic region (partly of the phthalimide group and of impurities), and an additional signal at 1.26 ppm between the signal of the CH₂ groups (1.4 ppm) and methyl groups of TEMPO (1.03 ppm), which could be assigned to CH₂ repeating units of PE.

Table 4: Overview of different reaction conditions used for the synthesis of poly(ethylene-*co*-TEMVP).

Entry	Polymer*	TEMPO derivative	eq. TEMPO	eq. H-donor	eq. HE	Comment
1	HP	TEMPO	0.20	1.20	1.00	Insoluble material
2	HP	TEMPO-OH	0.30	0.80	1.00	Signals of TEMPO-OH
3	HP	TEMPO-OH	0.30	1.30	1.10	<i>PhSiH₃ as H-donor</i>
4	HP	TEMPO-OH	3.00	0.50	0.50	<i>Two-step reaction, reduced eq. of HE</i>
5	HP	TEMPO-OH	1.20	0.50	0.50	<i>Two-step reaction, reduced reaction time</i>
6	BP	TEMPO-OH	0.50	2.00	2.00	<i>One-step reaction, HE as H-donor</i>

*HP = homopolymer, BP = block copolymer.

Noteworthy, the chemical shift of the signal of the methyl- and ethyl-groups of TEMPO did not fit to the shift observed in **Chapter 4.3.3** (slightly shifted towards higher ppm) and the signals are not broadened, but in contrast sharper and clearly distinguishable. The result indicated that i) the decarboxylation did not proceed quantitatively, but TEMPO-OH as well as hydrogen were added to the polymer backbone, ii) a copolymer with randomly distributed TEMPO-OH units was formed (indicated by the clearly distinguishable and not broadened signals) and iii) the ratio of TEMPO-OH to CH₂ units did not fit to the equivalents of the reactants employed for decarboxylation (too many TEMPO-OH groups attached to the polymer). Especially the latter mentioned issue will be evaluated in the following. Since the decarboxylation could not be performed in a quantitative fashion, the reaction conditions were further varied and the H-donor was exchanged from Bu₃SnH to PhSiH₃ (**Table 4**, entry #3). The ¹H NMR spectrum of the

Results and Discussion

reaction product showed signals assigned to TEMPO-OH (CH₂ (1.4 ppm), CH₃ (0.9 ppm)) and an additional signal at 1.26 ppm overlaying with the TEMPO signals (**Figure 36**). Furthermore, a broad and intensive signal at 7.30 ppm was identified arising from side reaction of phenylsilane (compare **Chapter 4.1.4** and **0**). Since employing PhSiH₃ did not improve the reaction result (ratio and form of signals of TEMPO and PE units), but additional side reaction involving PhSiH₃ occurred, the approach was dismissed and Bu₃SnH was used as the H-donor for all following experiments.

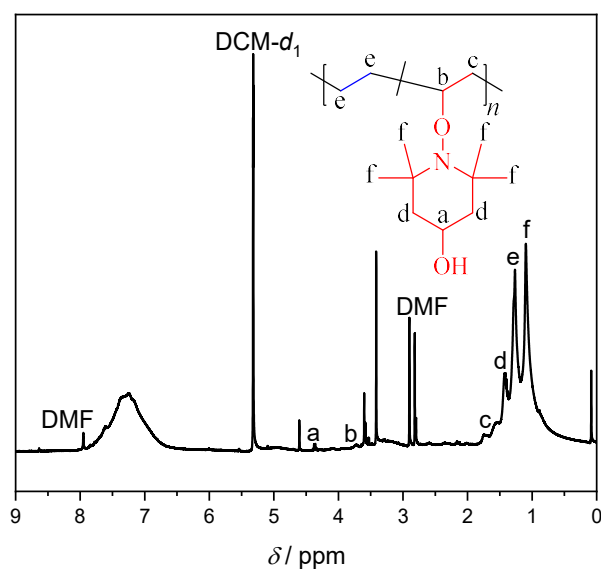
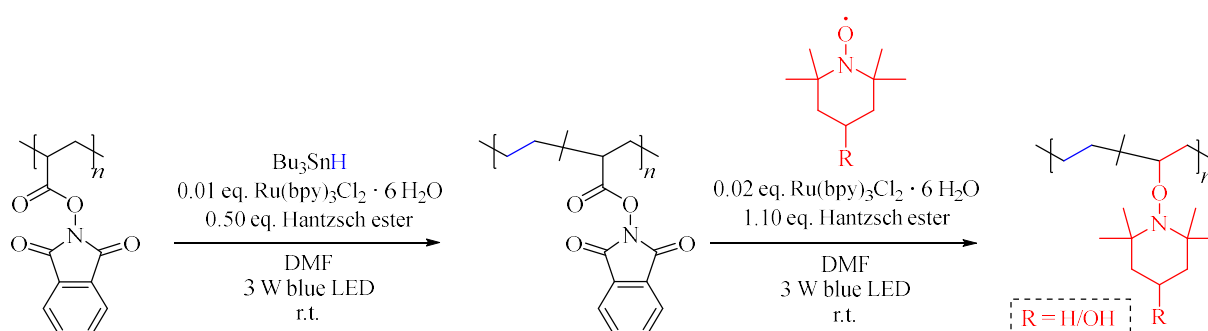


Figure 36: ¹H NMR spectra of the decarboxylation of PAP with TEMPO-OH and PhSiH₃ as H-donor.

McKie *et al.*¹⁴⁹ showed that the abstraction of hydrogen from Bu₃SnH is relatively slow ($k = 2 \cdot 10^6 \text{ M}^{-1} \text{ s}^{-1}$)¹⁵⁰ in comparison to the radical trapping by TEMPO ($k = 1.2 \cdot 10^9 \text{ M}^{-1} \text{ s}^{-1}$)¹⁵¹. Thus, the simultaneous addition of Bu₃SnH and TEMPO should result in a fast coupling of TEMPO with the carbon-centered radicals of the polymer backbone, while the addition of hydrogen is magnitudes slower. This also explains the observation that the ratio of TEMPO-OH to CH₂ groups did not fit. Since the TEMPO radicals couple much faster, they couple with the carbon-centered radical and are consumed in the first place. As long as TEMPO radicals are still present the H-abstraction from Bu₃SnH proceeds slow and CH₂ is formed at a low rate. When most of the TEMPO radicals have coupled, CH₂ is formed by H-abstraction from Bu₃SnH, contrary to the expected evenly distributed coupling of the TEMPO and H-radicals.

Furthermore, it was found that the tributyltin radical can react with TEMPO in a competing reaction during the decarboxylation.¹⁴⁹ This was also proven by an experiment, in which TEMPO (orange coloured solution) and Bu₃SnH were dissolved and mixed resulting in bleaching of the orange coloured solution. To circumvent side reactions between the H-donor and TEMPO, the reductive decarboxylation with Bu₃SnH and the decarboxylative functionalization with TEMPO was divided into two separate steps as demonstrated in **Scheme 46**.



Scheme 46: Synthesis of poly(ethylene-*co*-TEMVP) from PAP *via* a two-step reaction with the partly reductive decarboxylation with Bu₃SnH in the first step, followed by the decarboxylative functionalization with TEMPO.

To do so and to reach the actual goal to obtain a polymer with 50% PE units (to ensure that the partly decarboxylated polymer is still soluble), the reductive decarboxylation with Bu₃SnH was performed in a first step with 0.50 eq. H-donor and 0.50 eq. of HE, which should result in a decarboxylation of 50% of the phthalimide units. Even though it would be more suitable to perform the decarboxylative functionalization with TEMPO-OH in the first step to circumvent solubility issues, side reaction between PTEMVPO units at the polymer chain and Bu₃SnH should be avoided by performing the TEMPO-OH functionalization in the second step. Thus, it was intended to partly decarboxylate the polymer in the first step and use an excess of TEMPO (3.00 eq.) for the second decarboxylation in a two-step process (**Table 4**, entry #4). In the spectrum of the obtained polymer (**Figure 37**), three clear signals at 0.7 – 1.8 ppm were identified. While the middle signal at 1.25 ppm could be assigned to CH₂ repeating units, the other signals originated from the methyl and ethyl groups of TEMPO, even though their form is not as expected as discussed before. Additionally, the intensity of the signals of the proton next to the hydroxy group (4.2 ppm) and the backbone proton (3.6 ppm) did not fit to the intensity of the signals of the ethyl groups of TEMPO-OH (1.6 ppm).

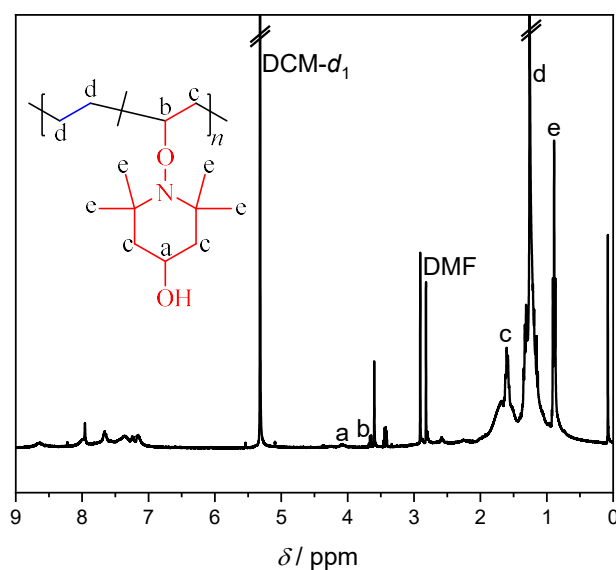


Figure 37: ¹H NMR spectrum of the decarboxylation of PAP with Bu₃SnH in the first step followed by decarboxylative functionalization with TEMPO in a second step with reduced equivalents of HE.

To further improve the reaction result, besides the reduced equivalents of H-donor and HE, the reaction time was adjusted and reduced to 15 minutes (**Table 4**, entry #5). This time frame is based on the kinetic investigations in **Chapter 4.1.4**, where the decarboxylation was found to proceed at a high reaction rate and the decarboxylation featured a quantitative conversion after 30 min under given conditions (time, concentration, reactants). In addition, the polymer obtained after the first decarboxylation with Bu₃SnH was analyzed by ¹H NMR spectroscopy, to examine whether the intended partly decarboxylation was successful. The analysis of the intermediate after the decarboxylation with Bu₃SnH for 15 min revealed the successful partly decarboxylation, since signals of the aromatic phthalimide protons (7.8 ppm) and a signal of low intensity assigned to CH₂ units were identified (**Figure 38a**). The ¹H NMR spectrum of the final product after the second decarboxylation with TEMPO-OH showed the three prominent signals in the range of 0.75 – 1.75 ppm and an additional, broad signal at 3.7 ppm (**Figure 38b**). The result indicated that the reduction of the reaction time did not further improve the reaction result. In contrast, the splitting of the decarboxylation into two steps improved the reaction result the most.

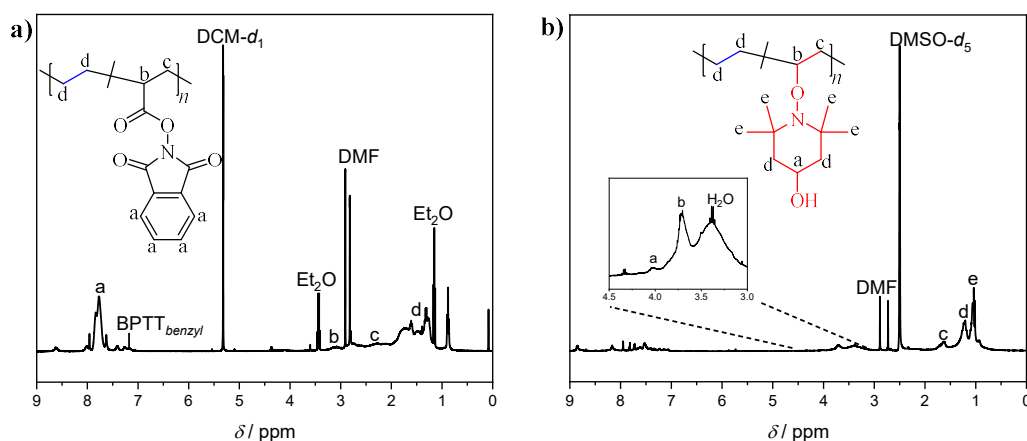


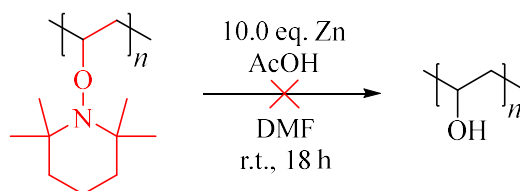
Figure 38: ^1H NMR spectra of the decarboxylation product **a)** after the first decarboxylation with Bu_3SnH as H-donor, 0.50 eq. HE and 15 min reaction time and **b)** after the second decarboxylation with TEMPO-OH.

In summary, the evaluation demonstrated that the synthesis of poly(ethylene-*co*-TEMVP) by decarboxylative functionalization with TEMPO and reduction with Bu_3SnH is in principle possible. Nevertheless, the reaction conditions have to be carefully evaluated and the competing reaction between Bu_3SnH and TEMPO has to be avoided. Therefore, the reaction has to be performed in a two-step process. Since performing a two-step process with two decarboxylation steps would not bring a great advantage over the common methods and because further evaluation is required to optimize the reaction to the final stage of operability, the project was postponed to further focus on the functionalization of **PTEMVP** or **PTEMVPO**.

4.3.4 Modification of TEMPO-functionalized Polymers

The modification of TEMPO moieties is a well-known subject in organic and polymer chemistry research.^{40,152,153} While in organic chemistry, the reduction of alkoxyamines based on TEMPO represents an efficient method to obtain alcohols, in polymer chemistry modifications of TEMPO are mostly performed on end groups of polymers synthesized by NMP.¹⁵⁴ In the case of TEMPO-functionalized polymers (**PTEMVP** and **PTEMVPO**), the reduction of the alkoxyamine should result in the formation of poly(vinyl alcohol) (PVA, **Scheme 47**). The standard synthesis of PVA is based on the hydrolysis of poly(vinyl acetate) (PVAc), mostly with sodium hydroxide, whereby reaching a quantitative conversion of the acetate is challenging. Herein, the reduction of **PTEMVP** synthesized by decarboxylation of **FP1** could be an alternative method.

Results and Discussion



Scheme 47: Reduction of **PTEMVP** to PVA with zinc and acetic acid.

To do so, reaction conditions used in literature were sorted and a procedure for **PTEMVP** developed. First, the homopolymer **PTEMVP** was used for the reduction with zinc (Zn, 10.0 eq.) and acetic acid (AcOH, 200 eq.) in DMF (**Table 5**, entry #1). Due to the limited solubility of **PTEMVP** in polar solvents, the ratio of DMF and AcOH had to be evaluated. For the reduction, the polymer was dissolved in DMF, AcOH was added and the solution was deoxygenated. Simultaneously, zinc was deoxygenated in a flask, the polymer/AcOH solution was then added and the reaction stirred overnight. The subsequent precipitation of the polymer resulted in high amounts of zinc acetate precipitating besides the polymer, making an analysis impossible. Therefore, the polymer was purified by dialysis (Spectra Pro, prewetted dialysis membrane with, MWCO = 1000 g mol⁻¹) in a methanol/water (80:20) mixture, which was chosen to i) dissolve the zinc acetate and ii) dissolve the possibly formed PVA. However, only an insoluble powder was obtained after purification. ATR-FT-IR spectroscopy was used to analyze the insoluble product as shown in **Figure 39**.

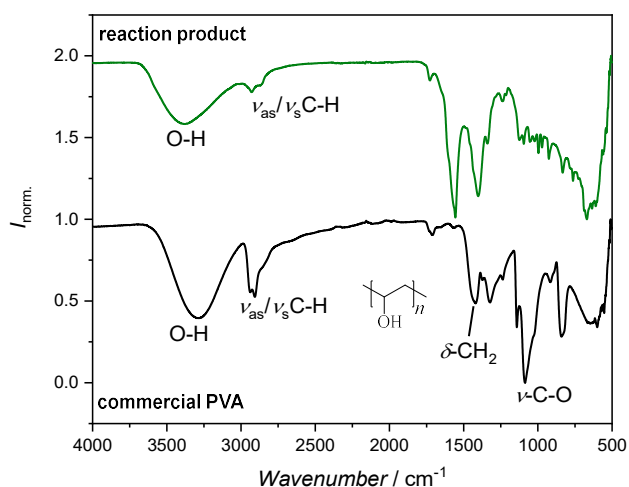


Figure 39: Comparison of the ATR-FT-IR spectra of the product after reduction of **PTEMVP** with Zn/AcOH in DMF (top, green) and of commercial PVA (black, bottom, Mowiol® 28-29, $M_w \sim 145.000$ g mol⁻¹, Sigma-Aldrich).

In the spectrum two intensive signals at 1556 cm^{-1} and 1397 cm^{-1} arose, as well as an intensive and broad signal at 3390 cm^{-1} originating from OH-groups, while the intensity of the $\nu_{\text{as}}\text{C-H}$ and $\nu_{\text{s}}\text{C-H}$ vibrations (2932 cm^{-1}) is rather low. Besides PVA, the signal of the OH-group could arise from water or methanol, which was used as solvent for purification by dialysis and zinc acetate which was not completely removed. In comparison to the ATR-FT-IR spectrum of commercial PVA (**Figure 39**, bottom), the signals of the obtained product are different, especially the intensive signal of the C-O vibration at 1082 cm^{-1} is missing in the spectrum of the product. Therefore, the procedure was further adapted.

Since PVA is insoluble in organic solvents, it was decided to use the **PTEMVP-*b*-POEGMEA** block copolymer to improve the solubility of the polymer during the reaction and facilitate the analysis (**Table 5**, entry #2). For the reduction 10.0 eq. of Zn and 200 eq. of AcOH were used, while the temperature was increased to $60\text{ }^{\circ}\text{C}$. As a result, a soluble polymer was obtained after purification by dialysis, which was analyzed *via* ^1H NMR spectroscopy. The spectrum revealed signals of the PEG side chain (4.24 ppm (COOCH_2), 3.5 ppm (OCH_2CH_2) and 3.2 ppm (CH_3)) stating the intact nature of the polymer (**Figure 40a**). Furthermore, prominent signals of TEMPO (0.8 – 1.9 ppm), but no signals of PVA (CHOH) could be identified, indicating that the reaction did not proceed as intended. A similar result was obtained changing the polymer to **PTEMVPO-*b*-POEGMEA** (**Table 5**, entry #3). The analysis of the ^1H NMR spectrum revealed signals of PEG (4.24 ppm (COOCH_2), 3.5 ppm (OCH_2CH_2) and 3.2 ppm (CH_3)) and TEMPO-OH (4.36 ppm (CHON), 1.25 ppm (CH_2), and 1.03 ppm (CH_3)) (**Figure 79**). The analysis of both reactions indicated that neither the alkoxyamines of TEMPO nor TEMPO-OH were even partly reduced by Zn/AcOH, which was unexpected, since the reaction usually features quantitative conversions on small molecules or end groups.^{113,152,154} Possibly, either the steric hindrance of the TEMPO units at the backbone or the low reactivity of Zn (activated Zn was not used) caused the reduction to fail.

Results and Discussion

Table 5: Variation of the reaction conditions for the reduction of **PTEMVP** / **PTEMVPO** homopolymers and block copolymers.

Entry	Polymer [†]	TEMPO derivative	Solvent	Temp. [°C]	Reductive system	Result*
1	HP	TEMPO	DMF	60	Zn/AcOH	Insoluble powder
2	BP	TEMPO	DMF	60	Zn/AcOH	PTEMVP signals
3	BP	<i>TEMPO-OH</i>	DMF	60	Zn/AcOH	PTEMVPO signals
4	BP	TEMPO-OH	DMF	60	Zn/AcOH	PTEMVPO , Zn(Ac) ₂ signals
5	BP	TEMPO-OH	DMF	80	Zn/AcOH	PTEMVPO , Zn(Ac) ₂ signals
6	BP	TEMPO-OH	<i>THF/H₂O</i>	60	Zn/AcOH	Not isolated
7	BP	<i>TEMPO</i>	THF/H ₂ O	60	Zn/AcOH	Signals of PEG
8	HP	TEMPO-OH	<i>MeOH/THF/H₂O</i>	<i>r.t.</i>	<i>Zn</i>	PTEMVPO signals

[†]HP = homopolymer, BP = block copolymer; *estimated by ¹H NMR spectroscopy.

Therefore, the equivalents of Zn (20.0 eq.) and acetic acid (250 eq.) were increased and the reduction was repeated with **PTEMVPO-*b*-POEGMEA**, which possessed a better solubility in polar solvents due to the additional hydroxy group. The reduction was performed once at 60 °C (**Table 5**, entry #4) and once at increased temperature (80 °C, **Table 5**, entry #5). The analysis of both polymers (reduction at 60 °C, **Figure 80**; reduction at 80 °C in **Figure 40b**) via ¹H NMR spectroscopy revealed similar spectra. In the spectrum of the polymer reduced at 80 °C, the signals of PEG (4.24 ppm (COOCH₂), 3.5 ppm (OCH₂CH₂) and 3.2 ppm (CH₃)) as well as of TEMPO-OH (4.36 ppm (CHON), 1.25 ppm (CH₂), and 1.03 ppm (CH₃)) could be clearly identified, stating the intact nature of the polymer after the reduction. Additionally, an intensive signal of Zn(Ac)₂ was found at 1.8 ppm since the polymer was not purified by dialysis but by precipitating and higher equivalents of Zn and AcOH were used. The analysis indicated that once again the TEMPO moieties were not reduced at all.

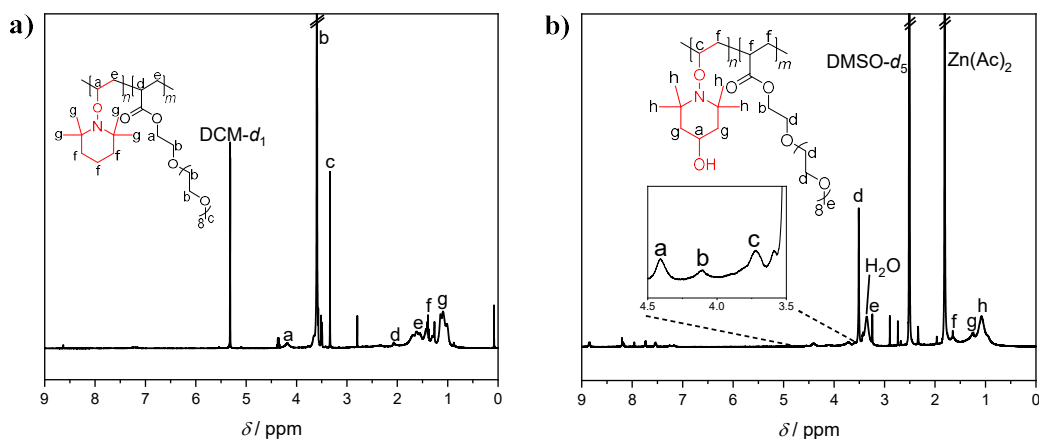


Figure 40: ^1H NMR spectra of reduction of **a) PTEMVP-*b*-POEGMEA** in DMF at 60 °C with Zn/AcOH (Table 5, entry #2) and **b) PTEMVPO-*b*-POEGMEA** in DMF at 80 °C with Zn/AcOH (Table 5, entry #5).

Contrary to DMF, which was used as the solvent for the reduction, in literature the reduction of alkoxyamines is mostly performed in THF or a mixture of THF and H_2O as solvent.^{152,153} Thus, it was suggested that the solvent could play a critical role for the reduction step. Therefore, **PTEMVPO-*b*-POEGMEA** and **PTEMVP-*b*-POEGMEA** were both used for reduction in THF/ H_2O mixture as solvent (Table 5, entry #6 and entry #7), since most literature procedures use THF/ H_2O as solvent. In the case of **PTEMVP-*b*-POEGMEA**, high dilution was necessary to dissolve the polymer (due to the limit solubility of the PTEMVP block in THF in contrast to TEMVPO). Nevertheless, the ^1H NMR spectrum only revealed signals of PEG and TEMPO (Figure 41a). In a last experiment, **PTEMVPO** was used for the reduction in a mixture of methanol, THF and water at room temperature with Zn, but without acetic acid. By doing so, the formation of $\text{Zn}(\text{Ac})_2$ should be avoided, while using the solvent mixture should provide excellent solubility for the precursor polymer as well as PVA. The analysis of the reaction product *via* ^1H NMR spectroscopy (Figure 41b) however revealed signals of **PTEMVPO** (4.36 ppm (CHON), 1.25 ppm (CH_2), and 1.03 ppm (CH_3)), but no signals of PVA.

Results and Discussion

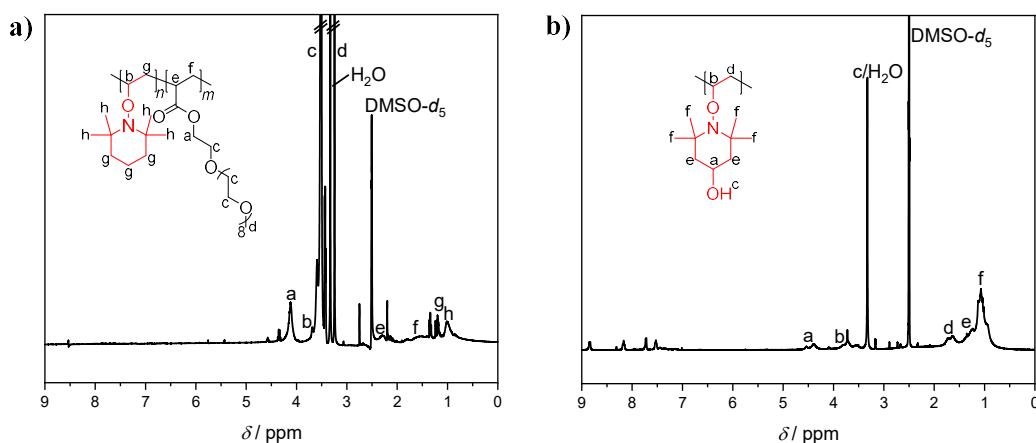
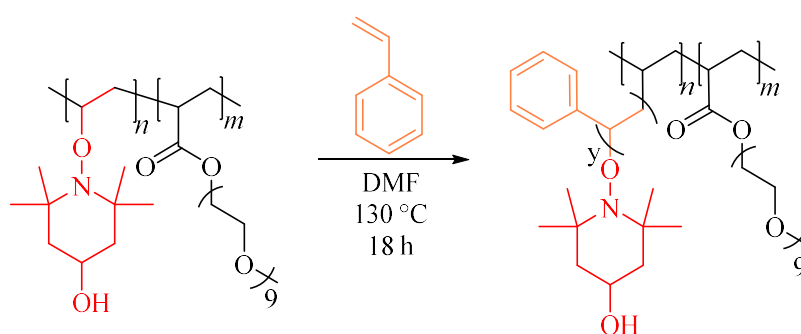


Figure 41: ^1H NMR spectra of the reduction of **a) PTEMVP-*b*-POEGMEA** in THF/H₂O at 60 °C with Zn/AcOH followed by dialysis (Table 5, entry #6) and **b) PTEMVPO** in MeOH/THF/H₂O at room temperature with Zn (Table 5, entry #9).

Finally, it was concluded, that the reason of the reaction to fail could be the high steric hindrance of the TEMPO groups at every repeating unit of the polymer. In various literature reports, TEMPO is mainly bound either to organic molecules or as an end group on a polymer, but not as a side group as in the case of the present chapter. However, the accessibility of zinc to the C-O bond is significantly better in the case of organic molecules and end groups than in the case of the functionalized polymers. Whether this assumption is correct was not further examined in this work, but could be checked by employing a **PTEMVP** copolymer in future studies. Nevertheless, since the results indicated that the reaction does not even proceed to low conversions, the approach was discarded.

The main application of TEMPO-functionalized polymers is the possibility of synthesizing graft polymers in a controlled manner. The grafting of side chains from a carbon-centered radical at the polymer backbone without a control agent or mediator usually results in a cross-linked material as demonstrated in **Chapter 4.3.1**. The reason behind this observation is an uncontrolled FRP. To gain control over a radical polymerization, RDRP techniques can be used. As described in detail in **Chapters 2.2.1** and **2.4**, NRC essentially is the basis of the RDRP technique NMP, in which nitroxides like TEMPO are used to mediate the polymerization by reversibly forming a dormant species. As explained in **Chapter 2.2.1**, NMP can be initiated by i) a bicomponent system *i.e.*, a radical initiator like AIBN and a nitroxide or ii) a monocomponent system, represented by a stable alkoxyamine which can be cleaved upon heating. Herein, the TEMPO-functionalized polymer intrinsically represents a monocomponent

system. Upon heating (125 - 135 °C, as explained in **Chapters 2.2.1** and **2.4**), the thermolabile C-O bond is homolytically cleaved and the carbon-centered radical as well as TEMPO are formed. Subsequently, the carbon-centered radical can initiate a polymerization in the presence of a suitable monomer, such as styrene (**Scheme 48**). **PTEMVPO-*b*-POEGMEA** was chosen as polymer since the POEGMEA block facilitates ^1H NMR analysis by integration of the signals and styrene was chosen as monomer due to its good polymerizability and to have a direct comparison to the crosslinking experiment in **Chapter 4.3.1**. Consequently, polystyrene should be grafted from **PTEMVPO-*b*-POEGMEA** as shown in **Scheme 48**.



Scheme 48: Grafting styrene from **PTEMVPO-*b*-POEGMEA** by NMP upon heating to 130 °C.

To do so, the TEMPO-OH-functionalized block copolymer **PTEMVPO-*b*-POEGMEA** was dissolved in DMF and 150 eq. of styrene per TEMPO unit were added (**Scheme 48**). After deoxygenating, the polymerization was conducted at 130 °C for 18 h without the addition of an initiator and the polymer was precipitated in cold diethyl ether and analyzed *via* ^1H NMR, ATR-FT-IR spectroscopy and SEC in DMAc as eluent. In **Figure 42a** the ^1H NMR spectrum of the graft polymer **poly(ethylene-*graft*-styrene)-*b*-POEGMEA** is presented. The characteristic aromatic proton signals of styrene could be identified as well as the signals of POEGMEA (4.2 ppm (COOCH_2), 3.7 ppm ($\text{CH}_2\text{CH}_2\text{O}$) and 3.2 ppm (CH_3)) and TEMPO (4.3 ppm (CHOH), 3.75 ppm (NOCH), and 1.4 - 1.0 ppm (CH_2 , CH_3)) indicating the successful graft polymerization. From the ^1H NMR spectrum a *DP* of 67 styrene units per macromolecule was calculated, resulting in an average side chain length of 4.5 styrene units. Additionally, SEC chromatography (**Figure 42c**) proved the successful graft polymerization by revealing a unimodal distribution of the polymer and an increase of the molar mass from $M_n = 7500 \text{ g mol}^{-1}$ to $M_n = 15500 \text{ g mol}^{-1}$.

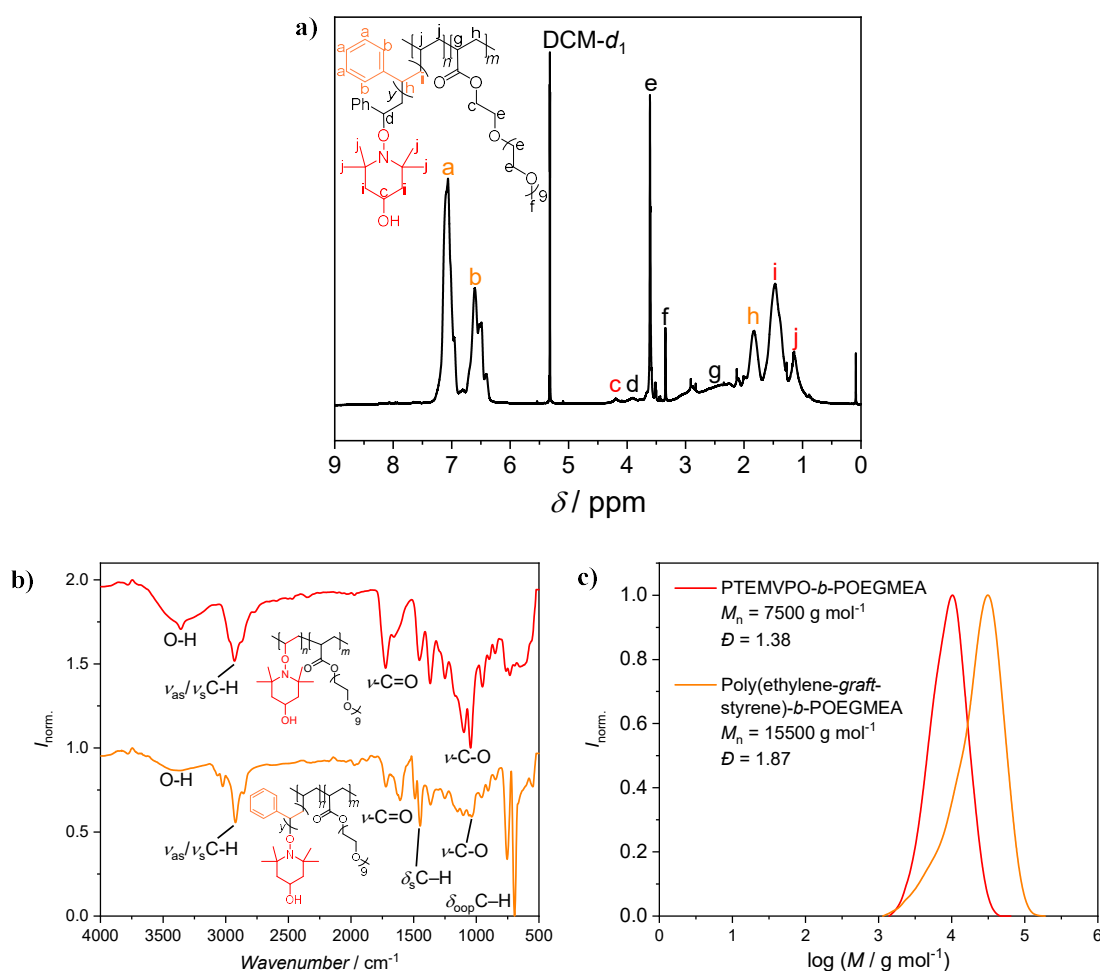


Figure 42: a) ^1H NMR spectrum of poly(ethylene-*graft*-styrene)-*b*-POEGMEA. b) Comparison of the ATR-FT-IR spectra of PTEMVPO-*b*-POEGMEA (top, red) and poly(ethylene-*graft*-styrene)-*b*-POEGMEA (bottom, orange) and c) comparison of the SEC chromatogram before (red) and after grafting of styrene (orange) in DMAc as eluent and PMMA calibration.

Based on the results of the SEC analysis, a DP of polystyrene of 77 per macromolecule was calculated, resulting in an average side chain length of 5 styrene units. This is in consistence with the DP calculated from the ^1H NMR spectrum. Furthermore, the comparison of the ATR-FT-IR spectra before (red) and after grafting (orange) shows additional signals of polystyrene ($\delta_{\text{oop}}\text{C-H}$ at 690 and 760 cm^{-1}), stating a successful graft polymerization. Thus, the results once more proved the successful decarboxylative NRC of TEMPO on PAP polymers.

4.3.5 Recapitulation

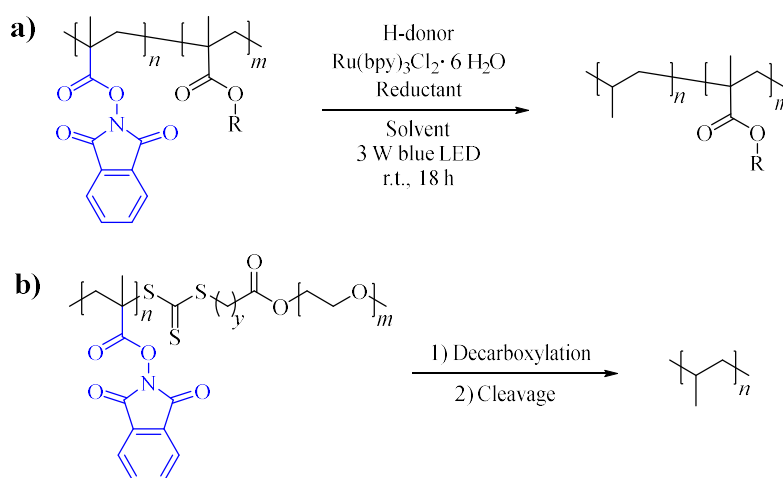
In summary, the functionalization of phthalimide-based precursor polymers by Michael-type addition as well as by NRC was successfully performed. The versatility of the Michael-type addition was demonstrated by employing two different acrylates and a vinyl ketone as Michael-acceptors, proving the variability of the decarboxylation and resulting in structurally new polymers. Additionally, NRC was performed on PAP homopolymers and block copolymers with two different TEMPO derivatives (TEMPO and TEMPO-OH) and a new synthetic route towards TEMPO-functionalized polymers was established. Furthermore, the synthesis of poly(ethylene-*co*-TEMVP) polymers was investigated and reaction conditions evaluated. The detailed analysis showed that the competing reaction between the tributyltin radical and TEMPO results in side reactions and diminished yields of the desired product. Dividing the decarboxylation into two steps improved the result (less side reactions were observed). Nevertheless, dividing the synthesis into two steps is contrary to the targeted goal to establish a straightforward and mild method towards poly(ethylene-*co*-TEMVP) polymers and the further optimization of the approach was postponed. Subsequently, **PTEMVP** and **PTEMVPO** polymers were used for reduction with Zn/AcOH to PVA. Despite extensive variation of the reaction parameters, suitable reaction conditions could not be found and the idea was dismissed. Finally, a TEMPO-functionalized block copolymer was employed for a successful graft polymerization, as shown by the controlled grafting of styrene from **PTEMVPO-*b*-POEGMEA**.

In conclusion, the Michael-type addition as well as the NRC with TEMPO derivatives on PAP polymers represents a versatile enrichment of synthetic methods suitable for the preparation of functional polymers by PPM.

Results and Discussion

4.4 Propylene-free Synthesis of Polypropylene *via* Decarboxylation

The synthesis of polypropylene (PP) homopolymers and block copolymers arose as a project from the first and the second project. PP is the second most used plastic worldwide after PE¹ and characterized by a higher thermal and mechanical stability⁵⁴ making the development of alternative synthesis methods particularly interesting. Once the decarboxylation of PAP was optimized to successfully yield PE homopolymers (**Chapter 4.2**) and block copolymers (**Chapter 4.1**), the decarboxylation of methacrylic phthalimide-based polymers should analogously yield PP. Correspondingly, the methacrylic monomer *N*-(methacryloyloxy)phthalimide (MAP) was synthesized and a suitable RAFT system evaluated. After the successful RAFT polymerization, the photochemical decarboxylation of the methacrylic precursor system was evaluated as shown in **Scheme 49**. The project was designed to aim on the synthesis of PP block copolymers and pure PP with the same strategy as in **Chapter 4.1** and **Chapter 4.2** to demonstrate the versatility of the decarboxylation in polymer chemistry.



Scheme 49: Intended concept of the propylene-free synthesis of **a)** PP block copolymers and **b)** PP homopolymers from methacrylate-based precursor polymers by photochemical decarboxylation.

In accordance with the findings of the present chapter, Sumerlin *et al.*¹⁵⁵ published a study about the decarboxylation of PMAP polymers in March, 2022. Their analysis of the decarboxylation process and products present an expansion to the study of the present chapter.

4.4.1 Synthesis of Precursor Polymers

As for the other projects of the present thesis, the phthalimide structural motif is the central aspect of the decarboxylation. To transfer the results and the decarboxylation process evaluated under **Chapters 4.1** and **4.2** to the methacrylic analogue, the acrylic monomer NAP was exchanged with the methacrylic analogous *N*-(methacryloyloxy)phthalimide (MAP), featuring an additional methyl group. Since this additional methyl group should not directly be affected by the decarboxylation, the resulting, decarboxylated polymer should possess the additional methyl group. Furthermore, the radical formed during the decarboxylation is a tertiary radical and not a secondary radical as in the case of PAP. From the polymerization of MAP, the polymer poly[*N*-(methacryloyloxy)phthalimide] (PMAP) should be obtained.

In the first step, the monomer MAP was synthesized analogously to NAP *via* Steglich esterification from methacrylic acid with *N*-hydroxyphthalimide, EDC·HCl, and DMAP as catalyst (**Figure 43a**). The monomer was obtained in high purity and a good yield (67%) as shown in **Figure 43b** and **Figure 43c**.

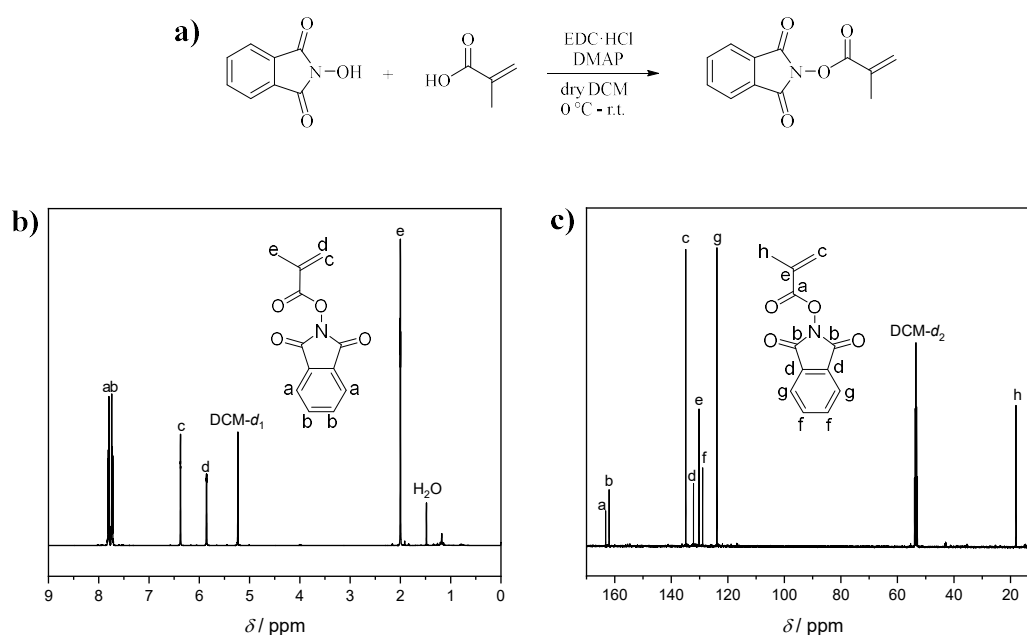


Figure 43: a) Synthesis of *N*-(methacryloyloxy)phthalimide (MAP) *via* Steglich esterification and analysis of the monomer by b) ¹H NMR spectroscopy and c) ¹³C NMR spectroscopy in DCM-*d*₂ as solvent.

MAP was readily used for RAFT polymerization using BPTT as RAFT agent in DMF at 80 °C to examine if the reactivity is suitable to control the polymerization. Nevertheless, the reactivity

Results and Discussion

of the methacrylate seemed to be higher in comparison to the acrylate and BPTT did not control the polymerization resulting in the formation of a shoulder and high dispersities were obtained (**Figure 81**). Therefore, a new RAFT agent had to be evaluated. At first, commercially available RAFT agents suitable for the polymerization of methacrylates were tested for their ability to control the polymerization of MAP and to conduct block copolymerizations with oligo(ethylene glycol) methyl ether methacrylate (OEGMEMA, $M_n = 500 \text{ g mol}^{-1}$, **Figure 44a**).

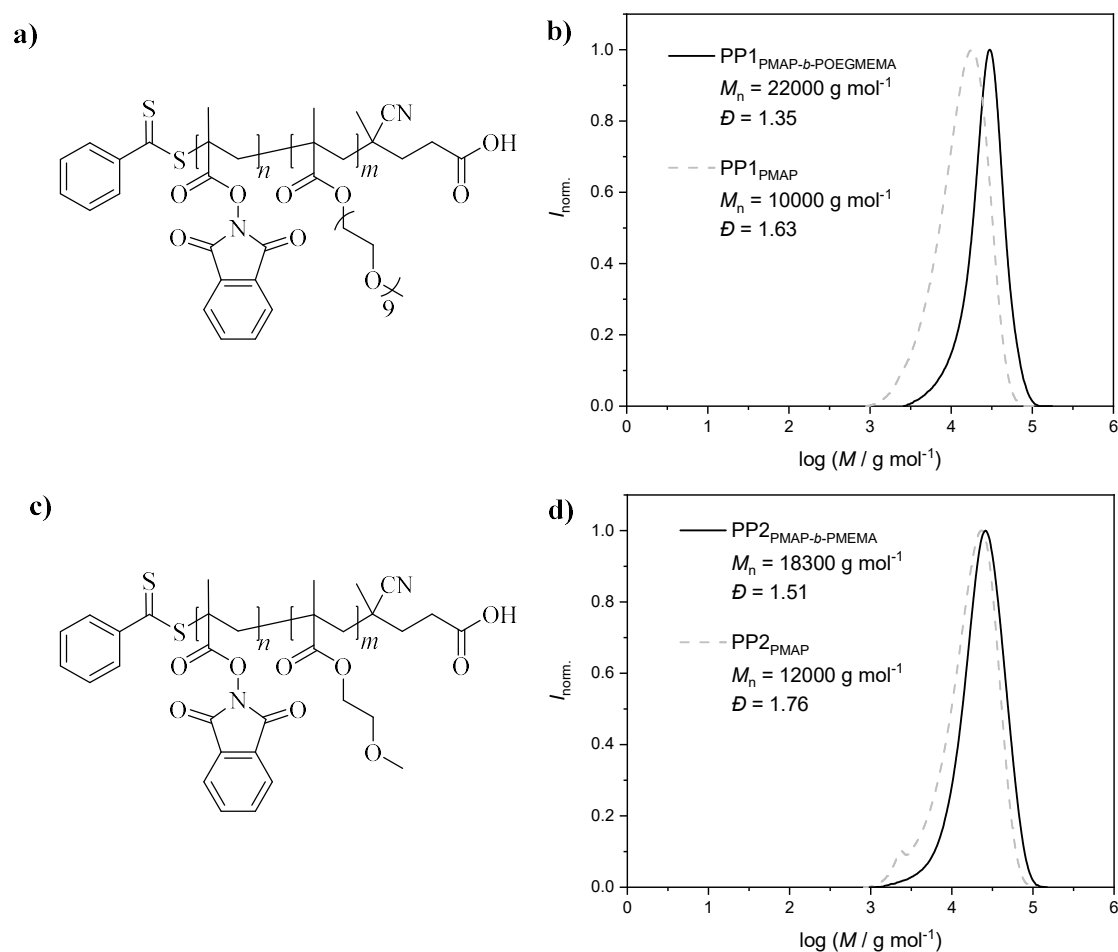


Figure 44: **a)** Structure of PMAP-*b*-POEGMEMA (**PP1**) polymerized by RAFT polymerization with 4-cyano-4-((phenylcarbonothioyl)thio)pentanoic acid (CTP). **b)** SEC chromatogram of PMAP (grey, dashed) and PMAP-*b*-POEGMEMA (**PP1**, black) in DMAc as eluent with PMMA calibration. **c)** Structure of PMAP-*b*-PMEMA (**PP2**) and **d)** SEC chromatogram of PMAP (grey, dashed) and PMAP-*b*-PMEMA (**PP2**, black) in DMAc as eluent with PMMA calibration

Finally, 4-cyano-4-((phenylcarbonothioyl)thio)pentanoic acid (CTP) proved itself to be suitable for the block copolymerization of MAP with OEGMEMA. The resulting block copolymer

PMAP-*b*-POEGMEMA (**PP1**) featured a degree of polymerization of the blocks of $DP_{\text{MAP}} = 43$ and $DP_{\text{OEGMEMA}} = 24$ evaluated by SEC in DMAc as eluent with PMMA calibration (**Figure 44b**, see **Table 21** for details). In the further course of the study, also PMAP-*b*-PMEMA (**PP2**) with 2-methoxy ethyl methacrylate (MEMA) as comonomer was synthesized (**Figure 44c**). The polymer featured a degree of polymerization of the blocks of $DP_{\text{MAP}} = 52$ and $DP_{\text{MEMA}} = 44$ evaluated by SEC in DMAc as eluent with PMMA calibration (**Figure 44d**, see **Table 22** for details). In accordance with the concept of **Chapter 4.2**, a macroRAFT agent based on CTP was synthesized to polymerize MAP and obtain a degradable block copolymer (**DPP1**, **Figure 82**, **Figure 83**).

4.4.2 Decarboxylation of Poly[*N*-(methacryloyloxy)phthalimide] Block Copolymers

After the successful synthesis of PMAP block copolymers, the decarboxylation of **PP1** with the optimized conditions evaluated in **Chapter 4.1.4**, meaning $\text{Ru}(\text{bpy})_3\text{Cl}_2 \cdot 6 \text{H}_2\text{O}$ (0.02 eq.), HE (1.00 eq.) and tributyltin hydride (1.50 eq.) in DMF under the irradiation of three 3 W blue LEDs (450 nm) at room temperature was investigated (**Figure 45a**). Unfortunately, transferring the reaction conditions described led to an unexpected result, which is documented by ^1H NMR spectroscopy as shown in **Figure 45b**.

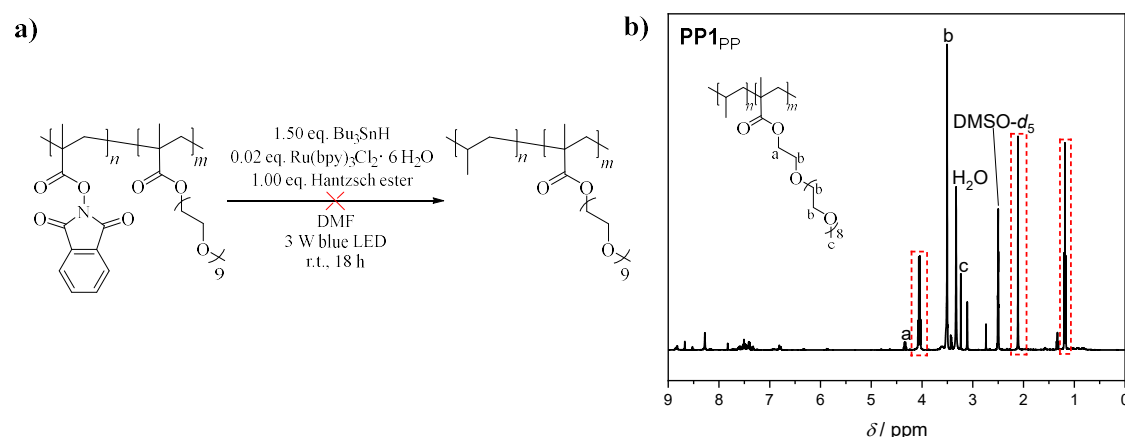
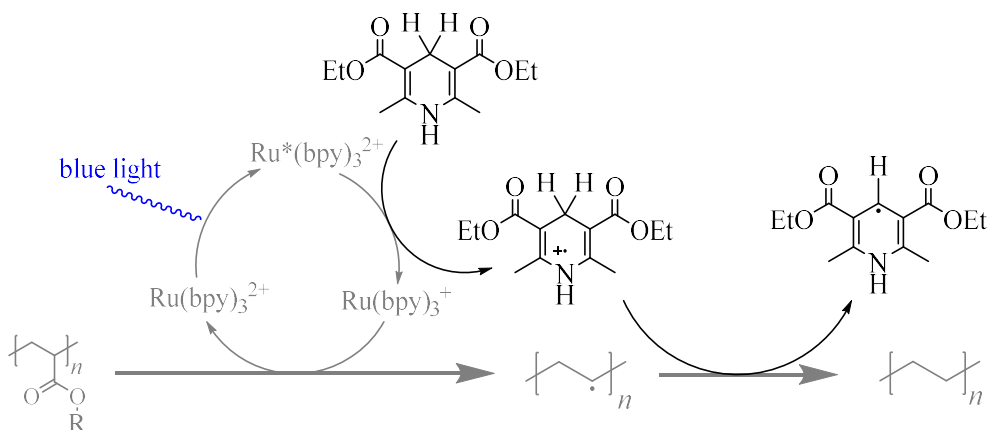


Figure 45: a) Decarboxylation of **PP1** with $\text{Ru}(\text{bpy})_3\text{Cl}_2 \cdot 6 \text{H}_2\text{O}$, HE and Bu_3SnH in DMF as solvent and b) the analysis of the resulting product *via* ^1H NMR spectroscopy.

Results and Discussion

In the spectrum the signals of the PEG chain (4.2 ppm (COOCH_2), 3.7 ppm ($\text{CH}_2\text{CH}_2\text{O}$), and 3.2 ppm (CH_3)) could be identified. Contrary to the expectation, the signals are not broadened as a result of the polymer architecture, but rather sharp with a splitting pattern. Additionally, backbone signals of POEGMEMA or PP (expected in the range of 0.9 – 1.5 ppm) could not be found. However, three additional and sharp signals at 4.06 ppm, 2.11 ppm, and 1.18 ppm arose, which could not be assigned to protons of the presumed product, but judging from their shift and their multiplicity they rather seem to originate from ethyl acetate (EA). However, EA was not part of the synthesis nor was used for purification. Thus, it was speculated that the signals originated from a side reaction or the decomposition of the polymer resulting in a product similar to EA. The signals could not originate from EA itself due to the precipitation of the polymer, which should result in the removal of EA and other organic molecules from the product. Furthermore, drying the product would remove organic molecules with a low boiling point. Hence, it was speculated that the side product must feature a comparably high molar mass with a at least partly EA-like structure. To find the reason for those side reactions or decomposition and to circumvent further issues, the reaction conditions were varied as shown in **Table 6**. In the first step, the equivalents of the H-donor Bu_3SnH were increased from 1.50 eq. to 10.0 eq. (**Table 6**, entry #2). The reason behind this idea was to provide an increased concentration of the H-donor in the reaction solution, resulting in the tertiary radical to couple with hydrogen abstracted by the H-donor instantly after its formation to avoid possible side reactions. This led to a similar spectrum with the EA-like signals than before (**Figure 84**). Since Bu_3SnH is known to be a highly reactive compound, it was considered that the tributyltin radical could be the cause for the side reactions or decomposition. Thus, the H-donor was exchanged with HE by increasing the equivalents of HE from 1.00 to 1.50 eq. (**Table 6**, entry #3), since HE can also abstract hydrogen (**Scheme 50**, see also **Chapter 2.5** for more details).¹¹⁵ Employing HE as H-donor resulted in a similar ^1H NMR spectrum with prominent EA-like signals (**Figure 85**). Based on the result it was considered that Bu_3SnH could not have caused the issues. Thus, other reactants were exchanged and HE was used as the catalyst instead of $\text{Ru}(\text{bpy})_3\text{Cl}_2 \cdot 6 \text{H}_2\text{O}$ (**Table 6**, entry #4), since Zheng *et al.*¹⁵⁶ demonstrated the catalyst-free decarboxylation of phthalimide activated esters based on HE. Yet again, side reactions or the decomposition of the polymer were observed, resulting in EA-like signals in the ^1H NMR spectrum (**Figure 86**).



Scheme 50: Mechanism of the photochemical decarboxylation with HE as H-donor.

So far, the variation of the H-donor and the catalyst could not improve the result and side reactions or the decomposition of the polymer were observed. Thus, the reductant (HE) was exchanged with DIPEA, while Bu_3SnH was used as H-donor (**Table 6**, entry #5) as shown in **Figure 46a**, which affected the decarboxylation result drastically.

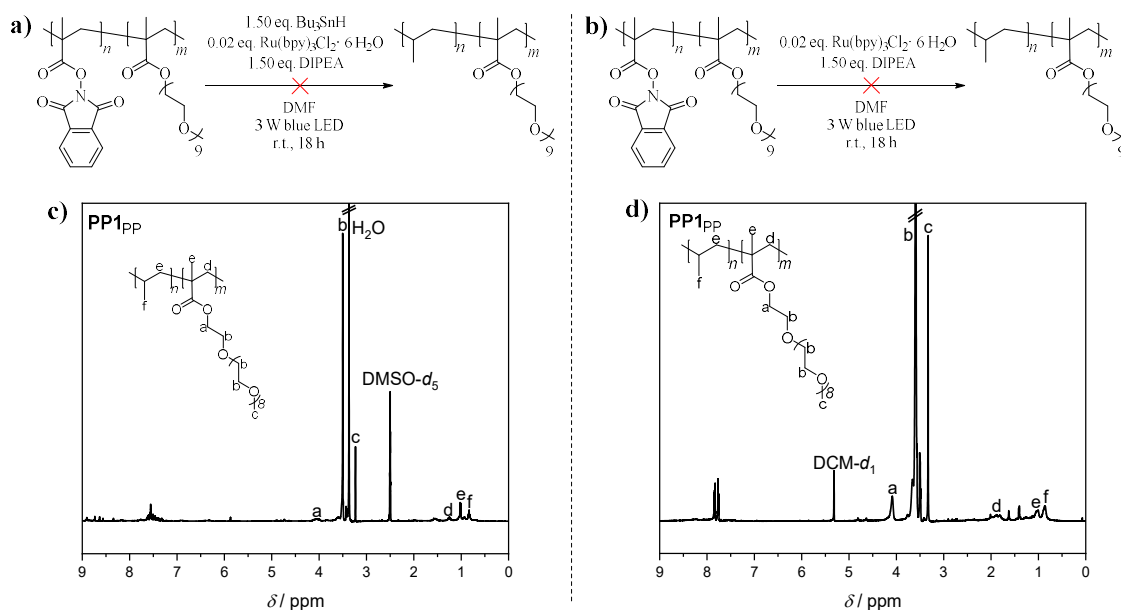
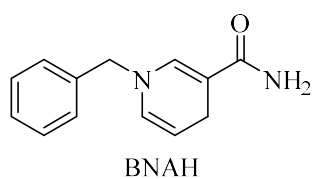


Figure 46: **a)** Decarboxylation of PP1 with $\text{Ru}(\text{bpy})_3\text{Cl}_2 \cdot 6 \text{H}_2\text{O}$, DIPEA as reductant, and Bu_3SnH as H-donor in DMF as solvent and **b)** decarboxylation of PP1 with $\text{Ru}(\text{bpy})_3\text{Cl}_2 \cdot 6 \text{H}_2\text{O}$ and DIPEA as reductant and H-donor in DMF as solvent as well as the corresponding analyses via **c)/d)** ^1H NMR spectroscopy.

Results and Discussion

In the ^1H NMR spectrum of the decarboxylation product, the signals of the PEG side chain (4.2 ppm (COOCH_2), 3.7 ppm ($\text{CH}_2\text{CH}_2\text{O}$) and 3.2 ppm (CH_3)) could be clearly identified, while EA-like signals could not be observed (**Figure 46c**). However, the signal of the backbone protons featured only a low intensity and could not be clearly assigned to either the POEGMEMA or the PP block. The result indicated that HE caused or increased the side reaction or decomposition of the polymer. Furthermore, it was concluded that decomposition of the polymer rather than a side reaction resulted in the EA-like signals, since the formation of a tertiary radical at the polymer backbone in combination with the HE radical could result in β -scission of the polymer backbone and that additional side reactions of the HE radical with the OEGMEMA side chain resulted in the EA-like signals in the ^1H NMR spectra. This would explain i) the sharp structure of the signals in the ^1H NMR spectra and ii) that the resulting products could not be removed by precipitation. Thus, the evaluation of suitable reaction parameters was continued with DIPEA as reductant. In the next step, only $\text{Ru}(\text{bpy})_3\text{Cl}_2 \cdot 6 \text{H}_2\text{O}$ and DIPEA were used as reactants while the solvent and DIPEA should abstract hydrogen (**Figure 46b**, and **Table 6**, entry #6). The analysis of the decarboxylation product *via* ^1H NMR spectroscopy revealed a similar result in comparison to the decarboxylation with Bu_3SnH , but the backbone signals featured a higher intensity and impurities could be identified in the aromatic region, probably resulting from cleaved phthalimide, which was not quantitatively removed by precipitation judging from its multiplicity (**Figure 46d**).

Besides $\text{Ru}(\text{bpy})_3\text{Cl}_2 \cdot 6 \text{H}_2\text{O}$, Eosin Y was found to be a suitable and highly efficient catalyst for the decarboxylation of phthalimide-based esters.^{98,134} Eosin Y is frequently used for the decarboxylation of secondary as well as tertiary phthalimide-based esters⁹⁸ and was used for the decarboxylation of **PP1** with DIPEA as reductant (1.50 eq.) and Bu_3SnH as H-donor (1.50 eq.). However, the decarboxylation did not proceed (**Table 6**, entry #7, **Figure 87**). Since the catalyst $\text{Ru}(\text{bpy})_3\text{Cl}_2 \cdot 6 \text{H}_2\text{O}$ did not seem to cause problems, the exchange was dismissed and the focus was further laid on the optimization of the H-donor/reductant combination and PhSiH_3 was used as H-donor, even though issues caused by phenylsilane have to be kept in



Scheme 51: Structure of 1-benzyl-1,4-dihydronicotinamide.

mind (**Table 6**, entry #8). Nevertheless, the analysis of the decarboxylation product revealed broad signals and impurities in the aromatic region (**Figure 88**), but no improvement of the backbone signals of POEGMEMA or PP. As explained in detail in **Chapter 4.1.2**, Okada *et al.*¹¹⁴ originally used 1-benzyl-1,4-dihydronicotinamide (BNAH, **Scheme 51**) as the reductant during the decarboxylation. Thus, in the following DIPEA was exchanged

Results and Discussion

with BNAH, which can be used as both reductant and H-donor (**Table 6**, entry #9).¹¹⁴ Unfortunately, the exchange of DIPEA with BNAH did also not improve the decarboxylation, but resulted in various impurities, even though no decomposition was observed (**Figure 89**). Hence, DIPEA was used as reductant in the following and the solvent DMF was exchanged with DCM to improve the solubility of the H-donor Bu₃SnH (**Table 6**, entry #10, **Figure 47a**). The analysis of the decarboxylation product *via* ¹H NMR spectroscopy showed, that the exchange resulted in the formation of two intensive signals at 1.44 ppm and 3.6 ppm, which could not be assigned. It was speculated that the signal at 1.44 ppm could arise from a CH chain, however its shift seems to be too high to originate from the polymer backbone.

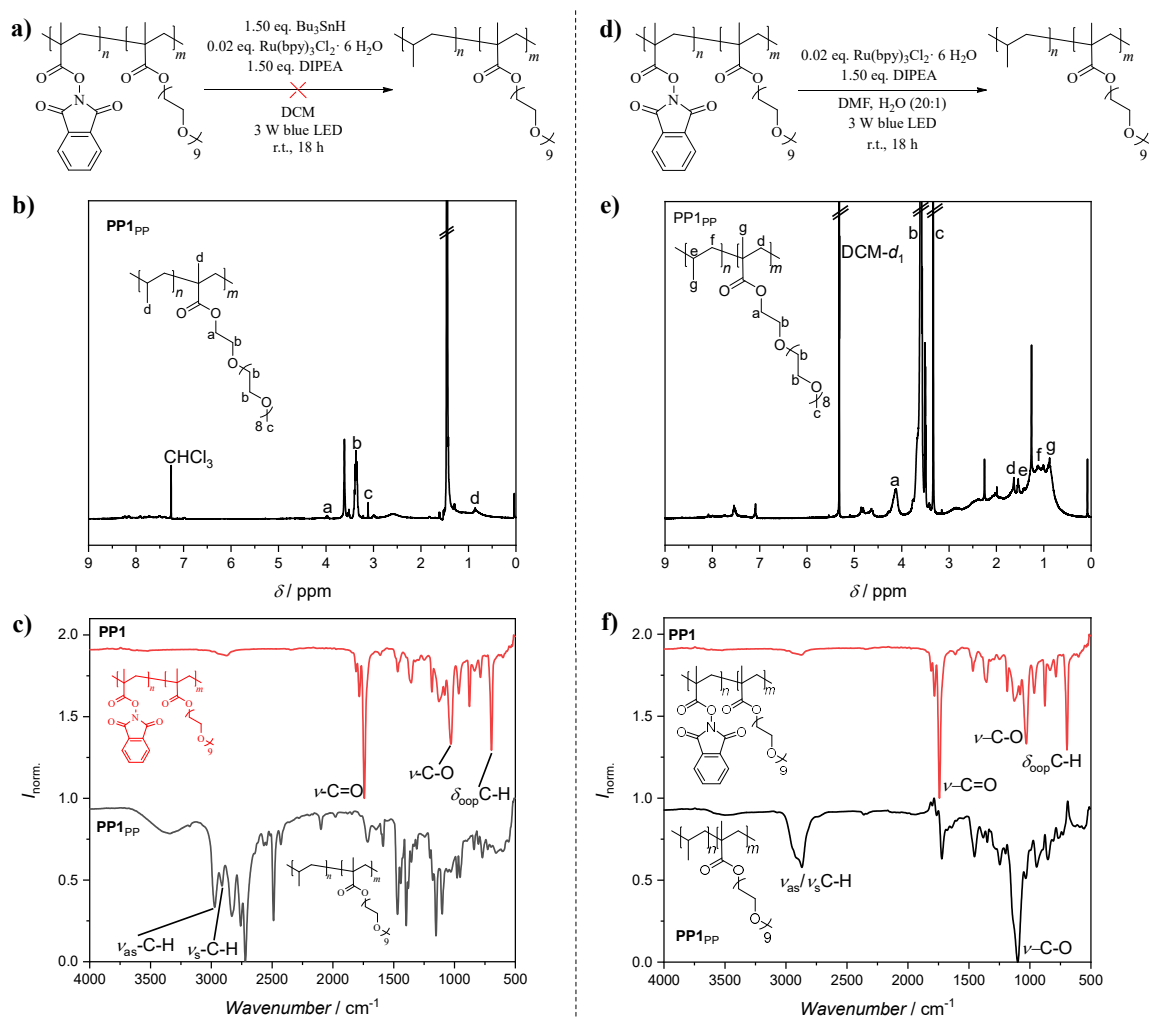


Figure 47: **a)** Decarboxylation of **PP1** with Ru(bpy)₃Cl₂ · 6 H₂O, DIPEA and Bu₃SnH in DCM as solvent and **b)** the analysis *via* ¹H NMR spectroscopy and **c)** the comparison of the ATR-FT-IR spectra before (top, red) and after (bottom, black) decarboxylation. **d)** Decarboxylation of PMAP-*b*-POEGMEMA (**PP1**) with Ru(bpy)₃Cl₂ · 6 H₂O, DIPEA in DMF/H₂O (20:1) and the analysis *via* **e)** ¹H NMR and **f)** ATR-FT-IR spectroscopy.

Results and Discussion

Further, a signal of low intensity at 0.9 ppm was assigned to the methyl groups of the polymer backbone (**Figure 47b**). This approach was thus already promising in comparison to the first decarboxylation results. The comparison of the ATR-FT-IR spectra (**Figure 47c**) before (top, red) and after (bottom, black) shows a change in the vibrational bands after the decarboxylation. Additional bands in the range of 2975 - 2715 cm^{-1} ($\nu_{\text{as}}\text{C-H}$, $\nu_{\text{s}}\text{C-H}$, $\nu_{\text{as}}\text{CH}_3$, and $\nu_{\text{a}}\text{CH}_3$) arising from C-H and CH_3 vibrations as well as an additional, unidentified band at 2488 cm^{-1} appeared after the decarboxylation. Furthermore, the intensity of the vibrational band of the ester (1720 cm^{-1}) and the $\delta_{\text{oop}}\text{C-H}$ vibration (690 cm^{-1}) is drastically reduced. The results indicated that on the one hand the decarboxylation of the phthalimide was successful and on the other hand that the amount of groups in the polymer consisting of C-H was increased. Thus, neither the ^1H NMR spectrum nor the ATR-FT-IR spectrum meet the expected form.

In the next step, the solvent was changed back to DMF, but Bu_3SnH was exchanged by water (**Table 6**, entry #11), since water can also act as a H-donor.¹¹¹ This exchange resulted in an excellent improvement of the decarboxylation result as shown in **Figure 47d**. In the ^1H NMR spectrum, the signals of the PEG side chain as well as of the CH_2 and CH_3 of the backbone of POEGMEMA could be identified. Additionally, the comparison of the ATR-FT-IR spectra (**Figure 47f**) before (top, red) and after (bottom, black) shows an additional band at 2870 cm^{-1} (ν_{as} and ν_{s}) arising from C-H and CH_3 vibrations and a removal of the aromatic C-H vibration at 694 cm^{-1} ($\delta_{\text{oop}}\text{C-H}$), while the intensity of the vibration of the ester is reduced but still present. The results can be interpreted that either the decarboxylation and formation of PP was at least partly successful, but the signals intensity is low in the ^1H NMR spectrum. Or the PMAP block could also be removed by decomposition, since no clear signals of the PP backbone can be identified in the ^1H NMR spectrum and the ATR-FT-IR spectrum is comparable to one of pure POEGMEMA.^{157,158}

Table 6: Variation of the reaction conditions of the decarboxylation of **PP1**.

Entry	Cat.*	Reductant [†]	Solvent	H-donor	Result [#]
1	Ru	HE	DMF	1.50 eq. Bu ₃ SnH	Decomposition, EA-like signals
2	Ru	HE	DMF	10.0 eq. Bu ₃ SnH	Decomposition, EA-like signals
3	Ru	HE	DMF	1.50 eq. HE	Decomposition, EA-like signals
4	(HE)	HE	DMF	1.50 eq. Bu ₃ SnH	Decomposition, no PEG signal
5	Ru	DIPEA	DMF	1.50 eq. Bu ₃ SnH	No decomposition, low signals intensity
6	Ru	DIPEA	DMF	(Solvent)	No decomposition, high signals intensity
7	Eosin Y	DIPEA	DMF	1.50 eq. Bu ₃ SnH	No decarboxylation
8	Ru	DIPEA	DMF	1.50 eq. PhSiH ₃	No decarboxylation, signal at 7.3 ppm
9	Ru	BNAH	DMF	1.50 eq. Bu ₃ SnH	No decomposition, impurities
10	Ru	DIPEA	DCM	1.50 eq. Bu ₃ SnH	No decomposition, signal at 1.44 ppm
11	Ru	DIPEA	DMF	H ₂ O	No decomposition, backbone signal

*cat. = catalyst; [†]reductant of the catalyst; [#]estimated by ¹H NMR spectroscopy.

For comparison, **PP1** was also decarboxylated with the thermal decarboxylation method, first introduced in **Chapter 4.1.2** and presented in **Figure 48a**. The intention was to examine whether the degradation would be also observed using a different decarboxylation method. The decarboxylation was performed with the conditions evaluated in **Chapter 4.1.4**, meaning 1.50 eq. of Bu₃SnH as H-donor, 0.10 eq. of NiCl₂·6 H₂O, 0.20 eq. of bbbpy as ligand and 0.50 eq. of zinc in DMF at 40 °C. The analysis of the reaction product *via* ¹H NMR spectroscopy revealed a quantitative decarboxylation of the polymer and an intensive, but broad signal of the polymer backbone as shown in **Figure 48b**. The result is in accordance with the

Results and Discussion

results evaluated in **Chapter 4.1.4**, while the signal of PP could not be clearly identified or featured a low intensity.

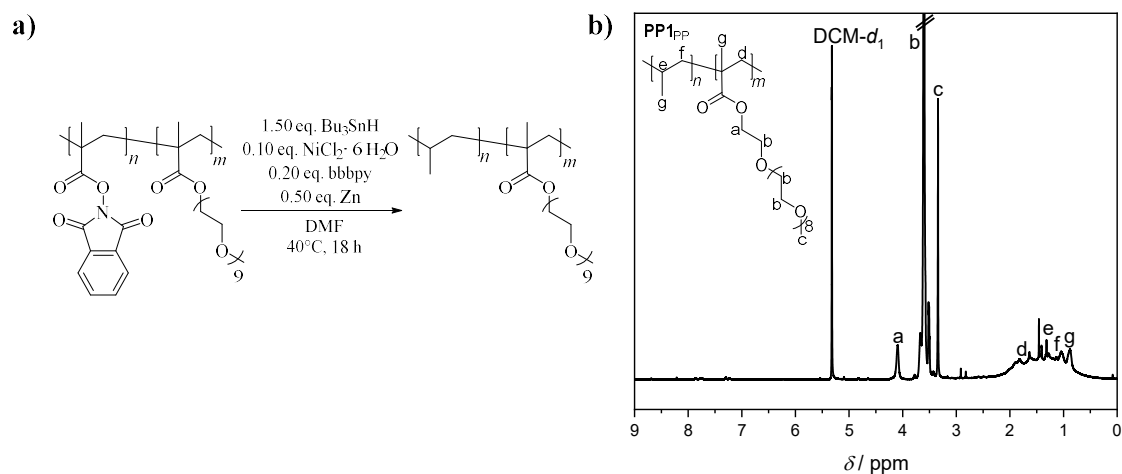


Figure 48: a) Thermal decarboxylation of **PP1** with NiCl₂ · 6 H₂O, bbbpy, Zn and Bu₃SnH as H-donor in DMF and b) the analysis *via* ¹H NMR spectroscopy.

To examine, whether the exchange of Bu₃SnH with water would be suitable for the thermal decarboxylation process, the reaction was repeated with water as primary H-donor as demonstrated in **Figure 49a**. On the one hand, the examination of the thermal decarboxylation did not reveal a comparable decomposition as the photochemical decarboxylation with HE, on the other hand a clear and intensive signal of PP could not be identified as well. Thus, by employing the thermal decarboxylation approach it was proven, that the decomposition of the backbone does not necessarily occur to the same extent as observed. Nevertheless, the issues regarding the thermal method discussed in detail in **Chapter 4.1.4** prevent a further analysis and the approach was dismissed.

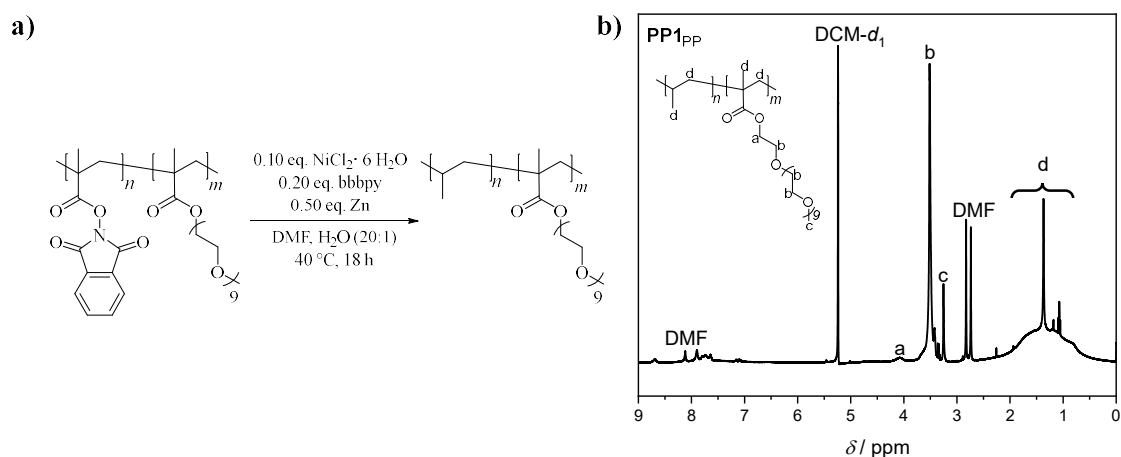


Figure 49: a) Thermal decarboxylation of **PP1** with $\text{NiCl}_2 \cdot 6 \text{H}_2\text{O}$, bbbpy and Zn in DMF/ H_2O (20:1) and b) the analysis *via* ^1H NMR spectroscopy.

In the next step, the block copolymer composition was varied and MEMA was used as a comonomer instead of OEGMEMA to obtain PMAP-*b*-PMEMA (**PP2**), which was synthesized by RAFT polymerization and employed for photochemical decarboxylation as shown in **Figure 50a**.

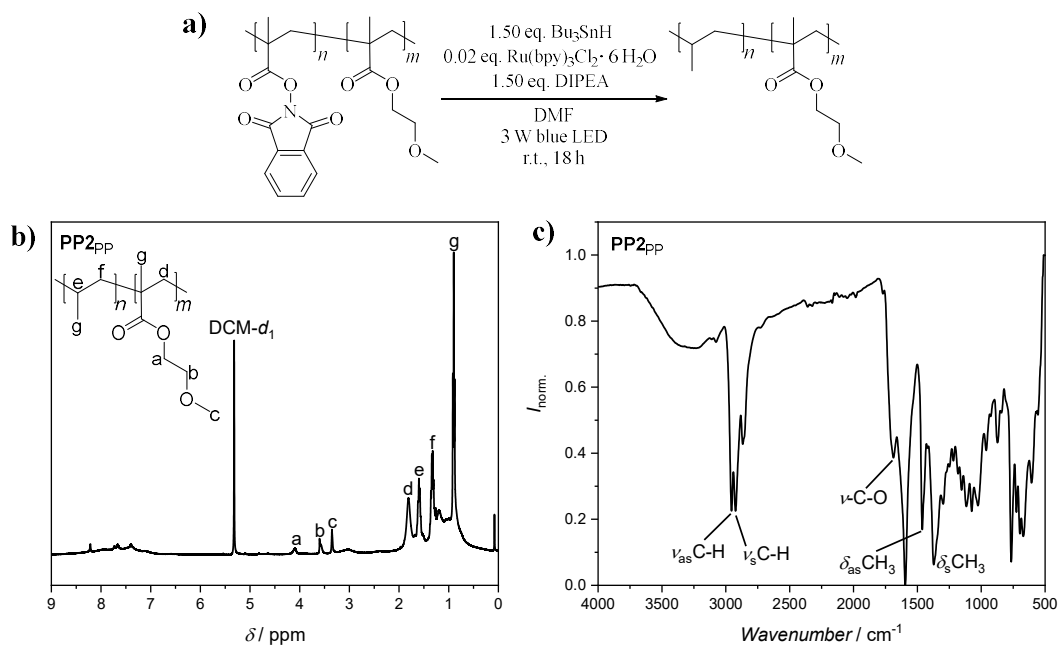
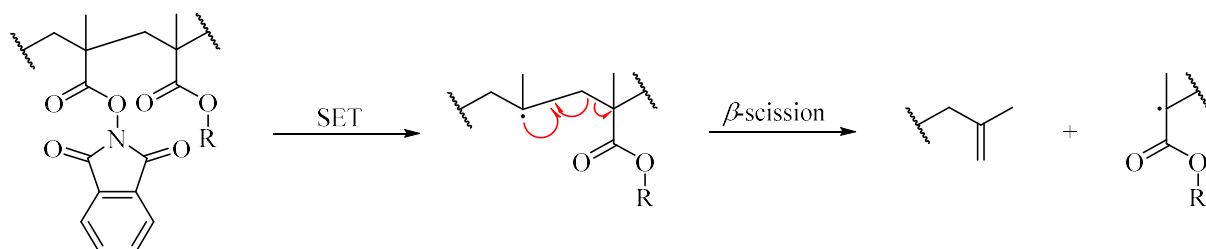


Figure 50: a) Decarboxylation of **PP2** with $\text{Ru}(\text{bpy})_3\text{Cl}_2 \cdot 6 \text{H}_2\text{O}$, DIPEA and Bu_3SnH as H-donor in DMF and the analysis of **PP2PP** *via* b) ^1H NMR and c) ATR-FT-IR spectroscopy.

Results and Discussion

In the ^1H NMR spectrum, beside the signals of the PEG chain, backbone signals at 0.9 ppm (CH_3 of PMEMA and PP), 1.1 ppm (CH of PP), 1.2 ppm (CH_2 of PP), and 1.6 ppm (CH_2 of PMEMA) could be identified, similar to the result before (**Figure 50b**). In the ATR-FT-IR spectrum, intensive signals at 2953 cm^{-1} (ν_{as}), 2858 cm^{-1} (ν_{s}) of the C-H vibrations and 1610 cm^{-1} (ester) as well as signals at $600 - 750\text{ cm}^{-1}$ could be identified. On the one hand the procedure of the decarboxylation of PMAP block copolymers could be optimized in terms of resulting in PP-based polymers without extensive decomposition of the material. On the other hand the polymers still did not feature the great purity comparable to the PE-based polymers in **Chapter 4.1.4** and **Chapter 4.2.2**. Therefore, the decarboxylation of the synthesized degradable block copolymer **DPP1** was not pursued.

As stated in the beginning of the chapter, in March 2022 Sumerlin *et al.*¹⁵⁵ published a study about the degradation of MAP-based copolymers. They performed the decarboxylation with Eosin Y as catalyst and DIPEA as reductant. To prevent quenching reactions of the backbone radical they did not add any H-donor (besides the reductant DIPEA). The detailed analysis revealed that the PMAP copolymer degrades under β -scission of the backbone (**Scheme 52**), which is in accordance with the results and the conclusions drawn in the present chapter. Furthermore, they found, that the same procedure with acrylate-based PAP copolymers leads to coupling of chains and thus, that in the case of an all-acrylate backbone the coupling is faster than the degradation. In the case of the PMAP copolymer the degradation by β -scission seems to be favoured over the coupling. After the decarboxylation Sumerlin *et al.* did not precipitate the product but removed the solvent (DCM) under reduced pressure to investigate all reaction products. Since the procedure of the present thesis aimed on the synthesis of PP and DMF was used as the solvent, the product was precipitated, removing all small molecules.



Scheme 52: Proposed mechanism of the SET-induced decarboxylative backbone degradation of PMAP copolymers by Sumerlin *et al.*¹⁵⁵

However, in contrast to the findings of the present study, Sumerlin *et al.* did not observe the formation of EA-like signals as described in the beginning of the chapter. This could be due to the use of OEGMEMA as comonomer and the employment of block copolymers in the present chapter instead of copolymers with styrene or methyl acrylate, as Sumerlin *et al.* did. Nevertheless, it could be demonstrated that the decarboxylation of PMAP block copolymers does not necessarily result in the degradation of the backbone, but the synthesis of PP polymers by decarboxylation still needs optimization of the reaction conditions to reach a high efficiency and purity of the product, while the findings of Sumerlin *et al.* expand the results of the present thesis.

4.4.3 Recapitulation

The synthesis of the monomer MAP and its RAFT polymerization with OEGMEMA and MEMA to obtain two different block copolymers was successfully accomplished. The results and procedures of the photochemical decarboxylation of PAP evaluated in **Chapter 4.1** and **4.2** were transferred to the decarboxylation of PMAP block copolymers. However, the direct transfer of the reaction conditions resulted in the degradation of the polymer backbone. To avoid the degradation, the reactants such as the H-donor, catalyst and reductant were varied, whereby the exchange of the reductant HE resulted in a reduced degradation. Thus, DIPEA was used as the reductant in the further course of the study. The analysis of the polymer obtained by the combination of DIPEA, $\text{Ru}(\text{bpy})_3\text{Cl}_2 \cdot 6 \text{H}_2\text{O}$ in DMF/water and water as the main H-donor, revealed signals of the backbone of PMEMA and most likely PP. Furthermore, the results were compared to the thermal decarboxylation process, which did not result in the degradation of the polymer. Finally, the findings of the present chapter were expanded by a study of Sumerlin *et al.*¹⁵⁵, in which they analyzed the degradation of PMAP copolymers in detail and found β -scission as the reason of the degradation. Their observation is in accordance with the conclusion drawn from the results of the present chapter. Furthermore, attempts were made to avoid the degradation by carefully evaluating every reactant.

5 Conclusion and Outlook

The wide range of possible applications and the increasing demand for functional PE has resulted in a rapid development of new synthesis methods for PE. However, most of these methods have the disadvantage of poor control and the use of hazardous, gaseous ethylene, especially on a laboratory scale. Therefore, within the present dissertation, a new and ethylene-free synthesis method was developed by transferring novel decarboxylation methods from organic chemistry to polymer chemistry.

Firstly, the synthesis of pure PE by photochemical and thermal decarboxylation of the homopolymer PAP was pursued. Herein, the solubility of the polymer during decarboxylation was identified as a crucial parameter to obtain a quantitative conversion. Therefore, the focus was laid on block copolymers of PAP with a second block (POEGMEA) ensuring the solubility during the decarboxylation, making use of polymer architectures to circumvent chemical challenges. A library of precursor block copolymers with different chains lengths and comonomers was synthesized by RAFT polymerization and the thermal as well as the photochemical decarboxylation yielded PE block copolymers. Yet, a side reaction caused by the H-donor phenylsilane (as also evaluated within the second project) resulted in the formation of a comonomer fraction, which was successfully identified by extensive analyses of the polymers (^1H NMR, ATR-FT-IR spectroscopy, DLS, and DSC) and thus the H-donor was exchanged with tributyltin hydride (see also second project). While the thermal decarboxylation method yielded PE with low purity (additional comonomer fraction, probably caused by the catalytic system), the photochemical decarboxylation successfully yielded PE block copolymers in high purity and high efficiency, as proven by ^1H NMR and ATR-FT-IR spectroscopy, DSC ($T_m = 92\text{ }^\circ\text{C}$) and DLS (increase of R_h). The results of the methods clearly revealed the superiority of the photochemical method and deep analyses of the procedure and the processes of decarboxylation reactions on polymers was provided. Furthermore, the importance of highly efficient reactions for PPM was highlighted and the development of a successful method for the synthesis of PE block copolymers from a polyacrylate-based precursor laid the foundation for the following projects within the present dissertation.

The second project focused on the initial aim of the present thesis *i.e.*, the synthesis of PE homopolymers from the polyacrylate-based precursor. To facilitate the synthesis of PE while circumventing the solubility limitation, the block copolymer system developed in the first project was modified accordingly. Herein, an advanced design of the RAFT agent featuring a PEG chain connected by an ester linkage was developed. Thus, a degradable block copolymer

was synthesized with the macroRAFT agent, which could be cleaved upon aminolysis after successful (photochemical) decarboxylation. The macroRAFT agent provided i) good control over the polymerization, ii) an excellent solubility during the decarboxylation allowing for a quantitative removal of the phthalimide units, and iii) could be cleaved quantitatively. The comprehensive analyses of the obtained PE polymers revealed the formation of a small comonomer fraction (as stated and identified in the first project). The subsequent extensive and wisely considered variations proved the comonomer to originate from a side reaction caused by phenylsilane, which was exchanged by tributyltin hydride. The photochemical decarboxylation method yielded degradable PE block copolymers in high purity. To further demonstrate the versatility of the decarboxylation approach, three different chain lengths of the precursor polymer were synthesized and successfully decarboxylated. Additionally, the following aminolysis step was further evaluated and a one-pot two-step process for the decarboxylation followed by aminolysis was successfully developed. Subsequently, the PEs obtained from all three precursor polymers were thoroughly characterized by spectroscopic and thermal analyses and the purity as well as the linear structure and the successful predefinition of the chain lengths were demonstrated. In summary, the initial aim of the present dissertation was achieved by establishing a straightforward procedure for the controlled synthesis of pure, crystalline and predefined PE from a polyacrylate-based precursor polymer by decarboxylation.

The third project dealt with the utilization of the decarboxylation of PAP polymers for functionalization reactions. A straightforward synthesis route towards unprecedented polymers was established and the limits of the method evaluated. Herein, the Michael-type addition of α , β -unsaturated carbonyl compounds was successfully implemented into the decarboxylation of PAP and demonstrated on three different Michael-acceptors. To widen the scope of functionalization reactions based on the decarboxylation of PAP, NRC with TEMPO was successfully demonstrated on PAP homopolymers as well as on block copolymers. Further, the addition of those alkoxyamines to the polymer backbone laid the foundation for a controlled synthesis of graft polymers by NMP. The approach was demonstrated by the controlled grafting of styrene from PAP-*b*-POEGMEA as proven by various analysis methods. Herein, various functionalization methods were implemented to the decarboxylation of PAP and thus the approaches successfully served as a new toolbox for the functionalization of polymers. Furthermore, the potential of the decarboxylation of PAP was further exploited and the knowledge gained in the course of this dissertation was used to develop and successfully implement further project ideas. With this additional step, the initial goal of the present thesis was exceeded by far.

Conclusion and Outlook

In the last project, the transfer of the optimized decarboxylation procedure to the corresponding methacrylate-based phthalimide polymer (PMAP) in order to obtain PP in a controlled fashion analogous to PE was described. After the successful synthesis of PMAP block copolymers, the analysis of the reaction product after the decarboxylation indicated a decomposition of the polymer by β -scission of the polymethacrylic backbone. The following extensive adaption of the reaction conditions decreased the decomposition successfully and a detailed insight on the processes during the decarboxylation was given, but the decarboxylation did not yield PP polymers in a comparable purity. Further, Sumerlin *et al.*¹⁵⁵ published a study of the degradation of the PMAP backbone by decarboxylation during the investigation within this thesis, thus proving the conclusion drawn from the decarboxylation results.

In summary, the present dissertation provided a powerful tool for the first ethylene-free and controlled synthesis of PE block copolymers and pure PE from a polyacrylate-based precursor system. The approach not only allowed for the predefinition of the polymer architecture and chain lengths but also impressively demonstrated the advantage of carefully designed architecture of polymers to circumvent common challenges in polymer chemistry such as solubility issues. Furthermore, the results underlined the requirement of highly efficient and quantitative reactions for PPM methods, while the challenge of directly transferring methods evaluated in the field of organic chemistry to polymer chemistry was highlighted and successfully solved. In addition, the combination of the decarboxylation approach with PPM methods such as the Michael-type addition and NRC allowed for the establishment of a new toolbox for polymer chemistry and ultimately enabled the access to new functional polymers. Therefore, the aim of the present dissertation was exceeded by far and laid the foundation for further research in PE-based functional polymers.

6 Experimental Section

6.1 Instrumentation

6.1.1 Nuclear Magnetic Resonance (NMR) spectroscopy

^1H -NMR and ^{13}C -NMR spectra were recorded on a Bruker Ascend III 400 MHz spectrometer at a frequency of $\nu = 400$ MHz and $\nu = 101$ MHz, respectively. All samples were dissolved in deuterated solvents; chemical shifts are reported relative to the residual solvent signals.

6.1.2 Size Exclusion Chromatography (SEC)

6.1.2.1 SEC using DMAc as Eluent

SEC measurements with DMAc as eluent were performed on an Agilent 1200 Series System, comprising an autosampler, a differential Refractive Index (RI) detector and two PLgel 5 μm Mixed C columns (300×7.5 mm). The measurements were performed at a temperature of $T = 50^\circ\text{C}$ and a flow rate of 0.5 mL min^{-1} . Samples were measured at a concentration of 2 mg mL^{-1} and filtered prior to measurement. All number-average molar mass M_n and dispersity D values were extrapolated from a range of linear polystyrene standards between 474 and $2.52 \times 10 \text{ g mol}^{-1}$.

6.1.2.2 High-Temperature-SEC (HT-SEC) using 1,2,4-TCB as Eluent

HT-SEC measurements were performed by PSS Polymer Standards Service GmbH in Mainz on with an evaporative light scattering detector (ELSC), a PSS POLEFIN, 20 μm , Guard, ID $8.00 \text{ mm} \times 50.00 \text{ mm}$ precolumn and four PSS POLEFIN linear XL, 20 μm , 0 \AA , ID $8.00 \text{ mm} \times 300.00 \text{ mm}$ columns. The measurements were performed at a temperature of $T = 160^\circ\text{C}$ and a flow rate of 1.0 mL min^{-1} . Samples were measured at a concentration of 3.0 g L^{-1} and filtered prior to measurement. All number-average molar mass M_n and dispersity D values were extrapolated from a range of polystyrene standards.

6.1.3 Attenuated Total Reflection (ATR) Fourier-Transform (FT) Infrared (IR) Spectroscopy (ATR-FT-IR)

ATR-FT-IR spectra were recorded on a Bruker Vertex 80 from $500 - 4000 \text{ cm}^{-1}$ at 25°C .

Experimental Section

6.1.4 Differential Scanning Calorimetry (DSC)

Differential scanning calorimetry was conducted using a DSC Q200 (TA Instruments) in ranges from 0 °C to 150 °C with a scan rate of 10 K min⁻¹.

6.1.5 Thermal Gravimetric Analysis (TGA)

Thermal gravimetric analysis (TGA) was carried out using a TGA 5500 (TA Instruments) at a heating rate of 10 K min⁻¹ under nitrogen atmosphere up to 1000 °C.

6.1.6 Dynamic Light Scattering (DLS)

Dynamic light scattering (DLS) measurements were performed on a Zetasizer Nano S system with a measurement range of 0.3 nm - 10.0 μm and a He-Ne laser with 633 nm and 4 mW at 25 °C. The samples were dissolved in DMAc at a concentration of 2 mg mL⁻¹.

6.1.7 Light-emitting Diodes (LED) Setup

Photochemical experiments were carried out using three Avonec 3 W high power LEDs on a star plate and a radiator with a wavelength maximum of 440 – 450 nm (actinic blue) in a Schlenk tube with a distance of app. 1.5 cm from the light source in a custom-built photoreactor (Figure 51).

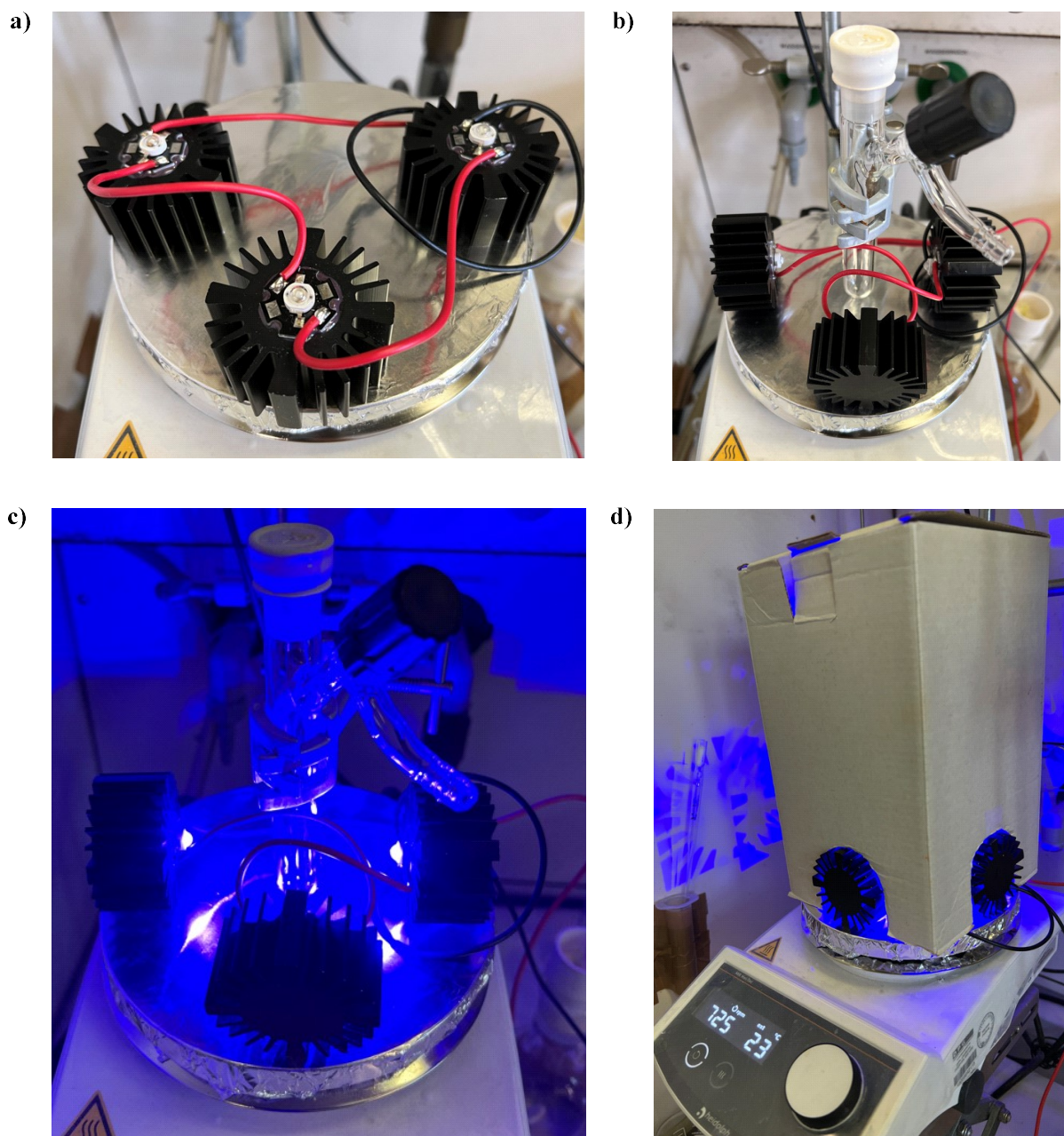


Figure 51: Photos of the LED setup used for photochemical reaction. **a)** Avonec 3 W high power LEDs on a star plate. **b)** LEDs with Schlenk tube used for the decarboxylation, placed in a distance of 1.5 cm around the tube. **c)** Schlenk tube with LEDs turned on. **d)** Final reaction setup with custom-build protection ensuring the removal of the heat produced by the LEDs.

Experimental Section

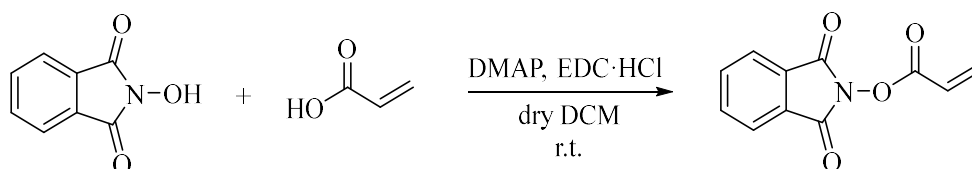
6.2 Materials

Oligo(ethylene glycol)methyl ether acrylate 480 (OEGMEA, Sigma-Aldrich, 99%), oligo(ethylene glycol)methyl ether methacrylate 500 (OEGMEMA, Sigma-Aldrich, 99%), 2-methoxyethyl acrylate (MEA, Sigma-Aldrich, 99%), 2-methoxyethyl methacrylate (MEMA, Sigma-Aldrich, 99%), methyl acrylate (MA, Sigma-Aldrich, 99%), methyl vinyl ketone (MVK, Fisher Scientific, 98%), and styrene (Sigma-Aldrich, 99%) were purified by passing through basic aluminium oxide for inhibitor removal prior to utilization. Acetic acid (AcOH, TCI, > 99.5%) acrylic acid (Sigma-Aldrich, 98%), 4,4'-di-tert-butyl-2,2'-dipyridyl (bbbpy, Sigma-Aldrich, 98%), acetone (VWR, reagent grade), anhydrous dichloromethane (DCM, Sigma-Aldrich, $\geq 99.8\%$), anhydrous *N,N*-dimethylformamide (DMF, Sigma-Aldrich, $\geq 99.8\%$), diisopropyl ethyl amine (DIPEA, Acros, 98%), anhydrous tetrahydrofuran (THF, Sigma-Aldrich, $\geq 99.8\%$), 2,2'-azobis(2-methylpropionitrile) (AIBN, Sigma-Aldrich, 98%), benzyl bromide (VWR, 98%), 1-benzyl-1,4-dihydronicotinamide (BNAH, TCI, 95%), carbon disulfide (Alfa Aesar, 99%), cyclohexane (VWR, reagent grade), dichloromethane (DCM, VWR, reagent grade), diethyl 1,4-dihydro-2,6-dimethyl-3,5-pyridinedicarboxylate (Hantzsch ester, TCI Chemicals, 98%), diethyl ether (VWR, reagent grade), 4-dimethylaminopyridine (DMAP, Acros Organics, 99%), Eosin Y (Fisher Scientific, $\geq 88\%$), 1-ethyl-3-(3-dimethylaminopropyl)-carbodiimide hydrochloride (EDC·HCl, Roth, 98%), ethyl acetate (VWR, reagent grade), ethylenediamine (Acros, 98%), *N*-hydroxyphthalimide (Sigma-Aldrich, 97%), 4-hydroxy-2,2,6,6-tetramethylpiperidinyloxy (TEMPO-OH, Sigma-Aldrich, 97%), isopropyl alcohol (VWR, reagent grade), methacrylic acid (Sigma-Aldrich, 99%), methanol (VWR, reagent grade) 4-methoxythiobenzamide (ABCR, 98%), bis-(4-methoxyphenyl)disulfide (ABCR, 98%), poly(ethylene glycol) methyl ether 1000 (mPEG₁₀₀₀, TCI), 3-mercaptopropionic acid (Fisher, 97%), 11-mercaptopundecanoic acid (Sigma-Aldrich, 98%), phenylsilane (Sigma-Aldrich, 97%), potassium carbonate (Alfa Aesar), propanethiol (Alfa Aesar, 98%), sodium hydroxide (Carl Roth, $\geq 98\%$) 2,2,6,6-tetramethylpiperidinyloxy (TEMPO, ABCR, 98%), tributyltin hydride (Alfa Aesar, 97%), triethylamin (TEA, Alfa Aesar, 99%), tris(2,2'-bipyridyl)dichlororuthenium(II)hexahydrate (Sigma-Aldrich, $\geq 99.5\%$), and zinc (Acros, 98%) were used as received.

All other solvents and reagents were of analytical grade or higher and were used without further purification.

6.3 Procedures for ‘Ethylene-free Synthesis of Polyethylene Copolymers and Block Copolymers’

6.3.1 Synthesis of *N*-(Acryloyloxy)phthalimide *via* Steglich esterification



Acrylic acid (1.20 eq.), *N*-hydroxyphthalimide (1.00 eq.), and 4-dimethylaminopyridine (0.05 eq.) were dissolved in DCM (0.15 mol L⁻¹) in a round bottom flask. The reaction mixture was stirred and 1-ethyl-3-(3-dimethylaminopropyl)carbodiimide hydrochloride (1.20 eq.) was added slowly at room temperature. The reaction mixture was then stirred overnight, after which the solution was concentrated using a rotary evaporator and the crude product purified by column chromatography using cyclohexane : ethyl acetate in a 3 : 1 ratio as eluents. The solvent was removed under reduced pressure yielding a white, crystalline product. (Yield: 31%)

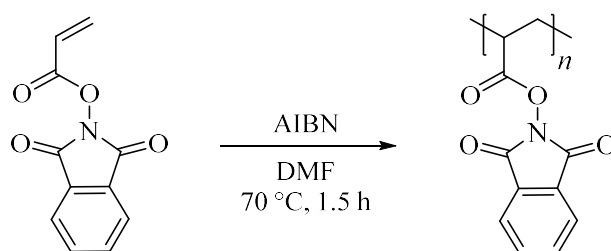
¹H NMR (400 MHz, DCM-*d*₂) δ / ppm = 8.24 - 7.27 (m, 4H, C_{aromatic}H), 6.73 (d, *J* = 17.3, 1.0 Hz, 1H, C_{vinyl}H), 6.40 (dd, *J* = 17.3, 10.7 Hz, 1H, C_{vinyl}H), 6.22 (d, *J* = 10.7, 1.0 Hz, 1H, C_{vinyl}H).

¹³C NMR (400 MHz, DCM-*d*₂) δ / ppm = 161.16 (C_{vinyl}COO), 161.85 (NCO), 136.19 (C_{vinyl}), 134.90 (C_{aromat.}), 128.86 (C_{vinyl}), 123.89 (C_{aromat.}), 122.92 (C_{aromat.}).

*R*_f (CH/EE, 3:1): 0.3

Experimental Section

6.3.2 Free Radical Polymerization of *N*-(Acryloyloxy)phthalimide



N-(Acryloyloxy)phthalimide and AIBN were dissolved in DMF in a round bottom flask. The flask was sealed with a septum and the solution was deoxygenated with a nitrogen flow for 20 min. Afterwards, the flask was placed in a preheated oil bath for 1.5 h at 70 °C and the polymer was precipitated in cold diethyl ether, centrifuged, washed with diethyl ether, and dried under reduced pressure at 40 °C.

$^1\text{H NMR}$ (400 MHz, $\text{DCM-}d_2$) δ / ppm = 7.66 (m, 4H), 3.69 – 3.39 (m, 1H), 2.43 (s, 2H).

ATR-FT-IR: ν (cm^{-1}) = 2930, 1811, 1784, 1670, 1467, 1357, 1055, 833, 760.

Table 7: Overview of PAP homopolymers **P1** – **P3**.

	M_n^* (g mol^{-1})	\bar{D}^*	DP^*	M_n^\dagger (g mol^{-1})	DP^\dagger	$M_n, \text{theo.}$ (g mol^{-1})	$\text{conv.}^\#$ (%)
P1	8300	2.25	39	8250	38	27130	30
P2	2500	1.22	11	1600	7	1600	> 90
P3	5600	1.56	26	6700	30	27130	25

*calculated by SEC with DMAc as eluent; † calculated by $^1\text{H NMR}$ spectroscopy; $^\#$ conversion calculated by $^1\text{H NMR}$ spectroscopy.

Table 8: Experimental details of the synthesis of **P1**.

	mass [mg]	[mmol]	eq.
<i>N</i> -(acryloyloxy)phthalimide	400	1.84	125
AIBN	2.43	0.01	1.00
DMF	0.75 mL	/	/

Table 9: Experimental details of the synthesis of **P2**.

	mass [mg]	[mmol]	eq.
<i>N</i> -(acryloyloxy)phthalimide	260	1.20	7.00
AIBN	30.0	0.18	1.00
DMF	2.00 mL	/	/

Table 10: Experimental details of the synthesis of **P3**.

	mass [mg]	[mmol]	eq.
<i>N</i> -(acryloyloxy)phthalimide	500	2.30	125
AIBN	3.00	0.018	1.00
DMF	2.50 mL	/	/

6.3.3 Free Radical Copolymerization of *N*-(Acryloyloxy)phthalimide and Oligo(ethylene glycol) methyl ether acrylate

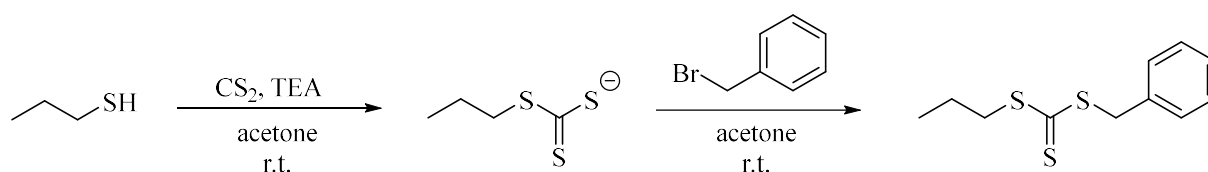
Oligo(ethylene glycol) methyl ether acrylate (1.00 g, 2.10 mmol, 3.00 eq.), *N*-(acryloyloxy)phthalimide (0.15 g, 0.69 mmol, 1.00 eq.) and AIBN (3.40 mg, 0.013 mmol, 0.008 eq.) were dissolved in 1.00 mL of DMF in a round bottom flask. Subsequently, the flask was sealed with a septum and the solution was deoxygenated with a nitrogen flow for 20 min. After deoxygenation, the flask was placed in a preheated oil bath for 1.5 h at 80 °C and the copolymer was precipitated in cold diethyl ether, centrifuged, washed three times with cold diethyl ether, and dried under reduced pressure at 40 °C. The ratio of *N*-(acryloyloxy)phthalimide to oligo(ethylene glycol) methyl ether acrylate was found to be 1 : 3.

¹H NMR (400 MHz, CDCl₃) δ/ ppm = 7.82 (m, 4H), 4.19 (m, 6H), 3.79 - 3.46 (m, 96H), 3.36 (s, 9H), 2.64 - 1.15 (m, 12H).

SEC (DMAc): $M_n = 28300 \text{ g mol}^{-1}$, $D = 2.17$.

Experimental Section

6.3.4 Synthesis of *S, S'*- Benzyl propyl trithiocarbonate (BPTT)



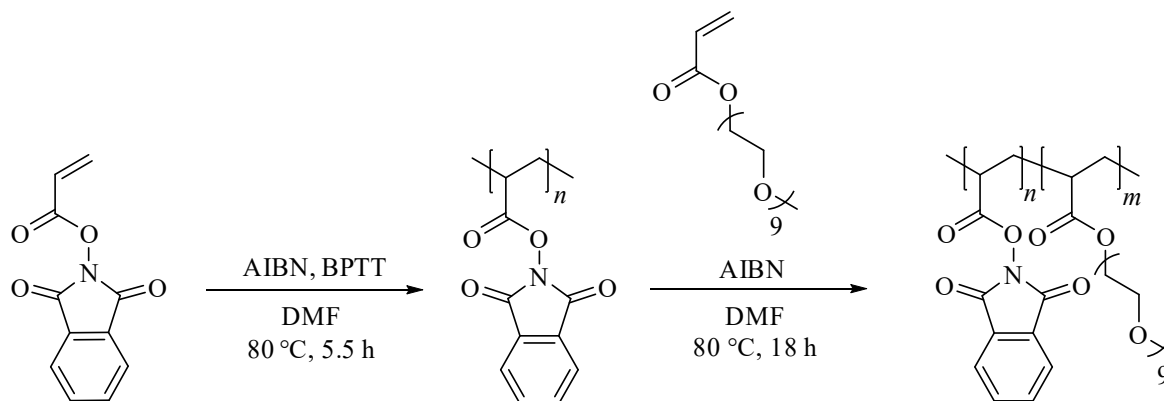
In a 25 mL round bottom flask propanethiol (0.30 g, 3.94 mmol, 1.00 eq.) and triethylamine (0.40 g, 3.94 mmol, 1.00 eq.) were dissolved in 6.00 mL of acetone and carbon disulfide (0.75 g, 9.85 mmol, 2.50 eq.) was added dropwise while stirring. After 30 min, benzyl bromide (0.84 g, 4.95 mmol, 1.25 eq.) dissolved in 2.00 mL of acetone was added dropwise and the reaction was stirred for 2 h. Subsequently, 20.0 mL of DCM were added and the reaction mixture was washed with water, 1M HCl, and brine. The combined organic phases were dried with MgSO_4 and concentrated using a rotatory evaporator. (Yield: 1.08 g, 90%)

^1H NMR (400 MHz, $\text{DCM-}d_2$) δ /ppm = 7.42 - 7.23 (m, 5H, $\text{C}_{\text{aromatic}}\text{H}$), 4.63 (s, 2H, $\text{SCH}_2\text{C}_{\text{aromatic}}$), 3.45 – 3.32 (m, 2H, $\text{CH}_3\text{CH}_2\text{CH}_2\text{S}$) 1.75 (m, 2H, $\text{CH}_3\text{CH}_2\text{CH}_2\text{S}$), 1.02 (t, $J = 7.4$ Hz, 3H, $\text{CH}_3\text{CH}_2\text{CH}_2\text{S}$).

^{13}C NMR (400 MHz, $\text{DCM-}d_2$) δ /ppm = 135.91, 131.91 – 126.79, 41.79, 39.46, 22.14, 13.78.

6.3.5 Synthesis of Poly[*N*-(acryloyloxy)phthalimide] Block Copolymers via RAFT polymerization

6.3.5.1 Poly[*N*-(acryloyloxy)phthalimide]-*block*-Poly[(ethylene glycol) methyl ether acrylate] (P5-P9)



N-(Acryloyloxy)phthalimide, AIBN, and *S*-benzyl *S'*-propyltrithiocarbonate (BPTT) were dissolved in DMF in a pear-shaped flask. The flask was sealed with a septum and the solution was deoxygenated with a nitrogen flow for 20 minutes. Afterwards, the flask was placed in a preheated oil bath for 5.5 h at 80 °C and deinhibited oligo(ethylene glycol) methyl ether acrylate and AIBN were dissolved in DMF in a pear-shaped flask and the solution was deoxygenated with a nitrogen flow for 20 min. The quantitative conversion of *N*-(acryloyloxy)phthalimide was checked by taking a sample for ¹H NMR spectroscopy. The second monomer was added to the polymerization flask and the reaction mixture was stirred overnight at 80 °C. The polymer was precipitated in cold diethyl ether, centrifuged, washed with diethyl ether, and dried at 40 °C under reduced pressure.

P5: ¹H NMR (400 MHz, DCM-*d*₂) δ/ ppm = 8.13 (m, 4H), 4.44 (s, 3H), 3.88 (m, 58H), 3.64 (s, 5H), 2.97 – 2.42 (m, 3H), 2.12 (m, 3H).

P6: ¹H NMR (400 MHz, DCM-*d*₂) δ/ ppm = 8.13 (m, 37H), 4.44 (s, 2H), 3.88 (m, 42H), 3.64 (s, 3H), 2.97 – 2.42 (m, 20H), 2.12 (m, 2H).

P7: ¹H NMR (400 MHz, DCM-*d*₂) δ/ ppm = 8.13 (m, 37H), 4.44 (s, 2H), 3.88 (m, 42H), 3.64 (s, 3H), 2.97 – 2.42 (m, 20H), 2.12 (m, 2H).

P8: ¹H NMR (400 MHz, DCM-*d*₂) δ/ ppm = 8.13 (m, 10H), 4.44 (s, 2H), 3.88 (m, 36H), 3.64 (s, 3H), 2.97 – 2.42 (m, 6H), 2.12 (m, 2H).

P9: ¹H NMR (400 MHz, DCM-*d*₂) δ/ ppm = 8.13 (m, 10H), 4.44 (s, 2H), 3.88 (m, 36H), 3.64 (s, 3H), 2.97 – 2.42 (m, 6H), 2.12 (m, 2H).

Experimental Section

ATR-FT-IR: ν (cm⁻¹) = 2930, 1811, 1784, 1670, 1467, 1357, 1055, 833, 760.

Table 11: Overview of block copolymers **P5 - P9**.

	$M_{n, \text{phth.}}^*$ [g mol ⁻¹]	$M_{n, \text{phth.}}^\dagger$ [g mol ⁻¹]	$M_{n, \text{phth.,}}^{\text{theo.}}$ [g mol ⁻¹]	$M_{n, \text{block}}^*$ [g mol ⁻¹]	$M_{n, \text{block}}^\dagger$ [g mol ⁻¹]	$M_{n, \text{block,}}^{\text{theo.}}$ [g mol ⁻¹]	$\text{conv.}^\#$ [%]	D^*_{block}
P5	3400	4220	4340	17500	20640	52340	30	2.25
P6	5000	6180	6510	5400	7620	7950	60	1.62
P7	4000	5980	6510	5200	7390	7950	60	1.56
P8	3800	5210	6510	9500	10000	28340	20	1.75
P9	4700	3690	6510	8500	9450	28340	24	1.64

*calculated by SEC with DMAc as eluent; [†]calculated by ¹H NMR spectroscopy; [#]conversion of OEGMEA monomer, calculated by ¹H NMR spectroscopy.

Table 12: Experimental details of the synthesis of **P5**.

	mass [mg]	[mmol]	eq.
N-(acryloxyloxy)phthalimide	200	0.92	20.0
AIBN	0.76	0.005	0.10
BPTT	11.2	0.05	1.00
OEGMEA	2212	4.61	100
DMF	2.00 mL	/	/

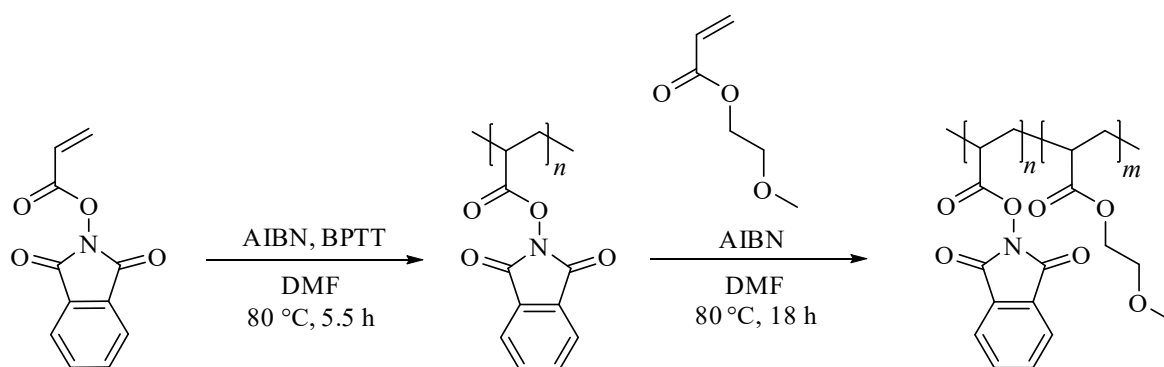
Table 13: Experimental details of the synthesis of **P6/P7**.

	mass [mg]	[mmol]	eq.
N-(acryloxyloxy)phthalimide	750	3.46	30.0
AIBN	1.89	0.01	0.10
BPTT	27.9	0.12	1.00
OEGMEA	276	0.57	5.00
DMF	1.00 mL	/	/

Table 14: Experimental details of the synthesis of **P8/P9**.

	mass [mg]	[mmol]	eq.
<i>N</i>-(acryloyloxy)phthalimide	750	3.46	30.0
AIBN	1.89	0.01	0.10
BPTT	27.9	0.12	1.00
OEGMEA	828	1.71	15.0
DMF	1.0 mL	/	/

6.3.5.2 Poly[*N*-(acryloyloxy)phthalimide]-*block*-Poly(2-methoxyethyl acrylate) (P10 and P11)



N-(Acryloyloxy)phthalimide, AIBN, and *S*-benzyl *S'*-propyltrithiocarbonate (BPTT) were dissolved in DMF in a pear-shaped flask. The flask was sealed with a septum and the solution was deoxygenated with a nitrogen flow for 20 minutes. Afterwards, the flask was placed in a preheated oil bath for 5.5 h at 80 °C and deinhibited 2-(methoxyethyl) acrylate and AIBN were dissolved in DMF in a pear-shaped flask and the solution was deoxygenated with a nitrogen flow for 20 min. The quantitative conversion of *N*-(acryloyloxy)phthalimide was checked by taking a sample for ¹H NMR spectroscopy and the second monomer was added to the polymerization flask and the reaction mixture was stirred overnight at 80 °C. The polymer was precipitated in cold diethyl ether, centrifuged, washed with diethyl ether, and dried at 40 °C under reduced pressure.

¹H NMR (400 MHz, DCM-*d*₂) δ / ppm = 8.12 (m, 7H), 4.12 (s, 2H), 3.49 (m, 4H), 3.28 (s, 3H), 2.42 (m, 5H), 2.12 (m, 2H).

ATR-FT-IR: ν (cm⁻¹) = 2880, 1738-1809, 1096, 696.

Experimental Section

Table 15: Experimental details of the synthesis of **P10/P11**.

	mass [mg]	[mmol]	eq.
<i>N</i>-(acryloyloxy)phthalimide	200	0.92	30.0
AIBN	0.50	0.003	0.10
BPTT	7.45	0.03	1.00
MEA	200	1.54	50.0
DMF	0.50 mL	/	/

6.3.6 Thermal Decarboxylation of Poly[*N*-(acryloyloxy)phthalimide] Polymers

Zinc (0.50 eq. per active ester group) was placed in a dry Schlenk tube equipped with a stirring bar. The tube was evacuated and backfilled with nitrogen three times. Simultaneously, NiCl₂ · 6 H₂O (0.10 eq. per active ester group) and bbbpy (0.20 eq. per active ester group) in anhydrous DMF (0.5 mL), H-donor (phenylsilane or tributyltin hydride) (1.50 eq. per active ester group) in anhydrous DMF (0.5 mL) and precursor polymer (1.00 eq.) in anhydrous DMF (0.015 mmol mL⁻¹) were deoxygenated with a nitrogen flow for 20 min in separate vials and added *via* a gas-tight syringe under nitrogen atmosphere afterwards. The reaction mixture was stirred at 40 °C for 18 h, precipitated in cold diethyl ether, centrifuged, washed with diethyl ether and dried under reduced pressure at 40 °C.

P1_{PE}: ¹H NMR (400 MHz, DMF-*d*₇) δ/ ppm = 7.77 - 6.64 (m, 4H), 3.68 - 3.09 (m, 1H), 1.99 - 0.38 (m, 49H).

P4_{PE}: ¹H NMR (400 MHz, DCM-*d*₂) δ/ ppm = 4.22 (s, 2H), 3.93 - 3.49 (m, 34H), 3.37 (s, 3H), 2.3 (m, 1H), 2.09 - 0.51 (m, 4H).

P5_{PE}: ¹H NMR (400 MHz, DCM-*d*₂) δ/ ppm = 4.18 (s, 2H), 3.73 - 3.54 (m, 34H), 3.33 (s, 3H), 2.26 (s, 1H), 1.89 (s, 2H), 1.58 (s, 1H).

P7_{PE}: ¹H NMR (400 MHz, DCM-*d*₂) δ/ ppm = 4.16 (s, 2H), 3.68 - 3.42 (m, 34H), 3.36 (s, 3H), 2.26 (s, 1H), 1.89 - 0.68 (s, 77H).

P9_{PE}: ¹H NMR (400 MHz, DCM-*d*₂) δ/ ppm = 4.17 (s, 2H), 3.59 (m, 34H), 3.34 (s, 3H), 2.32 (s, 1H), 1.77 - 1.46 (s, 12H).

P11_{PE}: ¹H NMR (400 MHz, DCM-*d*₂) δ/ ppm = 4.19 (m, 2H), 3.38 (m, 2H), 3.35 (s, 3H), 2.31 (m, 1H), 1.98 - 1.45 (m, 9H).

6.3.7 Photochemical Decarboxylation of Poly[*N*-(acryloyloxy)phthalimide] Polymers

Ru(bpy)₃Cl₂ · 6 H₂O (0.02 eq. per active ester group) and Hantzsch ester (1.00 eq. per active ester group) were placed in a dry Schlenk tube equipped with a stirring bar. The tube was evacuated and backfilled with nitrogen three times. Simultaneously, H-donor (phenylsilane or tributyltin hydride) (1.50 eq. per active ester group) in anhydrous DMF (0.5 mL) and precursor polymer (1.00 eq.) in anhydrous DMF (0.015 mmol mL⁻¹) in a separate vial were deoxygenated with a nitrogen flow for 20 min and added *via* a gas-tight syringe under nitrogen atmosphere. The reaction mixture was stirred under the irradiation of three 3 W blue LEDs (distance app. 1.5 cm from the light source, wavelength maximum 440 - 450 nm) at room temperature for 18 h, after which the polymer was precipitated in cold diethyl ether, centrifuged, washed with diethyl ether, and dried under reduced pressure at 40 °C.

P1_{PE}: ¹H NMR (400 MHz, DMSO-*d*₆) δ/ ppm = 7.73 – 7.38 (m, 4H), 3.69 - 3.03 (m), 2.82 – 2.21 (s), 1.99 - 0.38 (m, 50H).

P5_{PE}: ¹H NMR (400 MHz, DCM-*d*₂) δ/ ppm = 4.23 (s, 2H), 3.69 – 3.42 (m, 34H), 3.32 (s, 3H), 2.23 (m, 1H), 1.86 – 1.26 (s, 4H).

P6_{PE}: ¹H NMR (400 MHz, DCM-*d*₂) δ/ ppm = 4.18 (s, 2H), 3.73 – 3.42 (m, 34H), 3.35 (s, 3H), 2.23 (m, 1H), 1.52 (m, 2H), 1.26 (s, 37H).

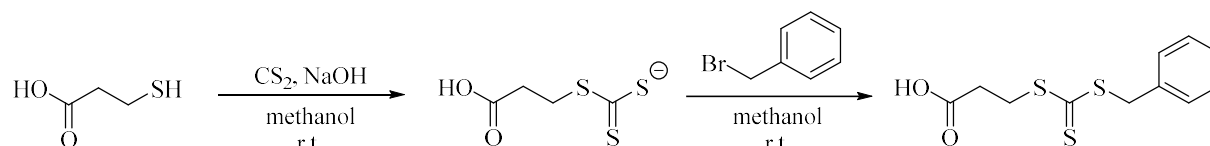
P8_{PE}: ¹H NMR (400 MHz, DCM-*d*₂) δ/ ppm = 4.22 (s, 2H), 3.74 – 3.48 (m, 34H), 3.31 (s, 3H), 2.18 (m, 1H), 1.61 (m, 2H), 1.26 (s, 10H).

P10_{PE}: ¹H NMR (400 MHz, DCM-*d*₂) δ/ ppm = 4.14 (m, 2H), 3.34 (m, 2H), 3.34 (s, 3H), 2.65 – 2.1 (m, 1H), 1.72 – 1.38 (m, 2H), 1.24 (m, 7H).

Experimental Section

6.4 Procedures for ‘Synthesizing Polyethylene from Polyacrylates: A Decarboxylation Approach’

6.4.1 Synthesis of 3-(((Benzylthio)carbonothioyl)thio)propanoic acid (BTTP)

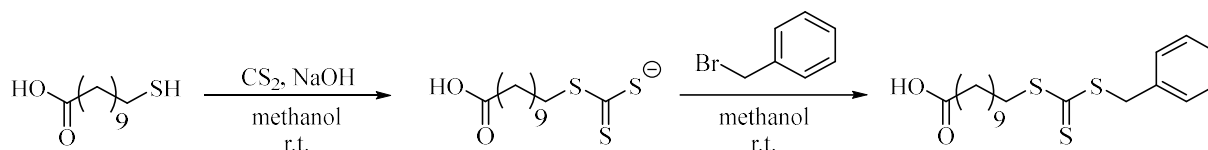


Sodium hydroxide (0.80 g, 20.0 mmol, 2.00 eq.) was dissolved in 20 mL of methanol and 3-mercaptopropionic acid (0.87 mL, 10.0 mmol, 1.00 eq.) was added. Subsequently, carbon disulfide (3.08 mL, 50.0 mmol, 5.00 eq.) was added and the colour of the solution immediately turned deep yellow. After 30 min benzyl bromide (1.31 mL, 11.0 mmol, 1.10 eq.) was added and the mixture was stirred overnight. The solvent was then removed under vacuum in a rotatory evaporator. The residue was dissolved in dichloromethane, washed with water and 1 M HCl and dried under reduced pressure to obtain a crystalline yellow solid. (Yield: 3.09 g, 89%)

¹H NMR (400 MHz, DCM-*d*₂) δ /ppm = 7.43 – 7.22 (m, 5H, C_{aromatic}H), 4.63 (s, 2H, C_{benzyl}H₂), 3.63 (t, *J* = 6.9 Hz, 2H, CSSCH₂), 2.85 (t, *J* = 6.9 Hz, 2H, HOOCCH₂).

¹³C NMR (400 MHz, DCM-*d*₂) δ /ppm = 223.54, 177.71, 135.59, 129.78, 129.22, 128.33, 41.96, 33.31, 31.54.

6.4.2 Synthesis of 11-(((Benzylthio)carbonothioyl)thio)undecanoic acid (BTTU)

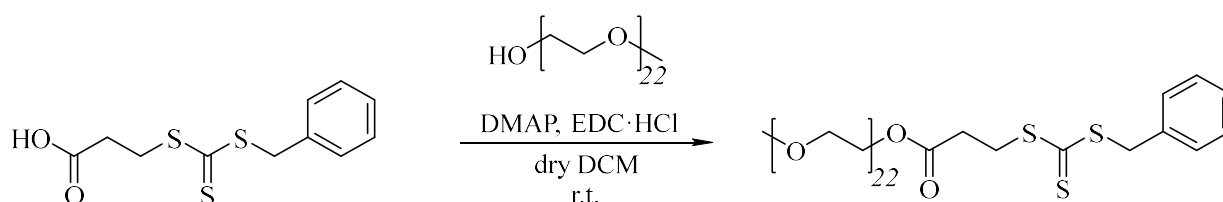


11-Mercapto undecanoic acid (1.09 g, 5.00 mmol, 1.00 eq.) was added to a solution of sodium hydroxide (0.40 g, 10.0 mmol, 2.00 eq.) in methanol (10.0 mL), then carbon disulfide (1.54 mL, 25.0 mmol, 5.00 eq.) was added. The colour of the solution immediately turned deep orange. After 30 min benzyl bromide (0.65 mL, 5.50 mmol, 1.10 eq.) was added and the mixture was stirred overnight, the solvent was then removed under vacuum in a rotating evaporator. The residue was dissolved in dichloromethane, washed with water and 1 M HCl and dried under reduced pressure to obtain a crystalline yellow solid. (Yield: 2.12 g, 88%)

¹H NMR (400 MHz, DCM-*d*₂) δ / ppm = 7.37 – 7.22 (m, 5H, C_{aromatic}H), 4.62 (s, 2H, C_{benzyl}H), 3.48 – 3.31 (m, 2H, SCH₂), 2.34 (t, *J* = 7.5 Hz, 2H, CH₂COO), 1.81 – 1.57 (m, 2H, SCH₂CH₂), 1.48 – 1.21 (m, 14H, (CH₂)₇).

Experimental Section

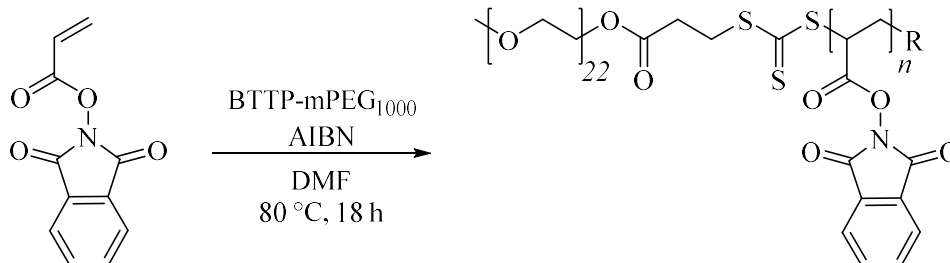
6.4.3 Synthesis of macroRAFT Agent



BTTP (250 mg, 0.92 mmol, 1.00 eq.) was dissolved in anhydrous DCM (8.00 mL) in a dry flask and DMAP (11.2 mg, 0.09 mmol, 0.10 eq.) and EDC·HCl (194 mg, 1.01 mmol, 1.10 eq.) were added. Into the flask mPEG₁₀₀₀ (459 mg, 0.46 mmol, 0.50 eq.) was added and the reaction was allowed to proceed for 4 days at room temperature with magnetic stirring. The polymer was precipitated two times in cold diethyl ether and petroleum ether and washed with 1M HCl three times and dried at 40 °C under reduced pressure.

¹H NMR (400 MHz, DCM-*d*₂) δ / ppm = 7.40 - 7.22 (m, 5H, C_{aromatic}H), 4.65 - 4.61 (m, 2H, C_{benzyl}H₂), 4.27 - 4.09 (m, 2H, COOCH₂), 3.73 - 3.54 (m, 86H, (CH₂CH₂O)₂₂), 3.53 - 3.48 (m, 2H, H₂SCSS), 3.33 (s, 3H, OCH₃), 2.85 - 2.68 (m, 2H OOCCH₂).

6.4.4 Synthesis of Poly[*N*-(acryloyloxy)phthalimide]-*block*-Poly(ethylene glycol)



N-(acryloyloxy)phthalimide, BTTP-mPEG₁₀₀₀ (1.00 eq.) and AIBN (0.10 eq.) were dissolved in DMF in a pear-shaped flask. The flask was sealed with a septum and the solution was deoxygenated with a nitrogen flow for 20 min. Subsequently, the flask was placed in a preheated oil bath for overnight at 80 °C. The polymer was precipitated in cold diethyl ether, centrifuged, washed with diethyl ether, and dried under reduced pressure at 40 °C.

DP1:

¹H NMR (400 MHz, DCM-*d*₂) δ /ppm = 8.11 – 7.08 (m, 84H), 4.21 (s, 2H), 3.76 – 3.40 (m, 107H), 3.34 (m, 3H), 2.43 (s, 42H).

SEC (DMAc): $M_n = 5900 \text{ g mol}^{-1}$, $D = 1.74$.

DP2:

¹H NMR (400 MHz, DCM-*d*₂) δ /ppm = 8.10 – 7.06 (m, 148H), 4.21 (s, 2H), 3.76 – 3.40 (m, 123H), 3.34 (m, 3H), 2.43 (s, 74H).

SEC (DMAc): $M_n = 9400 \text{ g mol}^{-1}$, $D = 1.90$.

DP3:

¹H NMR (400 MHz, DCM-*d*₂) δ /ppm = 8.15 – 7.11 (m, 240H), 4.21 (s, 2H), 3.76 – 3.40 (m, 146H), 3.34 (m, 3H), 2.43 (s, 120H).

SEC (DMAc): $M_n = 13700 \text{ g mol}^{-1}$, $D = 2.37$.

DP4:

¹H NMR (400 MHz, DCM-*d*₂) δ /ppm = 8.09 – 7.08 (m, 80H), 4.21 (s, 2H), 3.76 – 3.40 (m, 106H), 3.34 (m, 3H), 2.43 (s, 40H).

SEC (DMAc): $M_n = 5200 \text{ g mol}^{-1}$, $D = 1.81$.

ATR-FT-IR: $\nu \text{ (cm}^{-1}\text{)} = 1784, 1734, 1668, 1186, 1049, 873, 694$.

Experimental Section

Table 16: Experimental details of the synthesis of **DP1/DP4**.

	mass [mg]	[mmol]	eq.
<i>N</i> -(acryloxyloxy)phthalimide	1000	4.61	20.0
AIBN	3.78	0.02	0.10
BTTP-mPEG ₁₀₀₀	293	0.23	1.00
DMF	1.50 mL	/	/

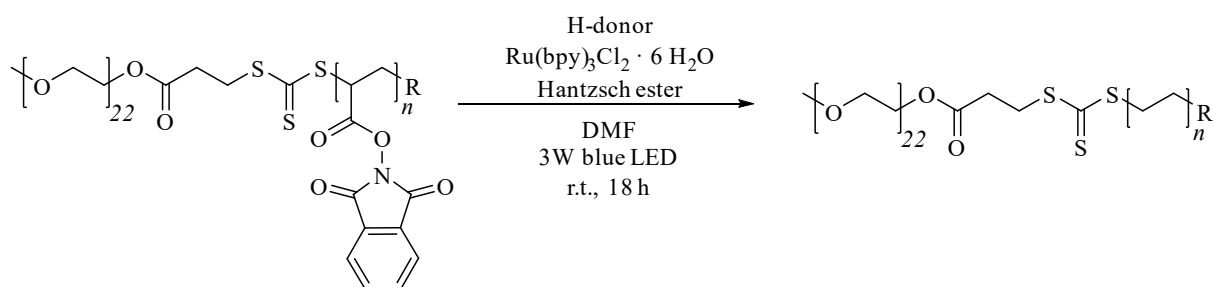
Table 17: Experimental details of the synthesis of **DP2**.

	mass [mg]	[mmol]	eq.
<i>N</i> -(acryloxyloxy)phthalimide	1000	4.61	50.0
AIBN	1.50	0.009	0.10
BTTP-mPEG ₁₀₀₀	117	0.09	1.00
DMF	1.50 mL	/	/

Table 18: Experimental details of the synthesis of **DP3**.

	mass [mg]	[mmol]	eq.
<i>N</i> -(acryloxyloxy)phthalimide	1000	4.61	500.0
AIBN	0.15	0.0009	0.10
BTTP-mPEG ₁₀₀₀	11.7	0.009	1.00
DMF	1.50 mL	/	/

6.4.5 Photochemical Decarboxylation of Poly[*N*-(acryloyloxy)phthalimide]-*block*-Poly(ethylene glycol)



Ru(bpy)₃Cl₂ · 6 H₂O (0.02 eq. per active ester group) and Hantzsch ester (1.00 eq. per active ester group) were placed in a dry Schlenk tube equipped with a stirring bar. The tube was evacuated and backfilled with nitrogen three times. Simultaneously, H-donor (phenylsilane or tributyltin hydride) (1.50 eq. per active ester group) and PAP-*b*-PEG (1.00 eq.) in anhydrous DMF (0.015 mmol mL⁻¹) were deoxygenated with a nitrogen flow for 20 min in separate vials and added *via* a gas-tight syringe under nitrogen atmosphere afterwards. The reaction mixture was stirred under the irradiation of three 3 W blue LEDs (distance app. 1.5 cm from the light source, wavelength maximum 440 - 450 nm) at room temperature for 18 h, precipitated in cold diethyl ether, centrifuged, and washed with diethyl ether and dried under reduced pressure.

6.4.5.1 Calculation for the improvement of reaction conditions:

The signal of the methyl end group of the PEG chain (3.25 ppm, three protons) was set to three, the integral of the signal of the ethylene oxide repeating units (3.51 ppm, ~87 protons) was taken as a second reference. The signal arising from side reactions at 7.35 ppm was integrated and the reduction of the signals intensity calculated by the following equation:

$$Reduction [\%] = 100 - \left[\frac{Integral\ at\ 7.35\ ppm\ Standard}{Integral\ at\ 7.35\ ppm\ Variation} 100 \right]$$

Experimental Section

6.4.5.2 Physical data of PE-*block*-PEG obtained with optimized conditions:

DP1_{PE}

¹H NMR (400 MHz, DCM-*d*₂) δ / ppm = 4.21 (s, 2H), 3.60 (m, 86H), 3.41 (m, 3H), 1.26 (s, 84H).

DP2_{PE}

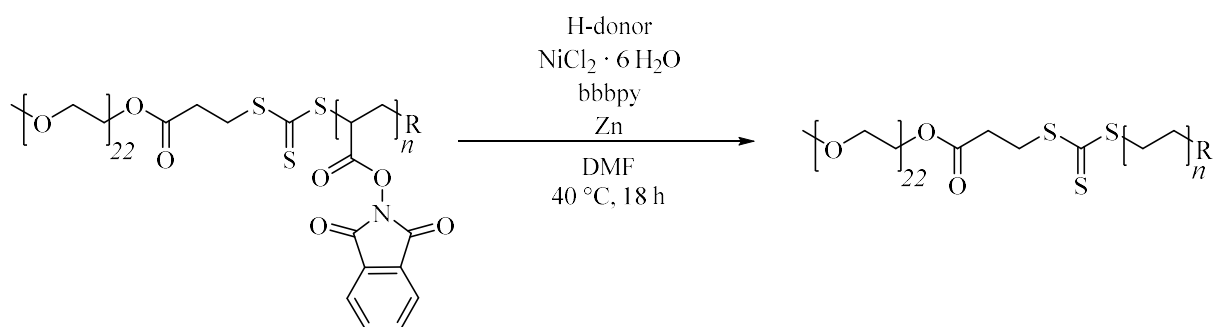
¹H NMR (400 MHz, DCM-*d*₂) δ / ppm = 4.21 (s, 2H), 3.60 (m, 86H), 3.41 (m, 3H), 1.26 (s, 147H).

DP3_{PE}

¹H NMR (400 MHz, DCM-*d*₂) δ / ppm = 4.21 (s, 2H), 3.60 (m, 86H), 3.41 (m, 3H), 1.26 (s, 246H).

ATR-FT-IR: ν (cm⁻¹) = 2921, 2845, 1683, 1305, 1060, 759, 698.

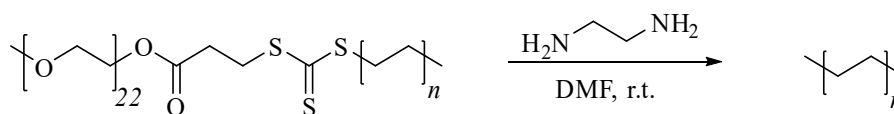
6.4.6 Thermal Decarboxylation of Poly[*N*-(acryloyloxy)phthalimide]-*block*-Poly(ethylene glycol)



Zinc (0.50 eq. per active ester group) was placed in a dry Schlenk tube equipped with a stirring bar. The tube was evacuated and backfilled with nitrogen three times. Simultaneously, $\text{NiCl}_2 \cdot 6 \text{H}_2\text{O}$ (0.10 eq. per active ester group) and bbbpy (0.20 eq. per active ester group) in anhydrous DMF (0.5 mL), H-donor (phenylsilane or tributyltin hydride) (1.50 eq. per active ester group) in anhydrous DMF (0.5 mL) and PAP-*b*-PEG (1.00 eq.) in anhydrous DMF ($0.015 \text{ mmol mL}^{-1}$) were deoxygenated with a nitrogen flow for 20 min in separate vials and added *via* a gas-tight syringe under nitrogen atmosphere afterwards. The reaction mixture was stirred at 40 °C for 18 h, precipitated in cold diethyl ether, centrifuged, washed with diethyl ether and dried under reduced pressure at 40 °C.

Experimental Section

6.4.7 Aminolysis of Polyethylene-*block*-Poly(ethylene glycol)



PE-*b*-PEG (1.00 eq.) was dissolved in DMF/TCB ($0.50 \text{ mmol mL}^{-1}$) in a pear shaped flask equipped with a stirring bar and deoxygenated with a nitrogen flow for 20 min. Ethylenediamine (5.00 eq.) was dissolved in DMF (0.50 mL), deoxygenated with a nitrogen flow for 20 min and added *via* a gas-tight syringe. The reaction was stirred overnight at $80 \text{ }^\circ\text{C}$ and the resulting suspension was precipitated in methanol at room temperature and centrifuged. The resulting PE was purified by stirring in methanol under reflux, followed by centrifugation of the hot suspension. The product was dried at $40 \text{ }^\circ\text{C}$ under reduced pressure.

6.4.7.1 Physical data of PE obtained from optimized conditions:

PE1:

$^1\text{H NMR}$ (400 MHz, $80 \text{ }^\circ\text{C}$, TCE- d_2) δ / ppm = 1.22 (s, 4H).

$^{13}\text{C NMR}$ (400 MHz, $80 \text{ }^\circ\text{C}$, TCE- d_2) δ / ppm = 28.07.

SEC (1,2,4-TCB, $160 \text{ }^\circ\text{C}$): $M_n = 1050 \text{ g mol}^{-1}$, $D = 2.52$.

ATR-FT-IR: ν (cm^{-1}) = 2919, 2847, 1470, 715.

DSC: $T_m = 96 \text{ }^\circ\text{C}$.

PE2:

$^1\text{H NMR}$ (400 MHz, $80 \text{ }^\circ\text{C}$, TCE- d_2) δ / ppm = 1.22 (s, 4H).

$^{13}\text{C NMR}$ (400 MHz, $80 \text{ }^\circ\text{C}$, TCE- d_2) δ / ppm = 28.07, 26.37, 25.16, 16.00, 11.86.

ATR-FT-IR: ν (cm^{-1}) = 2921, 2845, 1471, 712.

DSC: $T_m = 95 \text{ }^\circ\text{C}$.

PE3:

$^1\text{H NMR}$ (400 MHz, $80 \text{ }^\circ\text{C}$, TCE- d_2) δ / ppm = 1.22 (s, 4H).

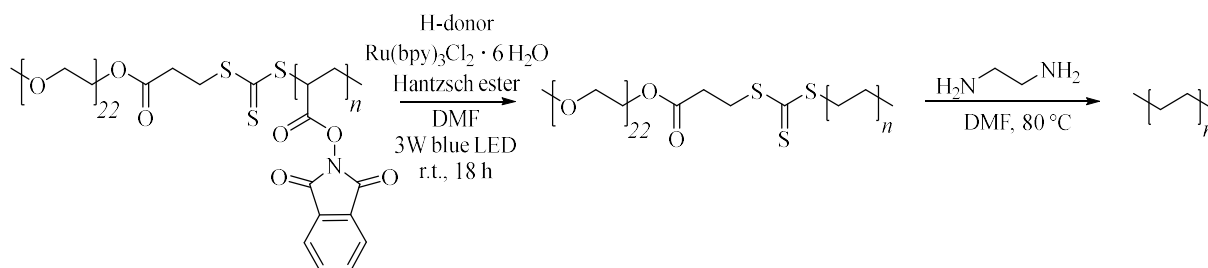
$^{13}\text{C NMR}$ (400 MHz, $80 \text{ }^\circ\text{C}$, TCE- d_2) δ / ppm = 28.07, 26.26, 25.11, 16.08, 11.89.

SEC (1,2,4-TCB, $160 \text{ }^\circ\text{C}$): $M_n = 1320 \text{ g mol}^{-1}$, $D = 2.73$.

ATR-FT-IR: ν (cm^{-1}) = 2919, 2847, 1470, 715.

DSC: $T_m = 97 \text{ }^\circ\text{C}$.

6.4.8 One-Pot Two-Step Photochemical Decarboxylation and Aminolysis



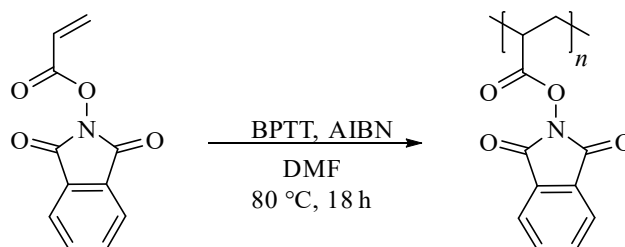
Ru(bpy)₃Cl₂ · 6 H₂O (0.02 eq. per active ester group) and Hantzsch ester (1.00 eq. per active ester group) were placed in a dry Schlenk tube equipped with a stirring bar. The tube was evacuated and backfilled with nitrogen three times. Simultaneously, H-donor (phenylsilane or tributyltin hydride) (1.50 eq. per active ester group) in anhydrous DMF (0.5 mL) and PAP-*b*-PEG (1.00 eq.) in anhydrous DMF (0.015 mmol mL⁻¹) were deoxygenated with a nitrogen flow for 20 min in separate vials and added *via* a gas-tight syringe under nitrogen atmosphere afterwards. The reaction mixture was stirred under the irradiation of three 3 W blue LEDs (distance app. 1.5 cm from the light source, wavelength maximum 440 - 450 nm) at room temperature for 18 h. Subsequently, the LED were removed, a balloon filled with nitrogen was added and the tube was placed in a preheated oil bath at 80 °C. Simultaneously, ethylenediamine (5.00 eq. per polymer) was dissolved in DMF (0.50 mL), deoxygenated with a nitrogen flow for 20 min and added to the Schlenk tube *via* a gas-tight syringe. The reaction was stirred overnight at 80 °C and the resulting suspension was precipitated in methanol at room temperature and centrifuged. The resulting PE was purified by stirring in methanol under reflux, followed by centrifugation of the hot suspension. The product was dried at 40 °C under reduced pressure.

Experimental Section

6.5 Procedures for ‘Decarboxylation of Poly[*N*-(acryloyloxy)phthalimide as a Versatile Tool for Post-Polymerization Modification’

6.5.1 Synthesis of Precursor Polymers

6.5.1.1 Synthesis of Poly[*N*-(acryloyloxy)phthalimide] (FP1)



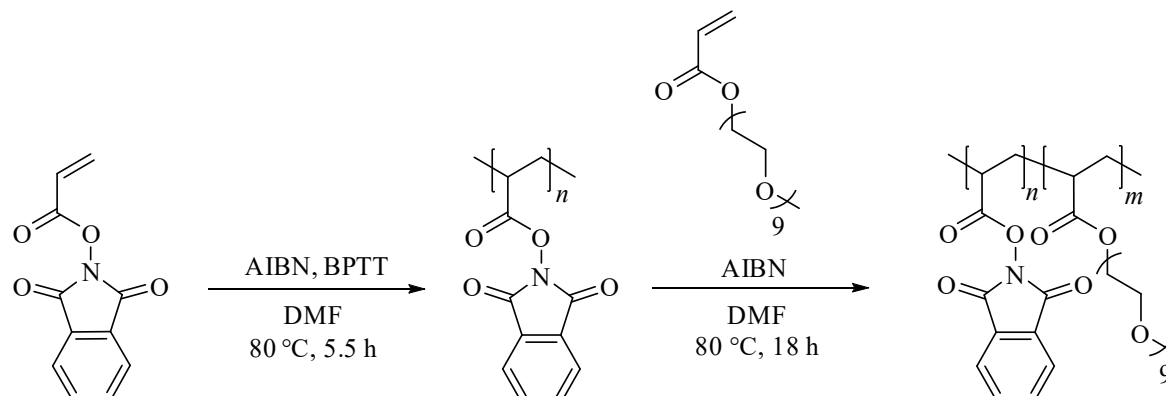
N-(Acryloyloxy)phthalimide (0.50 g, 2.30 mmol, 30.0 eq.), AIBN (1.26 mg, 0.01 mmol, 0.10 eq.), and BPTT (18.6 mg, 0.08 mmol, 1.0 eq.) were dissolved in 1.50 mL of DMF in a pear-shaped flask. The flask was sealed with a septum, the solution was deoxygenated with a nitrogen flow for 20 min and the flask was placed in a preheated oil bath for overnight at 80 °C. The polymer was precipitated in cold diethyl ether, centrifuged, washed with diethyl ether, and dried at room temperature.

¹H NMR (400 MHz, DCM-*d*₂) δ / ppm = 7.66 (m, 4H), 3.69 – 3.39 (m, 1H), 2.43 (s, 2H).
ATR-FT-IR: ν (cm⁻¹) = 2932, 1809, 1787, 1659, 1472, 1357, 1061, 835, 762.

Table 19: Analysis results of FP1 by SEC in DMAc as eluent with PMMA calibration and ¹H NMR spectroscopy.

	$M_{n, SEC}$ [g mol ⁻¹]	\bar{D}_{SEC}	DP_{SEC}	$M_{n, NMR}$ [g mol ⁻¹]	DP_{NMR}
FP1	6700	1.20	30	7500	34

6.5.1.2 Synthesis of Poly[*N*-(acryloyloxy)phthalimide]-*block*-Poly[(ethylene glycol) methyl ether acrylate] (FP2)



N-(Acryloyloxy)phthalimide (0.50 g, 2.30 mmol, 20.0 eq.), AIBN (1.89 mg, 0.01 mmol, 0.10 eq.), and BPTT (27.9 mg, 0.12 mmol, 1.00 eq.) were dissolved in 1.50 mL of DMF in a pear-shaped flask. The flask was sealed with a septum, the solution was deoxygenated with a nitrogen flow for 20 min and the flask was placed in a preheated oil bath for 5.5 h at 80 °C. Subsequently, a ¹H NMR sample was taken to check for full conversion of AP and deinhibited oligo(ethylene glycol) methyl ether acrylate (553 mg, 1.15 mmol, 10.0 eq.) was added and the polymerization conducted over night. The polymer was precipitated in cold diethyl ether, centrifuged, washed with diethyl ether, and dried at room temperature.

¹H NMR (400 MHz, DCM-*d*₂) δ / ppm = 8.13 (m, 36H), 4.44 (s, 2H), 3.88 (m, 41H), 3.64 (s, 3H), 2.97 – 2.42 (m, 9H), 2.12 (m, 2H).

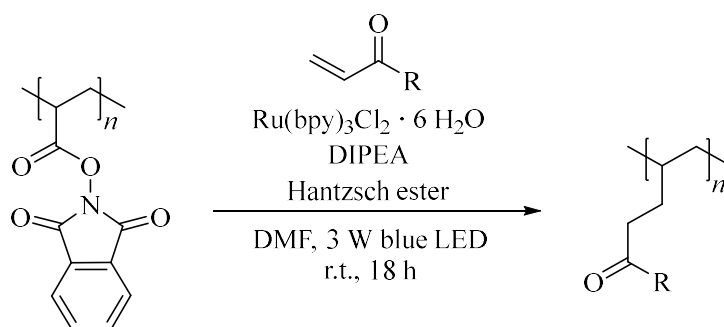
ATR-FT-IR: ν (cm⁻¹) = 2930, 1811, 1784, 1670, 1467, 1357, 1055, 833, 760.

Table 20: Analysis results of FP2 by SEC in DMAc as eluent with PMMA calibration and ¹H NMR spectroscopy.

	M_n , SEC. [g mol ⁻¹]	D_{SEC} .	DP_{SEC} .	M_n , NMR [g mol ⁻¹]	DP_{NMR}
PAP	4000	1.61	18	4800	22
POEGMEA	900	1.58	2	1700	4

Experimental Section

6.5.2 Michael-type Addition



$\text{Ru}(\text{bpy})_3\text{Cl}_2 \cdot 6 \text{H}_2\text{O}$ (0.02 eq. per active ester group) and Hantzsch ester (1.00 eq. per active ester group) were placed in a dry Schlenk tube equipped with a stirring bar. The tube was evacuated and backfilled with nitrogen three times. Simultaneously, Michael acceptor (1.50 eq. per active ester group) and DIPEA (1.50 eq. per active ester group) in separate vials dissolved in anhydrous DMF (0.5 mL) as well as PAP (1.00 eq.) was dissolved in anhydrous DMF ($0.015 \text{ mmol mL}^{-1}$) and all vials were deoxygenated with a nitrogen flow for 20 min each and added *via* a gas-tight syringe under nitrogen atmosphere afterwards. The reaction mixture was stirred under the irradiation of three 3 W blue LEDs (distance app. 1.5 cm from the light source, wavelength maximum 440 - 450 nm) at room temperature for 18 h, precipitated in cold diethyl ether, centrifuged, and washed with diethyl ether.

FP1-MEA

$^1\text{H NMR}$ (400 MHz, CDCl_3) δ / ppm = 4.33 – 4.05 (m, 2H), 3.55 (s, 2H), 3.33 (s, 3H), 2.63 – 2.14 (m, 2H), 1.90 – 1.42 (m, 2H), 1.42 – 0.80 (m, 3H).

ATR-FT-IR: ν (cm^{-1}) = 2926, 1731, 1444, 1121, 760.

SEC (DMAc): $M_n = 7700 \text{ g mol}^{-1}$, $D = 1.45$.

FP1-MA

$^1\text{H NMR}$ (400 MHz, CDCl_3) δ / ppm = 3.65 (s, 3H), 2.58 – 2.17 (m, 2H), 1.95 – 1.46 (m, 2H), 1.46 – 0.80 (m, 3H).

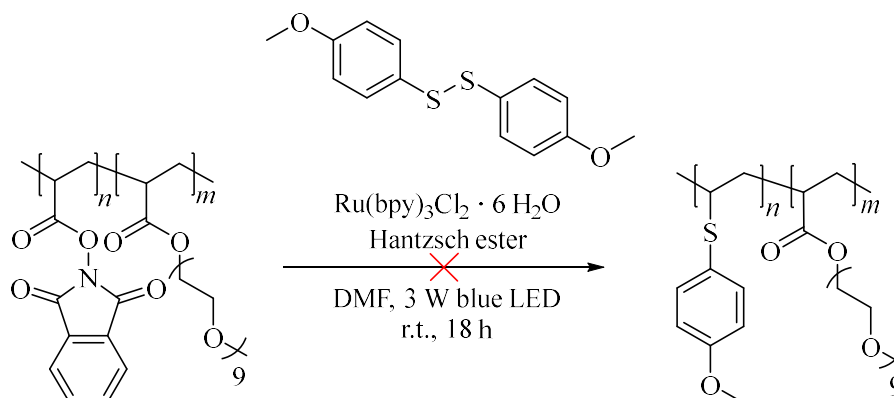
ATR-FT-IR: ν (cm^{-1}) = 2931, 2854, 1730, 1439, 1157, 762.

FP1-MVK

$^1\text{H NMR}$ (400 MHz, CDCl_3) δ / ppm = 2.68 – 2.27 (m, 2H), 2.23 – 1.90 (m, 3H), 1.82 – 1.39 (m, 2H), 1.37 – 0.73 (m, 3H).

ATR-FT-IR: ν (cm^{-1}) = 2925, 2851, 1708, 1358, 1161, 761.

6.5.3 Functionalization of Poly[*N*-(acryloyloxy)phthalimide]-*block*-Poly[oligo(ethylene glycol) methyl ether acrylate] with Bis-(4-methoxyphenyl)disulfide

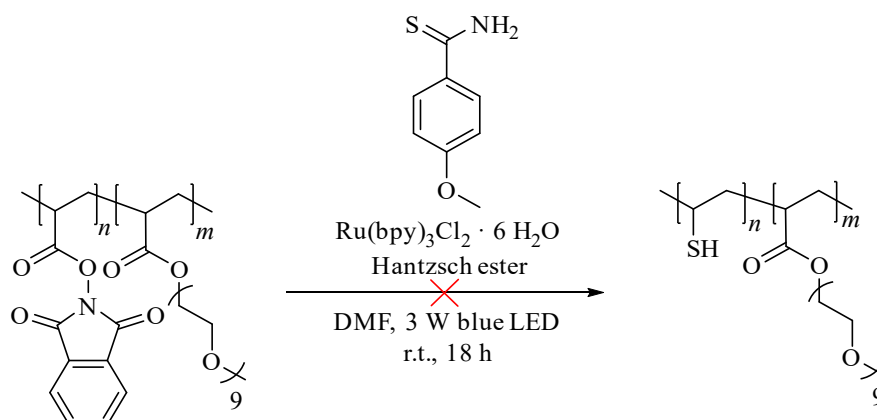


Ru(bpy)₃Cl₂ · 6 H₂O (13.8 mg, 0.02 mmol, 0.02 eq. per active ester group) and Hantzsch ester (241 mg, 1.01 mmol, 1.10 eq. per active ester group) were placed in a dry Schlenk tube equipped with a stirring bar. The tube was evacuated and backfilled with nitrogen three times. Simultaneously, bis(4-methoxyphenyl)disulfide (257 mg, 0.92 mmol, 1.00 eq. per active ester group) in 1.00 mL of anhydrous DMF and **FP2** (200 mg, 0.03 mmol, 1.00 eq.) in anhydrous DMF (0.015 mmol mL⁻¹) were deoxygenated with a nitrogen flow for 20 min and added *via* a gas-tight syringe under nitrogen atmosphere afterwards. The reaction mixture was stirred under the irradiation of three 3 W blue LEDs (distance app. 1.5 cm from the light source, wavelength maximum 440 - 450 nm) at room temperature for 18 h, precipitated in cold petroleum ether, centrifuged, washed with diethyl ether.

Experimental Section

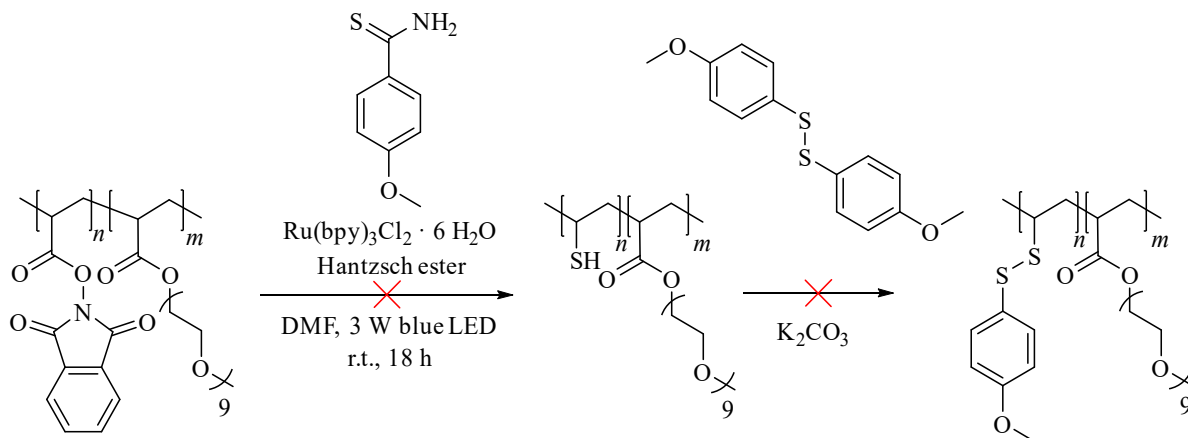
6.5.4 Decarboxylative Thiolation of Poly[*N*-(acryloyloxy)phthalimide]

6.5.4.1 Decarboxylation of PAP (FP1) with 4-Methoxythiobenzamide



Ru(bpy)₃Cl₂ · 6 H₂O (10.3 mg, 0.01 mmol, 0.02 eq. per ester group) and Hantzsch ester (181 mg, 0.76 mmol, 1.10 eq. per ester group) were placed in a dry Schlenk tube equipped with a stirring bar. The tube was evacuated and backfilled with nitrogen three times. Simultaneously, 4-methoxythiobenzamide (302 mg, 1.04 mmol, 1.00 eq. per ester group) in 1.00 mL of anhydrous DMF and **FP2** (360 mg, 0.04 mmol, 1.00 eq.) in anhydrous DMF (0.015 mmol mL⁻¹) were deoxygenated with a nitrogen flow for 20 min and added *via* a gas-tight syringe under nitrogen atmosphere afterwards. The reaction mixture was stirred under the irradiation of three 3 W blue LEDs (distance app. 1.5 cm from the light source, wavelength maximum 440 - 450 nm) at room temperature for 18 h, precipitated in cold petroleum ether, centrifuged, washed with diethyl ether.

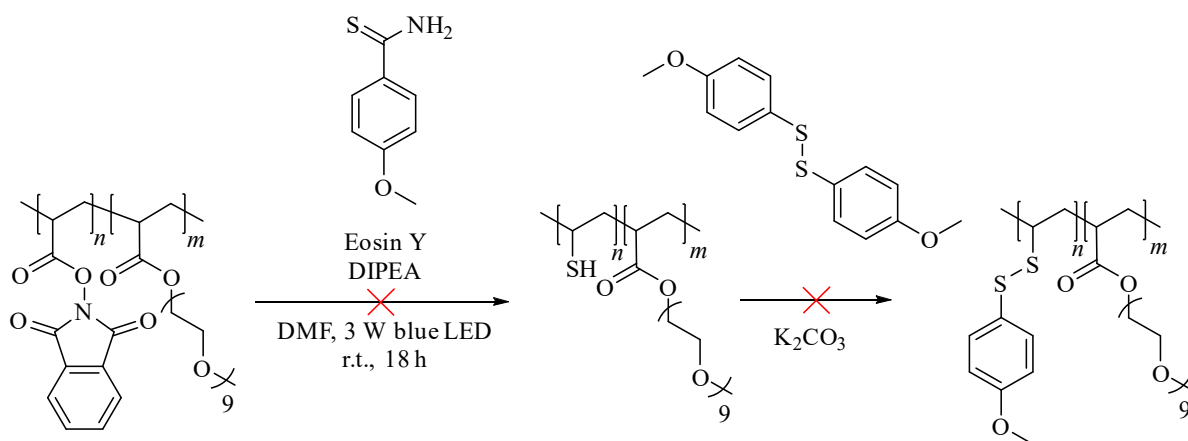
6.5.4.2 Decarboxylation of PAP-*b*-POEGMEA (FP2) with 4-Methoxybenzamide and Bis-(4-methoxyphenyl)disulfide



Ru(bpy)₃Cl₂ · 6 H₂O (13.1 mg, 0.03 mmol, 0.02 eq. per active ester group) and Hantzsch ester (229 mg, 0.96 mmol, 1.10 eq. per active ester group) were placed in a dry Schlenk tube equipped with a stirring bar. The tube was evacuated and backfilled with nitrogen three times. Simultaneously, 4-methoxythiobenzamide (292 mg, 1.75 mmol, 1.00 eq. per active ester group) in 1.00 mL of anhydrous DMF and **FP2** (250 mg, 0.03 mmol, 1.00 eq.) in anhydrous DMF (0.015 mmol mL⁻¹) were deoxygenated with a nitrogen flow for 20 min and added *via* a gas-tight syringe under nitrogen atmosphere afterwards. The reaction mixture was stirred under the irradiation of three 3 W blue LEDs (distance app. 1.5 cm from the light source, wavelength maximum 440 - 450 nm) at room temperature for 18 h. Subsequently, potassium carbonate (242 mg, 1.75 mmol, 2.00 eq.) and bis-(4-methoxyphenyl)disulfide (487 mg, 1.75 mmol, 2.00 eq.) dissolved in DMF (0.5 mL) and were added under nitrogen atmosphere. The solution was stirred for 18 h and the polymer precipitated in cold diethyl ether, washed and dried under reduced pressure.

Experimental Section

6.5.4.3 Decarboxylation of PAP-*b*-POEGMEA (FP2) with Eosin Y as Photocatalyst, 4-Methoxythiobenzamide, and Bis-(4-methoxyphenyl)disulfide



Eosin Y (55.8 mg, 0.08 mmol, 0.02 eq. per ester group) was placed in a dry Schlenk tube equipped with a stirring bar. The tube was evacuated and backfilled with nitrogen three times. Simultaneously, 4-methoxythiobenzamide (269 mg, 1.62 mmol, 1.00 eq. per ester group), DIPEA (115 mg, 0.89 mmol, 1.10 eq. per ester group) were dissolved in anhydrous DMF (0.5 mL) as well as FP2 (200 mg, 0.04 mmol, 1.00 eq.) in anhydrous DMF (0.015 mmol mL⁻¹) were deoxygenated with a nitrogen flow for 20 min in separate vials and added *via* a gas-tight syringe under nitrogen atmosphere afterwards. The reaction mixture was stirred under the irradiation of three 3 W blue LEDs (distance app. 1.5 cm from the light source, wavelength maximum 440 - 450 nm) at room temperature for 18 h. Subsequently, the solution was transferred into a deoxygenated Schlenk flask with potassium carbonate (223 mg, 1.61 mmol, 2.00 eq.) and bis-(4-methoxyphenyl)disulfide (449 mg, 1.61 mmol, 2.00 eq.) dissolved in DMF (1.00 mL). The solution was stirred for 18 h and the polymer precipitated in cold diethyl ether, washed and dried under reduced pressure.

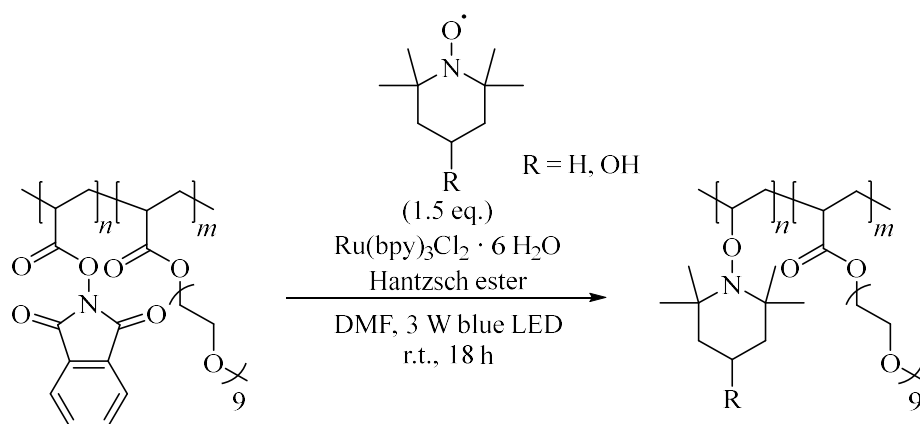
6.5.5 Crosslinking of Poly[*N*-(acryloyloxy)phthalimide] with Styrene

Ru(bpy)₃Cl₂ · 6 H₂O (0.02 eq. per active ester group) and Hantzsch ester (1.00 eq. per active ester group) were placed in a dry Schlenk tube equipped with a stirring bar. The tube was evacuated and backfilled with nitrogen three times. Simultaneously, styrene (30.0 eq. per active ester group) in anhydrous DMF (0.5 mL) and **FP1** (1.00 eq.) dissolved in anhydrous DMF (0.015 mmol/mL) in a separate vial were deoxygenated with a nitrogen flow for 20 min each and added *via* a gas-tight syringe under nitrogen atmosphere afterwards. The reaction mixture was stirred under the irradiation of three 3 W blue LEDs (distance app. 1.5 cm from the light source, wavelength maximum 440 - 450 nm) at room temperature for 18 h, precipitated in cold diethyl ether, centrifuged, and washed with diethyl ether.

ATR-FT-IR: ν (cm⁻¹) = 3024, 2928, 2844, 1781, 1735, 1446, 1374, 1185, 1046, 874, 751, 697.

Experimental Section

6.5.6 Nitroxide Radical Coupling



Ru(bpy)₃Cl₂ · 6 H₂O (0.02 eq. per active ester group) and Hantzsch ester (1.00 eq. per active ester group) were placed in a dry Schlenk tube equipped with a stirring bar. The tube was evacuated and backfilled with nitrogen three times. Simultaneously, TEMPO/TEMPO-OH (1.50 eq. per active ester group) and DIPEA (1.50 eq. per ester group) were dissolved in anhydrous DMF (0.5 mL) as well as **FP1/FP2** (1.00 eq.) in anhydrous DMF (0.015 mmol/mL) in separate vials were deoxygenated with a nitrogen flow for 20 min each and added *via* a gas-tight syringe under nitrogen atmosphere afterwards. The reaction mixture was stirred under the irradiation of three 3 W blue LEDs (distance app. 1.5 cm from the light source, wavelength maximum 440 - 450 nm) at room temperature for 18 h, precipitated, centrifuged, and washed. **PTEMVP** was precipitated in cold methanol, **PTEMVPO**, **PTEMVP-*b*-POEGMEA**, and **PTEMVPO-*b*-POGEMA** were precipitated in cold diethyl ether

PTEMVP

¹H NMR (400 MHz, DCM-*d*₂) δ / ppm = 4.11 – 3.55 (m, 1H), 2.62 – 2.04 (m, 2H), 1.96 – 1.15 (m, 6H), 1.14 – 0.76 (m, 12H).

ATR-FT-IR: ν (cm⁻¹) = 2931, 1751, 1463, 1363, 1134, 951, 717.

SEC (DMAc): M_n = 7500 g mol⁻¹, D = 1.26.

PTEMVPO

¹H NMR (400 MHz, DMSO-*d*₆) δ / ppm = 4.47 (m, 1H), 4.14 – 3.58 (m, 1H), 3.58 – 3.09 (m, 1H), 1.91 – 1.51 (m, 2H), 1.30 (m, 2H), 1.18 (s, 3H).

ATR-FT-IR: ν (cm⁻¹) = 3340, 2941, 1751, 1442, 1373, 1176, 1051, 736, 603.

SEC (DMAc): M_n = 8300 g mol⁻¹, D = 1.27.

PTEMVP-*b*-POEGMEA

¹H NMR (400 MHz, DCM-*d*₂) δ / ppm = 4.18 (s, 20H), 3.99 – 3.82 (m, 9H), 3.80 – 3.42 (m, 32H), 3.34 (s, 3H), 2.65 (s, 1H), 2.34 (s, 2H), 1.89 – 1.25 (m, 56H), 1.09 (m, 108H).

ATR-FT-IR: ν (cm⁻¹) = 2918, 1737, 1461, 1091.

PTEMVPO-*b*-POEGMEA

¹H NMR (400 MHz, DMSO-*d*₆) δ / ppm = 4.48 (m, 9H), 4.11 (s, 20H), 3.94 – 3.64 (m, 18H), 3.51 (s, 32H), 3.24 (s, 3H), 2.24 (m, 2H), 1.69 (m, 2H), 1.44 – 1.21 (m, 36H), 1.20 – 0.78 (m, 118H).

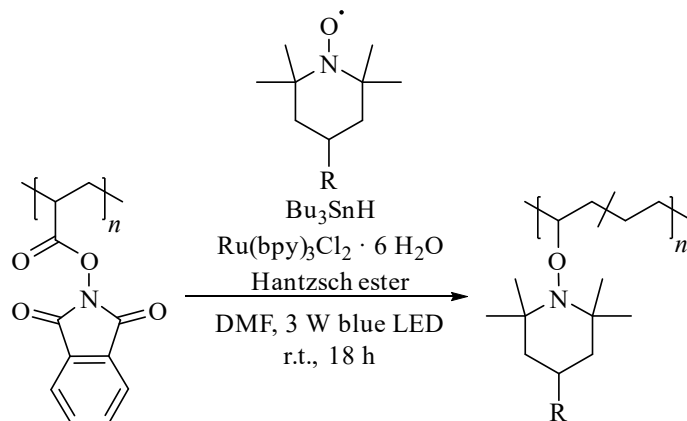
ATR-FT-IR: ν (cm⁻¹) = 3415, 2931, 1743, 1456, 1361, 1099, 1049, 727.

SEC (DMAc): $M_n = 7500$ g mol⁻¹, $D = 1.38$.

Experimental Section

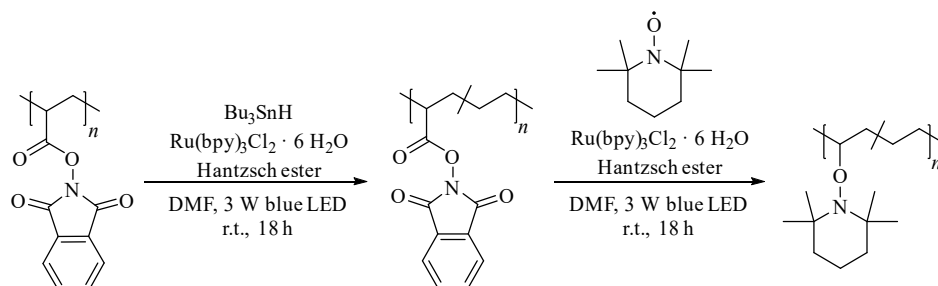
6.5.7 Synthesis of Poly[2,2,6,6-tetramethyl-1-(vinylloxy)piperidine)-co-ethylene]

6.5.7.1 One-Step Decarboxylation



$\text{Ru}(\text{bpy})_3\text{Cl}_2 \cdot 6 \text{H}_2\text{O}$ and Hantzsch ester were placed in a dry Schlenk tube equipped with a stirring bar. The tube was evacuated and backfilled with nitrogen three times. Simultaneously, the TEMPO-derivative dissolved in anhydrous DMF ($0.30 \text{ mmol mL}^{-1}$), **FP1** dissolved in anhydrous DMF ($0.01 \text{ mmol mL}^{-1}$), and Bu_3SnH dissolved in anhydrous DMF ($3.00 \text{ mmol mL}^{-1}$) were deoxygenated with a nitrogen flow for 20 min and added *via* a gas-tight syringe under nitrogen atmosphere afterwards. The reaction mixture was stirred under the irradiation of three 3 W blue LEDs (distance app. 1.5 cm from the light source, wavelength maximum 440 - 450 nm) at room temperature and precipitated in cold petroleum ether, centrifuged, washed with petroleum ether.

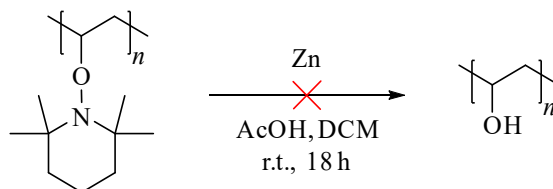
6.5.7.2 Two-Step Decarboxylation



Ru(bpy)₃Cl₂ · 6 H₂O (13.8 mg, 0.02 mmol, 0.02 eq. per active ester group) and Hantzsch ester (328 mg, 1.38 mmol, 1.50 eq. per active ester group) were placed in a dry Schlenk tube equipped with a stirring bar. The tube was evacuated and backfilled with nitrogen three times. Simultaneously, Bu₃SnH (215 mg, 0.74 mmol, 0.80 eq. per active ester group) in 2.00 mL of anhydrous DMF and **FP1** (200 mg, 0.03 mmol, 1.00 eq.) dissolved in 2.00 mL of anhydrous DMF were deoxygenated with a nitrogen flow for 20 min and added *via* a gas-tight syringe under nitrogen atmosphere afterwards. The reaction mixture was stirred under the irradiation of three 3 W blue LEDs (distance app. 1.5 cm from the light source, wavelength maximum 440 - 450 nm) at room temperature for 10 min. Subsequently, TEMPO (431 mg, 2.77 mmol, 3.00 eq. per ester group) in 1.00 mL of anhydrous DMF was added *via* a gas-tight syringe and the reaction stirred for additional 18 h and precipitated in cold methanol, centrifuged, and washed with methanol.

Experimental Section

6.5.8 Reduction of Poly[2,2,6,6-tetramethyl-1-(vinyloxy)piperidine] Polymers

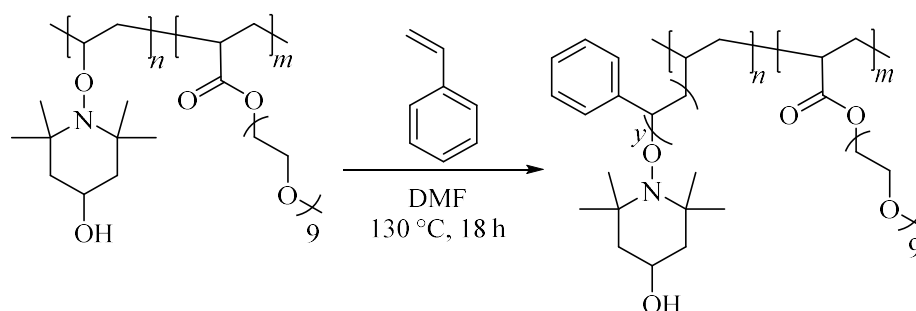


A crimp vial was charged with Zn powder (300 mg, 4.61 mmol, 20.0 eq. per TEMPO group) and deoxygenated with a nitrogen flow for 20 min. Simultaneously, **PTEMVP** (50.0 mg, 0.008 mmol, 1.00 eq.) was dissolved in a mixture of 6.00 ml of DCM, 1.00 ml of AcOH and 1.00 ml of water in a vial, deoxygenated for 20 min and added *via* a gas-tight syringe. The reaction mixture was stirred over the weekend and excess of Zn was filtered. The product was isolated by precipitation or by dialysis with a prewetted Spectra Pro dialysis membrane (MWCO = 1000 g mol⁻¹) in methanol/water (80:20).

6.5.8.1 Reduction of PTEMVPO-*b*-POEGMEA

A crimp vial was charged with Zn powder (20.0 eq. per TEMPO group) and deoxygenated with a nitrogen flow for 20 min. Simultaneously, **PTEMVPO-*b*-POEGMEA** (1.00 eq.) was dissolved in a mixture of DCM/THF, AcOH and water (8:1:1) in a vial, deoxygenated for 20 min and added *via* a gas-tight syringe. The reaction mixture was stirred over the weekend and excess of Zn was filtered. The product was isolated by precipitation or by dialysis with a prewetted Spectra Pro dialysis membrane (MWCO = 1000 g mol⁻¹) in methanol/water (80:20).

6.5.9 Grafting of Styrene



PTEMVPO-*b*-POEGMEA (50.0 mg, 0.007 mmol, 1.00 eq.) and styrene (1.13 g, 10.9 mmol, 150 eq. per TEMPO group) were dissolved in 2.00 mL of DMF in a pear shaped flask. The flask was sealed with a septum, the solution was deoxygenated with a nitrogen flow for 20 min and the flask was placed in a preheated oil bath for overnight (18 h) at 130 °C. The polymer was precipitated in cold diethyl ether, centrifuged, washed with diethyl ether, and dried at room temperature.

¹H NMR (400 MHz, DCM-*d*₂) δ / ppm = 7.43 – 6.23 (m, 272H), 4.19 (s, 2H), 3.76 – 3.47 (m, 32H), 3.34 (s, 32H), 2.29 – 1.13 (m, 328).

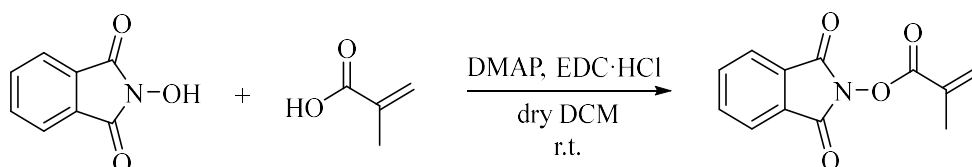
ATR-FT-IR: ν (cm⁻¹) = 2931, 1751, 1463, 1363, 1134, 951, 717.

SEC (DMAc): M_n = 15500 g mol⁻¹, D = 1.87.

Experimental Section

6.6 Procedures for ‘Propylene-free Synthesis of Polypropylene *via* Decarboxylation’

6.6.1 Synthesis of *N*-(Methacryloyloxy)phthalimide



Methacrylic acid (1.20 eq.), *N*-hydroxyphthalimide (1.00 eq.), and 4-dimethylaminopyridine (0.050 eq.) were dissolved in DCM (0.15 mol L⁻¹) in a round bottom flask. The reaction mixture was stirred and 1-ethyl-3-(3-dimethylaminopropyl)carbodiimide hydrochloride (1.20 eq.) was added slowly at room temperature. The reaction mixture was then stirred overnight, after which the solution was concentrated using a rotary evaporator and the crude product purified by column chromatography using cyclohexane : ethyl acetate in a 3 : 1 ratio as eluents. The solvent was removed under reduced pressure yielding a white, crystalline product. (Yield: 60 %)

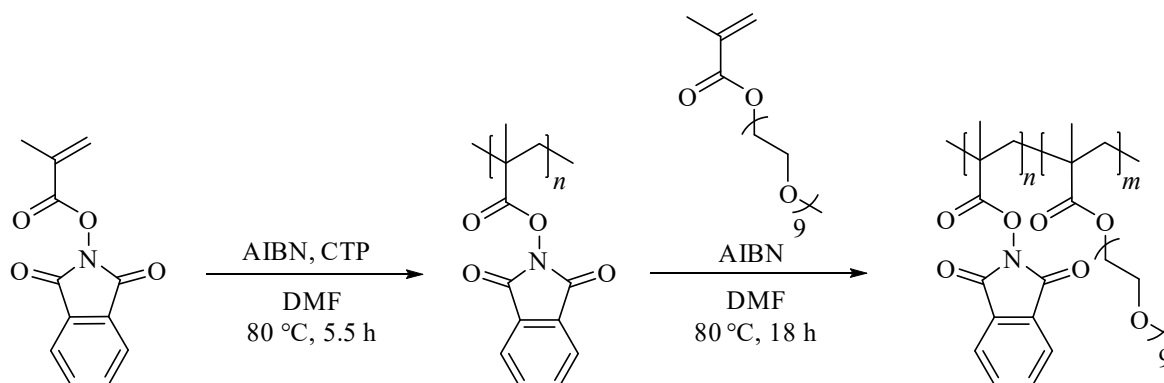
¹H NMR (400 MHz, DCM-*d*₂) δ / ppm = 7.99 - 7.87 (m, 2H, C_{aromatic}H), 7.87 – 7.75 m, 2H, C_{aromatic}H), 6.46 (1H, C_{vinyl}H), 5.98 – 5.91 (m, 1H, C_{vinyl}H), 2.11 – 2.05 (s, 3H, CH₃).

¹³C NMR (400 MHz, DCM-*d*₂) δ / ppm = 163.60 (C_{vinyl}COO), 162.40 (NCO), 135.26 (C_{vinyl}), 132.54 (C_{aromat.}), 130.59 (C_{vinyl}), 129.29 (C_{aromat.}), 124.24 (C_{aromat.}), 18.45 (CH₃).

*R*_f (CH/EE, 3:1): 0.3

6.6.2 Synthesis of Poly[*N*-(methacryloyloxy)phthalimide] Block Copolymers

6.6.2.1 Poly[*N*-(methacryloyloxy)phthalimide]-*block*-Poly[(ethylene glycol) methyl ether methacrylate] (PP1)



N-(Methacryloyloxy)phthalimide (250 mg, 1.08 mmol, 50.0 eq.), AIBN (0.35 mg, 0.002 mmol, 0.10 eq.), and 4-cyano-4-((phenylcarbonothioyl)thio)pentanoic acid (CTP, 6.04 mg, 0.02 mmol, 1.00 eq.) were dissolved in 0.75 mL of DMF in a pear-shaped flask. The flask was sealed with a septum and the solution was deoxygenated with a nitrogen flow for 20 min. Subsequently, the flask was placed in a preheated oil bath for 5.5 h at 80 °C. Deinhibited oligo(ethylene glycol) methyl ether methacrylate (649 mg, 1.30 mmol, 60.0 eq.) and AIBN (0.35 mg, 0.002 mmol, 0.10 eq.) were dissolved in 0.10 mL of DMF in a vial and the solution was deoxygenated with a nitrogen flow for 20 min. The quantitative conversion of *N*-(methacryloyloxy)phthalimide was checked by ¹H NMR spectroscopy. OEGMEMA was added polymerization was stirred overnight at 80 °C. The polymer was precipitated in cold diethyl ether, centrifuged, washed, and dried at 40 °C under reduced pressure.

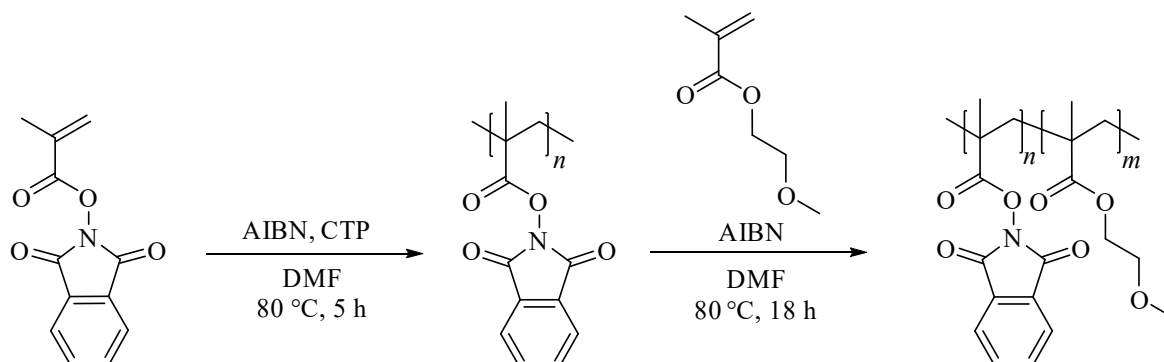
¹H NMR (400 MHz, DCM-*d*₂) δ/ppm = 8.19 – 7.29 (m, 7H), 4.24 (m, 2H), 3.58 (m, 32H), 3.33 (s, 3H), 2.84 – 2.33 (m, 4H) 1.75 (m, 2H), 1.47 – 0.91 (s, 8H).

Table 21: Analysis results of **PP1** by SEC in DMAc as eluent with PMMA calibration and ¹H NMR spectroscopy.

	$M_{n, SEC}$ [g mol ⁻¹]	\bar{D}_{SEC}	DP_{SEC}	$M_{n, NMR}$ [g mol ⁻¹]	DP_{NMR}
PMAP	10000	1.63	43	10925	47
POEGMEMA	12000	1.35	24	12893	26

Experimental Section

6.6.2.2 Poly[*N*-(methacryloyloxy)phthalimide]-*block*-Poly(2-methoxyethyl methacrylate) (PP2)



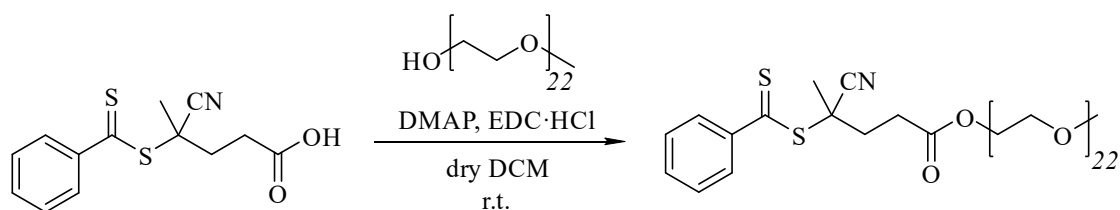
N-(Methacryloyloxy)phthalimide (250 mg, 1.08 mmol, 55.0 eq.), AIBN (0.32 mg, 0.002 mmol, 0.10 eq.), and 4-cyano-4-((phenylcarbonothioyl)thio)pentanoic acid (CTP, 5.50 mg, 0.02 mmol, 1.00 eq.) were dissolved in 0.75 mL of DMF in a pear-shaped flask. The flask was sealed with a septum and the solution was deoxygenated with a nitrogen flow for 20 minutes. Afterwards, the flask was placed in a preheated oil bath for 5.0 h at 80 °C. Deinhibited 2-methoxyethyl methacrylate (MEMA, 141 mg, 0.98 mmol, 50.0 eq.) and AIBN (0.32 mg, 0.002 mmol, 0.10 eq.) were dissolved in 0.10 mL of DMF in a vial and the solution was deoxygenated with a nitrogen flow for 20 min. The quantitative conversion of *N*-(methacryloyloxy)phthalimide was checked by taking a sample for ¹H NMR spectroscopy. MEMA was added to the polymerization flask and the reaction mixture was stirred overnight at 80 °C. The polymer was precipitated in cold diethyl ether, centrifuged, washed with diethyl ether, and dried at 40 °C under reduced pressure.

¹H NMR (400 MHz, DCM-*d*₂) δ /ppm = 7.86 (m, 5H), 4.05 (m, 2H), 3.54 (m, 2H), 3.28 – 3.13 (s, 3H), 2.78 – 2.41 (m, 2H) 1.82 (m, 2H) 1.82 (m, 2H), 1.23 – 0.95 (s, 7H).

Table 22: Analysis results of PP2 by SEC in DMAc as eluent with PMMA calibration and ¹H NMR spectroscopy.

	$M_{n, SEC}$ [g mol ⁻¹]	D_{SEC}	DP_{SEC}	$M_{n, NMR}$ [g mol ⁻¹]	DP_{NMR}
PMAP	12000	1.76	52	12850	56
PMEMA	6300	1.51	44	6920	48

6.6.2.3 Synthesis of macroRAFT Agent

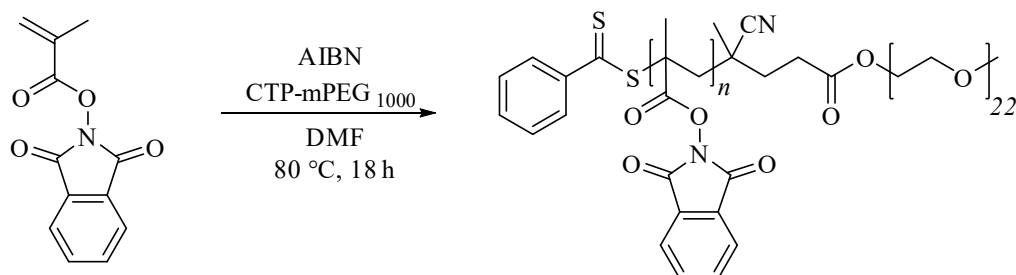


4-Cyano-4-((phenylcarbonothioyl)thio)pentanoic acid (100 mg, 0.38 mmol, 1.00 eq.) was dissolved in anhydrous DCM (3.00 mL) in a dry flask and DMAP (4.40 mg, 0.04 mmol, 0.10 eq.) and EDC·HCl (75.5 mg, 0.39 mmol, 1.10 eq.) were added. Into the flask mPEG₁₀₀₀ (179 mg, 0.18 mmol, 0.50 eq.) was added and the reaction was allowed to proceed for 4 d at room temperature with magnetic stirring. The polymer was precipitated two times in cold diethyl ether and washed with 1M HCl three times.

¹H NMR (400 MHz, CDCl₃) δ / ppm = 7.97 – 7.84 (m, 2H, C_{aromatic}H), 7.66 – 7.33 (m, 2H, C_{aromatic}H), 4.35 – 4.14 (m, 2H, COOCH₂), 3.74 – 3.48 (m, 86H, (CH₂CH₂O)₂₂), 3.37 (s, 3H, OCH₃), 2.77 – 2.59 (m, 2H, CNCCH₂), 2.50 – 2.33 (m, 2H, CH₂COO), 1.90 – 1.67 (m, 3H, CCH₃CN).

Experimental Section

6.6.2.4 Synthesis of Poly[*N*-(methacryloyloxy)phthalimide]-*block*-Poly(ethylene glycol) (DPP1)



N-(methacryloyloxy)phthalimide (1.00 g, 4.30 mmol, 70.0 eq.), CTP-mPEG₁₀₀₀ (79.1 mg, 0.06 mmol, 1.00 eq.) and AIBN (1.00 mg, 0.006 mmol, 0.10 eq.) were dissolved in 3.50 mL of DMF in a pear-shaped flask. The flask was sealed with a septum and the solution was deoxygenated with an argon flow for 20 min. Subsequently, the flask was placed in a preheated oil bath for overnight at 80 °C. The polymer was precipitated in cold diethyl ether, centrifuged, washed with diethyl ether, and dried under reduced pressure at 40 °C.

¹H NMR (400 MHz, DCM-*d*₂) δ / ppm = 7.89 – 7.50 (m, 4H), 4.24 (s, 2H), 3.60 (m, 86H), 3.33 (m, 3H), 2.86 (m, 2H), 2.06 – 1.43 (m, 3H).

SEC (DMAc): $M_n = 10500 \text{ g mol}^{-1}$, $D = 2.22$.

6.6.3 Decarboxylation of Poly[*N*-(methacryloyloxy)phthalimide] Block Copolymers

Ru(bpy)₃Cl₂ · 6 H₂O (0.02 eq. per active ester group) and the reductant (1.00 eq. per active ester group) were placed in a dry Schlenk tube equipped with a stirring bar. The tube was evacuated and backfilled with nitrogen three times. Simultaneously, the H-donor (1.50 eq. per active ester group) in anhydrous DMF (0.5 mL) and the precursor polymer (1.00 eq.) in anhydrous DMF (0.015 mmol mL⁻¹) in a separate vial were deoxygenated with a nitrogen flow for 20 min and added *via* a gas-tight syringe under nitrogen atmosphere afterwards. The reaction mixture was stirred under the irradiation of three 3 W blue LEDs (distance app. 1.5 cm from the light source, wavelength maximum 440 - 450 nm) at room temperature for 18 h, after which the polymer was precipitated in cold diethyl ether, centrifuged, washed with diethyl ether, and dried under reduced pressure at 40 °C.

7 Abbreviations

7.1 List of Abbreviations

%	Percentage
°C	Degree Celsius
AcOH	Acetic acid
AIBN	2,2'-Azobis(2-methylpropionitrile)
AP	Anionic polymerization
Aq.	Aqueous
ATR-FT-IR	Attenuated Total Reflection Fourier-Transform Infrared Spectroscopy
ATRP	Atom-transfer radical polymerization
Bbbpy	4,4'-Di-tert-butyl-2,2'-dipyridyl
BDMAP	1,6-Bis(dimethylamino)pyrene
BNAH	1-Benzyl-1,4-dihydronicotinamide
CH	Cyclohexane
cm	Centimeter
CMRP	Cobalt-Mediated Radical Polymerization
CP	Cationic polymerization
CSIRO	Commonwealth Scientific and Industrial Research Organization
CT	Charge-transfer
CTA	Chain-transfer agent
CTP	4-Cyano-4-((phenylcarbonothioyl)thio)pentanoic acid
CuAAC	Copper-catalyzed alkyne-azide cycloaddition
<i>D</i>	Dispersity
Δ	Delta
δ	Chemical shift in NMR spectroscopy
d	Day

Abbreviations

DCC	<i>N,N'</i> -Dicyclohexylcarbodiimide
DCM	Dichloromethane
DIB	1,3-Diisopropenylbenzene
DIPEA	<i>N,N</i> -Diisopropylethylamine
DMAP	4-Dimethylaminopyridine
DMF	Dimethylformamide
DMSO	Dimethyl sulfoxide
<i>DP</i>	Degree of polymerization
DSC	Differential scanning calorimetry
e.g.	Exempli gratia
EA	Ethyl acetate
EDC	1-Ethyl-3-(3-dimethylaminopropyl)carbodiimide
<i>et al.</i>	Et alii
Et ₃ N	Triethylamine
FRP	Free radical polymerization
h	Hour
HE	Hantzsch ester
HCl	Hydrochloric acid
IC	Internal Conversion
<i>i.e.</i>	Id est
<i>i</i> -PrOH	Isopropanol
IR	Infrared
ISC	Intersystem crossing
ITP	Iodine-transfer polymerization
K	Kelvin
LiTFSI	Lithium bis(trifluoromethanesulfonyl)imide
LMCT	Ligand-to-metal charge-transfer

M	Molar
MA	Methyl acrylate
MAO	Methylaluminoxane
MAP	<i>N</i> -(Methacryloyloxy)phthalimide
M_n	Number average molar mass
M_w	Weight average molar mass
MEA	2-Methoxyethyl acrylate
MeOH	Methanol
MEMA	2-Methoxyethyl methacrylate
min	Minute
mL	Milliliter
MLCT	Metal-to-ligand charge transfer
mM	Millimolar
mmol	Millimole
mol	Mole
mol%	Mole percentage
MVK	Methylvinyl ketone
MWCO	Molecular weight cut-off
NADH	Nicotinamide adenine dinucleotide
NaOH	Sodium hydroxide
NAP	<i>N</i> -(Acryloyloxy)phthalimide
NAS	<i>N</i> -(Acryloyloxy)succinimide
NiCl ₂	Nickel(II) chloride
NHP	<i>N</i> -hydroxyphthalimide
NHS	<i>N</i> -hydroxysuccinimide
NMP	Nitroxide-mediated polymerization
NMR	Nuclear magnetic resonance

Abbreviations

NRC	Nitroxide radical coupling
OEGMEA	Oligo(ethylene glycol) methyl ether acrylate
OEGMEMA	Oligo(ethylene glycol) methyl ether methacrylate
PAP	Poly[<i>N</i> -(acryloyloxy)phthalimide]
PE	Polyethylene
PET	Poly(ethylene terephthalate)
PFP	Pentafluorophenyl
PFPA	Pentafluorophenyl acrylate
PMAP	Poly[<i>N</i> -(methacryloyloxy)phthalimide]
PMEA	Poly(2-methoxyethyl acrylate)
PMEMA	Poly(2-methoxyethyl methacrylate)
POEGMEA	Poly[oligo(ethylene glycol) methyl ether acrylate]
POEGMEMA	Poly[oligo(ethylene glycol) methyl ether methacrylate]
PP	Polypropylene
PPM	Post-polymerization modification
ppm	Parts per million
PS	Polystyrene
PTEMVP	Poly[2,2,6,6-tetramethyl-1-(vinylloxy)piperidine]
PTEMVPO	Poly[2,2,6,6-tetramethyl-1-(vinylloxy)piperidin-4-ol]
PUR	Polyurethane
PVA	Poly(vinyl alcohol)
PVAc	Poly(vinyl acetate)
PVC	Poly(vinyl chloride)
r.t.	Room temperature
RAFT	Reversible addition-fragmentation chain-transfer
RDRP	Reversible-deactivation radical polymerization
RI	Refractive index

SEC	Size-exclusion chromatography
T	Temperature
t -BuSH	<i>tert</i> -Butylthiol
TEA	Triethylamine
T_g	Glass transition temperature
TGA	Thermogravimetric analysis
THF	Tetrahydrofuran
T_m	Melting temperature
VAc	Vinyl acetate
vs.	Versus
ν	Wavenumber
ν_{as} C-H	Asymmetrical C-H stretch
ν_s C-H	Symmetrical C-H stretch
δ_{oop} C-H	Out-of-plane deformation C-H stretch
δ_r	Rocking deformation C-H stretch
δ_s	Symmetrical deformation C-H stretch

8 List of Schemes, Figures, and Tables

8.1 List of Schemes

Scheme 1: Mechanism of free radical polymerization with three main steps: initiation, propagation, and termination.....	4
Scheme 2: Initiation of nitroxide-mediated polymerization by a) a bicomponent system with an initiator or b) by a monocomponent system with heat and the mechanism of NMP based on the equilibrium between dormant species (left) and the active species (right) with the propagating radical.....	6
Scheme 3: General structures of four different RAFT agents: dithioester, trithiocarbonate, xanthate, and dithiocarbamate with the stabilizing group Z and leaving group R.....	7
Scheme 4: Examples for MAMs: styrene, acrylates, methacrylates, acrylonitrile, and LAMs: vinylacetates, <i>N</i> -vinylpyrrolidone, and <i>N</i> -vinylcarbazol. ⁴⁶	8
Scheme 5: Mechanism of RAFT polymerization including the a) initiation, b) pre-equilibrium, c) reinitiation of a new chain, d) main-equilibrium, and e) termination. ⁴⁶	8
Scheme 6: Mechanism of the Ziegler-Natta process with the exemplary catalytic system TiCl ₄ with diethylaluminiumchloride. a) Formation of the titanium-aluminium complex and the addition of the first ethylene unit (blue) to the free coordination position (grey box). b) Rearrangement of the electrons in the complex after addition of ethylene and insertion of ethylene into the titanium-carbon bond for the formation of a polymer chain.	11
Scheme 7: Mechanism of the synthesis of PE by a metallocene-catalyzed process with a zirconium-based Kaminsky catalyst. a) The formation of the active metallocenium ion ZrCp ₂ CH ₃ ⁺ from the zirconium-based metallocene catalyst and methylaluminoxane (MAO) and the first addition of a ethylene unit (blue) to the free coordination position. b) Insertion of the ethylene unit into the zirconium-carbon bond opening a new coordination position.	12
Scheme 8: Production share of different plastics in Europe in 2021. ¹ PE is subdivided into low-density PE (LDPE) and high-density PE (HDPE). PP = polypropylene, PVC = poly(vinyl chloride), PUR = polyurethane, PET = poly(ethylene terephthalate), and PS = polystyrene. .	13
Scheme 9: Presentation of the molecular structure of different types of PE: rarely branched high-density PE (HDPE), slightly branched linear low-density PE (LLDPE) and highly branched low-density PE (LDPE).	14
Scheme 10: Polymerization of ethylene with two different xanthates as demonstrated by Monteil <i>et al.</i> ¹¹	15

List of Schemes, Figures, and Tables

Scheme 11: Mechanism of the cobalt-mediated radical polymerization of ethylene demonstrated by Detrembleur <i>et al.</i> ¹⁶	16
Scheme 12: a) Polymerization of ethylene using 1,3-diisopropenylbenzene (DIB), Cp ₂ ZrCl ₂ as catalyst, methylaluminoxane (MAO) as cocatalyst and hydrogen with the following block formation as demonstrated by Scott <i>et al.</i> ⁶¹ b) Simplified mechanism of the polymerization of ethylene with DIB and Cp ₂ ZrCl ₂ . ⁶¹	17
Scheme 13: Simplified mechanism of the NRC between a carbon-centered radical and a nitroxide. ³⁵	19
Scheme 14: Different steps of the mechanism of NRC on a PE with a TEMPO derivative (red) as the nitroxide: a) The decomposition of the peroxide by heat or under irradiation of light, b) the peroxide-induced radical formation at the backbone under H-abstraction and c) NRC of TEMPO with the carbon-centered radical at the backbone.....	21
Scheme 15: The three main steps of the mechanism of grafting side chains from a TEMPO-functionalized PE by NMP with a) the initiation upon heating to form the nitroxide and carbon-centered radical which initiates the polymerization by reacting with the monomer, b) the propagation step, in which monomeric units are added to the side chain and c) the equilibrium between the propagating chain and the nitroxide with the stable alkoxyamine.....	22
Scheme 16: Different active esters commonly used in organic synthesis.	23
Scheme 17: Amidation of an activated phthalimide-based ester with the reduced electron-density (marked in red) of the carbonyl carbon due to the electron-withdrawing group.	23
Scheme 18: Synthesis of the Barton ester (marked in blue) <i>via</i> Steglich esterification with <i>N,N'</i> -dicyclohexylcarbodiimide (DCC) and 4-dimethylaminopyridine (DMAP) followed by the Barton decarboxylation with tributyltin hydride and AIBN upon heating. ¹⁰⁸	25
Scheme 19: Synthesis of <i>N</i> -acyloxyphthalimide (marked in blue) <i>via</i> Steglich esterification with <i>N,N'</i> -dicyclohexylcarbodiimide (DCC) and 4-dimethylaminopyridine (DMAP) followed by the metal-catalyzed decarboxylation. ^{111,112}	26
Scheme 20: Mechanism of the photochemical decarboxylation of the phthalimide activated ester <i>N</i> -(acyloxy)phthalimide as used in the present thesis with Ru(bpy) ₃ Cl ₂ as metal catalyst and HE (green) as reductant. ^{113,115}	27
Scheme 21: Simplified Jablonski diagram of a) excitement of the catalyst Ru(bpy) ₃ ²⁺ , followed by MLCT and ISC to Ru*(bpy) ₃ ²⁺ and b) reduction of Ru*(bpy) ₃ ²⁺ by HE (green) to Ru(bpy) ₃ ⁺ and c) SET from Ru(bpy) ₃ ⁺ to the carbonyl of the phthalimide (red). ¹²⁰	28

List of Schemes, Figures, and Tables

Scheme 22: Mechanism of the photochemical decarboxylation of <i>N</i> -(acyloxy)phthalimide with Ru(bpy) ₃ Cl ₂ · 6 H ₂ O as metal catalyst, HE (green) or DIPEA (purple) as reductant and radical quencher and the electron-deficient alkene (Michael-acceptor, blue). ¹¹⁵	29
Scheme 23: Mechanism of the thermally-induced, nickel-catalyzed decarboxylation of <i>N</i> -(acyloxy)phthalimide as used in the present thesis with NiCl ₂ as metal catalyst and zinc as reductant. ¹²⁵	30
Scheme 24: Pathway of the intended concept of the present thesis. The decarboxylation of the phthalimide-based precursor polymer poly[<i>N</i> -(acryloyloxy)phthalimide] (PAP) by either photochemical, ruthenium-catalyzed (top) or thermal, nickel-catalyzed decarboxylation results in the formation of a carbon-centered radical at the polymer backbone. The radical should then be used for a) the main goal of the present thesis <i>i.e.</i> , the decarboxylative reduction of PAP to obtain pure PE and b) the decarboxylative reduction of PAP block copolymers to obtain PE block copolymers.	31
Scheme 25: Ethylene-free synthesis of PE block copolymers by either thermal or photochemical decarboxylation using an acrylate-based precursor polymer.....	34
Scheme 26: Structure of phenylsilane.....	38
Scheme 27: a) Approach A: The thermal decarboxylation of the PAP homopolymer with phenylsilane as H-donor, NiCl ₂ · 6 H ₂ O and bbbpy as catalytic system and zinc as reductant. b) Approach B: The photochemical decarboxylation of the PAP homopolymer with phenylsilane as H-donor, Ru(bpy) ₃ Cl ₂ · 6 H ₂ O as catalytic system and HE as reductant.....	39
Scheme 28: Structure of the catalyst Ru(bpy) ₃ Cl ₂ · 6 H ₂ O.....	40
Scheme 29: Thermally-induced decarboxylation of block copolymer PAP- <i>b</i> -POEGMEA yielding PE- <i>b</i> -POEGMEA.	46
Scheme 30: Photochemically-induced decarboxylation of block copolymer PAP- <i>b</i> -POEGMEA yielding PE- <i>b</i> -POEGMEA.	48
Scheme 32: Structure of lithium bis(trifluoromethanesulfonyl)imide.....	53
Scheme 32: Schematic depiction of the effect of the LiTFSI addition The salt accumulates exclusively in the POEGMEA phase, increasing the microphase separation and thus enables the crystallization of PE.	53
Scheme 34: Structure of tributyltin hydride.	55
Scheme 34: Schematic depiction of the crystallinity of PE- <i>b</i> -POEGMEA after decarboxylation with H-donor Bu ₃ SnH (left) and hindered crystallization of the PE block due to a small comonomer fraction after the decarboxylation with PhSiH ₃ (right). Reduced crystal length (R_D) and increased lamella thickness (R_L) resulting in a decreased crystal size marked.	57

List of Schemes, Figures, and Tables

Scheme 35: Overview of the project idea to obtain pure PE from a) a soluble, degradable block copolymer which can be quantitatively decarboxylated to yield b) a degradable PE block copolymer which can be cleaved to yield c) PE.....	64
Scheme 36: a) Synthesis of the basic structure of the RAFT agents and b) detailed structure of the RAFT agents 3-(((benzylthio)carbonothioyl)thio)propanoic acid (BTTP) and 11-(((benzylthio)carbonothioyl)thio)undecanoic acid (BTTU) evaluated for the synthesis of the degradable PAP block copolymers.	66
Scheme 37: Photochemical decarboxylation of PAP- <i>b</i> -PEG with phenylsilane as H-donor to yield PE- <i>b</i> -PEG.	69
Scheme 38: Aminolysis of PE- <i>b</i> -PEG cleaving the connection between both blocks, to obtain pure PE.	71
Scheme 39: Functionalization of PAP <i>via</i> photochemical decarboxylation using the carbon-centered radical formed at the polymer backbone.....	85
Scheme 40: Decarboxylative Michael-type addition of PAP with α , β -unsaturated carbonyl compounds 2-methoxyethyl acrylate (MEA), methyl acrylate (MA), and methyl vinyl ketone (MVK).	87
Scheme 41: Decarboxylative functionalization of FP1 with bis-(4-methoxyphenyl)disulfide.	92
Scheme 42: Decarboxylative thiolation of FP2 with 4-methoxythiobenzamide followed by functionalization with bis-(4-methoxyphenyl)disulfide.....	93
Scheme 43: Decarboxylative NRC on PAP with TEMPO or TEMPO-OH.	96
Scheme 44: Decarboxylative NRC on PAP- <i>b</i> -POEGMEA with TEMPO or TEMPO-OH. ...	98
Scheme 45: Synthesis of poly(ethylene- <i>co</i> -TEMVP) from PAP by simultaneous decarboxylation with TEMPO/TEMPO-OH and Bu ₃ SnH as H-donor.	100
Scheme 46: Synthesis of poly(ethylene- <i>co</i> -TEMVP) from PAP <i>via</i> a two-step reaction with the partly reductive decarboxylation with Bu ₃ SnH in the first step, followed by the decarboxylative functionalization with TEMPO.	103
Scheme 47: Reduction of PTEMVP to PVA with zinc and acetic acid.	106
Scheme 48: Grafting styrene from PTEMVPO-<i>b</i>-POEGMEA by NMP upon heating to 130 °C.....	111
Scheme 49: Intended concept of the propylene-free synthesis of a) PP block copolymers and b) PP homopolymers from methacrylate-based precursor polymers by photochemical decarboxylation.	114
Scheme 50: Mechanism of the photochemical decarboxylation with HE as H-donor.	119

List of Schemes, Figures, and Tables

Scheme 52: Structure of 1-benzyl-1,4-dihydronicotinamide.....	120
Scheme 52: Proposed mechanism of the SET-induced decarboxylative backbone degradation of PMAP copolymers by Sumerlin <i>et al.</i> ¹⁵⁵	126

8.2 List of Figures

Figure 1: a) Synthesis of the monomer <i>N</i> -(acryloyloxy)phthalimide by Steglich esterification as well as the corresponding b) ¹ H NMR and c) ¹³ C NMR spectrum.....	36
Figure 2: a) Polymerization of NAP to PAP and the analysis of PAP (P1) by b) SEC with DMAc as eluent and PMMA calibration. c) Copolymerization of NAP with OEGMEA yielding P[AP- <i>co</i> -OEGMEA] (P4) and d) the corresponding SEC chromatogram in DMAc as eluent using PMMA calibration.....	37
Figure 3: a) Thermal decarboxylation of P[AP- <i>co</i> -OEGMEA] (P4) and the analysis of the product via b) ¹ H NMR spectroscopy.....	41
Figure 4: a) Structure of RAFT-agent <i>S</i> , <i>S'</i> - benzyl propyl trithiocarbonate (BPTT) and the analysis via b) ¹ H NMR and c) ¹³ C NMR spectroscopy.....	42
Figure 5: a) Synthesis of PAP- <i>b</i> -POEGMEA by chain extension of PAP via RAFT polymerization. b) ¹ H NMR spectrum of P5 . c) ¹ H NMR spectrum of P6 and the corresponding SEC chromatograms in DMAc as eluent with PMMA calibration of d) P5 and e) P6	43
Figure 6: a) ¹ H NMR spectrum of PAP- <i>b</i> -PMEA (P10) and b) the corresponding SEC chromatogram in DMAc as eluent with PMMA calibration.....	45
Figure 7: a) Schematic depiction of the block ratios of block copolymer P5_{PE} , with PE (black) and POEGMEA (blue) blocks, as well as the analysis of P5_{PE} via b) ¹ H NMR spectroscopy, c) ATR-FT-IR spectroscopy, and the analysis of the block copolymers before and after decarboxylation by d) SEC with DMAc as eluent and PMMA calibration.....	47
Figure 8: a) Schematic depiction of the block ratios of block copolymer P5_{PE} , with PE (black) and POEGMEA (blue) blocks, as well as the analysis of P5_{PE} via b) ¹ H NMR spectroscopy, c) ATR-FT-IR spectroscopy, and the analysis of the block copolymers before and after decarboxylation by d) SEC with DMAc as eluent and PMMA calibration.....	49
Figure 9: a) ¹ H NMR spectra of PAP- <i>b</i> -POEGMEA (P6) and PE- <i>b</i> -POEGMEA (P6_{PE}) after photochemically-induced decarboxylation, b) schematic depiction of the block ratios of block copolymer P6_{PE} , with PE (black) and POEGMEA (blue) blocks and c) comparison of the ATR-FT-IR spectra before (top) and after (bottom) photochemically-induced decarboxylation.....	50
Figure 10: a) DLS analysis of PAP- <i>b</i> -POEGMEA (P6 , black) and PE- <i>b</i> -POEGMEA (P6_{PE} , red) after photochemically-induced decarboxylation as well as b) DSC characterization of P6_{PE} after the addition of LiTFSI to favor the microphase separation and c) schematic depiction of the formation of agglomerates with partly crystalline PE in the core. As a result of the formation of agglomerates, the hydrodynamic radius R_h increases as demonstrated by DLS.....	52

List of Schemes, Figures, and Tables

- Figure 11:** **a)** Schematic depiction of block ratios of block copolymer **P7_{PE}**, with PE (black) and POEGMEA (blue) blocks, as well as the analysis of **P7_{PE}** via **b)** ¹H NMR spectroscopy (additional, broad signal at 7.3 ppm marked in red), **c)** ATR-FT-IR spectroscopy, and the analysis of the block copolymers before and after decarboxylation by **d)** DLS. 54
- Figure 12:** **a)** Photochemical decarboxylation of PAP-*b*-POEGMEA (**P8**) with tributyltin hydride and the analysis of **P8_{PE}** via **b)** ¹H NMR spectroscopy, **c)** ATR-FT-IR spectroscopy, **d)** DLS and **e)** DSC revealing $T_m = 92$ °C and $T_c = 54$ °C. 56
- Figure 13:** **a)** Thermal decarboxylation of **P9** with tributyltin hydride and the analysis of **P9_{PE}** via **b)** ¹H NMR spectroscopy, **c)** ATR-FT-IR spectroscopy, **d)** DLS, and **e)** DSC, which did not reveal a melting or crystallization of the material. 58
- Figure 14:** Comparison of the ¹H NMR spectra of **P10** (top) and **P10_{PE}** (bottom). The removal of the aromatic proton signal is marked in red, while the arising signal of PE is marked in black. 60
- Figure 15:** Comparison of the ¹H NMR spectra of **P10** (top) and **P10_{PE}** (bottom). The removal of the δ_{oop} C-H vibration is marked in red, while the arising signal of the C-H vibration of PE is marked in black. 60
- Figure 16:** **a)** Structure of the macroRAFT-agent BTTP-mPEG₁₀₀₀ and the ¹H NMR spectra of **b)** BTTP and **c)** BTTP-mPEG₁₀₀₀. 67
- Figure 17:** **a)** Structure of the precursor polymer PAP-*b*-PEG and **b)** the SEC chromatograms of the three different polymers **DP1-3** in DMAc as eluent and PMMA calibration and **c)** overview of the molar masses of the precursor polymers. 68
- Figure 18:** **a)** Comparison of the ¹H NMR spectra of **DP2** before (top) and after (**DP2_{PE}**, bottom) the decarboxylation. **b)** ¹H NMR spectrum of **DP1_{PE}**. **c)** ¹H NMR spectrum of **DP3_{PE}**. 70
- Figure 19:** **a)** ATR-FT-IR spectra of the **DP2** precursor (top, black), after decarboxylation (**DP2_{PE}**, middle, grey) and after cleavage (**PE2**, bottom, light grey). **b)** DSC chromatogram of **PE2** obtained after decarboxylation and cleavage of **DP2**. 72
- Figure 20:** ¹H NMR spectra of PE-*b*-PEG (**DP2_{PE}**) after photochemically-induced decarboxylation with **a)** reduced equivalents of phenylsilane, **b)** reduced concentration with respect to the polymer, **c)** additional *i*-PrOH and **d)** reduced concentration and additional *i*-PrOH. Solvent: DCM-*d*₂. 74
- Figure 21:** **a)** Decarboxylation of PAP-*b*-PEG under optimized conditions followed by cleavage with ethylenediamine. **b)** ¹H NMR spectrum of **DP3_{PE}** after decarboxylation with Bu₃SnH, solvent: DCM-*d*₂. **c)** HT-¹H NMR spectrum of **PE3** derived from **DP3_{PE}** after

List of Schemes, Figures, and Tables

cleavage with ethylenediamine, solvent: TCE- d_2 and d) HT- ^{13}C NMR spectrum of PE3 derived from DP3 after cleavage with ethylenediamine, solvent: TCE- d_2	75
Figure 22: a) Comparison of the ATR-FT-IR spectra of DP3_{PE} before (top, black) and PE3 after (bottom, grey) cleavage with ethylenediamine at room temperature. Analysis of PE3 by b) DSC and c) HT-SEC in 1,2,4-TCB at 160 °C.	76
Figure 23: a) Formation of ethylene thiourea (ETU) from ethylenediamine in the presence of a trithiocarbonate like BTTP. b) ^1H NMR spectrum of PE- <i>b</i> -PEG (DP2_{PE}), solvent: DCM- d_2 . Analysis of PE2 via c) HT- ^1H NMR spectroscopy, benzyl end group and ETU marked, solvent: TCE- d_2 and d) HT- ^{13}C NMR spectroscopy, solvent: TCE- d_2 . e) ATR-FT-IR spectrum and f) DSC chromatogram of PE2	78
Figure 24: a) ^1H NMR spectrum of PE- <i>b</i> -PEG (DP1), solvent: DCM- d_2 . Analysis of PE1 via b) HT- ^1H NMR spectroscopy, benzyl end group and ETU marked, solvent: TCE- d_2 , c) HT- ^{13}C NMR spectroscopy, solvent: TCE- d_2 , d) ATR-FT-IR spectroscopy, e) HT-SEC in 1,2,4-TCB at 160 °C and f) DSC.....	79
Figure 25: a) ^1H NMR spectrum of DP4_{PE} after thermally-induced decarboxylation of DP4 with phenylsilane and b) analysis via ATR-FT-IR spectroscopy of DP4 (top, black), DP4_{PE} (middle, grey) and PE4 (bottom, light grey).....	81
Figure 26: a) ^1H NMR spectrum of DP4_{PE} after thermally-induced decarboxylation with Bu_3SnH and the corresponding b) comparison of the ATR-FT-IR spectra of DP4_{PE} and PE4	82
Figure 27: DSC analysis of the different approaches for the cleavage of DP2_{PE} with ethylenediamine: a) Cleavage in DMF at 80 °C, b) cleavage in DMF at 80 °C, after direct addition of ethylenediamine to the decarboxylation mixture (one-pot two-step procedure, c) cleavage in 1,2,4-TCB at 80 °C and d) cleavage of PE- <i>b</i> -PEG with LiAlH_4	83
Figure 28: a) Comparison of the ^1H NMR spectra of PAP (FP1) (top, black) and after the Michael-type addition of MEA (FP1-MEA , bottom, blue); solvent: DCM- d_2 . b) SEC chromatogram of FP1 (black) and FP1-MEA (blue). c) Comparison of the ATR-FT-IR spectra of FP1 (top, black) and FP1-MEA (bottom, blue).	88
Figure 29: Analysis of FP1-MA via a) ^1H NMR spectroscopy and b) ATR-FT-IR spectroscopy.	89
Figure 30: Analysis of FP1-MVK via a) ^1H NMR spectroscopy and b) ATR-FT-IR spectroscopy.	90

List of Schemes, Figures, and Tables

- Figure 31:** **a)** Side chain polymerization of styrene on **FP1** in the absence of DIPEA and formation of a cross-linked polymer (**FP1-CL**). **b)** Comparison of ATR-FT-IR spectra of **FP1** (PAP) (top, black) with **FP1-CL** (bottom, blue). 91
- Figure 32:** ¹H NMR spectra of **a)** the decarboxylative thiolation of **FP2** with 4-methoxythiobenzamide and **b)** the following functionalization in a one-pot two-step process with bis-(4-methoxyphenyl)disulfide. 94
- Figure 33:** **a)** Decarboxylative thiolation with Eosin Y as the catalyst as used by Cao *et al.*¹³⁴ and **b)** the comparison of the ¹H NMR spectra of the first step (top) and the second step (bottom) of the reaction. 95
- Figure 34:** **a)** ¹H NMR spectrum of **PTEMVPO** after decarboxylation of PAP with TEMPO-OH; solvent: DMSO-*d*₆. **b)** Comparison of ATR-FT-IR spectra of **FP1** (top, black) and **PTEMVPO** (bottom, red). **c)** ¹H NMR spectrum of **PTEMVP** after decarboxylation of PAP with TEMPO; solvent: DCM-*d*₂. **d)** SEC chromatogram of **PTEMVP** and precursor **FP1** in DMAC as eluent with PMMA calibration. 97
- Figure 35:** **a)** ¹H NMR spectrum of **PTEMVP-*b*-POEGMEA** after decarboxylation of PAP-*b*-POEGMEA (**FP2**) with TEMPO; solvent: DCM-*d*₂. **b)** Comparison of ATR-FT-IR spectra of **FP2** (top, black) and **PTEMVP-*b*-POEGMEA** (bottom, red). **c)** ¹H NMR spectrum of **PTEMVPO-*b*-POEGMEA** after decarboxylation with TEMPO-OH; solvent: DMSO-*d*₆. **d)** SEC chromatogram of **PTEMVPO-*b*-POEGMEA** and precursor **FP2** with DMAc as eluent and PMMA calibration. 99
- Figure 36:** ¹H NMR spectra of the decarboxylation of PAP with TEMPO-OH and PhSiH₃ as H-donor. 102
- Figure 37:** ¹H NMR spectrum of the decarboxylation of PAP with Bu₃SnH in the first step followed by decarboxylative functionalization with TEMPO in a second step with reduced equivalents of HE. 104
- Figure 38:** ¹H NMR spectra of the decarboxylation product **a)** after the first decarboxylation with Bu₃SnH as H-donor, 0.50 eq. HE and 15 min reaction time and **b)** after the second decarboxylation with TEMPO-OH. 105
- Figure 39:** Comparison of the ATR-FT-IR spectra of the product after reduction of **PTEMVP** with Zn/AcOH in DMF (top, green) and of commercial PVA (black, bottom, Mowiol® 28-29, *M*_w ~ 145.000 g mol⁻¹, Sigma-Aldrich). 106
- Figure 40:** ¹H NMR spectra of reduction of **a)** **PTEMVP-*b*-POEGMEA** in DMF at 60 °C with Zn/AcOH (**Table 5**, entry #2) and **b)** **PTEMVPO-*b*-POEGMEA** in DMF at 80 °C with Zn/AcOH (**Table 5**, entry #5). 109

List of Schemes, Figures, and Tables

Figure 41: ^1H NMR spectra of the reduction of a) PTEMVP- <i>b</i> -POEGMEA in THF/H ₂ O at 60 °C with Zn/AcOH followed by dialysis (Table 5, entry #6) and b) PTEMVPO in MeOH/THF/H ₂ O at room temperature with Zn (Table 5, entry #9).	110
Figure 42: a) ^1H NMR spectrum of poly(ethylene- <i>graft</i> -styrene)- <i>b</i> -POEGMEA. b) Comparison of the ATR-FT-IR spectra of PTEMVPO- <i>b</i> -POEGMEA (top, red) and poly(ethylene- <i>graft</i> -styrene)- <i>b</i> -POEGMEA (bottom, orange) and c) comparison of the SEC chromatogram before (red) and after grafting of styrene (orange) in DMAc as eluent and PMMA calibration.....	112
Figure 43: a) Synthesis of <i>N</i> -(methacryloyloxy)phthalimide (MAP) <i>via</i> Steglich esterification and analysis of the monomer by b) ^1H NMR spectroscopy and c) ^{13}C NMR spectroscopy in DCM- <i>d</i> ₂ as solvent.	115
Figure 44: a) Structure of PMAP- <i>b</i> -POEGMEMA (PP1) polymerized by RAFT polymerization with 4-cyano-4-((phenylcarbonothioyl)thio)pentanoic acid (CTP). b) SEC chromatogram of PMAP (grey, dashed) and PMAP- <i>b</i> -POEGMEMA (PP1 , black) in DMAc as eluent with PMMA calibration. c) Structure of PMAP- <i>b</i> -PMEMA (PP2) and d) SEC chromatogram of PMAP (grey, dashed) and PMAP- <i>b</i> -PMEMA (PP2 , black) in DMAc as eluent with PMMA calibration	116
Figure 45: a) Decarboxylation of PP1 with Ru(bpy) ₃ Cl ₂ · 6 H ₂ O, HE and Bu ₃ SnH in DMF as solvent and b) the analysis of the resulting product <i>via</i> ^1H NMR spectroscopy.....	117
Figure 46: a) Decarboxylation of PP1 with Ru(bpy) ₃ Cl ₂ · 6 H ₂ O, DIPEA as reductant, and Bu ₃ SnH as H-donor in DMF as solvent and b) decarboxylation of PP1 with Ru(bpy) ₃ Cl ₂ · 6 H ₂ O and DIPEA as reductant and H-donor in DMF as solvent as well as the corresponding analyses <i>via</i> c)/d) ^1H NMR spectroscopy.....	119
Figure 47: a) Decarboxylation of PP1 with Ru(bpy) ₃ Cl ₂ · 6 H ₂ O, DIPEA and Bu ₃ SnH in DCM as solvent and b) the analysis <i>via</i> ^1H NMR spectroscopy and c) the comparison of the ATR-FT-IR spectra before (top, red) and after (bottom, black) decarboxylation. d) Decarboxylation of PMAP- <i>b</i> -POEGMEMA (PP1) with Ru(bpy) ₃ Cl ₂ · 6 H ₂ O, DIPEA in DMF/H ₂ O (20:1) and the analysis <i>via</i> e) ^1H NMR and f) ATR-FT-IR spectroscopy.	121
Figure 48: a) Thermal decarboxylation of PP1 with NiCl ₂ · 6 H ₂ O, bbbpy, Zn and Bu ₃ SnH as H-donor in DMF and b) the analysis <i>via</i> ^1H NMR spectroscopy.	124
Figure 49: a) Thermal decarboxylation of PP1 with NiCl ₂ · 6 H ₂ O, bbbpy and Zn in DMF/H ₂ O (20:1) and b) the analysis <i>via</i> ^1H NMR spectroscopy.	125
Figure 50: a) Decarboxylation of PP2 with Ru(bpy) ₃ Cl ₂ · 6 H ₂ O, DIPEA and Bu ₃ SnH as H-donor in DMF and the analysis of PP2PP <i>via</i> b) ^1H NMR and c) ATR-FT-IR spectroscopy.	125

List of Schemes, Figures, and Tables

Figure 51: Photos of the LED setup used for photochemical reaction. a) Avonec 3 W high power LEDs on a star plate. b) LEDs with Schlenk tube used for the decarboxylation, placed in a distance of 1.5 cm around the tube. c) Schlenk tube with LEDs turned on. d) Final reaction setup with custom-build protection ensuring the removal of the heat produced by the LEDs.	133
Figure 52: ^1H NMR spectrum of PAP (P1). Solvent $\text{DCM-}d_2$	211
Figure 53: ^1H NMR spectrum of P1 _{PE} after thermally-induced decarboxylation. Solvent: 50:50 mixture of $\text{DMF-}d_7$ and $\text{DMSO-}d_6$	211
Figure 54: ^1H NMR spectrum of P1 _{PE} after photochemically-induced decarboxylation. Solvent: $\text{DMSO-}d_6$	212
Figure 55: ^1H NMR spectrum of PAP (P1) after thermally-induced decarboxylation with tributyltin hydride in $\text{DMF}/1,2,4\text{-TCB}$ (1:1) at 120 °C. Solvent: $\text{DMSO-}d_6$, $\text{DMF-}d_7$	212
Figure 56: Thermogravimetical analysis of P5 , heating rate 10 K min ⁻¹	213
Figure 57: Thermogravimetical analysis of P5 _{PE} in comparison to P5 , heating rate 10 K min ⁻¹	213
Figure 58: DSC characterization of P5 , heating rate 10 K min ⁻¹	214
Figure 59: DLS analysis of P5 and P5 _{PE} after thermally-induced decarboxylation with phenylsilane.....	214
Figure 60: DLS analysis of P5 and P5 _{PE} after photochemically-induced decarboxylation with phenylsilane.....	215
Figure 61: Thermogravimetical analysis of P6 , heating rate 10 K min ⁻¹	215
Figure 62: Thermogravimetical analysis of P6 _{PE} in comparison to P6 , heating rate 10 K min ⁻¹	216
Figure 63: Thermogravimetical analysis of P7 _{PE} in comparison to P7 , heating rate 10 K min ⁻¹	216
Figure 64: Reaction monitoring of photochemically-induced decarboxylation of PAP- <i>b</i> -POEGMEA (P10). Solvent: CDCl_3	217
Figure 65: Reaction monitoring of thermally-induced decarboxylation of PAP- <i>b</i> -POEGMEA (P11). Solvent: CDCl_3	218
Figure 66: Thermogravimetical analysis of P10 _{PE} in comparison to P10 , heating rate 10 K min ⁻¹	219
Figure 67: ^1H NMR spectrum of P11 _{PE} (<i>PE-b</i> -PMEA) after thermal decarboxylation. Solvent: $\text{DCM-}d_2$	219
Figure 68: ATR-FT-IR spectrum of P11 _{PE} (<i>PE-b</i> -PMEA) after thermal decarboxylation...	220

List of Schemes, Figures, and Tables

Figure 69: SEC chromatogram of PAP-BTTP-mPEG ₂₀₀₀ in DMAc as eluent with PMMA calibration.....	221
Figure 70: ¹ H NMR spectrum (raw spectrum) of DP2_{PE} after decarboxylation under standard conditions (1.50 eq. phenylsilane). The integrals of relevant signals at 3.25 ppm, 3.51 ppm, and 7.35 ppm for the calculation of the improvement of the decarboxylation result are marked.	221
Figure 71: ¹ H NMR of DP2_{PE} after decarboxylation with reduced equivalents of phenylsilane. Integrals of relevant signals at 3.25 ppm, 3.51 ppm, and 7.35 ppm for the calculation of the improvement of the decarboxylation result are marked.	222
Figure 72: ¹ H NMR of DP2_{PE} after decarboxylation with reduced concentration. Integrals of relevant signals at 3.25 ppm, 3.51 ppm, and 7.35 ppm for the calculation of the improvement of the decarboxylation result are marked.	222
Figure 73: ¹ H NMR of DP2_{PE} after decarboxylation with additional <i>i</i> -PrOH. Integrals of relevant signals at 3.25 ppm, 3.51 ppm, and 7.35 ppm for the calculation of the improvement of the decarboxylation result are marked.	223
Figure 74: ¹ H NMR of DP2_{PE} after decarboxylation with reduced concentration and additional <i>i</i> -PrOH. Integrals of relevant signals at 3.25 ppm, 3.51 ppm, and 7.35 ppm for the calculation of the improvement of the decarboxylation result are marked.....	223
Figure 75: ATR-FT-IR spectrum of commercial PE (Polyethylene, Sigma Aldrich, average $M_n = 7700 \text{ g mol}^{-1}$, 427799-250G).	224
Figure 76: DSC analysis of commercial PE (Polyethylene, Sigma Aldrich, average $M_n = 7700 \text{ g mol}^{-1}$, 427799-250G).	224
Figure 77: ¹ H NMR spectrum of FP1 after decarboxylation in the presence of bis-(4-methoxyphenyl)disulphide. Solvent: DCM- <i>d</i> ₂	225
Figure 78: ¹ H NMR spectrum of poly(ethylene- <i>co</i> -TEMVPO) after decarboxylation with Bu ₃ SnH and TEMPO-OH. Solvent: DMSO- <i>d</i> ₆	225
Figure 79: ¹ H NMR spectrum of PTEMVPO-<i>b</i>-POEGMEA after reduction with Zn/AcOH in DMF at 60 °C; solvent: DMSO- <i>d</i> ₆	226
Figure 80: ¹ H NMR spectrum of PTEMVPO-<i>b</i>-POEGMEA after reduction with Zn/AcOH in DMF at 60 °C; solvent: DMSO- <i>d</i> ₆	226
Figure 81: SEC chromatogram of PMAP (grey, dashed) and PMAP- <i>b</i> -POEGMEMA (black) polymerized with BPTT as RAFT agent in DMAc as eluent with PMMA calibration.	227
Figure 82: ¹ H NMR spectrum of DPP1 . Solvent: DCM- <i>d</i> ₂	227
Figure 83: SEC chromatogram of DPP1 in DMAc as eluent and PMMA calibration.	228

List of Schemes, Figures, and Tables

Figure 84: ^1H NMR spectrum PP1_{PE} after decarboxylation with $\text{Ru}(\text{bpy})_3\text{Cl}_2$, HE and 10 eq. of Bu_3SnH . Solvent: $\text{DCM-}d_2$	228
Figure 85: ^1H NMR spectrum of PP1_{PE} after decarboxylation with $\text{Ru}(\text{bpy})_3\text{Cl}_2$ and HE as reductant and H-donor. Solvent: $\text{DCM-}d_2$	229
Figure 86: ^1H NMR spectrum of PP1_{PE} after decarboxylation with HE as catalyst and Bu_3SnH as H-donor. Solvent: $\text{DMSO-}d_6$	229
Figure 87: ^1H NMR spectrum of PP1_{PE} after decarboxylation with Eosin Y as catalyst and DIPEA as H-donor. Solvent: $\text{DCM-}d_2$	230
Figure 88: ^1H NMR spectrum of PP1_{PE} after decarboxylation with $\text{Ru}(\text{bpy})_3\text{Cl}_2 \cdot 6 \text{H}_2\text{O}$, DIPEA and PhSiH_3 as H-donor. Solvent: $\text{DMSO-}d_6$	230
Figure 89: ^1H NMR spectrum of PP1_{PE} after decarboxylation with $\text{Ru}(\text{bpy})_3\text{Cl}_2 \cdot 6 \text{H}_2\text{O}$, BNAH as reductant and Bu_3SnH as H-donor. Solvent: $\text{DMSO-}d_6$	231

8.3 List of Tables

Table 1: Overview of the synthesis of different PAP polymers.	38
Table 2: Summary of block copolymers synthesized and their calculated and theoretical molar masses as well as dispersity.	44
Table 3: Variation of the reaction parameters of the decarboxylation reactions with PAP- <i>b</i> -PEG.	73
Table 4: Overview of different reaction conditions used for the synthesis of poly(ethylene- <i>co</i> -TEMVP).	101
Table 5: Variation of the reaction conditions for the reduction of PTEMVP / PTEMVPO homopolymers and block copolymers.	108
Table 6: Variation of the reaction conditions of the decarboxylation of PP1	123
Table 7: Overview of PAP homopolymers P1 – P3	136
Table 8: Experimental details of the synthesis of P1	137
Table 9: Experimental details of the synthesis of P2	137
Table 10: Experimental details of the synthesis of P3	137
Table 11: Overview of block copolymers P5 - P9	140
Table 12: Experimental details of the synthesis of P5	140
Table 13: Experimental details of the synthesis of P6/P7	140
Table 14: Experimental details of the synthesis of P8/P9	141
Table 15: Experimental details of the synthesis of P10/P11	142
Table 16: Experimental details of the synthesis of DP1/DP4	148
Table 17: Experimental details of the synthesis of DP2	148
Table 18: Experimental details of the synthesis of DP3	148
Table 19: Analysis results of FP1 by SEC in DMAc as eluent with PMMA calibration and ¹ H NMR spectroscopy.	154
Table 20: Analysis results of FP2 by SEC in DMAc as eluent with PMMA calibration and ¹ H NMR spectroscopy.	155
Table 21: Analysis results of PP1 by SEC in DMAc as eluent with PMMA calibration and ¹ H NMR spectroscopy.	169
Table 22: Analysis results of PP2 by SEC in DMAc as eluent with PMMA calibration and ¹ H NMR spectroscopy.	170

9 Danksagung

An dieser Stelle möchte ich allen danken, die mich während der Promotion und auf dem Weg dorthin begleitet haben.

Mein großer Dank gilt vor allem Prof. Dr. Patrick Théato. Danke, dass du mir die Möglichkeit gegeben hast meine Promotion bei dir durchzuführen und dass du mir alle Freiheiten gewährt hast diese Arbeit umzusetzen.

Des Weiteren möchte ich mich bei Prof. Dr. Christoph Weder bedanken, der mich im Rahmen meines Auslandsforschungsaufenthalts in seine Gruppe aufgenommen und mir diesen damit ermöglicht hat. Ich bin sehr dankbar, 3 Monate am AMI gearbeitet zu haben. Dieser Aufenthalt hat mich sowohl persönlich als auch wissenschaftlich sehr bereichert. Diesbezüglich möchte ich auch allen Mitgliedern des Bereichs Polymer Chemistry & Materials des AMIs für die umfassende Unterstützung, Offenheit und tolle Arbeitsatmosphäre danken. Hierbei möchte ich vor allem auch Stephen Schrettl danken, der immer eine offene Tür für wissenschaftlichen Austausch hatte. Ferner gilt mein Dank besonders Livius Muff, Derek Kiebala, James „Jimmy“ Hemmer und Chris Rader sowie Franziska Marx für die umfassende Unterstützung während meines Aufenthalts.

An dieser Stelle möchte ich mich auch beim Karlsruhe House of Young Scientist (KHYS) für die Förderung meines Auslandsaufenthalts bedanken. Ich bin sehr dankbar für die Unterstützung, mittels derer ich diese wertvolle Erfahrung erleben konnte.

Ein großes Dankeschön gilt außerdem Katharina Elies. Danke für deine nette Art und deine unendliche Hilfsbereitschaft und Unterstützung.

Ein weiteres Dankeschön möchte ich an Dr. Dominik Voll aussprechen. Danke für die umfassende organisatorische Unterstützung.

Auch möchte ich mich bei Bärbel Seufert-Dausmann und Martina Ritter für die bürokratische und organisatorische Unterstützung bedanken.

Mein großer Dank gilt außerdem meinen beiden Freunden und Coautoren Andreas Butzelaar und Edgar Molle. Danke, dass die letzten drei Jahre im Labor so grandios und lustig waren. Vielen Dank natürlich auch für die Korrektur dieser Arbeit.

Des Weiteren möchte ich mich bei Martin „Goethe“ Gauthier-Jaques, Sergej Baraban, Sven Schneider und Nico Zuber für die lustige Gemeinschaft bedanken.

Ein weiteres Dankeschön geht an meinen Studenten Cornelius Hub.

Natürlich möchte ich mich auch bei allen Mitgliedern des AK Théato für die Zusammenarbeit bedanken.

Nicht vergessen möchte ich natürlich auch die „Freunde der Chemie“: Stefan, Lea, Maxi, Michelle, Peter, Antoine und Stephanie.

Des Weiteren gilt mein großer Dank meinem langjährigen Freund Tobias Schiestel, für die vielen interessanten Gespräche, lustigen Weinfeste und natürlich die Korrektur dieser Arbeit. Daneben möchte ich auch meinen langjährigen Freunden Frederick „Freddy“ Luft und Benedikt Kielwein danken.

Des Weiteren möchte ich noch Claudia danken, die während meiner gesamten Promotion immer an meiner Seite standst. Danke, dass du immer für mich da warst.

Zu guter Letzt und damit an wichtigster Stelle möchte ich mich bei meinen Eltern, denen diese Arbeit gewidmet ist, danken. Danke für all die Unterstützung die ich durch euch erfahren habe, ihr habt diese Arbeit und den Doktor erst möglich gemacht. Danke Papa, dass Du mir damals schon die Welt erklärt und die hohe Bedeutung einer guten Ausbildung gezeigt und mir damit alle Türen geöffnet hast. Danke Mama, dass du mich in allem organisatorischem unterstützt hast und für deine liebevolle Fürsorge. Danke, dass ich mich immer auf euch verlassen kann. Im Zuge dessen möchte ich mich noch bei meinem Bruder Thomas für die Unterstützung bedanken.

10 References

- (1) Plastics Europe. *Plastics - The Facts 2021*. <https://plasticseurope.org/knowledge-hub/plastics-the-facts-2021/> **2021** (accessed 2022-03-03).
- (2) Jeremic, D. Polyethylene **2014**, 1–42. DOI: 10.1002/14356007.a21_487.pub3.
- (3) v. Pechmann, H. Ueber Diazomethan und Nitrosoacylamine. *Ber. Dtsch. Chem. Ges.* **1898**, *31* (3), 2640–2646. DOI: 10.1002/cber.18980310314.
- (4) Ronca, S. Polyethylene. *Brydson's Plastic Materials* **2017**, 247–278. DOI: 10.1016/B978-0-323-35824-8.00010-4.
- (5) Fawcett, E. W.; Gibson, R. O.; Perrin, M. W.; Paton, J. G.; Williams, E. G.; ICI LTD. Improvements in or relating to the polymerisation of ethylene. **1936**, GB471590A.
- (6) Böhm, L. L. Die Ethylenpolymerisation mit Ziegler-Katalysatoren 50 Jahre nach der Entdeckung. *Angew. Chem.* **2003**, *115* (41), 5162–5183. DOI: 10.1002/ange.200300580.
- (7) Sinn, H.; Kaminsky, W. Ziegler-Natta Catalysis **2008**, *18*, 99–149. DOI: 10.1016/S0065-3055(08)60307-X.
- (8) Liu, T. M.; Baker, W. E. The effect of the length of the short chain branch on the impact properties of linear low density polyethylene. *Polymer Engineering & Science* **1992**, *32* (14), 944–955. DOI: 10.1002/pen.760321406.
- (9) Kurtz, S. M. The UHMWPE handbook: ultra-high molecular weight polyethylene in total joint replacement. *Elsevier* **2004**.
- (10) McKellop, H.; Shen, F. - w.; Lu, B.; Campbell, P.; Salovey, R. Development of an extremely wear-resistant ultra high molecular weight polyethylene for total hip replacements. *Journal of Orthopaedic Research* **1999**, *17* (2), 157–167. DOI: 10.1002/jor.1100170203.
- (11) Dommanget, C.; D'Agosto, F.; Monteil, V. Polymerization of ethylene through reversible addition-fragmentation chain transfer (RAFT). *Angewandte Chemie (International ed. in English)* **2014**, *53* (26), 6683–6686. DOI: 10.1002/anie.201403491.

(12) Haifeng Gao; Krzysztof Matyjaszewski. Synthesis of functional polymers with controlled architecture by CRP of monomers in the presence of cross-linkers: From stars to gels. *Progress in Polymer Science* **2009**, *34* (4), 317–350. DOI: 10.1016/j.progpolymsci.2009.01.001.

(13) Matyjaszewski, K.; Tsarevsky, N. V. Nanostructured functional materials prepared by atom transfer radical polymerization. *Nature chemistry* **2009**, *1* (4), 276–288. DOI: 10.1038/nchem.257.

(14) Blasco, E.; Sims, M. B.; Goldmann, A. S.; Sumerlin, B. S.; Barner-Kowollik, C. 50th Anniversary Perspective: Polymer Functionalization. *Macromolecules* **2017**, *50* (14), 5215–5252. DOI: 10.1021/acs.macromol.7b00465.

(15) Chen, Q.-B.; Zeng, T.-Y.; Xia, L.; Zhang, Z.; Hong, C.-Y.; Zou, G.; You, Y.-Z. A RAFT/MADIX method finely regulating the copolymerization of ethylene and polar vinyl monomers under mild conditions. *Chemical Communications* **2017**, *53* (78), 10780–10783. DOI: 10.1039/C7CC06341E.

(16) Demarteau, J.; Scholten, P. B. V.; Kermagoret, A.; Winter, J. de; Meier, M. A. R.; Monteil, V.; Debuigne, A.; Detrembleur, C. Functional polyethylene (PE) and PE-based block copolymers by organometallic-mediated radical polymerization. *Macromolecules* **2019**, *52* (22), 9053–9063. DOI: 10.1021/acs.macromol.9b01741.

(17) Kermagoret, A.; Debuigne, A.; Jérôme, C.; Detrembleur, C. Precision design of ethylene- and polar-monomer-based copolymers by organometallic-mediated radical polymerization. *Nature chemistry* **2014**, *6* (3), 179–187. DOI: 10.1038/nchem.1850.

(18) Scholten, P. B. V.; Cartigny, G.; Grignard, B.; Debuigne, A.; Cramail, H.; Meier, M. A. R.; Detrembleur, C. Functional Polyethylenes by Organometallic-Mediated Radical Polymerization of Biobased Carbonates. *ACS Macro Letters* **2021**, *10* (3), 313–320. DOI: 10.1021/acsmacrolett.1c00037.

(19) Aggarwal, S. L.; Sweeting, O. J. Polyethylene: preparation, structure, and properties. *Chemical Reviews* **1957**, *57* (4), 665–742. DOI: 10.1021/cr50016a004.

(20) Fan, Z.-q.; Zhang, Y.-q.; Xu, J.-t.; Wang, H.-t.; Feng, L.-x. Structure and properties of polypropylene/poly (ethylene-co-propylene) in-situ blends synthesized by spherical Ziegler–Natta catalyst. *Polymer* **2001**, *42* (13), 5559–5566. DOI: 10.1016/S0032-3861(01)00062-3.

References

- (21) Chen, M.; Chen, C. A Versatile Ligand Platform for Palladium - and Nickel - Catalyzed Ethylene Copolymerization with Polar Monomers. *Angewandte Chemie International Edition* **2018**, *57* (12), 3094–3098. DOI: 10.1002/anie.201711753.
- (22) Luo, Y.; Baldamus, J.; Hou, Z. Scandium half-metallocene-catalyzed syndiospecific styrene polymerization and styrene– ethylene copolymerization: Unprecedented incorporation of syndiotactic styrene-styrene sequences in styrene-ethylene copolymers. *Journal of the American Chemical Society* **2004**, *126* (43), 13910–13911. DOI: 10.1021/ja046063p.
- (23) Boasen, N. K.; Hillmyer, M. A. Post-polymerization functionalization of polyolefins. *Chemical Society Reviews* **2005**, *34* (3), 267–275. DOI: 10.1039/B311405H.
- (24) Braun, D. Origins and development of initiation of free radical polymerization processes. *International Journal of Polymer Science* **2009**. DOI: 10.1155/2009/893234.
- (25) Berthelot, M.; Deville, H. E. S.-C.; Luynes, V. d.'A. de. *Lecons de Chimie Professées en 1864 et 1865*; Librairie Hachette, **1866**.
- (26) Hermann Staudinger. Ueber Polymerisation. *Berichte Der Deutschen Chemischen Gesellschaft* **1920** (53(6)), 1073–1085. DOI: 10.1002/cber.19200530627.
- (27) Staudinger, H.; Kohlschütter, H. W. Über hochpolymere Verbindungen, 55. Mitteil.: Über Poly-acrylsäure. *Berichte der deutschen chemischen Gesellschaft (A and B Series)* **1931**, *64* (8), 2091–2098. DOI: 10.1002/cber.19310640835.
- (28) Nesvadba, P. Radical Polymerization in Industry. In *Encyclopedia of Radicals in Chemistry, Biology and Materials*; John Wiley & Sons, Ltd, **2012**. DOI: 10.1002/9781119953678.rad080.
- (29) Lechner, M. D.; Gehrke, K.; Nordmeier, E. H. *Makromolekulare Chemie*; Springer, **2003**.
- (30) David H. Solomon, Ezio Rizzardo, Paul Cacioli. Polymerization process and polymers produced thereby. **1984**, US4581429A.
- (31) Moad, G.; Rizzardo, E. Alkoxyamine-initiated living radical polymerization: Factors affecting alkoxyamine homolysis rates. *Macromolecules* **1995**, *28* (26), 8722–8728. DOI: 10.1021/ma00130a003.

- (32) Hawker, C. J. Molecular weight control by a "living" free-radical polymerization process. *Journal of the American Chemical Society* **1994**, *116* (24), 11185–11186. DOI: 10.1021/ja00103a055.
- (33) Chong, Y. K.; Ercole, F.; Moad, G.; Rizzardo, E.; Thang, S. H.; Anderson, A. G. Imidazolidinone nitroxide-mediated polymerization. *Macromolecules* **1999**, *32* (21), 6895–6903. DOI: 10.1021/ma9904868.
- (34) Malmström, E.; Miller, R. D.; Hawker, C. J. Development of a new class of rate-accelerating additives for nitroxide-mediated 'living' free radical polymerization. *Tetrahedron* **1997**, *53* (45), 15225–15236. DOI: 10.1016/S0040-4020(97)00959-9.
- (35) Coiai, S.; Passaglia, E.; Cicogna, F. Post-polymerization modification by nitroxide radical coupling. *Polymer International* **2019**, *68* (1), 27–63. DOI: 10.1002/pi.5664.
- (36) Ciftci, M.; Arslan, M.; Buchmeiser, M.; Yagci, Y. Polyethylene-g-Polystyrene Copolymers by Combination of ROMP, Mn₂(CO)₁₀-Assisted TEMPO Substitution and NMRP. *ACS Macro Letters* **2016**, *5* (8), 946–949. DOI: 10.1021/acsmacrolett.6b00460.
- (37) Marque, S. Influence of the Nitroxide Structure on the Homolysis Rate Constant of Alkoxyamines: A Taft–Ingold Analysis. *The Journal of organic chemistry* **2003**, *68* (20), 7582–7590. DOI: 10.1021/jo030036k.
- (38) Marque, S.; Fischer, H.; Baier, E.; Studer, A. Factors Influencing the C–O Bond Homolysis of Alkoxyamines: Effects of H– Bonding and Polar Substituents. *The Journal of organic chemistry* **2001**, *66* (4), 1146–1156. DOI: 10.1021/jo001190z.
- (39) Marque, S.; Le Mercier, C.; Tordo, P.; Fischer, H. Factors influencing the C–O– bond homolysis of trialkylhydroxylamines. *Macromolecules* **2000**, *33* (12), 4403–4410. DOI: 10.1021/ma9918452.
- (40) Tebben, L.; Studer, A. Nitroxides: applications in synthesis and in polymer chemistry. *Angewandte Chemie International Edition* **2011**, *50* (22), 5034–5068. DOI: 10.1002/anie.201002547.
- (41) Hawker, C. J.; Barclay, G. G.; Orellana, A.; Dao, J.; Devonport, W. Initiating systems for nitroxide-mediated "living" free radical polymerizations: synthesis and evaluation. *Macromolecules* **1996**, *29* (16), 5245–5254. DOI: 10.1021/ma951905d.

References

- (42) YK, C. J. C.; Ercole, F.; Krstina, J.; Jeffery, J.; Le, T.; Mayadunne, R. T. A.; Meijs, G.; Moad, C. L.; Moad, G.; Rizzardo, E.; Thang, S. H. Living free-radical polymerization by reversible addition– fragmentation chain transfer: the RAFT process. *Macromolecules* **1998**, *31* (16), 5559–5562. DOI: 10.1021/ma9804951.
- (43) Mayadunne, R. T. A.; Jeffery, J.; Moad, G.; Rizzardo, E. Living free radical polymerization with reversible addition– fragmentation chain transfer (raft polymerization): Approaches to star polymers. *Macromolecules* **2003**, *36* (5), 1505–1513. DOI: 10.1021/ma021219w.
- (44) Moad, G.; Rizzardo, E.; Thang, S. H. End - functional polymers, thiocarbonylthio group removal/transformation and reversible addition - fragmentation - chain transfer (RAFT) polymerization. *Polymer International* **2011**, *60* (1), 9–25. DOI: 10.1002/pi.2988.
- (45) Moad, G.; Chong, Y. K.; Postma, A.; Rizzardo, E.; Thang, S. H. Advances in RAFT polymerization: the synthesis of polymers with defined end-groups. *Polymer* **2005**, *46* (19), 8458–8468. DOI: 10.1016/j.polymer.2004.12.061.
- (46) Perrier, S. 50th Anniversary Perspective: RAFT Polymerization - A User Guide. *Macromolecules* **2017**, *50* (19), 7433–7447. DOI: 10.1021/acs.macromol.7b00767.
- (47) Jeremic, D. Polyethylene. *Ullmann's encyclopedia of industrial chemistry* **2000**, 1–42.
- (48) Bamberger, E.; Tschirner, F. Ueber die Einwirkung von Diazomethan auf β - Arylhydroxylamine. *Ber. Dtsch. Chem. Ges.* **1900**, *33* (1), 955–959. DOI: 10.1002/cber.190003301166.
- (49) H. H. Windsor. *Popular Mechanics Magazine*, Volume 92, **1949**.
- (50) McDaniel, M. P. Review of Phillips chromium catalyst for ethylene polymerization. *Handbook of Transition Metal Polymerization Catalysts* **2018**, 401–571.
- (51) Kaiser, W. *Kunststoffchemie für Ingenieure: von der Synthese bis zur Anwendung*; Carl Hanser Verlag GmbH Co KG, **2021**.
- (52) Natta, G. Stereospezifische Katalysen und isotaktische Polymere. *Angewandte Chemie* **1956**, *68* (12), 393–403. DOI: 10.1002/ange.19560681202.

- (53) Kaminsky, W. New polymers by metallocene catalysis. *Macromolecular Chemistry and Physics* **1996**, *197* (12), 3907–3945. DOI: 10.1002/macp.1996.021971201.
- (54) Gilbert, M., Ed. *Brydson's Plastics Materials*, 8th Edition; Elsevier, **2016**.
- (55) Kurtz, S. M.; Gawel, H. A.; Patel, J. D. History and systematic review of wear and osteolysis outcomes for first-generation highly crosslinked polyethylene. *Clinical Orthopaedics and Related Research*® **2011**, *469* (8), 2262–2277. DOI: 10.1007/s11999-011-1872-4.
- (56) Rose, R. M.; Cimino, W. R.; Ellis, E.; an Crugnola. Exploratory investigations on the structure dependence of the wear resistance of polyethylene. *Wear* **1982**, *77* (1), 89–104. DOI: 10.1016/0043-1648(82)90048-5.
- (57) Bergerbit, C.; Baffie, F.; Wolpers, A.; Dugas, P. - Y.; Boyron, O.; Taam, M.; Lansalot, M.; Monteil, V.; D'Agosto, F. Ethylene polymerization-induced self-assembly (PISA) of poly(ethylene oxide)-*block*-polyethylene copolymers via RAFT. *Angew. Chem.* **2020**, *132* (26), 10471–10476. DOI: 10.1002/ange.202001741.
- (58) Wolpers, A.; Baffie, F.; Verrioux, L.; Perrin, L.; Monteil, V.; D'Agosto, F. Iodine-transfer polymerization (ITP) of ethylene and copolymerization with vinyl acetate. *Angewandte Chemie International Edition* **2020**, *59* (43), 19304–19310. DOI: 10.1002/anie.202008872.
- (59) Arriola, D. J.; Carnahan, E. M.; Hustad, P. D.; Kuhlman, R. L.; Wenzel, T. T. Catalytic production of olefin block copolymers via chain shuttling polymerization. *Science* **2006**, *312* (5774), 714–719. DOI: 10.1126/science.1125268.
- (60) Zeng, T.; You, W.; Chen, G.; Nie, X.; Zhang, Z.; Xia, L.; Hong, C.; Chen, C.; You, Y. Degradable PE-Based Copolymer with Controlled Ester Structure Incorporation by Cobalt-Mediated Radical Copolymerization under Mild Condition. *Iscience* **2020**, *23* (3), 100904. DOI: 10.1016/j.isci.2020.100904.
- (61) Kay, C. J.; Goring, P. D.; Burnett, C. A.; Hornby, B.; Lewtas, K.; Morris, S.; Morton, C.; McNally, T.; Theaker, G. W.; Waterson, C. Polyolefin–Polar Block Copolymers from Versatile New Macromonomers. *Journal of the American Chemical Society* **2018**, *140* (42), 13921–13934. DOI: 10.1021/jacs.8b09039.

References

- (62) Dong, J. Y.; Chung, T. C. Synthesis of polyethylene containing a terminal p-methylstyrene group: Metallocene-mediated ethylene polymerization with a consecutive chain transfer reaction to p-methylstyrene and hydrogen. *Macromolecules* **2002**, *35* (5), 1622–1631. DOI: 10.1021/ma011622n.
- (63) Luo, J.; Shea, K. J. Polyhomologation. A living C1 polymerization. *Accounts of chemical research* **2010**, *43* (11), 1420–1433. DOI: 10.1021/ar100062a.
- (64) Shea, K. J.; Walker, J. W.; Zhu, H.; Paz, M.; Greaves, J. Polyhomologation. A living polymethylene synthesis. *Journal of the American Chemical Society* **1997**, *119* (38), 9049–9050. DOI: 10.1021/ja972009f.
- (65) Chapman, R.; Melodia, D.; Qu, J.-B.; Stenzel, M. H. Controlled poly(olefin)s via decarboxylation of poly(acrylic acid). *Polymer Chemistry* **2017**, *8* (43), 6636–6643. DOI: 10.1039/C7PY01466J.
- (66) Garrison, J. B.; Hughes, R. W.; Young, J. B.; Sumerlin, B. S. Photoinduced SET to access olefin-acrylate copolymers. *Polymer Chemistry* **2022**. DOI: 10.1039/D1PY01643A.
- (67) Theato, P.; Klok, H.-A. *Functional polymers by post-polymerization modification: concepts, guidelines and applications*; John Wiley & Sons, **2013**.
- (68) Xue, W.; Mutlu, H.; Theato, P. Post-polymerization modification of polymeric active esters towards TEMPO containing polymers: A systematic study. *European Polymer Journal* **2020**, *130*, 109660. DOI: 10.1016/j.eurpolymj.2020.109660.
- (69) Guise-Richardson, C. Redefining Vulcanization: Charles Goodyear, patents, and industrial control, 1834-1865. *Technology and Culture* **2010**, *51* (2), 357–387.
- (70) Fisher, H. L. Vulcanization of rubber. *Industrial & Engineering Chemistry* **1939**, *31* (11), 1381–1389. DOI: 10.1021/ie50359a015.
- (71) Oesper, R. E. Christian Friedrich Schonbein. Part II. Experimental labors. *Journal of Chemical Education* **1929**, *6* (4), 677. DOI: 10.1021/ed006p677.
- (72) Arslan, M.; Acik, G.; Tasdelen, M. A. The emerging applications of click chemistry reactions in the modification of industrial polymers. *Polymer Chemistry* **2019**, *10* (28), 3806–3821. DOI: 10.1039/C9PY00510B.

- (73) Arslan, M.; Tasdelen, M. A. Click chemistry in macromolecular design: complex architectures from functional polymers. *Chemistry Africa* **2019**, *2* (2), 195–214. DOI: 10.1007/s42250-018-0030-8.
- (74) Binder, W. H.; Sachsenhofer, R. ‘Click’chemistry in polymer and materials science. *Macromolecular Rapid Communications* **2007**, *28* (1), 15–54. DOI: 10.1002/marc.200600625.
- (75) Liang, L.; Astruc, D. The copper(I)-catalyzed alkyne-azide cycloaddition (CuAAC)“click” reaction and its applications. An overview. *Coordination Chemistry Reviews* **2011**, *255* (23-24), 2933–2945. DOI: 10.1016/j.ccr.2011.06.028.
- (76) Lowe, A. B. Thiol-ene “click” reactions and recent applications in polymer and materials synthesis: a first update. *Polymer Chemistry* **2014**, *5* (17), 4820–4870. DOI: 10.1039/C4PY00339J.
- (77) Sobek, J.; Martschke, R.; Fischer, H. Entropy control of the cross-reaction between carbon-centered and nitroxide radicals. *Journal of the American Chemical Society* **2001**, *123* (12), 2849–2857. DOI: 10.1021/ja0036460.
- (78) Fischer, H. The persistent radical effect in controlled radical polymerizations. *J. Polym. Sci. A Polym. Chem.* **1999**, *37* (13), 1885–1901. DOI: 10.1002/(SICI)1099-0518(19990701)37:13<1885:AID-POLA1>3.0.CO;2-1.
- (79) Fischer, H. The persistent radical effect: a principle for selective radical reactions and living radical polymerizations. *Chemical Reviews* **2001**, *101* (12), 3581–3610. DOI: 10.1021/cr990124y.
- (80) Chaudhary, B. I.; Chopin, L.; Klier, J. Nitroxyls for scorch suppression, cure control, and functionalization in free-radical crosslinking of polyethylene. *Polymer Engineering & Science* **2007**, *47* (1), 50–61. DOI: 10.1002/pen.20664.
- (81) Cicogna, F.; Coiai, S.; Rizzarelli, P.; Carroccio, S.; Gambarotti, C.; Domenichelli, I.; Yang, C.; Dintcheva, N. T.; Filippone, G.; Pinzino, C. Functionalization of aliphatic polyesters by nitroxide radical coupling. *Polymer Chemistry* **2014**, *5* (19), 5656–5667. DOI: 10.1039/C4PY00641K.

References

(82) Domenichelli, I.; Coiai, S.; Cicogna, F.; Pinzino, C.; Passaglia, E. Towards a better control of the radical functionalization of poly(lactic acid). *Polymer International* **2015**, *64* (5), 631–640. DOI: 10.1002/pi.4799.

(83) Bodley, M. W.; Parent, J. S. A new approach to dynamic vulcanization: Use of functional nitroxyls to control reaction dynamics and outcomes. *Industrial & engineering chemistry research* **2017**, *56* (43), 12247–12255. DOI: 10.1021/acs.iecr.7b02681.

(84) Coiai, S.; Cicogna, F.; Yang, C.; Tempesti, V.; Carroccio, S. C.; Gorrasi, G.; Mendichi, R.; Dintcheva, N. T.; Passaglia, E. Grafting of hindered phenol groups onto ethylene/ α -olefin copolymer by nitroxide radical coupling. *Polymers* **2017**, *9* (12), 670. DOI: 10.3390/polym9120670.

(85) Molloy, B. M.; Johnson, K.-a.; Ross, R. J.; Parent, J. S. Functional group tolerance of AOTEMPO-mediated peroxide cure chemistry. *Polymer* **2016**, *99*, 598–604. DOI: 10.1016/j.polymer.2016.07.067.

(86) Dakin, J. M.; Shanmugam, K. V. S.; Twigg, C.; Whitney, R. A.; Parent, J. S. Isobutylene-rich macromonomers: Dynamics and yields of peroxide-initiated crosslinking. *J. Polym. Sci. A Polym. Chem.* **2015**, *53* (1), 123–132. DOI: 10.1002/pola.27462.

(87) Twigg, C.; Mueller, E.; Molloy, B. M.; Scott Parent, J. Peroxide-initiated chemical modification of poly(isobutylene-*co*-isoprene): H-atom transfer yields and regioselectivity. *J. Polym. Sci. A Polym. Chem.* **2016**, *54* (19), 3102–3109. DOI: 10.1002/pola.28194.

(88) Batz, H. -G.; Franzmann, G.; Ringsdorf, H. Model reactions for synthesis of pharmacologically active polymers by way of monomeric and polymeric reactive esters. *Angewandte Chemie International Edition in English* **1972**, *11* (12), 1103–1104. DOI: 10.1002/anie.197211031.

(89) Ferruti, P.; Bettelli, A.; Fere, A. High polymers of acrylic and methacrylic esters of *N*-hydroxysuccinimide as polyacrylamide and polymethacrylamide precursors. *Polymer* **1972**, *13* (10), 462–464. DOI: 10.1016/0032-3861(72)90084-5.

(90) Günay, K. A.; Theato, P.; Klok, H. -A. Standing on the shoulders of Hermann Staudinger: Post-polymerization modification from past to present. *J. Polym. Sci. A Polym. Chem.* **2013**, *51* (1), 1–28. DOI: 10.1002/9783527655427.ch1.

- (91) Das, A.; Theato, P. Activated Ester Containing Polymers: Opportunities and Challenges for the Design of Functional Macromolecules. *Chemical Reviews* **2016**, *116* (3), 1434–1495. DOI: 10.1021/acs.chemrev.5b00291.
- (92) Qin, T.; Cornella, J.; Li, C.; Malins, L. R.; Edwards, J. T.; Kawamura, S.; Maxwell, B. D.; Eastgate, M. D.; Baran, P. S. A general alkyl-alkyl cross-coupling enabled by redox-active esters and alkylzinc reagents. *Science* **2016**, *352* (6287), 801. DOI: 10.1126/science.aaf6123.
- (93) Paul, T. J.; Strzelczyk, A. K.; Feldhof, M. I.; Schmidt, S. Temperature-Switchable Glycopolymers and Their Conformation-Dependent Binding to Receptor Targets. *Biomacromolecules* **2020**, *21* (7), 2913–2921. DOI: 10.1021/acs.biomac.0c00676.
- (94) Handké, N.; Trimaille, T.; Luciani, E.; Rollet, M.; Delair, T.; Verrier, B.; Bertin, D.; Gigmes, D. Elaboration of densely functionalized polylactide nanoparticles from *N*-acryloxysuccinimide-based block copolymers. *J. Polym. Sci. A Polym. Chem.* **2011**, *49* (6), 1341–1350. DOI: 10.1002/pola.24553.
- (95) Choi, J.; Schattling, P.; Jochum, F. D.; Pyun, J.; Char, K.; Theato, P. Functionalization and patterning of reactive polymer brushes based on surface reversible addition and fragmentation chain transfer polymerization. *J. Polym. Sci. A Polym. Chem.* **2012**, *50* (19), 4010–4018. DOI: 10.1002/pola.26200.
- (96) Woodfield, P. A.; Zhu, Y.; Pei, Y.; Roth, P. J. Hydrophobically modified sulfobetaine copolymers with tunable aqueous UCST through postpolymerization modification of poly(pentafluorophenyl acrylate). *Macromolecules* **2014**, *47* (2), 750–762. DOI: 10.1021/ma402391a.
- (97) Molle, E.; Frech, S.; Grüger, T.; Theato, P. Electrochemically-initiated polymerization of reactive monomers via 4-fluorobenzenediazonium salts. *Polymer Chemistry* **2021**, *12* (41), 5970–5978. DOI: 10.1039/D1PY00536G.
- (98) Parida, S. K.; Mandal, T.; Das, S.; Hota, S. K.; Sarkar, S. de; Murarka, S. Single electron transfer-induced redox processes involving *N*-(acyloxy)phthalimides. *ACS Catalysis* **2021**, *11* (3), 1640–1683. DOI: 10.1021/acscatal.0c04756.
- (99) Murarka, S. *N*-(acyloxy) phthalimides as redox-active esters in cross-coupling reactions. *Advanced Synthesis & Catalysis* **2018**, *360* (9), 1735–1753. DOI: 10.1002/adsc.201701615.

References

- (100) Oliver, D. J. The glycine decarboxylase complex from plant mitochondria. *Annual review of plant biology* **1994**, *45* (1), 323–337. DOI: 10.1146/annurev.pp.45.060194.001543.
- (101) Douce, R.; Bourguignon, J.; Neuburger, M.; Rébeillé, F. The glycine decarboxylase system: a fascinating complex. *Trends in plant science* **2001**, *6* (4), 167–176. DOI: 10.1016/S1360-1385(01)01892-1.
- (102) David, J.-C.; Dairman, W.; Udenfriend, S.; David, J. C.; Dairman, W.; Udenfriend, S. Decarboxylation to tyramine: a major route of tyrosine metabolism in mammals. *Proceedings of the National Academy of Sciences* **1974**, *71* (5), 1771–1775. DOI: 10.1073/pnas.71.5.1771.
- (103) Walton, N. J.; Butt, V. S. Metabolism and decarboxylation of glycollate and serine in leaf peroxisomes. *Planta* **1981**, *153* (3), 225–231. DOI: 10.1007/BF00383891.
- (104) Iding, H.; Siegert, P.; Mesch, K.; Pohl, M. Application of α -keto acid decarboxylases in biotransformations. *Biochimica et Biophysica Acta (BBA)-Protein Structure and Molecular Enzymology* **1998**, *1385* (2), 307–322. DOI: 10.1016/S0167-4838(98)00076-4.
- (105) Kolbe, H. Zersetzung der Valeriansäure durch den elektrischen Strom. *Ann. Chem. Pharm* **1848**, *64*, 339–341. DOI: 10.1002/jlac.18480640346.
- (106) Kochi, J. K. A new method for halodecarboxylation of acids using lead (IV) acetate. *Journal of the American Chemical Society* **1965**, *87* (11), 2500–2502. DOI: 10.1021/ja01089a041.
- (107) Hunsdiecker, H.; Hunsdiecker, C. Über den Abbau der Aalze aliphatischer Säuren durch Brom. *Berichte der deutschen chemischen Gesellschaft (A and B Series)* **1942**, *75* (3), 291–297. DOI: 10.1002/cber.19420750309.
- (108) Barton, D. H. R.; Crich, D.; Motherwell, W. B. New and improved methods for the radical decarboxylation of acids. *Journal of the Chemical Society, Chemical Communications* **1983** (17), 939–941. DOI: 10.1039/C39830000939.
- (109) Barton, D. H. R. *Some recollections of gap jumping*; American Chemical Society, **1991**.
- (110) Barton, D. H. R.; McCombie, S. W. A new method for the deoxygenation of secondary alcohols. *Journal of the Chemical Society, Perkin Transactions I* **1975** (16), 1574–1585. DOI: 10.1039/P19750001574.

- (111) Okada, K.; Okamoto, K.; Oda, M. A new and practical method of decarboxylation: photosensitized decarboxylation of *N*-acyloxyphthalimides *via* electron-transfer mechanism. *Journal of the American Chemical Society* **1988**, *110* (26), 8736–8738. DOI: 10.1021/ja00234a047.
- (112) Okada, K.; Okamoto, K.; Oda, M. Photochemical chlorodecarboxylation *via* an electron transfer mechanism. *Journal of the Chemical Society, Chemical Communications* **1989** (21), 1636–1637. DOI: 10.1039/C39890001636.
- (113) Zheng, C.; Wang, Y.; Xu, Y.; Chen, Z.; Chen, G.; Liang, S. H. Ru-Photoredox-Catalyzed Decarboxylative Oxygenation of Aliphatic Carboxylic Acids through *N*-(acyloxy)phthalimide. *Organic letters* **2018**, *20* (16), 4824–4827. DOI: 10.1021/acs.orglett.8b01885.
- (114) Okada, K.; Okamoto, K.; Morita, N.; Okubo, K.; Oda, M. Photosensitized decarboxylative Michael addition through *N*-(acyloxy)phthalimides *via* an electron-transfer mechanism. *Journal of the American Chemical Society* **1991**, *113* (24), 9401–9402. DOI: 10.1021/ja00024a074.
- (115) Pratsch, G.; Lackner, G. L.; Overman, L. E. Constructing quaternary carbons from *N*-(acyloxy)phthalimide precursors of tertiary radicals using visible-light photocatalysis. *The Journal of organic chemistry* **2015**, *80* (12), 6025–6036. DOI: 10.1021/acs.joc.5b00795.
- (116) Jiang, M.; Jin, Y.; Yang, H.; Fu, H. Visible-light photoredox synthesis of unnatural chiral α -amino acids. *Scientific reports* **2016**, *6* (1), 1–8. DOI: 10.1038/srep26161.
- (117) Schwarz, J.; Koenig, B. Metal-free, visible-light-mediated, decarboxylative alkylation of biomass-derived compounds. *Green Chemistry* **2016**, *18* (17), 4743–4749. DOI: 10.1039/C6GC01101B.
- (118) Chowdhury, R.; Yu, Z.; Tong, M. L.; Kohlhepp, S. V.; Yin, X.; Mendoza, A. Decarboxylative alkyl coupling promoted by NADH and blue light. *Journal of the American Chemical Society* **2020**, *142* (47), 20143–20151. DOI: 10.1021/jacs.0c09678.
- (119) Damrauer, N. H.; Cerullo, G.; Yeh, A.; Boussie, T. R.; Shank, C. V.; McCusker, J. K. Femtosecond dynamics of excited-state evolution in $[\text{Ru}(\text{bpy})_3]^{2+}$. *Science* **1997**, *275* (5296), 54–57. DOI: 10.1126/science.275.5296.54.

References

(120) Kalyanasundaram, K. Photophysics, photochemistry and solar energy conversion with tris (bipyridyl) ruthenium (II) and its analogues. *Coordination Chemistry Reviews* **1982**, *46*, 159–244. DOI: 10.1016/0010-8545(82)85003-0.

(121) Tucker, J. W.; Stephenson, C. R. J. Shining light on photoredox catalysis: theory and synthetic applications. *The Journal of organic chemistry* **2012**, *77* (4), 1617–1622. DOI: 10.1021/jo202538x.

(122) Harrigan, R. W.; Hager, G. D.; Crosby, G. A. Evidence for multiple-state emission from ruthenium (II) complexes. *Chemical Physics Letters* **1973**, *21* (3), 487–490. DOI: 10.1016/0009-2614(73)80290-8.

(123) Narayanam, J.; Tucker, J. W.; Stephenson, C. R. J. Electron-transfer photoredox catalysis: development of a tin-free reductive dehalogenation reaction. *Journal of the American Chemical Society* **2009**, *131* (25), 8756–8757. DOI: 10.1021/ja9033582.

(124) Prier, C. K.; Rankic, D. A.; MacMillan, D. W. C. Visible light photoredox catalysis with transition metal complexes: applications in organic synthesis. *Chemical Reviews* **2013**, *113* (7), 5322–5363. DOI: 10.1021/cr300503r.

(125) Qin, T.; Malins, L. R.; Edwards, J. T.; Merchant, R. R.; Novak, A. J. E.; Zhong, J. Z.; Mills, R. B.; Yan, M.; Yuan, C.; Eastgate, M. D.; Baran, P. S. Nickel-Catalyzed Barton Decarboxylation and Giese Reactions: A Practical Take on Classic Transforms. *Angewandte Chemie (International ed. in English)* **2017**, *56* (1), 260–265. DOI: 10.1002/anie.201609662.

(126) Frech, S.; Molle, E.; Butzelaar, A. J.; Theato, P. Ethylene-Free Synthesis of Polyethylene Copolymers and Block Copolymers. *Macromolecules* **2021**, *54* (21), 9937–9946. DOI: 10.1021/acs.macromol.1c01257.

(127) Theato, P.; Frech, S. Decarboxylation of n-oxyphthalimide-based polymers. **2020**, EP3798242A1.

(128) Stefan Frech. *Novel Post-Polymerization Functionalization Methods of Phthalimide-based Polymers towards Polyethylene and further functionalized Polymer Systems*, **2019**.

(129) Butzelaar, A. J.; Röring, P.; Mach, T. P.; Hoffmann, M.; Jeschull, F.; Wilhelm, M.; Winter, M.; Brunklaus, G.; Théato, P. Styrene-Based Poly(ethylene oxide) Side-Chain Block

Copolymers as Solid Polymer Electrolytes for High-Voltage Lithium-Metal Batteries. *ACS Applied Materials & Interfaces* **2021**, *13* (33), 39257–39270. DOI: 10.1021/acsami.1c08841.

(130) Frech, S.; Theato, P. Synthesizing Polyethylene from Polyacrylates: A Decarboxylation Approach. *ACS Macro Letters* **2022**, *11* (2), 161–165. DOI: 10.1021/acsmacrolett.1c00723.

(131) Mayadunne, R. T. A.; Rizzardo, E.; Chiefari, J.; Krstina, J.; Moad, G.; Postma, A.; Thang, S. H. Living polymers by the use of trithiocarbonates as reversible addition-fragmentation chain transfer (RAFT) agents: ABA triblock copolymers by radical polymerization in two steps. *Macromolecules* **2000**, *33* (2), 243–245. DOI: 10.1021/ma991451a.

(132) Obradors, C.; Martinez, R. M.; Shenvi, R. A. Ph(*i*-PrO)SiH₂: An Exceptional Reductant for Metal-Catalyzed Hydrogen Atom Transfers. *Journal of the American Chemical Society* **2016**, *138* (14), 4962–4971. DOI: 10.1021/jacs.6b02032.

(133) Brandhofer, T.; Mancheño, O. G. Versatile Ru - Photoredox - Catalyzed Functionalization of Dehydro-Amino Acids and Peptides. *ChemCatChem* **2019**, *11* (16), 3797–3801. DOI: 10.1002/cctc.201900446.

(134) Cao, T.; Xu, T.; Xu, R.; Shu, X.; Liao, S. Decarboxylative thiolation of redox-active esters to free thiols and further diversification. *Nature communications* **2020**, *11* (1), 1–8. DOI: 10.1038/s41467-020-19195-w.

(135) Shu, X.; Xu, R.; Ma, Q.; Liao, S. Accessing alkyl boronic esters *via* visible light-mediated decarboxylative addition reactions of redox-active esters. *Organic Chemistry Frontiers* **2020**, *7* (15), 2003–2007. DOI: 10.1039/D0QO00440E.

(136) Cerit, N.; Cakir, N.; Dag, A.; Sirkecioglu, O.; Durmaz, H.; Hizal, G.; Tunca, U. Various brush polymers through ring opening metathesis polymerization and nitroxide radical coupling reaction. *J. Polym. Sci. A Polym. Chem.* **2011**, *49* (13), 2850–2858. DOI: 10.1002/pola.24719.

(137) Frech, S.; Molle, E.; Hub, C.; Theato, P. Decarboxylation of Poly [*N*-(acryloyloxy) phthalimide] as a Versatile Tool for Post-Polymerization Modification. *Macromolecular Rapid Communications* **2022**, *43*, 2200068. DOI: 10.1002/marc.202200068.

(138) Xu, R.; Xu, T.; Yang, M.; Cao, T.; Liao, S. A rapid access to aliphatic sulfonyl fluorides. *Nature communications* **2019**, *10* (1), 1–7. DOI: 10.1038/s41467-019-11805-6.

References

- (139) Jiang, M.; Jin, Y.; Yang, H.; Fu, H. Visible-light photoredox synthesis of unnatural chiral α -amino acids. *Scientific reports* **2016**, *6* (1), 1–8. DOI: 10.1038/srep26161.
- (140) Feng, C.; Li, Y.; Yang, D.; Hu, J.; Zhang, X.; Huang, X. Well-defined graft copolymers: from controlled synthesis to multipurpose applications. *Chemical Society Reviews* **2011**, *40* (3), 1282–1295. DOI: 10.1039/B921358A.
- (141) Thakur, V. K.; Tan, E. J.; Lin, M.-F.; Lee, P. S. Polystyrene grafted polyvinylidene fluoride copolymers with high capacitive performance. *Polymer Chemistry* **2011**, *2* (9), 2000–2009. DOI: 10.1039/C1PY00225B.
- (142) Hyslop, D. K.; Parent, J. S. Functional nitroxyls for use in delayed-onset polyolefin cross-linking. *Macromolecules* **2012**, *45* (20), 8147–8154. DOI: 10.1021/ma3016135.
- (143) Scott, M. E.; Parent, J. S.; Dupont, J.; Whitney, R. A. Controlled radical grafting: Nitroxyl-mediated maleation of model hydrocarbons. *Industrial & engineering chemistry research* **2003**, *42* (16), 3662–3670. DOI: 10.1021/ie020888v.
- (144) Passaglia, E.; Coiai, S.; Cicogna, F.; Ciardelli, F. Some recent advances in polyolefin functionalization. *Polymer International* **2014**, *63* (1), 12–21. DOI: 10.1002/pi.4598.
- (145) Yang, D.; Feng, C.; Hu, J. Nitroxide radical coupling reaction: a powerful tool in polymer and material synthesis. *Polymer Chemistry* **2013**, *4* (8), 2384–2394. DOI: 10.1039/C2PY20987J.
- (146) Nicolas, J.; Guillaneuf, Y.; Lefay, C.; Bertin, D.; Gimes, D.; Charleux, B. Nitroxide-mediated polymerization. *Progress in Polymer Science* **2013**, *38* (1), 63–235. DOI: 10.1016/j.progpolymsci.2012.06.002.
- (147) Grubbs, R. B. Nitroxide-mediated radical polymerization: limitations and versatility. *Polymer Reviews* **2011**, *51* (2), 104–137. DOI: 10.1080/15583724.2011.566405.
- (148) Gimes, D. *Nitroxide mediated polymerization: from fundamentals to applications in materials science*, Vol. 19; Royal Society of Chemistry, **2016**.
- (149) Boger, D. L.; McKie, J. A. An efficient synthesis of 1, 2, 9, 9a-tetrahydrocyclopropa [c] benz [e] indol-4-one CBI: an enhanced and simplified analog of the CC-1065 and duocarmycin alkylation subunits. *The Journal of organic chemistry* **1995**, *60* (5), 1271–1275. DOI: 10.1021/jo00110a034.

- (150) Newcomb, M. Competition methods and scales for alkyl radical reaction kinetics. *Tetrahedron* **1993**, *49* (6), 1151–1176. DOI: 10.1016/S0040-4020(01)85808-7.
- (151) Johnston, L. J.; Scaiano, J. C.; Ingold, K. U. Kinetics of cyclopropyl radical reactions. 1. Absolute rate constants for some addition and abstraction reactions. *Journal of the American Chemical Society* **1984**, *106* (17), 4877–4881. DOI: 10.1021/ja00329a041.
- (152) Hartmann, M.; Li, Y.; Studer, A. Transition-metal-free oxyarylation of alkenes with aryl diazonium salts and TEMPO_{Na}. *Journal of the American Chemical Society* **2012**, *134* (40), 16516–16519. DOI: 10.1021/ja307638u.
- (153) Vogler, T.; Studer, A. Applications of TEMPO in Synthesis. *Synthesis* **2008**, *2008* (13), 1979–1993. DOI: 10.1055/s-2008-1078445.
- (154) Guillaneuf, Y.; Dufils, P.-E.; Autissier, L.; Rollet, M.; Gigmes, D.; Bertin, D. Radical chain end chemical transformation of SG1-based polystyrenes. *Macromolecules* **2010**, *43* (1), 91–100. DOI: 10.1021/ma901838m.
- (155) Garrison, J. B.; Hughes, R. W.; Sumerlin, B. S. Backbone Degradation of Polymethacrylates via Metal-Free Ambient-Temperature Photoinduced Single-Electron Transfer. *ACS Macro Letters* **2022**, *11*, 441–446. DOI: 10.1021/acsmacrolett.2c00091.
- (156) Zheng, C.; Wang, G. - Z.; Shang, R. Catalyst-free Decarboxylation and Decarboxylative Giese Additions of Alkyl Carboxylates through Photoactivation of Electron Donor-Acceptor Complex. *Advanced Synthesis & Catalysis* **2019**, *361* (19), 4500–4505. DOI: 10.1002/adsc.201900803.
- (157) Alejo, T.; Prieto, M.; Garcia-Juan, H.; Andreu, V.; Mendoza, G.; Sebastian, V.; Arruebo, M. A facile method for the controlled polymerization of biocompatible and thermoresponsive oligo (ethylene glycol) methyl ether methacrylate copolymers. *Polymer Journal* **2018**, *50* (2), 203–211. DOI: 10.1038/s41428-017-0004-8.
- (158) Montoya-Villegas, K. A.; Licea-Claverie, Á.; Zapata-González, I.; Gómez, E.; Ramírez-Jiménez, A. The effect in the RAFT polymerization of two oligo (ethylene glycol) methacrylates when the CTA 4-cyano-4-(propylthiocarbonothioylthio) pentanoic acid is auto-hydrolyzed to its corresponding amide. *Journal of Polymer Research* **2019**, *26* (3), 1–11. DOI: 10.1007/s10965-019-1718-4.

References

11 Appendix

Additional information and spectra for the different projects are given in the following.

11.1 Additional Results for ‘Ethylene-free Synthesis of Polyethylene Copolymers and Block Copolymers’

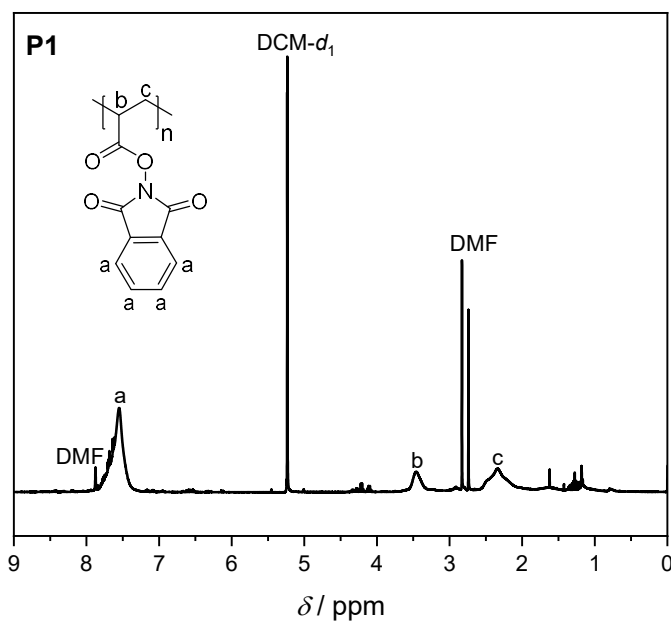


Figure 52: ^1H NMR spectrum of PAP (P1). Solvent $\text{DCM-}d_2$.

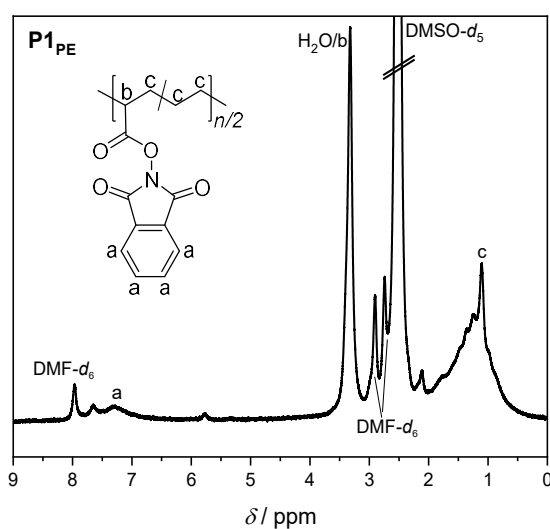


Figure 53: ^1H NMR spectrum of P1_{PE} after thermally-induced decarboxylation. Solvent: 50:50 mixture of $\text{DMF-}d_7$ and $\text{DMSO-}d_6$.

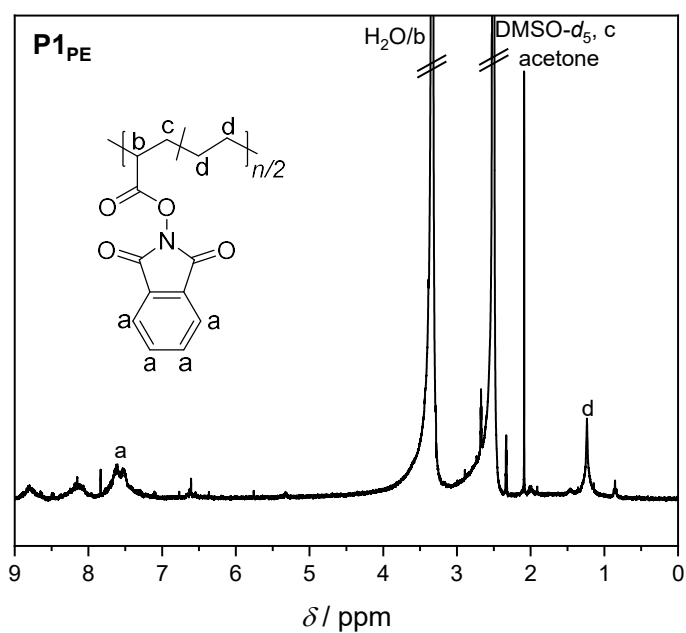


Figure 54: ¹H NMR spectrum of **P1_{PE}** after photochemically-induced decarboxylation. Solvent: DMSO-*d*₆.

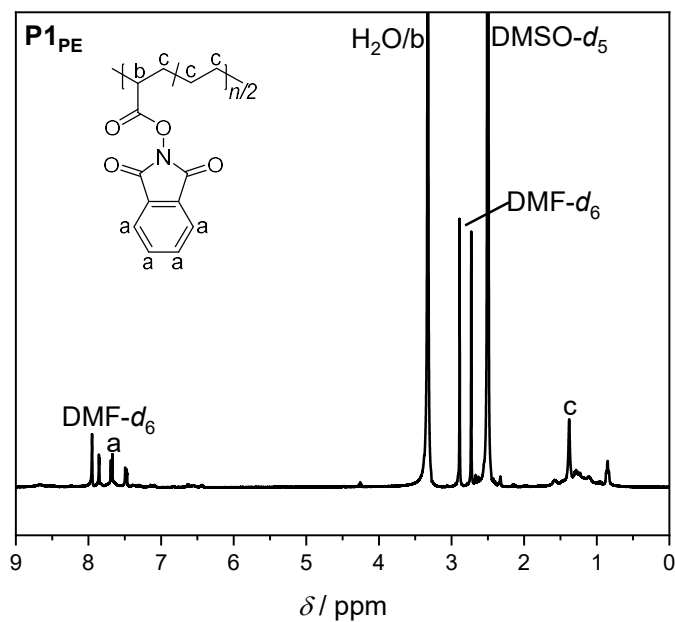


Figure 55: ¹H NMR spectrum of PAP (**P1**) after thermally-induced decarboxylation with tributyltin hydride in DMF/1,2,4-TCB (1:1) at 120 °C. Solvent: DMSO-*d*₆, DMF-*d*₇.

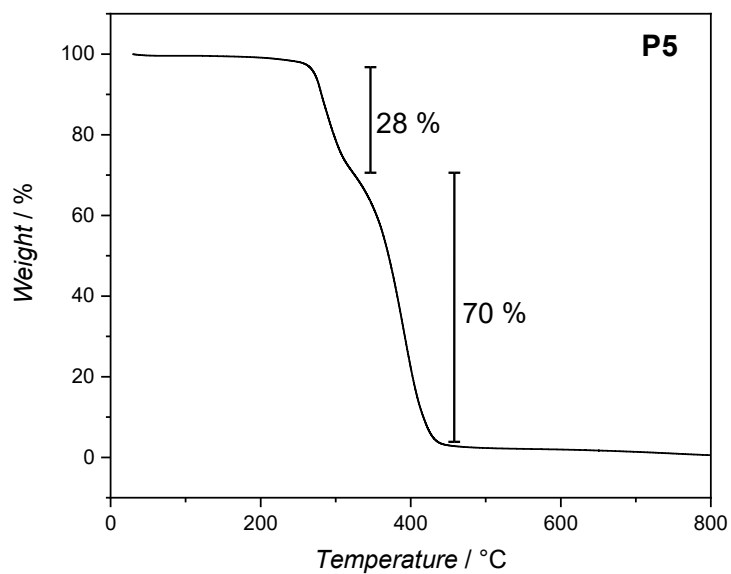


Figure 56: Thermogravimetric analysis of **P5**, heating rate 10 K min^{-1} .

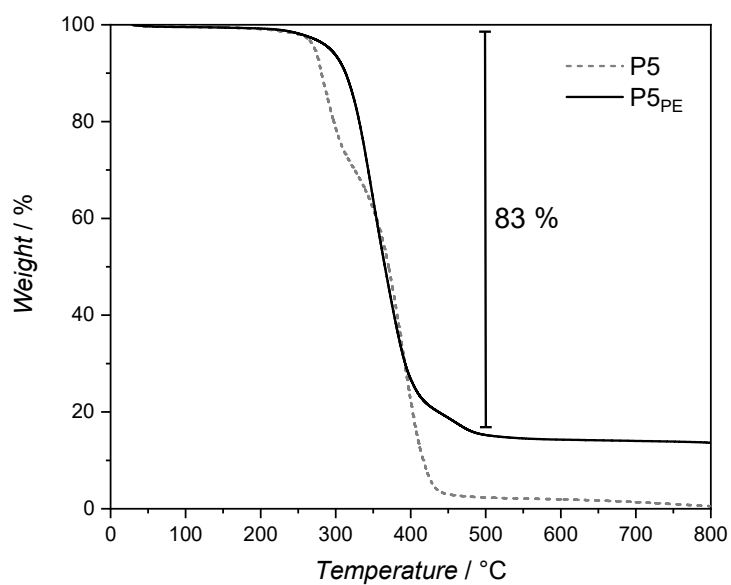


Figure 57: Thermogravimetric analysis of **P5PE** in comparison to **P5**, heating rate 10 K min^{-1} .

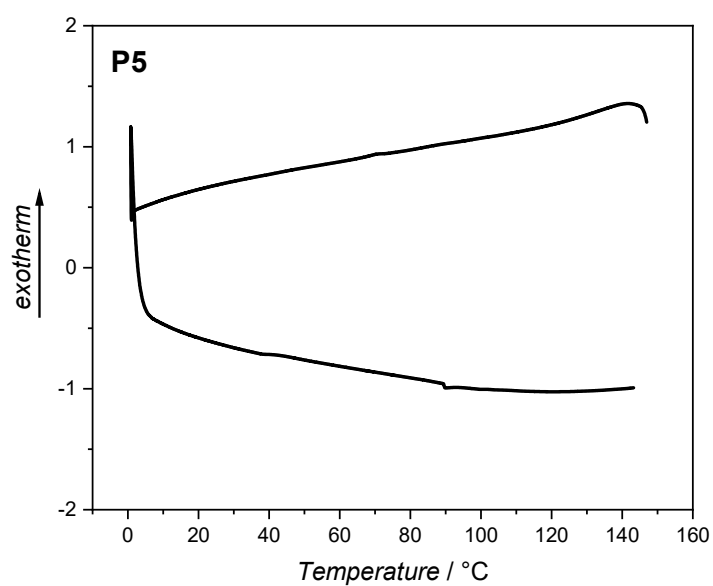


Figure 58: DSC characterization of **P5**, heating rate 10 K min⁻¹.

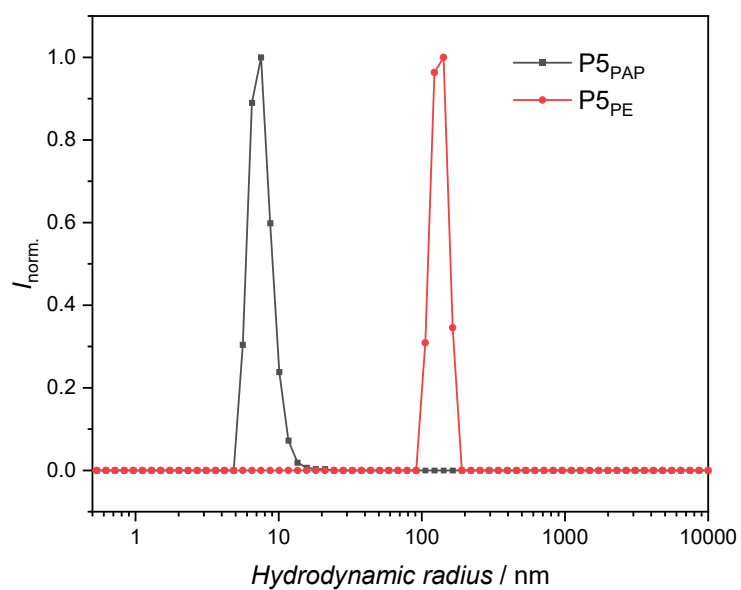


Figure 59: DLS analysis of **P5** and **P5_{PE}** after thermally-induced decarboxylation with phenylsilane.

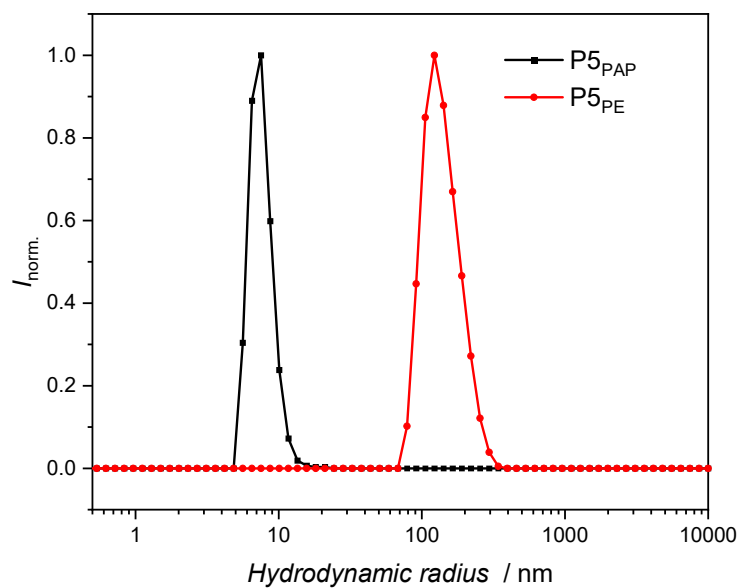


Figure 60: DLS analysis of **P5** and **P5_{PE}** after photochemically-induced decarboxylation with phenylsilane.

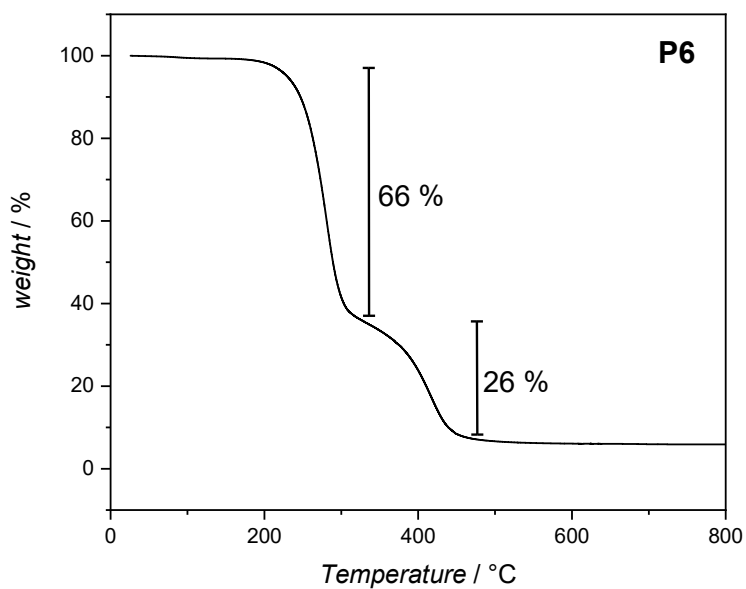


Figure 61: Thermogravimetric analysis of **P6**, heating rate 10 K min⁻¹.

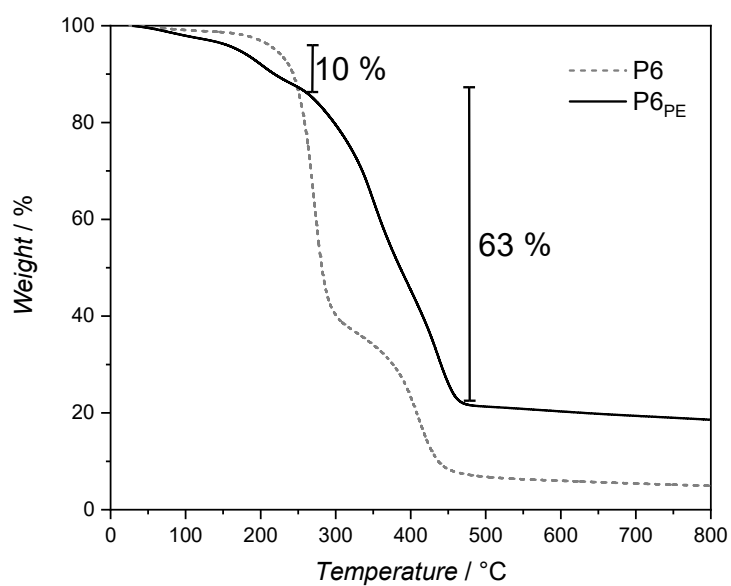


Figure 62: Thermogravimetric analysis of **P6_{PE}** in comparison to **P6**, heating rate 10 K min^{-1} .

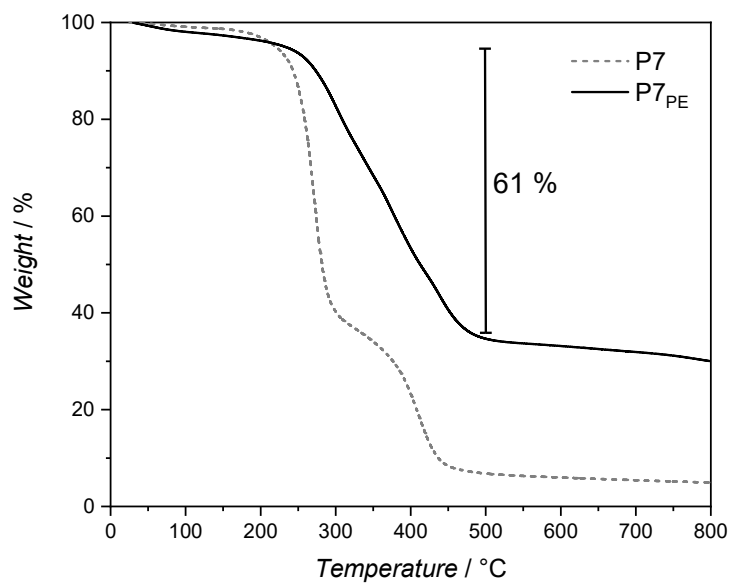


Figure 63: Thermogravimetric analysis of **P7_{PE}** in comparison to **P7**, heating rate 10 K min^{-1} .

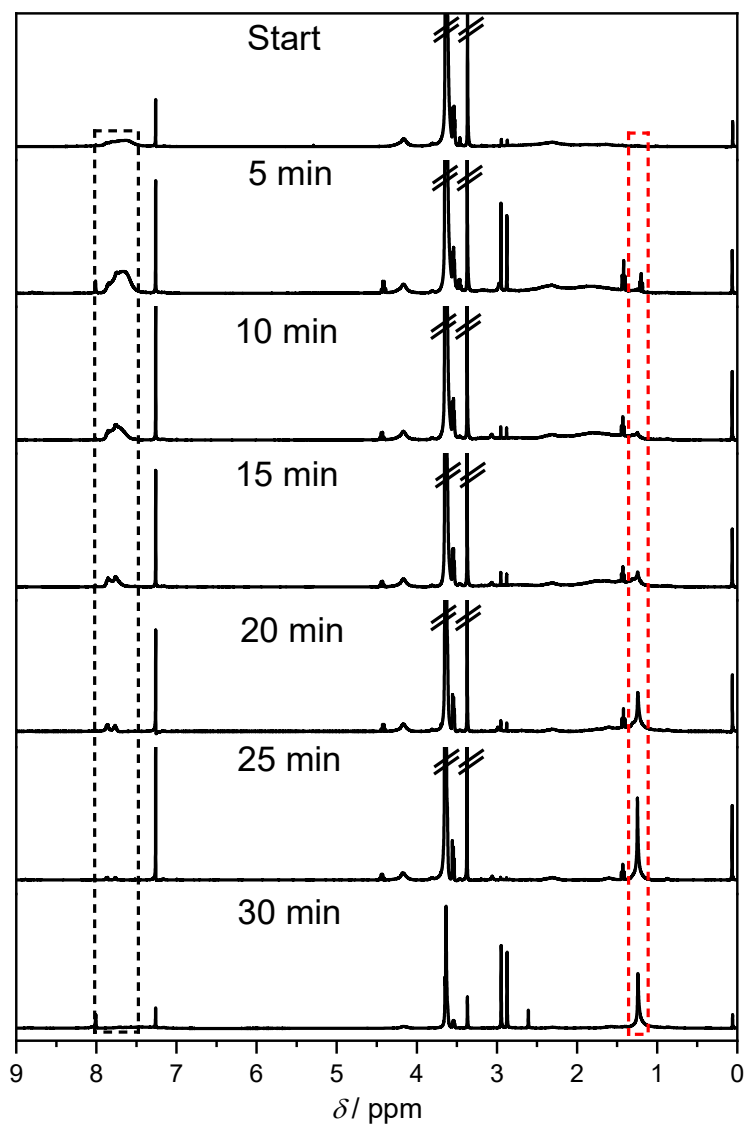


Figure 64: Reaction monitoring of photochemically-induced decarboxylation of PAP-*b*-POEGMEA (**P10**). Solvent: CDCl_3 .

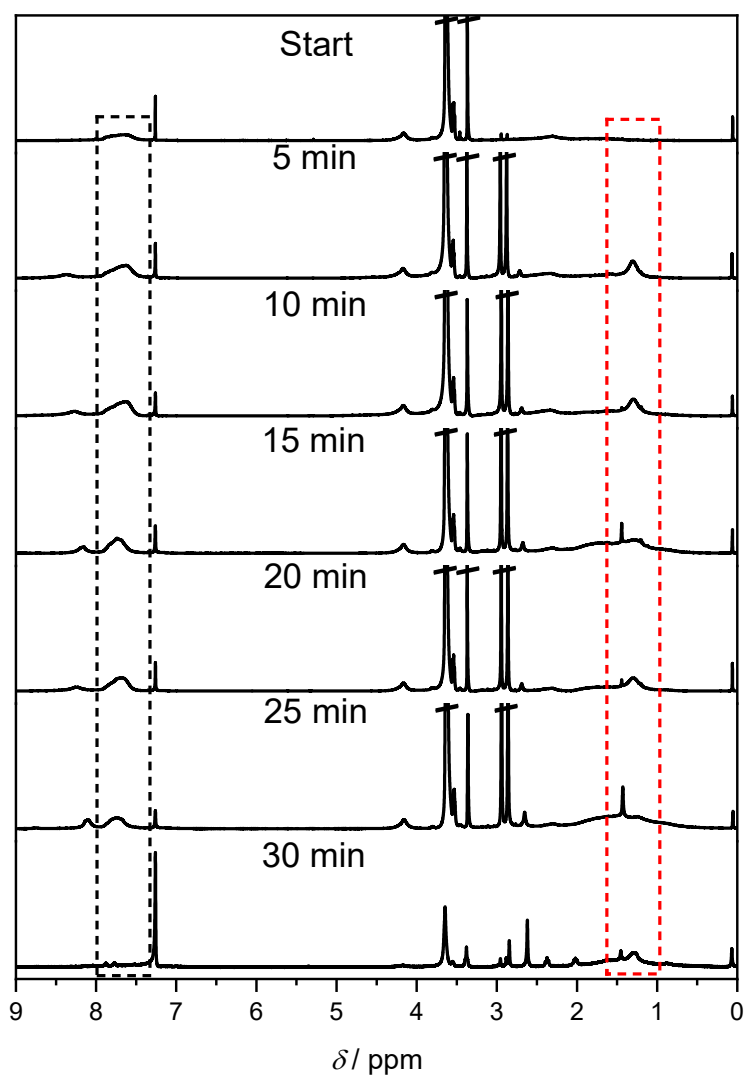


Figure 65: Reaction monitoring of thermally-induced decarboxylation of PAP-*b*-POEGMEA (P11). Solvent: CDCl_3 .

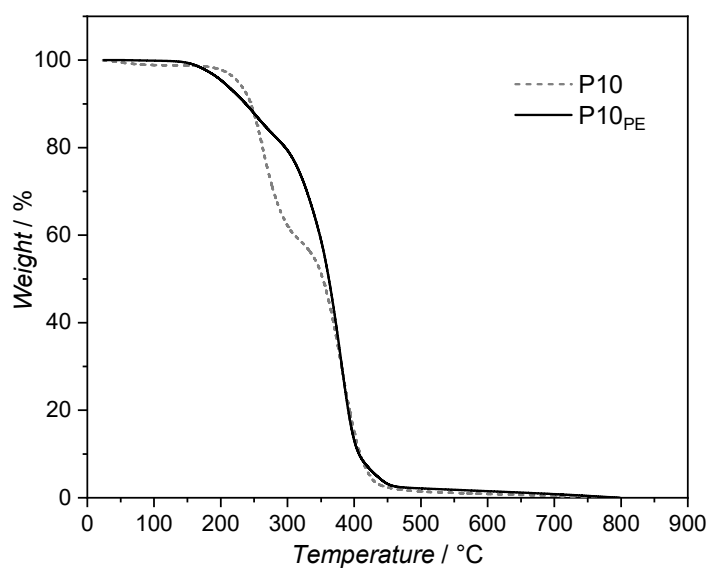


Figure 66: Thermogravimetric analysis of **P10_{PE}** in comparison to **P10**, heating rate 10 K min⁻¹.

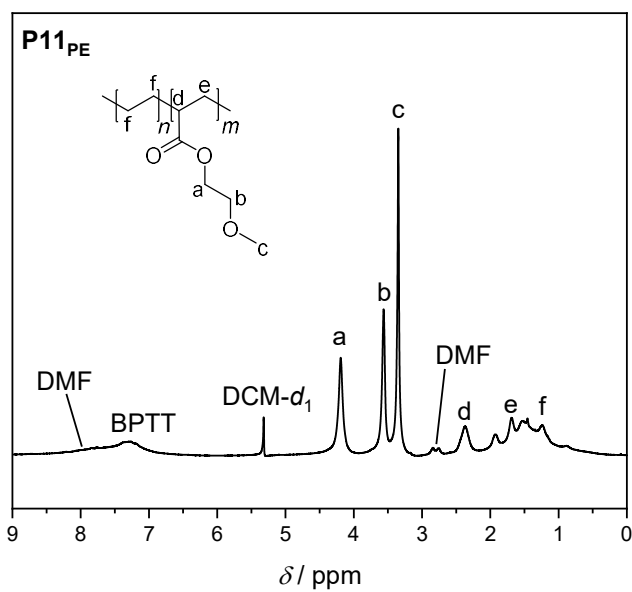


Figure 67: ¹H NMR spectrum of **P11_{PE}** (PE-*b*-PMEA) after thermal decarboxylation. Solvent: DCM-*d*₂.

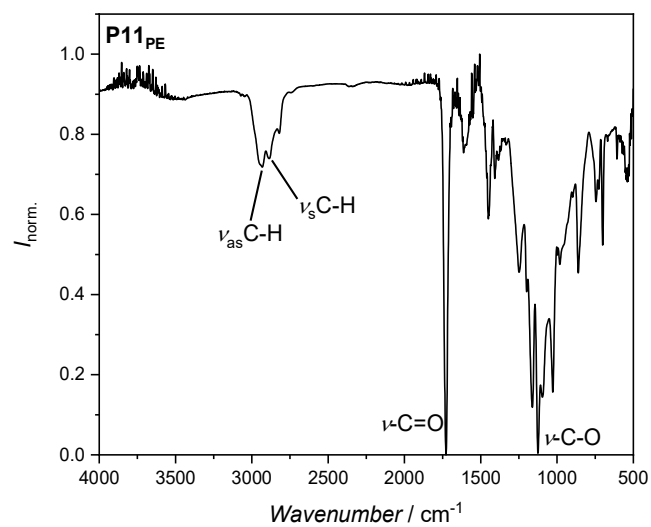


Figure 68: ATR-FT-IR spectrum of **P11_{PE}** (PE-*b*-PMEA) after thermal decarboxylation.

11.2 Additional Results for ‘Synthesizing Polyethylene from Polyacrylates: A Decarboxylation Approach’

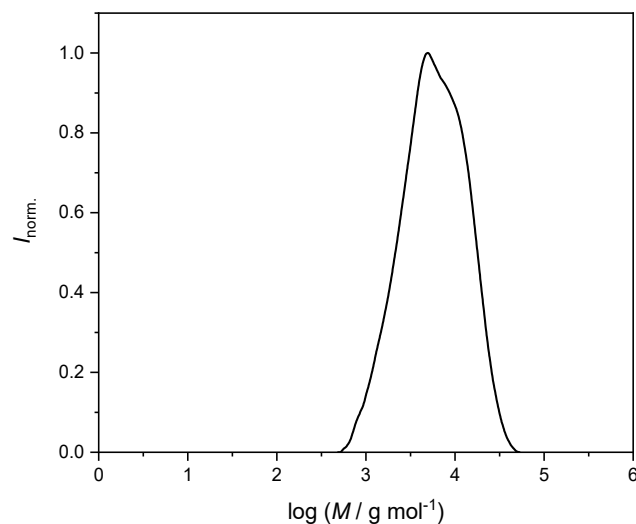


Figure 69: SEC chromatogram of PAP-BTTP-mPEG₂₀₀₀ in DMAc as eluent with PMMA calibration.

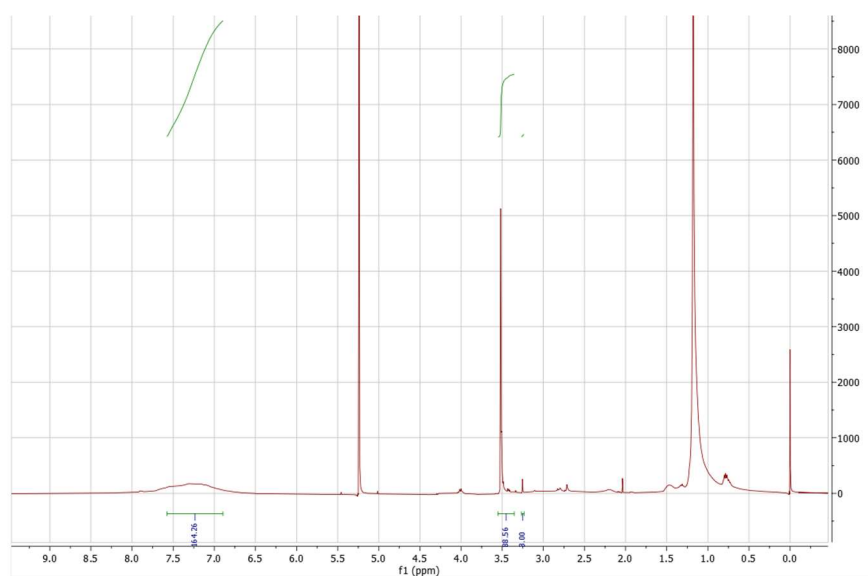


Figure 70: ¹H NMR spectrum (raw spectrum) of DP₂PE after decarboxylation under standard conditions (1.50 eq. phenylsilane). The integrals of relevant signals at 3.25 ppm, 3.51 ppm, and 7.35 ppm for the calculation of the improvement of the decarboxylation result are marked.

Integrals: 3.25 (s, 3H, (OCH₂CH₂)₂₂CH₃): 3.00

3.51 (s, 88H, (OCH₂CH₂)₂₂CH₃): 87.87

7.35: 163.63

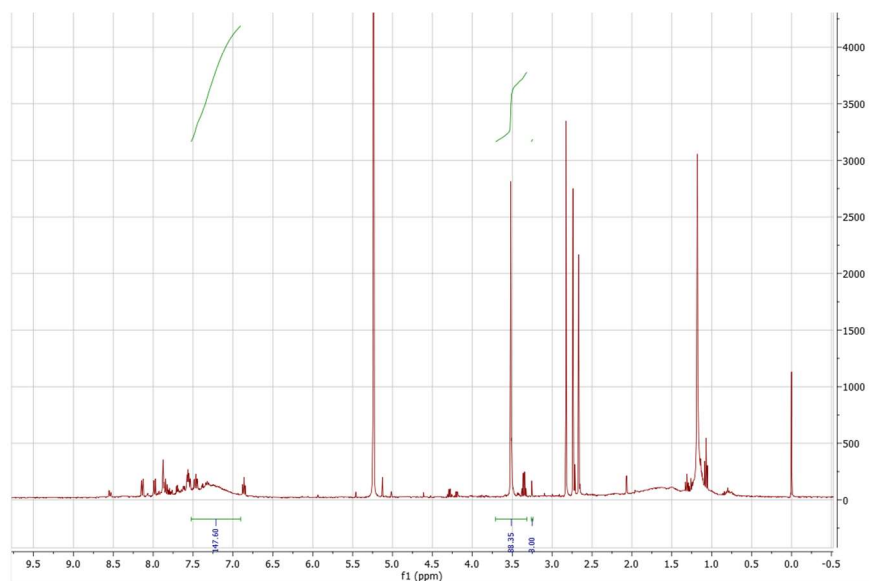


Figure 71: ^1H NMR of **DP2PE** after decarboxylation with reduced equivalents of phenylsilane. Integrals of relevant signals at 3.25 ppm, 3.51 ppm, and 7.35 ppm for the calculation of the improvement of the decarboxylation result are marked.

Integrals: 3.25 (s, 3H, $(\text{OCH}_2\text{CH}_2)_{22}\text{CH}_3$): 3.00

3.51 (s, 88H, $(\text{OCH}_2\text{CH}_2)_{22}\text{CH}_3$): 88.35

7.35: 147.60

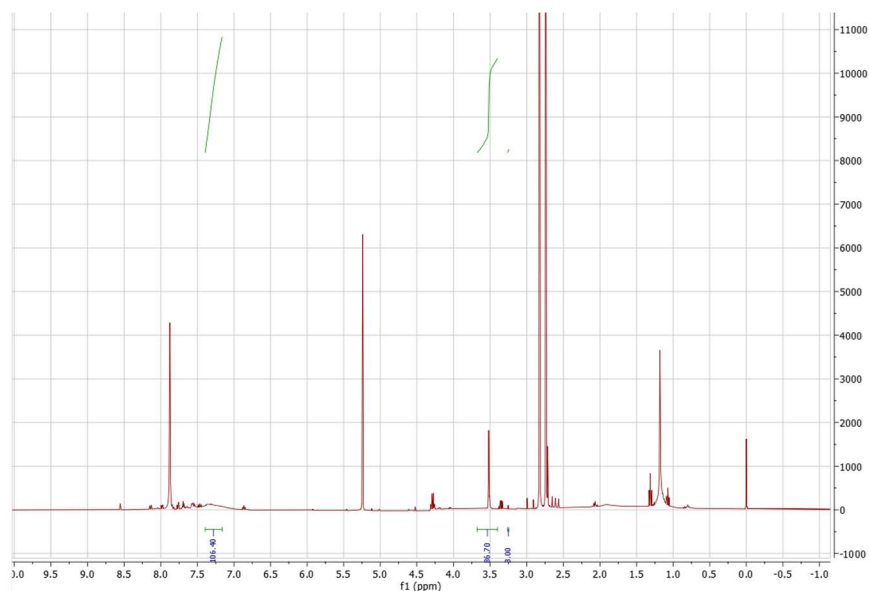


Figure 72: ^1H NMR of **DP2PE** after decarboxylation with reduced concentration. Integrals of relevant signals at 3.25 ppm, 3.51 ppm, and 7.35 ppm for the calculation of the improvement of the decarboxylation result are marked.

Integrals: 3.25 (s, 3H, $(\text{OCH}_2\text{CH}_2)_{22}\text{CH}_3$): 3.00

3.51 (s, 88H, $(\text{OCH}_2\text{CH}_2)_{22}\text{CH}_3$): 86.70

7.35: 106.4

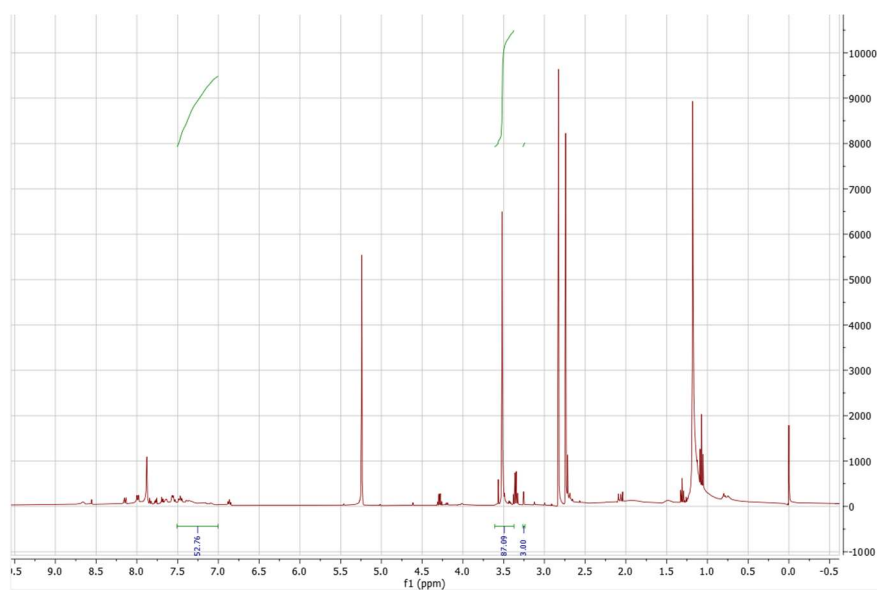


Figure 73: ^1H NMR of DP2PE after decarboxylation with additional *i*-PrOH. Integrals of relevant signals at 3.25 ppm, 3.51 ppm, and 7.35 ppm for the calculation of the improvement of the decarboxylation result are marked.

Integrals: 3.25 (s, 3H, $(\text{OCH}_2\text{CH}_2)_{22}\text{CH}_3$): 3.00

3.51 (s, 88H, $(\text{OCH}_2\text{CH}_2)_{22}\text{CH}_3$): 87.09

7.35: 52.76

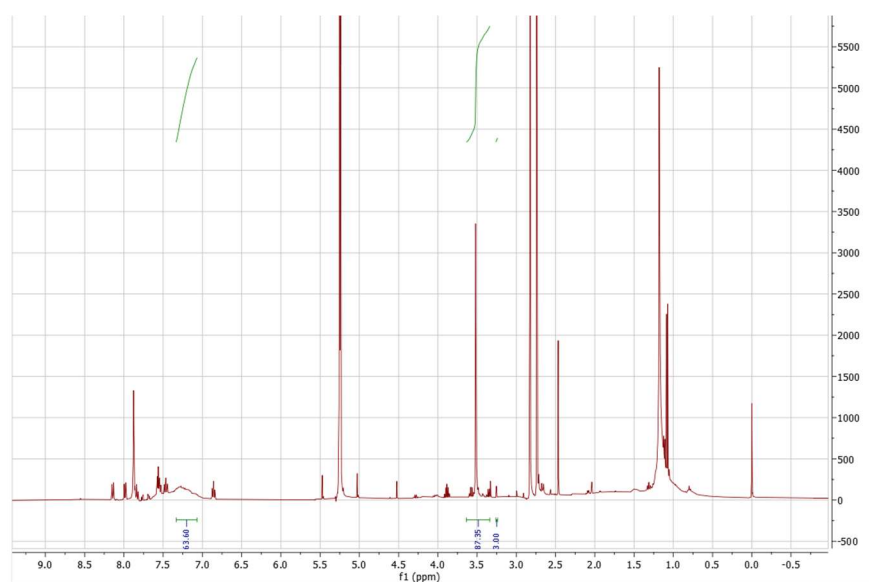


Figure 74: ^1H NMR of DP2PE after decarboxylation with reduced concentration and additional *i*-PrOH. Integrals of relevant signals at 3.25 ppm, 3.51 ppm, and 7.35 ppm for the calculation of the improvement of the decarboxylation result are marked.

Integrals: 3.25 (s, 3H, $(\text{OCH}_2\text{CH}_2)_{22}\text{CH}_3$): 3.00

3.51 (s, 88H, $(\text{OCH}_2\text{CH}_2)_{22}\text{CH}_3$): 87.35

7.35: 63.60

Appendix

Commercial Polyethylene (Sigma Aldrich, $M_n = 7700 \text{ g mol}^{-1}$)

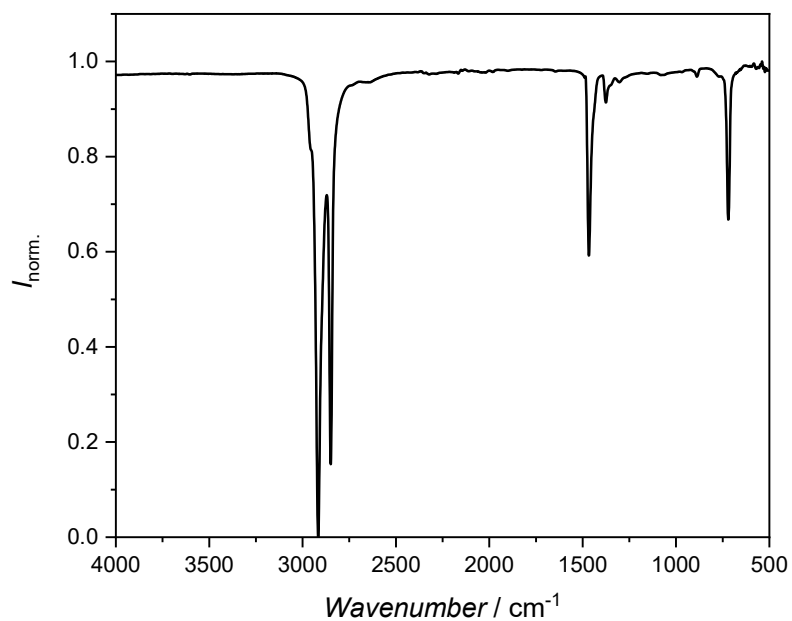


Figure 75: ATR-FT-IR spectrum of commercial PE (Polyethylene, Sigma Aldrich, average $M_n = 7700 \text{ g mol}^{-1}$, 427799-250G).

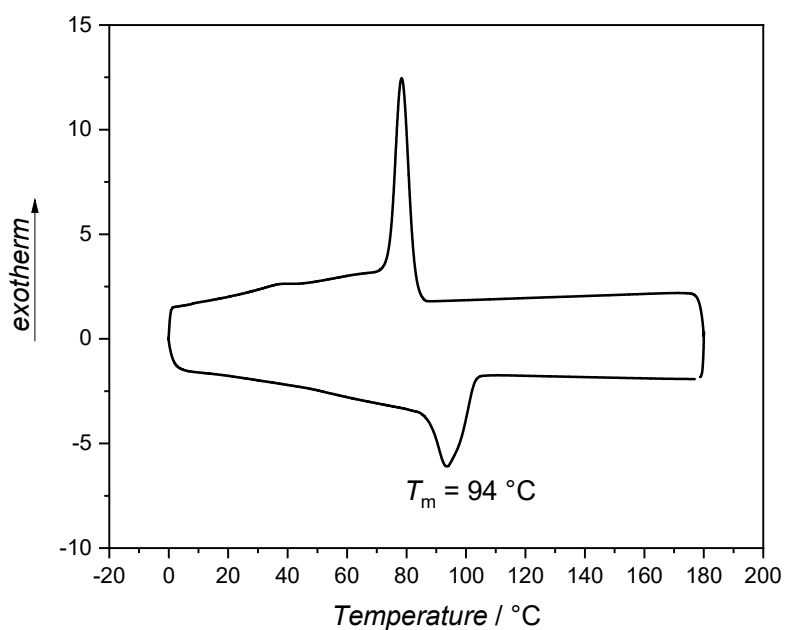


Figure 76: DSC analysis of commercial PE (Polyethylene, Sigma Aldrich, average $M_n = 7700 \text{ g mol}^{-1}$, 427799-250G).

11.3 Additional Results for ‘Decarboxylation of Poly[*N*-(acryloyloxy)phthalimide as a Versatile Tool for Post-Polymerization Modification’

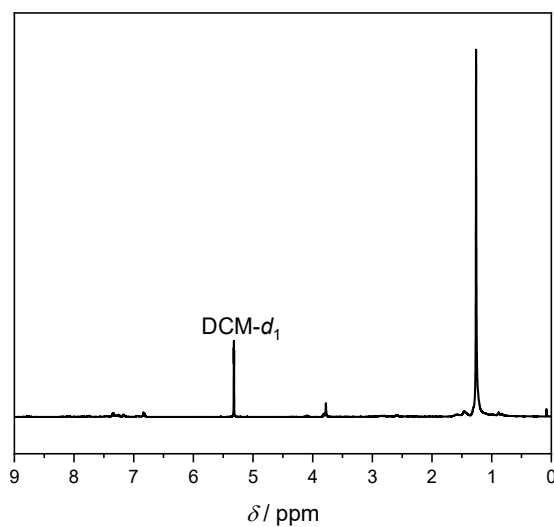


Figure 77: ^1H NMR spectrum of **FP1** after decarboxylation in the presence of bis-(4-methoxyphenyl)disulphide. Solvent: $\text{DCM-}d_2$.

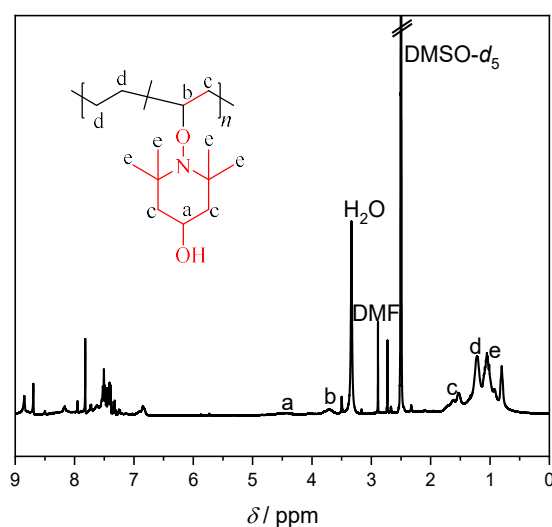


Figure 78: ^1H NMR spectrum of poly(ethylene-*co*-TEMVPO) after decarboxylation with Bu_3SnH and TEMPO-OH . Solvent: $\text{DMSO-}d_6$.

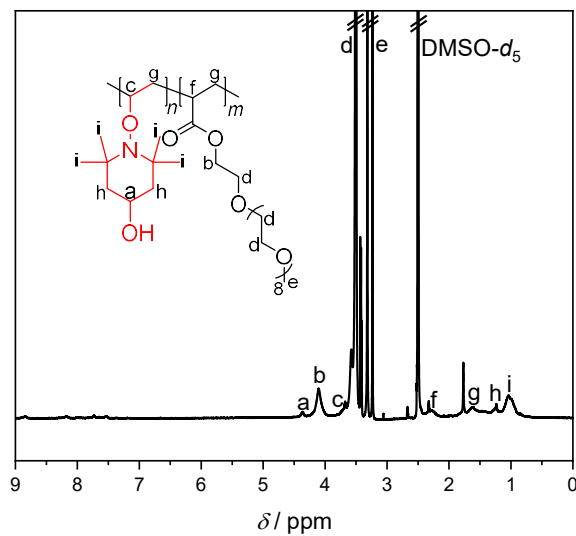


Figure 79: ¹H NMR spectrum of PTEMVPO-*b*-POEGMEA after reduction with Zn/AcOH in DMF at 60 °C; solvent: DMSO-*d*₆.

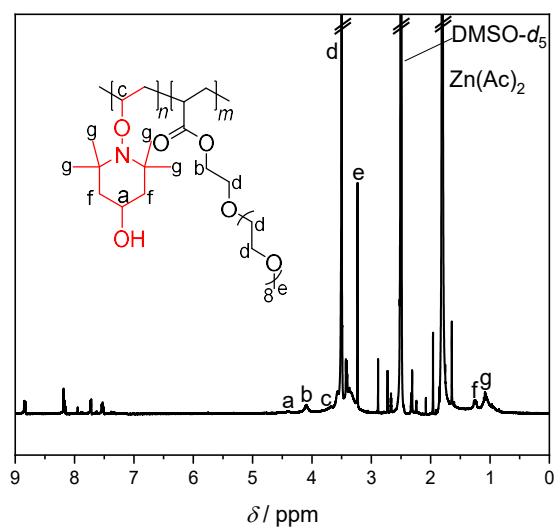


Figure 80: ¹H NMR spectrum of PTEMVPO-*b*-POEGMEA after reduction with Zn/AcOH in DMF at 60 °C; solvent: DMSO-*d*₆.

11.4 Additional Results for ‘Propylene-free Synthesis of Polypropylene *via* Decarboxylation’

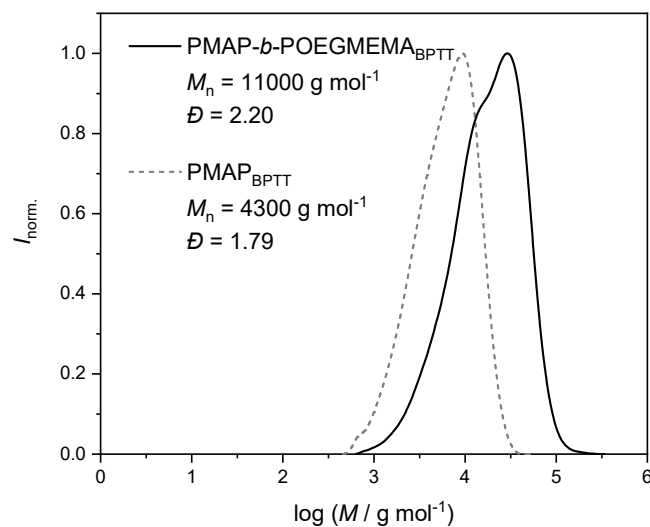


Figure 81: SEC chromatogram of PMAP (grey, dashed) and PMAP-*b*-POEGMEMA (black) polymerized with BPTT as RAFT agent in DMAc as eluent with PMMA calibration.

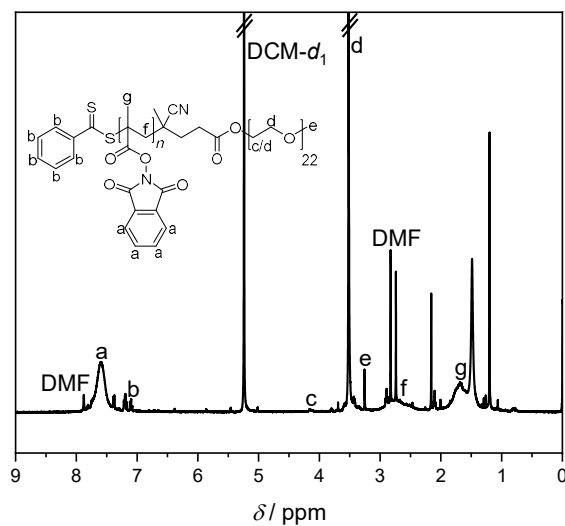


Figure 82: ^1H NMR spectrum of DPP1. Solvent: DCM- d_2 .

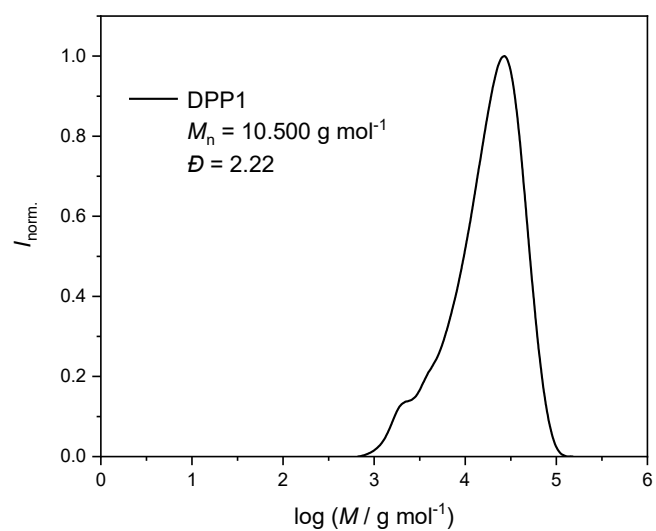


Figure 83: SEC chromatogram of **DPP1** in DMAc as eluent and PMMA calibration.

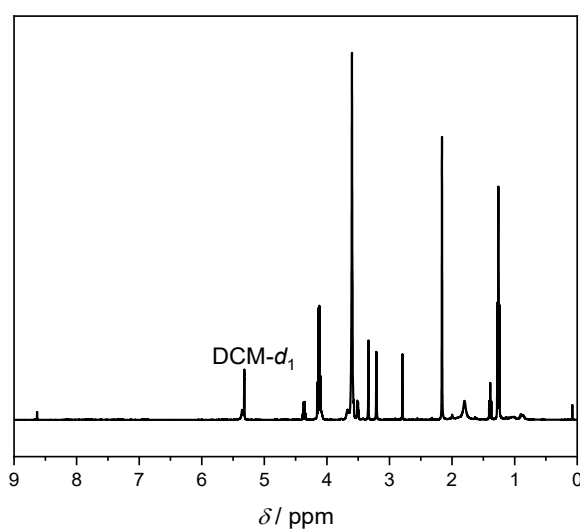


Figure 84: ^1H NMR spectrum **PP1PE** after decarboxylation with $\text{Ru}(\text{bpy})_3\text{Cl}_2$, HE and 10 eq. of Bu_3SnH . Solvent: $\text{DCM-}d_2$.

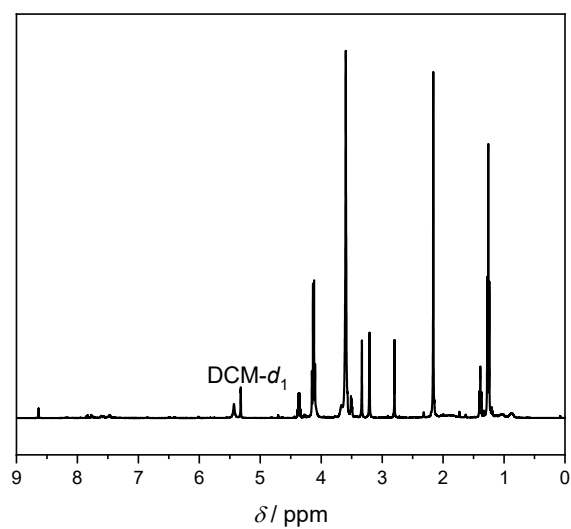


Figure 85: ¹H NMR spectrum of **PP1PE** after decarboxylation with Ru(bpy)₃Cl₂ and HE as reductant and H-donor. Solvent: DCM-*d*₂.

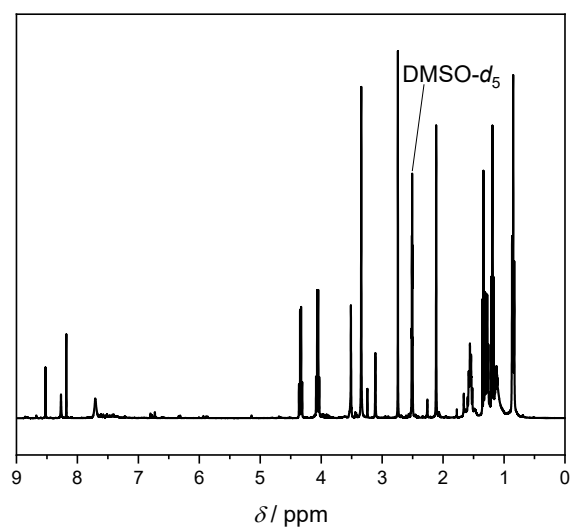


Figure 86: ¹H NMR spectrum of **PP1PE** after decarboxylation with HE as catalyst and Bu₃SnH as H-donor. Solvent: DMSO-*d*₆.

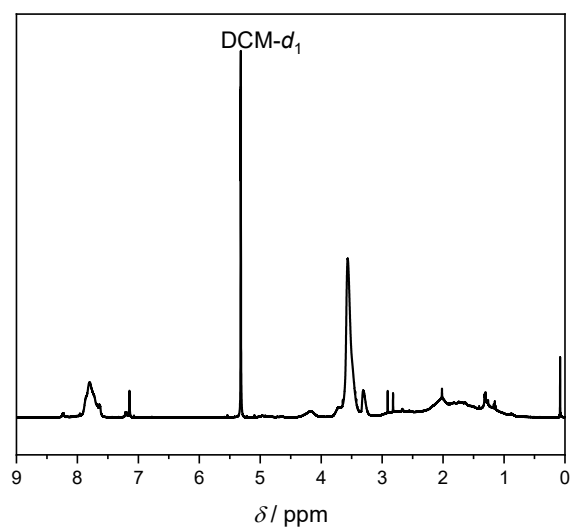


Figure 87: ¹H NMR spectrum of **PP1PE** after decarboxylation with Eosin Y as catalyst and DIPEA as H-donor. Solvent: DCM-*d*₂.

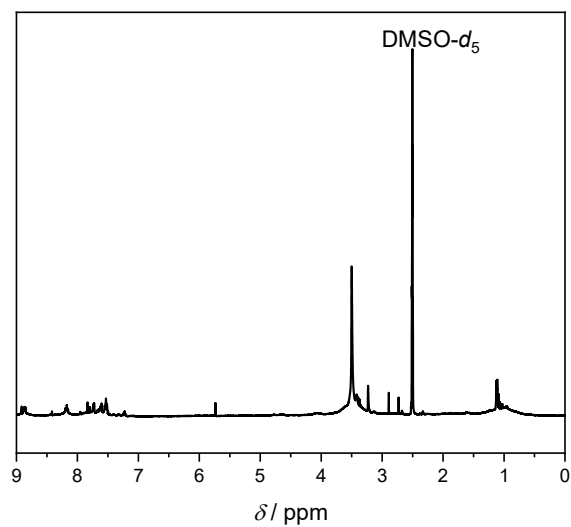


Figure 88: ¹H NMR spectrum of **PP1PE** after decarboxylation with Ru(bpy)₃Cl₂ · 6 H₂O, DIPEA and PhSiH₃ as H-donor. Solvent: DMSO-*d*₆.

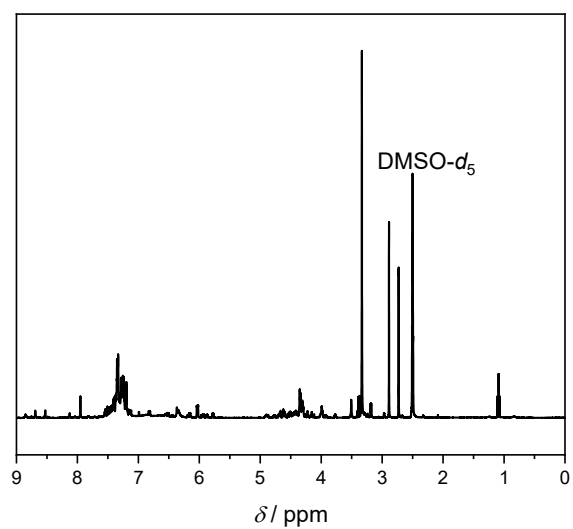


Figure 89: ^1H NMR spectrum of **PP1_{PE}** after decarboxylation with $\text{Ru}(\text{bpy})_3\text{Cl}_2 \cdot 6 \text{H}_2\text{O}$, BNAH as reductant and Bu_3SnH as H-donor. Solvent: $\text{DMSO-}d_6$.